The Electrochemistry of Diaza-Functionalized Quinone Compounds and their Application in Aqueous Redox Flow Batteries

Dem Fachbereich Biologie und Chemie

der Justus-Liebig-Universität Gießen

vorgelegte Dissertation

zur Erlangung des akademischen Grades

Doktor der Naturwissenschaften

–Dr. rer. nat. –

von

Jonas David Hofmann

Gießen, November 2020

Dekan / Dean	Prof. Dr. Jürgen Janek
1. Gutachter / 1st Reviewer	Prof. Dr. Jürgen Janek (Justus-Liebig-Universität Gießen)
2. Gutachter / 2nd Reviewer	Prof. Dr. Hermann Wegner (Justus-Liebig-Universität Gießen)

Eingereicht / submitted	23.11.2020
Disputation / disputation	12.02.2021

Danksagung

An dieser Stelle möchte ich mich ganz herzlich bei all jenen bedanken, die mich beim Anfertigen dieser Arbeit begleitet und unterstützt haben:

Mein besonderer Dank gilt Prof. Dr. Jürgen Janek für die Gelegenheit diese Arbeit in seiner Arbeitsgruppe anzufertigen, die hervorragende und professionelle Betreuung sowie die anregenden fachlichen Gespräche während dieser Zeit. Auch möchte ich mich für die Möglichkeit zur Einbringung und Umsetzung eigener Ideen in diesem neu erschlossenen Fachgebiet und das in diesem Zusammenhang entgegengebrachte Vertrauen bedanken.

Ebenso möchte ich mich bei Dr. Daniel Schröder für seine individuelle und zu jeder Zeit engagierte Betreuung bedanken. Der regelmäßige Austausch sowie seine wertvollen fachlichen Ratschläge haben mich stets vorangebracht und somit maßgeblich zum Erfolg dieser Arbeit beigetragen.

Darüber hinaus danke ich Prof. Dr. Hermann Wegner für die Übernahme des Korreferats dieser Arbeit sowie die über die Zeit meiner Promotion stets fruchtbare und freundliche Zusammenarbeit im gemeinsamen Forschungsprojekt. Ebenso möchte ich mich bei Prof. Dr. Doreen Mollenhauer für die gute Zusammenarbeit bedanken, die diese Arbeit sehr bereichert hat.

Ein besonderer Dank gilt auch Dominik Emmel, Felix Kerner sowie Felix Pfanschilling, deren wissenschaftliche Abschlussarbeiten ich betreuen durfte. Die durch ihr Engagement gewonnenen Erkenntnisse leisteten einen wertvollen Beitrag zu dieser Arbeit.

Mein weiterer Dank gilt der gesamten Arbeitsgruppe für eine schöne Zeit in angenehmer und freundschaftlicher Arbeitsatmosphäre. Ganz besonders danke ich an dieser Stelle Dr. Peter Schmitz, Dr. Sean Culver, Julian Zahnow und Michele Bastianello. Ebenso geht ein großer Dank an Kathrin Michel und die alte sowie neue Besetzung des Büros B75 für eine wunderbare Atmosphäre, die kurzweiligen Gespräche jeder Art und die stets große Hilfsbereitschaft.

Mein größter Dank gilt meiner Familie, meinem Vater Hans und meiner Mutter Monika, meiner Schwester Caroline und meinem Schwager Florian sowie meiner Freundin Anna für ihre unermüdliche und liebevolle Unterstützung.

Eidesstattliche Erklärung

Die vorliegende Arbeit wurde im Zeitraum vom 17.12.2015 bis 31.12.2019 am Physikalisch-Chemischen Institut der Justus-Liebig-Universität Gießen unter Betreuung von Prof. Dr. Jürgen Janek angefertigt.

Ich erkläre: Ich habe die vorgelegte Dissertation selbständig und ohne unerlaubte fremde Hilfe und nur mit den Hilfen angefertigt, die ich in der Dissertation angegeben habe. Alle Textstellen, die wörtlich oder sinngemäß aus veröffentlichten Schriften entnommen sind, und alle Angaben, die auf mündlichen Auskünften beruhen, sind als solche kenntlich gemacht. Bei den von mir durchgeführten und in der Dissertation erwähnten Untersuchungen habe ich die Grundsätze guter wissenschaftlicher Praxis, wie sie in der „Satzung der Justus-Liebig-Universität Gießen zur Sicherung guter wissenschaftlicher Praxis“ niedergelegt sind, eingehalten.

Gießen, den 23.11.2020

_____

Jonas David Hofmann

Abstract

In consequence of the increasing relevance of intermittent sustainable energy sources such as solar and wind energy, there is a growing demand for highly efficient and at the same time economic stationary storage concepts. In this context, redox flow batteries (RFBs) gained a lot of scientific interest in recent years. This especially applies to aqueous RFBs based on aromatic organic active materials such as quinones, which are characterized by a high natural abundance and favorable charge transfer characteristics. However, current concepts are restricted by severe drawbacks such as fast capacity fading due to active material degradation as well as insufficient cell voltages and voltage efficiencies. These issues primarily originate from a lack of suitable high-potential active materials, which are commonly prone to nucleophilic side reactions as a function of their redox potential. As current state-of-the-art active materials are not capable of providing high redox potentials together with stable cycling performances, new structural motifs are required. In this context, this work provides novel design strategies for the development of capable quinonoid active materials towards efficient concepts of stationary energy storage.

This thesis presents a systematic investigation of the structure-property relationships of nitrogen-functionalized quinone compounds. The class of diaza-quinones was thoroughly investigated according to different analytical techniques, in order to evaluate the benefit of this structural modification and to expand upon the existing knowledge of their homocyclic base structures. Performance-relevant key quantities – such as diffusion coefficients, redox potentials and kinetic rate constants – were determined by means of varying voltammetric techniques. The electrochemical stability of the compounds was investigated according to a combination of exhaustive electrolysis and a subsequent structural elucidation based on ^{1}H NMR spectroscopy. Based on the gained results, vulnerable sites could be identified thus shedding light on the mechanism of potential degradation reactions. Experiments were conducted in varying solvents, comprising aprotic as well as acidic and alkaline aqueous solution, in order to elucidate the impact of solvent-related effects – such as hydrogen bonding and protonation – on the charge transfer behavior of diaza-quinones. With these results, the structural motif of diaza-quinones was refined to obtain capable catholyte active materials for aqueous RFBs based on organic active materials (ORFBs). In addition, the experimental approach was complemented by theoretical considerations: experimental trends were successfully reconstructed by means of density functional theory (DFT) calculations. Based on the developed model, desirable diaza-quinone structures were defined to propel future research in this field.

Conclusively, this work provides useful guidance regarding the development of stable and capable quinonoid active materials for ORFBs and hence can contribute to meet the requirements for a commercial application of this promising technology.

Zusammenfassung

Im Hinblick auf den stetig zunehmenden Anteil regenerativer Energieträger wie Wind- oder Solarenergie am Energiemix steigt auch der Bedarf an gleichermaßen effizienten und wirtschaftlichen stationären Energiespeicherlösungen. Vor diesem Hintergrund erregten vor allem Redox-Flussbatterien in den vergangenen Jahren enormes wissenschaftliches Interesse. Dies gilt insbesondere für wässrige Flussbatterien auf Basis aromatischer, organischer Aktivmaterialien wie Chinonen, welche sich einerseits durch große natürliche Vorkommen und andererseits durch hervorragende Ladungstransfereigenschaften auszeichnen. Aktuelle Konzepte werden allerdings durch stetige Kapazitätsverluste sowie unzureichenden Zellspannungen und Spannungseffizienzen beeinträchtigt. Derartige Limitierungen sind in erster Linie auf das mangelnde Angebot an leistungsfähigen Katholyt-Aktivmaterialien zurückzuführen. Da nach aktuellem Stand der Forschung kein chinoides Aktivmaterial existiert, welches sowohl eine schnelle Reaktionskinetik als auch eine hohe Zyklenstabilität und Elektronenaffinität in sich vereint, bedarf es der Erschließung neuartiger Strukturmotive. Vor diesem Hintergrund befasst sich die vorliegende Arbeit mit der Untersuchung von Designstrategien zur Entwicklung leistungsfähiger, chinoider Aktivmaterialien.

Hierzu wurden die Struktur-Wirkungsbeziehungen stickstofffunktionalisierter Chinonverbindungen systematisch untersucht und sowohl elektro- als auch physikochemische Eigenschaften durch strukturelle Anpassungen gezielt modifiziert. Mithilfe verschiedener analytischer Methoden wurden die definierten Zielstrukturen charakterisiert und leistungsrelevante Kenngrößen bestimmt. So wurden Diffusionskoeffizienten, Redoxpotentiale und Ladungstransferraten ausgewählter Derivate anhand verschiedener voltammetrischer Methoden ermittelt. Die elektrochemische Stabilität der Verbindungen wurde durch deren vollständige elektrolytische Umsetzung mit anschließender Strukturaufklärung in Form von ^{1}H-NMR-Spektroskopie untersucht. Auf diese Weise konnten elektrochemisch anfällige Positionen im Molekül identifiziert und somit wertvolle Rückschlüsse auf den vorliegenden Degradationsmechanismus gezogen werden. Zur Bestimmung des Einflusses lösungsmittelspezifischer Effekte auf das elektrochemische Verhalten von Diaza-Chinonen fanden die Untersuchungen in verschiedenen Medien wie aprotischen, aziden und alkalischen Lösungen statt. Anhand der gewonnen Erkenntnisse wurde das Diaza-Chinon-Strukturmotiv systematisch weiterentwickelt und im Hinblick auf eine Anwendung als leistungsstarkes Katholyt-Aktivmaterial ausgearbeitet. Diese experimentelle Herangehensweise wurde dabei durch theoretische Aspekte ergänzt: Experimentelle Trends wurden mithilfe von DFT-basierten Rechnungen erfolgreich bestätigt und auf Basis des erhaltenen Modells weitere vielversprechende Zielstrukturen definiert.

Die vorliegende Arbeit leistet einen wichtigen Beitrag zur Entwicklung stabiler und leistungsstarker chinoider Aktivmaterialien für ORFBs und zeigt somit neue Wege für eine ökonomische Realisierung dieser vielversprechenden Technologie auf.

List of Abbreviations

AN	acetonitrile
AQ	anthraquinone
BC	1,2-butylene carbonate
BQDS	1,2-benzoquinone-3,5-disulfonic acid
CV	cyclic voltammogram
DAAQ	diaza-anthraquinone
DFT	density functional theory
DHDMBS	3,6-dihydroxy-2,4-dimethylbenzenesulfonic acid
DHP	dihydroxyphthalazine
DME	1,2-dimethoxyethane
EDL	electric double layer
ESW	electrochemical stability window
HER	hydrogen evolution reaction
HOMO	highest occupied molecular orbital
IEM	ion-exchange membrane
IL	ionic liquid
LIB	lithium-ion battery
LUMO	lowest unoccupied molecular orbital
NASA	National Aeronautic and Aerospace Administration
NMR	nuclear magnetic resonance
NQ	naphthoquinone
OER	oxygen evolution reaction
ORFB	aqueous redox flow battery based on organic active materials
PC	propylene carbonate
PCET	proton-coupled electron transfer
Q	quinone
$Q^{\bullet-}$	semiquinone anion radical
Q^{2-}	quinone dianion
$QH^{\bullet}$	protonated semiquinone radical
QH_2	fully protonated reduced quinone
RFB	redox flow battery
SES	stationary energy storage
THF	tetrahydrofuran
VRFB	all-vanadium redox flow battery

List of Symbols

μ_i	[m^2 $(V\ s)^{-1}$]	ion mobility
z		charge number
e	C	elementary charge
η	[Pa s]	dynamic viscosity
r	[m]	radius
F	[A s mol^{-1}]	Faraday constant
c_0	[mol L^{-1}]	concentration of active material
κ	[S m^{-1}]	ionic conductivity
ε_r		dielectric constant
ε_0	[F m^{-1}]	vacuum permittivity
L	[m]	distance of closest approach between ions
k_B	[J K^{-1}]	Boltzmann constant
T	[K]	absolute temperature
T_f	[°C]	freezing point
T_b	[°C]	boiling point
E_{app}	[V]	apparent equilibrium potential
k_{app}	[cm s]	apparent rate constant
pK_a		acid dissociation constant
k_r	[cm s]	actual kinetic rate constant
K_c		equilibrium constant of comproportionation
h		number of transferred protons
n		number of transferred electrons
E^0	[V]	redox potential
$E^{0'}$	[V]	formal potential
E_{exp}	[V]	experimentally observed potential
E_{hw}	[V]	polarographic half-wave potential
a_i		activity of reagent i
C		solvation energy discrepancy
σ		sigma (bond)
W_d	[Wh L^{-1}]	energy density
C_s	[Ah L^{-1}]	specific capacity
U	[V]	cell voltage
m	[g]	mass
M	[g mol^{-1}]	molar mass

V	[L]	volume
P_d	[W cm^{-2}]	areal power density
I	[A]	current
A	[cm^2]	surface area
R_i	[Ω]	inner cell resistance
R_{el}	[Ω]	electronic resistance
R_{ct}	[Ω]	charge transfer resistance
R_{mass}	[Ω]	mass transport resistance
k_0	[cm s]	standard rate constant
D	[cm^2 s^{-1}]	diffusion coefficient
ΔE_p	[V]	peak separation

Table of Contents

1 Introduction

1.1 Motivation and Outline

The increasing relevance of sustainable energy sources and the concomitant need for load compensation generates a large scientific interest with regard to different concepts of stationary energy storage (SES). Besides electrical double-layer capacitors, approaches involving the conversion of electrical energy to kinetic or potential energy such as flywheels or pumped hydroelectric storage have been successfully demonstrated.[1] However, drawbacks such as small energy contents, long response times and geographic constraints prevent a widespread application for those technologies.[2] As an alternative, technologies summarized under the term “chemical energy storage” such as batteries and fuel cells provide storage solutions based on electrochemical energy conversion. As a prime example lithium-ion batteries (LIBs) experienced great improvements regarding specific energies, energy densities and achievable cell voltages within the last three decades since their market introduction.[3,4] However, metrics concerning the size and dimensions of the system are considered less crucial for stationary applications. More importantly, batteries for grid storage should exhibit a high calendar life and round-trip efficiency combined with rapid response times at reasonable capital costs.[5,6]

Redox flow batteries (RFBs) are considered as a promising technology to fulfill those requirements due to their high power input and output, scalability and great variety of suitable active materials as well as solvents.[7] RFBs take advantage of two dissolved redox couples that are stored in separate reservoirs and can be pumped through an energy converter to release or store energy whenever needed. The first development of redox flow batteries in a modern sense occurred in the early 1970s at the National Aeronautic and Aerospace Administration (NASA): in consequence of the first oil crisis, NASA investigated solutions for cost-effective electrochemical energy storage. The studies comprising various low-cost electrolytes concluded with a system based on the redox couples Cr^{3+}/Cr^{2+} and Fe^{3+}/Fe^{2+}.[8–10] In the 1980s the concept was further developed and transferred to vanadium redox couples by Skyllas-Kazacos and coworkers.[11–13] Due to continuous technical improvements made since this pioneering work the all-vanadium redox flow battery (VRFB) was subject of a significant number of field studies.[14–18] At this point it is also commercially available to customers for a wide range of applications.[19,20]

However, a significant increase of the vanadium prices could be observed recently along with the growing demand for the required oxide raw materials.[21] As a consequence, new strategies are obligatory to enable the competitiveness of VRFBs against alternative stationary storage solutions.[22] The same applies for lithium-based systems such as lithium-sulfur, lithium-oxygen and LIBs in

particular, which may also experience a rise in manufacturing costs due to the steep and ongoing increase of lithium, cobalt and nickel prices.[3,23] Since the availability of utilized battery materials as well as their sustainable extraction gain further relevance with respect to environmental and economic aspects, alternative active materials have to be developed.

With regard to aqueous RFBs, aromatic organic compounds constitute a promising substance class for sustainable and cost-efficient SES.[24–28] Especially quinones, which may be derived from abundant resources such as lignin, have attracted wide scientific interest.[29–31] Many recent publications have investigated the structure-property relationships of quinonoid compounds and their application in redox flow batteries due to their fast charge transfer kinetics and tunable redox potentials.[32–38] Since the advent of aqueous redox flow batteries with organic active material (ORFB) that began with the studies of Aziz *et al*.[39] in 2014, many efforts have been made with respect to quinonoid electrolytes. The investigated, mostly anthraquinone-based molecules were optimized for their solubility in water as well as their redox potential by addition of electron donating and hydrophilic functional groups leading to high energy densities.[32,35,36,40–42] Furthermore, detrimental side reactions affecting the stability of active compounds such as Michael addition or self-polymerization have been addressed recently: sterically demanding functional groups such as ether-linked alkyl chains proved to be a successful measure to prevent decomposition, yielding a high cycling stability and calendar life.[37,43–45]

It is to be noted that these efforts refer to electron-rich compounds designed for the application as anolyte active material. However, promising candidates for the catholyte side of the battery are equally required to enable sustainable and cost-efficient all-quinone-based ORFBs. Yet, studies considering these high-potential molecules can only be found scarcely in the literature. The presented compounds further exhibit insufficient redox potentials or low cycling stabilities, preventing their efficient application as catholyte active material.[46–50]

To overcome these challenges, this thesis outlines pathways for the design and characterization of potent quinonoid active materials for ORFBs. Herein, design strategies concerning the incorporation of nitrogen into quinone base structures are presented as an effective measure to improve the electrochemical characteristics of the homocyclic compounds. Due to the more electron withdrawing nature of nitrogen compared to carbon the redox potential of the associated derivatives is significantly increased. Depending on the intrinsic electron affinity of the base structure favorably high redox potentials are achieved, which – in combination with appropriate anolyte active materials – enables high cell potentials of ORFBs. Additionally, the impact of the heterocyclic structure on the overall charge transfer characteristics is elucidated to provide a fundamental understanding of this new class of active materials. To classify the benefit for RFB applications, performance-relevant quantities are determined by selected analytical as well as voltammetric techniques. This work's studies reveal

favorable properties of the nitrogen-augmented derivatives surpassing their established homocyclic analogues. Experimental results are further complemented by density functional theory (DFT) calculations to predict the influence of structural modifications and to enable the tailored design of future catholyte active materials. Altogether, this thesis shows that diaza-quinones can contribute to more sustainable and efficient concepts of SES.

In order to provide a topical introduction, the basic principles of redox flow batteries are elucidated as part of the following section 1.2. Subsequently, section 1.3 summarizes relevant information with regard to quinonoid active materials for ORFBs, highlighting their redox behavior, structure-property relationships and potential degradation mechanisms. In this context, the performance-relevant quantities of ORFB active materials and the pitfalls in their investigation are outlined in section 1.4 as part of the publication "*Which Parameter is Governing for Aqueous Redox Flow Batteries with Organic Active Material?*". This is followed by section 1.5, providing an overview over state-of-the-art active materials applied in ORFBs as well as design strategies to maximize their performance.

Subsequently, the main results of this thesis are presented in terms of two scientific publications highlighting the characteristics, benefits and prospects of nitrogen-functionalized quinones. In the publication "*Quest for Organic Active Materials for Redox Flow Batteries: 2,3-Diaza-anthraquinones and Their Electrochemical Properties"* the compound class of diaza-anthraquinones (DAAQs) is introduced as an advanced form of the underlying homocyclic anthraquinone (AQ). Due to the modified base structure, the redox potential is positively shifted by 300 mV in acidic solution. Further insights into the structure-property relationships of DAAQs are given by the addition of peripheral substituents such as methoxy or hydroxyl moieties. It is found that adding a methoxy group proves to be an effective measure to increase the electrochemical stability of the compound. Hydroxyl moieties on the other hand evoke a negative shift of the redox potential, hence allowing for a tailored adjustment of the charge transfer characteristics. Hence, DAAQs are introduced as a versatile and adaptable class of active species regarding an application in aqueous RFBs. The results of this publication are complemented by subsequent studies focusing on the impact of solvent-related effects on the charge transfer characteristics of DAAQs. The impact of hydrogen bonding and protonation is investigated in varying solvents, revealing specific features such as an increased stabilization of the semiquinone intermediate as well as an additional protonation state at low pH values.

This concept was subsequently transferred to intrinsically more electron-deficient base structures in order to increase upon the benefit of the nitrogen-based positive potential shift found for DAAQs. As a result, naphthoquinone (NQ) with its comparably confined aromatic system was identified as a suitable template structure regarding catholyte active materials for ORFBs. In the publication *"Tailoring Dihydroxyphthalazines to Enable their Stable and Efficient Use in the Catholyte of Aqueous*

Redox Flow Batteries" the class of dihydroxyphthalazines (DHP) is consequently introduced as an evolution of the priorly investigated DAAQs. The reduced diaza-naphthoquinone DHP features fast and competitive charge transfer kinetics as well as a favorably high redox potential of 0.796 V vs SHE. This value clearly surpasses the potential of established homocyclic quinones, thus emphasizing the significance of the diaza-based design strategy with regard to the development of high-potential quinone active materials. Furthermore, the incorporation of methyl groups is presented as an effective measure to prevent potential nucleophilic degradation reactions. It is shown that long-term stable active materials are obtained, which enable high cycling efficiencies. In accordance with these findings, desirable DHP-based active materials are outlined by means of DFT calculations to further propel research in the field of quinonoid active materials for ORFBs.

In the last section, the results and insights of this PhD thesis are summarized and evaluated within the scientific context. Conclusively, based on the presented findings the prospects as well as future tasks in this field of research are addressed as part of a final outlook.

1.2 Redox flow batteries

The development of redox flow batteries dates back to the year 1949 when W. Kangro filed a patent for a novel technology to store electrical energy.[51] The concept described dissolved redox couples stored in separate tanks that can be transferred into different oxidation states while passing through an energy converter and was proposed as an effective measure for load levelling. Subsequently, a variety of elements was discussed to be used as potential active materials to fuel this new technology. However, it was not until 1962 that the combination of titanium and iron was proposed as an economically competitive alternative to lead- and nickel-iron batteries.[52] Research in this field was further propelled within the context of the first oil crisis in the early 1970s: NASA consequently started to investigate solutions for cost-effective electrochemical energy storage to focus on renewable intermittent energy sources. The studies comprising various low-cost electrolytes concluded with the concept of the first redox flow battery in a modern sense, which was based on the redox couples Cr^{3+}/Cr^{2+} and Fe^{3+}/Fe^{2+}.[8–10] The following transfer to vanadium redox couples in the 1980s initiated further investigations spanning several decades until the present day, making VRFB the most extensively studied concept in the field of RFBs.[12,53–57] . As a result, a high number of 90 installations with a total power of about 330 MW can be found all over the world at present.[22]

Within the last 15 years the number of publications investigating RFBs with non-aqueous electrolytes increased progressively along with alternative aqueous metal-based concepts such as the vanadium-polyhalide RFB.[58,59] However, with respect to economic and environmental aspects the scientific focus shifted towards ORFBs lately, starting with the publications of Huskinson and Yang in 2014.[39,50] In these studies low-cost aqueous solvents were combined together with organic active materials that may be derived from abundant resources to hold down the costs per kWh.[43] Within the last 6 years, great progress has been made in the field, especially regarding the design of anolyte active materials. Design strategies taking advantage of the structure-property relationships of organic compounds resulted in promising substances that could be optimized for an application at low potentials, high roundtrip efficiencies and high solubility in water.[32,37,43] However, commercialization of ORFBs has not been achieved yet due to limited achievements in the field of catholyte research. Assuming that these challenges can be overcome in the near future, ORFBs pose a promising technology to enable economic and widespread SES. It should be noted that besides the important role of active materials attention has to be devoted to the composition of the battery to position ORFBs as a capable alternative to other stationary concepts.

To introduce the reader to the general concept of ORFBs, its working principle and design opportunities are described in the following section. In this context, the major battery components and their impact on the process of energy conversion shall be elucidated in more detail.

1.2.1 Working principle

The unique feature of the most prominent RFB concept is that the active material is present in solution, which is why it is also denoted as all-liquid RFB.[60] By ways of illustration, a simplified scheme of this battery type is given in Figure 1. As already described by Kangro's patent in 1949, the redox couples involved in the process of energy conversion are present dissolved in a liquid and can therefore be stored separately in tanks.[51] This circumstance represents one of the most beneficial aspects that distinguishes all-liquid RFBs from established secondary batteries such as LIBs: the dimensions of the electrode material do not predetermine the stored capacity of an RFB but rather the volume of the storage tanks, which allows for a more flexible design of the system. The actual process of energy conversion takes place inside an energy converter that consists of two electrode chambers allocated to the occurring oxidation and reduction of active material. As suggested by the term "redox flow", the electrolyte is constantly pumped back and forth between storage tanks and the converter during application. In between the two electrode chambers, a separator allows for charge compensation while still maintaining spatial segregation of both circulatory systems. The charge transfer occurs within the converter at the interface between the liquid electrolyte and the porous electrodes. Since the porous electrodes in this case solely serve as current collectors, another major advantage of RFBs over conventional secondary batteries becomes apparent: the challenges associated with phenomena such as phase transformations or electrode morphology changes during charge and discharge are completely avoided.[61]

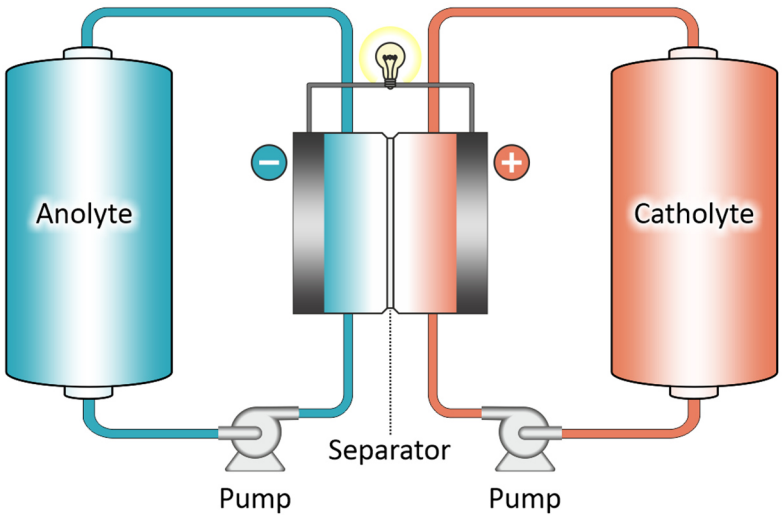

Figure 1: Schematic illustration of a redox flow battery and its components. Anolyte and catholyte are stored in separate tanks as part of two circulatory systems segregated by a separator such as an ion exchange membrane. The separator allows for charge compensation between the two chambers of the reactor entailing the porous current collectors.

In this context, the generatable power is determined by the size of the current collectors as well as the number and interconnection of stacks. Together with the fact that the amount of stored capacity can be scaled as desired according to the size of the electrolyte reservoirs, RFBs offer a high flexibility and can be adapted to certain applications.[60]

For the sake of completeness, it is to be noted that a multitude of varying RFB concepts has been reported to date, which share functional similarities with the described all-liquid approach. Those concepts may be classified by means of the aggregate state of the reactants involved in the process of energy conversion. One category of multiphase systems is classified by the comprehensive term "hybrid RFBs". This denotation refers to the fact that the active material of at least one half-cell is present in different aggregate states – e.g. solid/liquid – depending on the state of charge.[60] Consequently, the reactant is plated from and stripped back into solution during cycling. To give an example, zinc has been widely investigated in terms of hybrid RFBs in combination with different cathode counterparts such as halogens, vanadium or cerium.[62,63] Due to the highly negative standard potential of zinc, high cell voltages can be achieved, which holds especially true for alkaline solutions.[64,65] Yet, in the case of hybrid RFBs such as the zinc-iodine system solid material is deposited in the course of cell cycling. As a result, issues associated with phase transition such as dendrite formation or the clogging of pumps and pipelines are observed.[66] Consequently, one of the major advantages of all-liquid RFBs is annulled for this setup. To circumvent the negative aspects associated with the plating and stripping of solid material, alternative concepts combining a permanently liquid with a liquid/gaseous half-cell were proposed. Those were commonly based on a combination of the $H^+/\ \frac{1}{2}H_2$ redox couple as the liquid/gaseous component and varying halide solutions as the liquid component.[67,68] However, the need for noble metal catalysts, electrolyte crossover, poisoning of the catalyst by halide ions and corrosion issues prevented a widespread application to date.[69–72]

In an attempt to further increase the energy density of RFBs, the concept of flowable electrolytes was transferred to the electrode materials commonly used in the context of LIBs. Since the active material is present in the form of suspensions or conducting inks, this battery design allows to overcome the restrictions posed by the solubility limit of active species. The first lithium-flow battery was reported by Duduta *et al*.[73], which applied a suspension of $LiCoO_2$ with 1.5% Ketjen Black on the cathode side and a suspension of $Li_4Ti_5O_{12}$ with 2% Ketjen Black on the anode side, both dispersed in an alkyl carbonate solvent. Due to their high effective concentration of redox electrons in the range between 10 M and 40 M and the high theoretical cell voltages evoked by the use of lithium as active substance, such systems offer considerably high energy densities.[61] On the downside, due the high viscosity of the lithium inks high pumping losses are to be expected, which have a significantly negative impact on the operating efficiency at system level. Furthermore, safety concerns emanating from the

reactive nature of lithium and the volatility of commonly applied organic solvents may limit the implementation of semi-solid RFBs with regard to large scale applications.[74]

In general, much more elaborate technical solutions are required for the operational management of batteries with multiphase systems compared to the classical all-liquid RFB. Due to the special requirements associated with a uniform metal deposition or continuous gas feed and storage as well as the circulation of suspensions, more advanced electrolyte delivery systems are obligatory.[60,75] Thus, it may be more favorable to capitalize on the beneficial properties correlating with the use of all-liquid RFBs with regard to economic and sustainable SES. Leaving aside the favorable physicochemical peculiarities of aqueous RFBs – which shall be discussed in more detail later in section 1.2.2 – all-liquid batteries commonly provide a number of operational advantages: pumping losses are mitigated due to the use of inviscid electrolytes, reaction heat effectively dissipates along with the fluid transport and mechanical stress as well as morphological changes of the electrode are completely avoided because of the fluidic nature of the active material.

1.2.2 Components

Irrespective of the scaling opportunities for storage tanks and converter, the basic performance of RFBs is dictated by the components involved in the process of energy conversion and the nature of their materials. For instance, electrode materials may offer vastly different surface areas and geometries as well as chemical surface modifications depending on the respective redox chemistry and conditions.[76] The efficiency of the separator is closely intertwined with the nature and structural design of the applied active material as well as the solvent used.[77,78] The solvent in turn provides access to different temperature and potential ranges as well as a variety of different redox chemistries. Conclusively, it is to be noted that a clever choice of components contributes to the overall efficiency of RFBs. The performance-relevant components of RFBs and the underlying physico- and electrochemical principles shall be elucidated in more detail to take account of their importance in the process of energy conversion.

Electrode materials

As the electrode of an RFB provides the active surface area which moderates the heterogeneous charge transfer between the consumer and the active material, its texture and composition has a great significance in the process of energy conversion. In general, one would assume that high a surface area is beneficial to convert as much active material as possible at a time. However, in the case of RFBs the electrolyte must be pumped through the generator to undergo the desired redox processes.

Depending on the density and overall surface of the electrode, it may be harder to pass the active surface, which then may be associated with a loss of energy. As a result, there is a trade-off between the surface area required for an effective charge transfer and the energy required for a sufficient feed of electrolyte. This is especially important for commercial applications.

In general, there are two basic electrode configurations that find application in RFBs, which are denoted as *flow-through* and *flow-by* (see Figure 2).[79] In case of the *flow-through* configuration, a mesh or porous matrix of a conductive solid serves as the reactive surface that moderates the charge transfer between current collector and the active material dissolved in the electrolyte. During charge and discharge, the electrolyte is pumped through the porous network to undergo the desired redox reaction. The generated electrons are transferred into the external circuit, whereas ions migrate into the opposed electrode chamber for charge compensation. The most common electrode materials applied in *flow-through* configurations are fibrous and mostly carbon-based such as carbon or graphite felts. This is due to a combination of beneficial properties, namely an inert character versus corrosive media, high electrical conductivity, high oxygen and hydrogen overvoltages as well as a high porosity.[80] Furthermore, the intertwined structure of carbon felts enables a good turbulence of the electrolyte and hence a fast rate of active material conversion.[5]

In case of a *flow-by* configuration, the electrolyte containing the active species flows in a channel parallel to a planar electrode. Despite the fact that these electrodes commonly feature a spatially constrained three-dimensional surface layer formed by porous domains and catalyst particles, an interaction corresponding to a planar surface is observed.[5] The passing stream of electrolyte infuses the surface layer, forming an approximately stationary phase of suppressed convection.[81] In this phase, the active material diffuses laterally towards the planar electrode surface. Since in the case of *flow-by* configurations electrolyte percolation is negligible, energy losses associated with pumping can be effectively minimized. However, due to the stagnant layer within the porous electrode mass transfer and the conversion of active material takes place at a nearly constant rate, which can only be marginally increased by forced convection. The utilization of active material hence cannot be adapted as efficiently as in the case of *flow-through* designs. To circumvent these shortcomings, engineering approaches regarding the design of the electrolyte flow field are investigated. For instance, interdigitated or serpentine flow fields are used to increase the distance the electrolyte traverses in contact with the active surface area, which is also denoted as the residence time.[79,82] In the context of ORFBs, flow field modifications proved to be an effective measure to increase the overall limiting current as well as peak power density.[24,35,47]

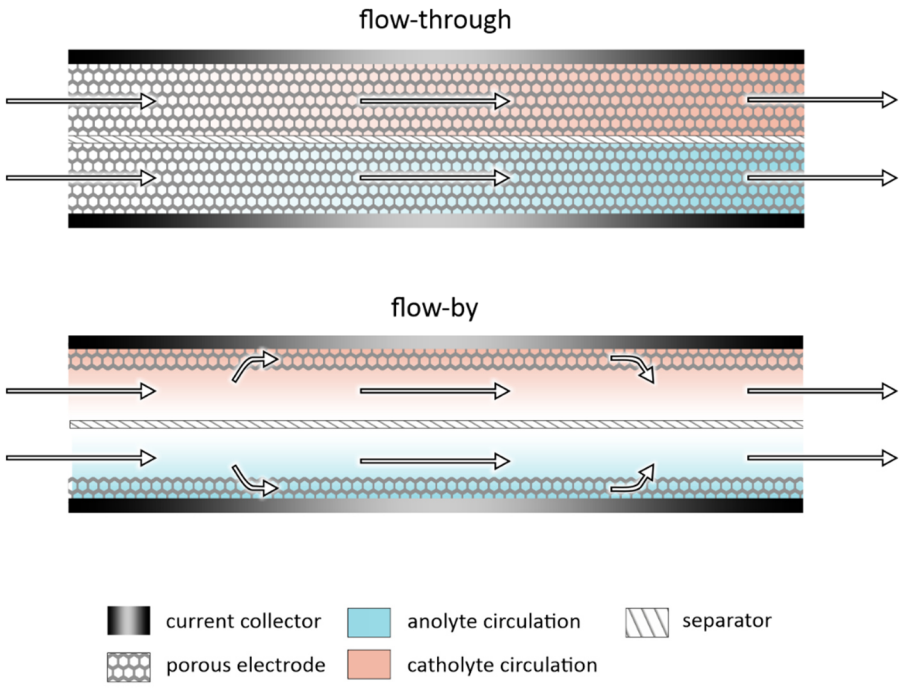

Figure 2: Schematic illustration of the two primary electrode concepts applied in RFBs, commonly denoted as flow-through and flow-by configuration. In the case of flow-through electrodes, the electrolyte is pumped through a porous network of a conductive solid material such as carbon felt. The flow-by concept on the other hand implies that the essentially unobstructed electrolyte passes a spatially confined porous electrode layer while partially infusing its surface.

Which of both configurations – *flow-through* or *flow-by* – is to be preferred is still subject of debate.[5,79,83] Surely it depends on a number of factors including the physicochemical properties of the flowing reactant, the nature of the occurring redox reaction and the associated phases. In the case of all-liquid RFBs such as ORFBs a *flow-through* configuration may be preferred: due to the highly fluid character of water, pumping losses are significantly mitigated. However, ORFBs commonly suffer from a low solubility of organic active material, which implies a rapid depletion of the dissolved reactive species during cycling, preventing high current densities. This drawback however may be compensated due to the high degree of forced mass transfer within the volumetric electrode at high pump rates. This also has a positive impact on organic active materials with low diffusion coefficients, which may be applied more efficiently as a result of the extrinsically enhanced rate of mass transfer. On the other hand, *flow-by* configurations may offer certain advantages in combination with active materials of high diffusivity (e.g. gases) or if solid substances are involved in the process of energy conversion. For instance, the plating of solid material is easier to realize for *flow-by* electrodes, since a free flow path for the electrolyte is permanently maintained.[84] In the case of a *flow-through* configuration however, solid material may block the obligatory pathways, preventing circulation and therefore leading to an increased pumping resistance or even complete failure of the system.

In general, many different factors need to be considered for the design of volumetric electrodes like carbon or graphite felts to achieve optimal performance. As mentioned earlier, a high active surface is desirable to maximize the conversion rate of active material. On the other hand, a high permeability of the electrode would minimize pressure drops and hence reduce pumping costs. Active surface area and permeability of felt electrodes are equally affected by the utilized fiber diameter. However, there is an inverse correlation between both quantities, thus requiring compromises in electrode design.[85,86]

Besides its geometry, the chemical nature can also have a significant impact on the overall performance of an electrode, as it may affect the kinetics of the occurring charge transfer. In order to classify the influence of surface modifications on the charge transfer kinetics, two different reaction mechanisms have to be distinguished, namely *inner-sphere* and *outer-sphere* reactions. In a heterogeneous *outer-sphere* electron transfer, the reactant center is located in the outer Helmholtz plane. This plane describes the closest distance to the electrode which can be attained by reactants that do not penetrate the layer of specifically adsorbed solvent molecules.[87] Consequently, the electron transfer occurs by a tunneling mechanism across the solvent layer, which is why there is no strong interaction of the electrode surface with the reactant. As opposed to this, *inner-sphere* reactions correspond to specifically adsorbed reactants that are located at the inner Helmholtz plane and hence in fact exhibit strong interactions with the electrode surface.[88] An experimental distinction can be made according to the electrode-dependent kinetics of the occurring charge transfer. Whereas *outer-sphere* reactions are rather insensitive to the nature of the applied electrode material, a strong dependence is observed in the case of *inner-sphere* reactions.[89] In the context of RFBs, the *outer-sphere* mechanism primarily applies to ligand-stabilized metal ions such as ferrocyanide or polyoxometalates.[88,90] Accordingly, the majority of active materials used in RFBs are allocated to the *inner-sphere* pathway. Thus, special care should be taken with respect to electrode pretreatment, since reaction rates may vary by several orders of magnitude.[80] Several measures have been reported to increase the charge transfer kinetics of carbon-based electrodes such as electrochemical activation[91], thermal treatment[92] or chemical etching[93] and doping[94]. In most cases, the increased coverage of the electrode surface with oxide-containing groups such as –C=O and –COOH was identified as the factor promoting the heterogeneous electron transfer between active material and electrode. However, the applicability and efficiency of these measures highly depends on the composition of the system referred to. As new designs of organic active materials emerge steadily, equally strong progress in the design of electrode materials will be required in the future.

Separators

The separator of an RFB ensures the charge compensation between both electrode compartments during charge and discharge while maintaining a spatial segregation between both circulatory systems. In an ideal case, the separator solely allows for the transition of species that are not directly involved in the process of energy conversion such as conducting salt ions or protons. Its main purpose is to prevent the crossover of active material, which may be highly detrimental, since the transferred material would not be available for subsequent cycles or may even trigger unwanted side reactions. Either way, an irreversible loss of capacity would be inherent, underlining the meaning of the separator for the overall efficiency of RFBs. Its composition and structure is highly dependent on the used system, that is to say the utilized active material as well as the solvent and additives used. The most prominent concepts, their fields of application and functional peculiarities shall be discussed in this section. Generally, there are four types of separators that are to be distinguished for the use in RFBs: (1) microporous separators, (2) ion-exchange membranes (IEMs), (3) hybrid and (4) ceramic membranes.[60] However, the application of ceramic separators is confined to a small number of RFB systems due to their low ionic conductivity .[95] Since they do not relate to the topic of this thesis, ceramic membranes thus will be omitted in the following detailed discussion for the sake of brevity.

(1) Microporous separators (pore size < 2 nm), which often are also denoted as size exclusion membranes are usually used in combination with rather bulky active materials such as polymers. As microporous membranes are based on charge-neutral polymer scaffolds, their efficiency is solely determined by the ratio of their pore diameter and the size of the incoming molecule. Measures to specifically adapt the dimensions of active substances to size exclusion membranes of a given pore radius hence proved to be very successful.[96,97] Due to the low costs of their base materials such as polyacrilnitrile[98], polyethersulfone[99] and polyvinylidene fluoride[100] microporous membranes can be produced very economically and hence reduce the overall costs of RFBs. In fact, Janoschka *et al*. investigated the application of a low-cost cellulose-based dialysis membrane in a polymer-based ORFB with positive results.[101] However, high energy densities can only be realized for molecules with high charge-to-mass-ratios.[102] This contradicts the application of bulky active materials such as polymers, which tend to suffer from electrochemical instability if their redox centers are packed too densely.[103] Consequently, with regard to high energy densities more advanced concepts are obligatory to improve the selectivity of separators towards more compact active materials.

In the case of (2) IEMs, a porous polymer network serves as the host structure similar to size exclusion membranes. Beyond that, IEMs are further augmented with acidic or basic side chains.[60] These functional groups enable an ionic bias that – depending on its polarity − supports the transfer of anions or cations for charge compensation and at the same time excludes redox-active molecules of the opposed charge. By way of example, these functional side chains can be incorporated into the

polymer-based host structure by infusing an ion-exchange resin together with a crosslinker.[104]IEMs can be categorized into cationic, anionic and amphoteric according to the polarity of their stationary phase. In terms of their base polymer, cationic IEMs are further divided into fluorinated and nonfluorinated membranes. At present especially perfluorinated membranes are widely used in RFB applications due to their beneficial properties: in the case of Nafion®, which is probably the most established system in this category, perfluorovinyl ether groups terminated with sulfonic acid moieties are incorporated into a tetrafluoro-ethylene (Teflon) host structure (see Figure 3a).[105] The Teflon backbone ensures a high mechanical stability of the polymer, whereas the incorporated sulfonic acid moieties provide a high ionic conductivity of up to 58.7 mS cm^{-1}.[5] Consequently, cations and especially protons can be easily transferred across the membrane, which allows for efficient charge balancing during electrochemical applications. The high ionic conductivity of Nafion® emanates from parallel channels, which are formed by the self-organized sulfonic acid moieties that are themselves encased by strands of the polymer backbone, forming inverted-micelle cylinders (see Figure 3b)[106].

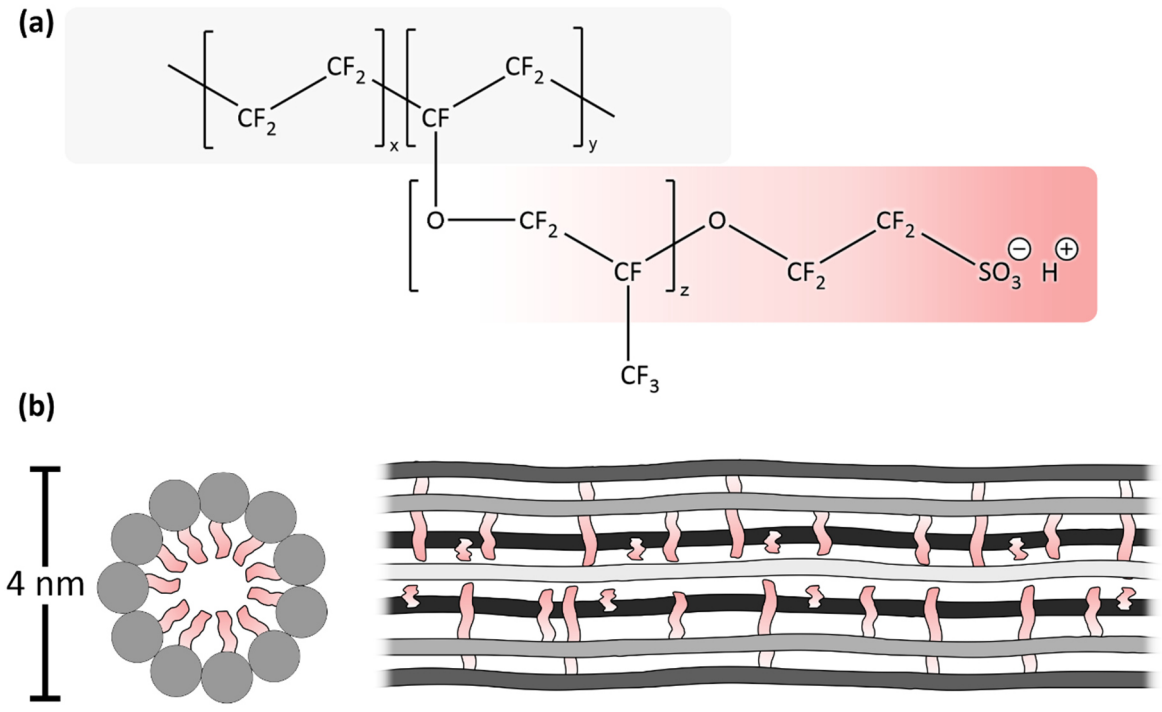

Figure 3: Chemical (a) and macroscopic structure (b) of Nafion®. The tetrafluoro-ethylene host structure (grey) is equipped with perfluorovinyl ether side chains, which in turn are terminated with sulfonic acid moieties (red). The self-organizing inverted micelle structure of the polymer generates parallel channels featuring high proton conductivities.

A major issue, directly referring to the high ionic conductivity of perfluorinated membranes, is denoted as electroosmotic drag. This describes the transport of water molecules across the membrane, which accompanies the desired movement of ions. At the interface between membrane and electrolyte an electric double layer (EDL) is formed comprising ionic charges from the electrolyte. When an electric field is applied − as in the case of RFBs during cycling − the ions within the fluid located at the EDL move as a result of the acting Coulomb force.[107] The moving ions drag bound solvent − e.g. water molecules − causing a bulk fluid motion.[108] Since the water content has a large impact on the membrane properties as well as the overall RFB performance, measures to maintain an optimal balance of the water content in both reservoirs are crucial.[109] Besides the unwanted water transport, most perfluorinated membranes exhibit insufficient ion selectivity leading up to the crossover of active material and hence nonideal Coulomb efficiencies.

In this context, (3) hybrid concepts are investigated to increase the permselectivity of the membranes. This is accomplished by a combination of IEMs such as Nafion® and inorganic substances that block the hydrophilic clusters represented by the aggregated sulfonic acid moieties. For instance, additives such as silicates[110], titaniumdioxide[111] or zirconium phosphate[112] are inserted into the polymer matrix, leading to a significant increase of the ion selectivity. However, in turn the overall ionic conductivity of the separator decreases, which emphasizes the need for further research in the field of IEMs.

Crossover and its prevention can not only be addressed in terms of separator design but rather also concerns the choice of active materials as implied earlier with regard to size exclusion membranes. In this context, so-called symmetrical RFBs present an unusual but promising approach: symmetrical systems take advantage of the application of the same parental active material in both electrode compartments. In this special case, the electrolyte composition is identical on both sides of the cell in the discharged state, whereas after charging, anolyte and catholyte solely distinguish by the oxidation state of the active substance.[113] If crossover occurs, this accordingly does not result in the mixing of disparate chemical compounds and therefore capacity can be restored in the following charge or discharge steps.[33] Furthermore, no chemical potential gradient can be observed in the discharged state, which otherwise may drive the crossover between both electrode compartments. Besides the studies focusing on metal-based complexes[113–116], several publications recently investigated the feasibility of symmetric RFBs based on organic molecules.[33,117–119] In this case, the sites involved in the charge transfer are located within the same molecule. Regarding electrochemical applications, the relative potential difference between the two associated redox events should be maximized to achieve high energy densities. The extent of their separation is determined by specific interactions, which depend on the number of moieties or molecular orbitals involved. If the charge transfer is allocated to

a single group as in the case of anthracene, electrostatic repulsion determines the relative potentials of the redox events. However, if multiple molecular orbitals are involved as in the case of two benzene rings connected by an alkyl chain, the measured potential difference is determined by the extent of their interaction.[82,120] As a result, specific adjustments of electrochemical characteristics may turn out to be very challenging from a synthetic point of view, especially with regard to active materials with a low molecular weight.[121] This becomes even more evident in the case of aqueous systems: besides the desired large relative potential difference required for high cell voltages, the intrinsic electron affinity – i.e. the absolute redox potentials − of an active compound have to conform to the operable potential window given by water as the solvent. Conclusively, despite the promising premise of symmetric systems, ORFBs based on structurally diverging anolyte and catholyte active materials are more viable at this point. However, this postulates the use of optimized separators maintaining a high ion conductivity, chemical stability and in particular ion selectivity during application.

Electrolyte

As a combination of the electrochemically active species, the solvent and conducting ions, the electrolyte comprises the supposedly most performance-relevant components of an RFB. These essential components have to meet certain individual requirements in order to achieve a high power and energy density. For instance, the active material should exhibit fast charge-transfer kinetics at a maximum relative potential difference between the redox potentials of both half cells. Furthermore, the solvent needs to provide a high capacity for the dissolution of active material, a low viscosity to reduce pump losses and a broad operable potential window so that high cell voltages can be achieved. In turn, the conducting ions have to maintain a high solution conductivity to prevent voltage losses while also featuring a high mobility and membrane compatibility to allow for an effective charge compensation during cycling.[122] Whereas the role of active materials shall be discussed in more detail in section 1.3, the following section will primarily focus on the choice of solvent and its implications for the overall performance of RFBs and their components.

A general distinction of electrolytes can be made according to the three major categories of solvents, namely the concepts based on ionic liquids (ILs), aqueous and nonaqueous electrolytes. The most apparent benefit regarding the use of ILs as a solvent in battery applications is their electrochemical stability over a wide potential span.[123] Accordingly, high cell voltages may be attained in combination with suitable active materials, leading to high energy densities. However, the choice of suitable IEMs is hindered by sterically demanding complexing ions, which limit the maximum current densities during cycling. In general, high viscosities and low ion conductivities prevent a widespread

application of ILs as solvents in RFBs. In order to mitigate these drawbacks, different combinations of anions and cations have been investigated.[124,125] The addition of water was further reported to decrease the viscosity and increase the ionic conductivity of electrolytes based on hydrophilic ILs.[126,127] However, many challenges related to their high viscosities remain unsolved and together with the high costs severely limit their application at system level.[75] Due to the low relevance of IL-based systems in the context of this thesis, a more detailed discussion of such is omitted at this point. For the sake of brevity, the reader is referred to the given specialized literature for more information.[128–130]

Instead, with focus on ORFBs, the different aspects of aqueous electrolytes shall be discussed in more detail while also considering nonaqueous electrolytes as a potential alternative. To begin with, aqueous electrolytes largely benefit from the favorable properties ascribed to their solvent: water is a non-hazardous, environmentally friendly substance that is abundantly available and therefore economically promising with respect to widespread SES. Water has a low viscosity, which according to equation (1) correlates with a high mobility u_i of the supporting ions and hence allows for a fast charge transport in solution. As reflected by equation (2), this turns out to be very beneficial for the conductivity of aqueous electrolytes.[131]

$$u_i = \frac{|z_i| e}{6 \pi \eta r_i} \tag{1}$$

$$\kappa = F \sum_i |z_i| u_i c_i \tag{2}$$

Here z is the charge of the considered ion, e is the elementary charge, η is the solvent viscosity, r is the ion radius, F is the Faraday constant, c_i is the concentration of supporting ions and κ is the resulting specific ionic conductivity. As can be seen, besides the viscosity of the solvent the concentration of ionic species largely contributes to the ionic conductivity of the electrolyte. In this regard, another significant parameter of the solvent has to be considered, which is denoted as the dielectric constant ε_r or relative permittivity. This quantity describes the ability of a material to adapt and align to an applied electric field and thus determines the solvation of ionic species. In general, the solubility of supporting salts increases together with ε_r.[58] Beyond that, the relative permittivity is a measure for the degree of ion pairing for a dissolved species, which is described by the Denison-Ramsey equation (3)[132]

$$-\ln(K_d) = \frac{e^2}{\varepsilon_0\ \varepsilon_r\ L\ k_B\ T} \qquad (3)$$

where K_d is the dissociation constant of the supporting salt, ε_r and ε_0 are the relative permittivity of the solvent and the permittivity of vacuum, L is the distance of closest approach of two associated ions, k_b is the Boltzmann constant and T is the absolute temperature. Due to the high relative permittivity of water (78.39), a high concentration of free charge carriers is inherent and voltage losses are mitigated.[133] Consequently, aqueous RFBs can be cycled at high currents, which enables high power densities and an effective charge balancing at system level, which is further substantiated by the availability of highly conductive IEMs: starting with the pioneering work of Skyllas-Kazacos in the mid-1980s, aqueous RFBs have been intensively investigated for more than 30 years to the present day. Thus, a lot of effort has been made in the area of membrane design and many performant concepts are readily available for a multitude of systems and applications.[98–100,104] Nonetheless, it is to be noted that there are drawbacks that come with the choice of water as a solvent: for instance, the application of aqueous electrolytes is confined to a temperature range between 0 °C and 100 °C. As a result, temperature management may be necessary to ensure full functionality in particularly hot or cold environments. The major disadvantage of aqueous electrolytes however is represented by the comparatively narrow electrochemical stability window (ESW), which is dictated by the electrolysis of water. By implication, at low potentials the hydrogen evolution reaction (HER) takes place on the cathode side:

Acidic: $$4\,H_3O^+ + 4\,e^- \rightarrow 2\,H_2 + 4\,H_2O \qquad (4)$$

Basic: $$4\,H_2O + 4\,e^- \rightarrow 2\,H_2 + 4\,OH^- \qquad (5)$$

On the other hand, oxygen forms on the anode side at high potentials as a result of the oxygen evolution reaction (OER):

Acidic: $$6\,H_2O \rightarrow O_2 + 4\,H_3O^+ + 4\,e^- \qquad (6)$$

Basic: $4\,OH^- \rightarrow O_2 + 2\,H_2O + 4\,e^-$ (7)

Overall: $2\,H_2O \rightarrow 2\,H_2 + 2\,O_2$ (8)

A combination of the cathodic and the anodic process yields the overall reaction described by equation (8). The potential span between HER and OER amounts to 1.23 V for kinetically ideal reactions, whereas the absolute potential of both events is determined by the pH value of the solution (for more information, see also section 1.3.1). However, considering the overpotentials of HER and ORR at carbon electrodes, the ESW of water can be further expanded by a clever choice of electrode materials.[60]

Table 1: Physicochemical quantities of water and selected nonaqueous solvents. T_f: freezing point of pure solvent. T_b: boiling point of pure solvent. Other quantities denoted as before. Data taken from ref.[133]

Solvent	T_f **[°C]**	T_b **[°C]**	η **[mPa s]**	ε_r
H_2O	0	100	0.89	78.4
Tetrahydrofuran (THF)	−108	66	0.46	7.6
Propylene carbonate (PC)	−55	242	2.53	64.9
1-Propanol	−176	97	1.94	20.5
Acetonitrile (AN)	−44	82	0.34	35.9
1,2-Dimethoxyethane (DME)	−69	85	0.46	7.2

In this context, nonaqueous solvents such as tetrahydrofuran (THF) or carbonates provide a larger operable potential window and temperature range, hence mitigating the major drawbacks of aqueous electrolytes. For instance, THF has a low freezing point of −108.4°C, which enables an application in particularly cold environments.[133] 1,2-Butylene carbonate (BC) in turn features a remarkably broad ESW of 7.2 V.[58] However, these benefits come at a price: to achieve a high current and hence power density, charge compensation must occur at a fast rate during cycling, which requires a high ionic conductivity of the applied electrolyte. As already mentioned for aqueous electrolytes, a high mobility and concentration of the supporting ionic species has to be given to ensure this. As described by equation (1) the charge carrier mobility u_i directly correlates with the viscosity η of the solvent. Unfortunately, a large amount of common nonaqueous solvents such as propylene carbonate (2.53 mPa s) and 1-propanol (1.94 mPa s) exhibits high viscosities (see Table 1), hence limiting the

charge transport compared to aqueous solvents (0.89 mPa s).[133] Besides these restrictions, these comparatively high viscosity of organic solvents also significantly increases the pumping costs at system level. One may argue that organic solvents with low viscosities such as acetonitrile (0.34 mPa s) or 1,2-dimethoxyethane (0.46 mPa s) may be used instead to circumvent the concomitant energy losses. However, for nonaqueous solvents there is a definite trade-off between their viscosity and relative permittivity ε_r, which constitutes a severe bottleneck for an application at high current densities.[58] In addition, IEMs show an unsatisfactory performance in nonaqueous solvents, leading to low power outputs and uncompetitive coulombic as well as voltage efficiencies compared to aqueous RFBs.[134,135] Another aspect that is to be considered is the additional costs for conductive additives, which are required to attain a practical conductivity of the electrolyte. Whereas in the case of aqueous electrolytes mostly cheap additives such as potassium hydroxide or sulfuric acid are used, which do not contribute significantly to the overall costs, rather costly additives such as tetrabuytlammonium hexafluorophosphate or sodium perchlorate are applied in nonaqueous systems.[58,136] Besides their detrimental impact on electrolyte costs, such additives were reported to interfere with the intended electrochemistry of the active material and to promote side reactions.[137] Furthermore, they may also limit the ESW of nonaqueous solvents, relativizing their greatest advantage over aqueous systems.[131] On top of all that, nonaqueous solvents are to be seen ecologically questionable, which contradicts the idea of green and sustainable energy storage.[138,139]

Conclusively, water-based electrolytes combine a multitude of beneficial properties with regard to sustainable and economic SES. Due to the low viscosity and high relative permittivity of water, aqueous electrolytes are rendered highly conductive, enabling high energy densities and efficient load levelling. In consequence of the nonflammable and non-toxic nature of water, these performance-relevant properties are paired with a reduced risk for health and environment. Additionally, the use of cheap additives to promote the conductivity of the electrolyte allows to cut costs and to position aqueous RFBs as an economically promising concept for future energy storage. However, in order to further improve upon the competitiveness of aqueous RFBs, it is equally necessary to reduce costs of other components of the battery, namely the separator, electrodes and the applied active material in particular.

1.3 Quinone active materials

Due to the growing demand for electrochemical energy storage, the prices of inorganic reactants such as vanadium or lithium are steadily increasing up to the present day.[21,23] Thus, other sources for active materials need to be harnessed in order to maintain a stable supply chain and to reduce the overall costs of stationary storage in particular. In this regard, the use of cheap and abundant organic redox materials poses a promising alternative, since such reactants may be extracted from plentifully available resources as organic waste products.[29,31] Besides the economic aspect, organic redox materials have a number of technological merits such as the abundant design space of structure motifs and highly tunable structures and properties.

In this context, the substance class of quinones represents a great example for organic compounds with potential for electrochemical applications. Quinones share the structural motif of a fully conjugated cyclic dione structure, whereas their general nomenclature follows the terminology of their parent hydrocarbons[140]: by way of illustration, the structures of benzo- (benzene), naphtho- (naphthalene) and anthraquinone (anthracene) are depicted in Figure 4. Another general distinction can be made according to the position of the two characteristic carbonyl groups: the prefix *ortho* is used in the case of an adjacent configuration, whereas quinones featuring carbonyl groups in opposite positions are denoted as *para*-quinones.

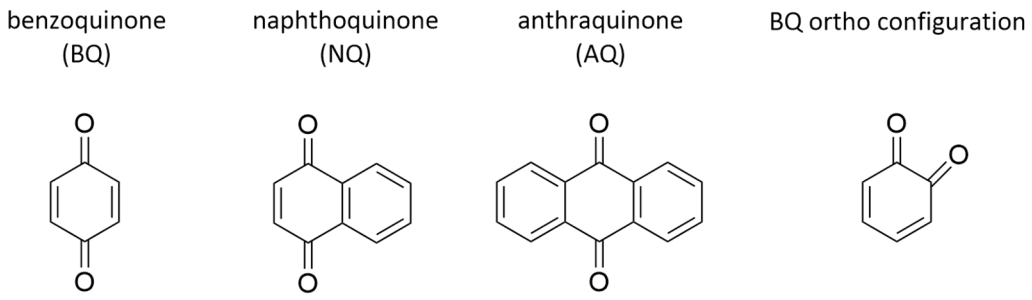

Figure 4: The primary quinone base structures derived from the parent hydrocarbons benzene, naphthalene and anthracene. BQ, NQ as well as AQ are illustrated in para configuration. For comparison, BQ is further depicted in ortho configuration on the right.

To return to the sustainable aspect of organic active materials, quinones can be derived from a waste product of the paper and pulp industry, namely lignocellulose. 15-30 wt% of this renewable biomass is ascribed to lignin, which poses a promising starting material for the production of bulk aromatics.[141] According to a process originally developed by Monsanto[142] (see Scheme 1), the oxidation of lignosulfonate yields vanillin, syringaldehyde and other phenolic compounds[143]:

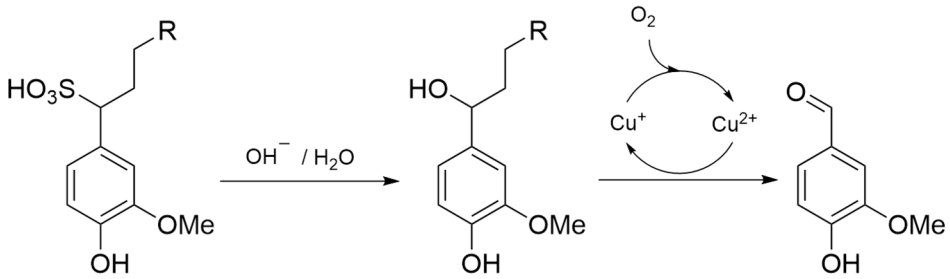

Scheme 1: Catalytic conversion of lignosulfonate. A hydrolysis step in alkaline solution yields a desulfonated product, which is oxidized by means of a copper-based catalyst. In this way, lignosulfonate can be refined to phenolic compounds such as vanillin or syringaldehyde, which serve as precursors for the preparation of quinone compounds.

Besides this homogeneous phase approach, similar results were reported for an electrochemical cleavage of lignin.[30,144,145] The obtained phenolic compounds subsequently can be adapted to electrochemical applications by hydroxylation in solutions of hydrogen peroxide.[146,147] The resulting dihydroxybenzenes consequently can be oxidized and thus are transferred into the desired quinonoid compounds, which have been thoroughly investigated due to their exemplarily redox behavior.[148,149] Another approach involves the coupling of aryl aldehydes like vanillin via Friedel-Crafts acylation to yield polycyclic systems such as AQs.[150] Overall, quinones pose a versatile class of compounds with highly favorable electro- and physicochemical properties, which makes them a promising candidate for the active material of ORFBs.[78] Furthermore, the potential for cost reduction of lignin-derived quinones presents a major advantage over other active materials and thus generated a lot of economic and scientific interest within the last few years. In the following section, the different aspects of quinones shall be elucidated by considering the redox chemistry and structure-property relationships as well as potential degradation mechanisms of this compound class.

1.3.1 Redox behavior

The reduction of quinones (Q) generally occurs by a transfer of two electrons, yielding the anion radical ($Q^{\bullet -}$) as an intermediate and the dianion (Q^{2-}) as the final product. With regard to the energy density of RFBs, this poses a great advantage over conventional metal-based redox couples such as vanadium, chromium and iron, since twice the number of electrons is transferred per mole of reactant. Due to the aromatic nature of the fully reduced species, quinones exhibit a high stability and reversibility with respect to charge transfer processes.[25] Furthermore, the associated redox reactions occur at fast rates, which implies fast charge transfer kinetics.[151] In consequence of their manifold beneficial properties, quinones are commonly considered as a promising active material for battery

applications and thus have been subject of a multitude of electrochemical studies within the last ten years.[152,153] However, the redox behavior of quinones is complex and depends on several direct as well as indirect factors: the absolute potentials of the occurring charge transfers are determined by the intrinsic electron density of the compound as well as dynamic contributions related to the applied solvent such as hydrogen bonding and protonation.[154] Whereas the aspects of molecular electron density and its modification will be discussed in detail in section 1.3.2, the following paragraph elucidates the impact of the solvent − e.g. hydrogen bonding and protonation − on the electrochemical behavior of quinones.

Aprotic media

In that respect, it may be favorable to begin with the lowest level of complexity: for nonaqueous, aprotic solvents such as acetonitrile, intermolecular hydrogen bonding and protonation are excluded, which allows for an independent consideration of the occurring charge transfer processes. In this case, the two-electron reduction of quinones takes place sequentially (see Scheme 2), forming the aforementioned anion radical $Q^{\bullet -}$, also denoted as semiquinone, and the dianion Q^{2-}.[155]

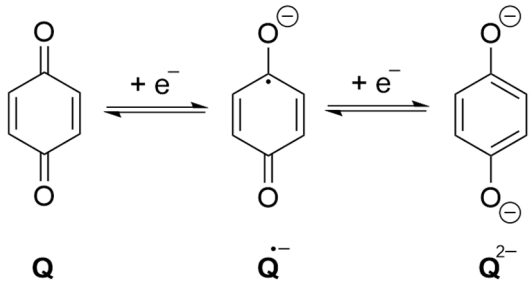

Scheme 2: The electrochemical reduction of quinones in aprotic solvents. Due to electrostatic reasons, electron transfer takes place sequentially, which manifests in two individual voltammetric waves in a cyclic voltammogram.

In aprotic solvents, the potential difference between the individual charge transfer steps is large enough so that two well-defined waves are observed in a cyclic voltammogram (CV). This appears to be reasonable from electrostatic arguments, since more energy should be required to add an electron to a molecule with a negative charge considering the first electron transfer.[156] Nevertheless, despite the absence of hydrogen bonds and proton donors in the solvent the observed characteristics may vary drastically as a result of intramolecular interactions. To give an example, the introduction of hydroxyl groups (−OH) evokes a positive potential shift of both individual redox processes (see Figure 5). Prima facie, this circumstance may seem counterintuitive, as hydroxyl groups are known to exhibit a positive mesomeric effect, hence increasing the overall electron density of the molecule.[154] However,

the observed behavior emphasizes the dominance of an opposite effect, which is denoted as intramolecular hydrogen bonding.[157] Accordingly, the positive shift of the redox potential results from the close proximity of the hydroxyl group and the carbonyl oxygen of the quinone: due to the exchange of the hydroxyl hydrogen between both moieties, the negative charge of the reduction products is effectively delocalized – e.g. stabilized – across the molecule.[158] If hydrogen-bond donors such as methanol or water are added to the aprotic electrolyte, a competition between intra- and intermolecular hydrogen bonding occurs. Although in most cases the intramolecular option is preferred, the stabilizing effect is outweighed with increasing molar fraction of the added donor.[159]

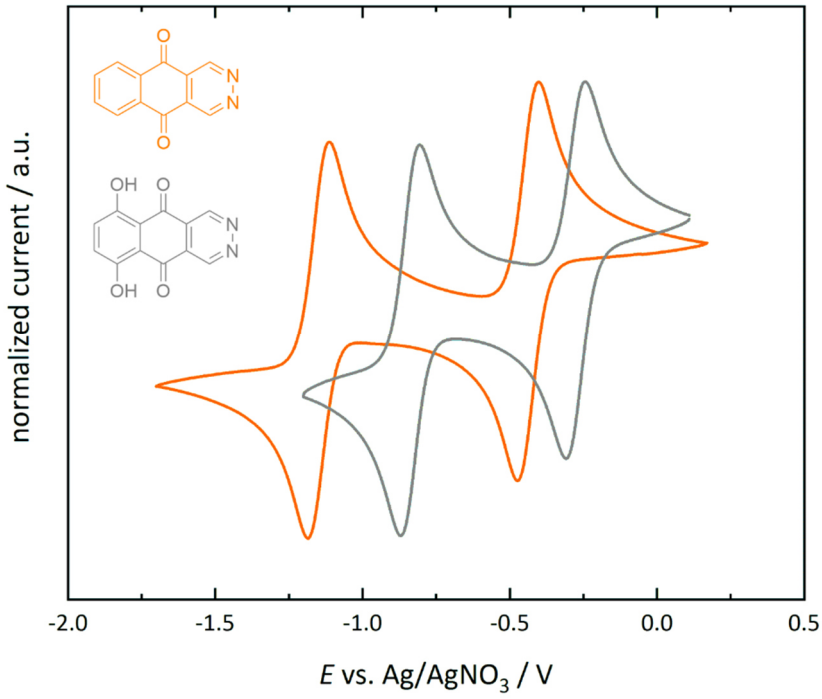

Figure 5: Intramolecular hydrogen bonding and its impact on the charge transfer characteristics of quinones. Due to the exchange of the –OH hydrogen between the hydroxyl and the carbonyl moieties of the dihydroxy-quinone (grey), the negative charge of the reduction products is effectively stabilized. This manifests in a positive potential shift compared to derivatives lacking the capability for intramolecular hydrogen bonding (orange). The measured currents were normalized to the maximum anodic current of the first redox event.

When water is incrementally added to an aprotic solution containing the quinone compound, the two voltammetric waves of the individual electron transfers move to more positive values of the potential scale.[160] However, it is to be noted that the two reduction products are not equally affected by intermolecular hydrogen bonding: the second signal associated with the formation of the quinone dianion Q^{2-} advances to a significantly higher extent than the signal related to the process of semiquinone $Q^{\bullet-}$ formation. If a sufficiently large amount of water is added, both signals eventually merge to a single voltammetric wave.[161] This may be explained by the increased capability for hydrogen bonding of Q^{2-} compared to $Q^{\bullet-}$. Due to the 2 x 3 lone pairs of the quinone dianion, up to six hydrogen

bonds may be considered, which are to be classified as strong or at least moderate in nature.[162] For the case of AQ in DMF, it was postulated that the hydrogen bond strength of the dianion needs to surpass the stabilization of the semiquinone by at least 72 kJ to enable the merging of the two voltammetric waves.[156] Considering six ligands, this corresponds to an energy discrepancy of 12 kJ per hydrogen bond. To put this into perspective, the hydrogen bond of a water-hydroxyl hydrogen bond (112 kJ) was determined to be 95.6 kJ stronger than a hydrogen bond between two water molecules (15.5 kJ).[163] With that in mind, it seems reasonable to assume a stabilization of Q^{2-} over $Q^{\bullet-}$ by an amount of 72 kJ.

Aqueous solutions

Moving on to exclusively aqueous solutions, the solvent itself poses an abundant and strong hydrogen bonding agent. The relative potential difference between the two redox processes is typically compensated by means of the hydrogen bonding interaction with the solvent and a single voltammetric wave is observed in the CV. Consequently, the individual electron transfers occur at approximately the same potential, which is why the reduction of quinones in alkaline aqueous solutions is formally referred to as a simultaneous two-electron transfer (see Scheme 3).[164] However, an independent stabilization of the semiquinone over the dianion may evoke a separation of both processes, even in an aqueous environment. This rare phenomenon was reported with regard to the addition of metal cations and supporting salts: due to an ion-pairing effect of the semiquinone intermediate with cations of specific dimensions, two distinct voltammetric waves were observed.[165,166] As part of this thesis, this was further achieved by a heterocyclic modification of the quinonoid base structure.[167] The peculiarities of such an intrinsic stabilization of the semiquinone intermediate and the implications for the overall charge transfer kinetics will be discussed more thoroughly in the following paragraph as well as section 2.2.

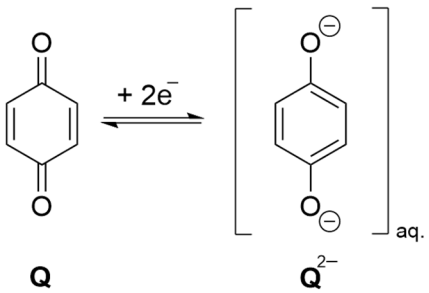

Scheme 3: The electrochemical reduction of quinones in alkaline, aqueous solution. In consequence of the increased hydrogen- bonding capability of Q^{2-} over the reduction intermediate $Q^{\bullet-}$, the two associated electron transfers occur at the same or at least very similar potentials. Consequently, quinone reduction in alkaline aqueous solution is commonly considered to take place as a simultaneous two-electron transfer.

Shifting the focus towards acidic aqueous solutions, the transition to the other end of the pH scale adds another layer of complexity to the redox behavior of quinones: besides the impact of hydrogen-bonding, protonation phenomena further have to be taken into account. In general, the reduction of quinones is considered to take place as a fast and highly driven two-electron/two-proton transfer in acidic media, yielding the fully protonated form of the reduced quinone QH_2.[168]

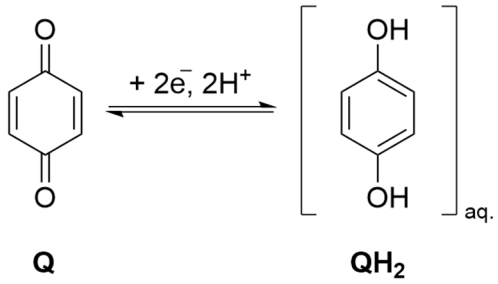

Scheme 4: The electrochemical reduction of quinones in acidic, aqueous solution. At low pH values, electron transfer is accompanied by protonation. If the semiquinone intermediate $Q^{\bullet -}$ is protonated to yield $QH^{\bullet}$, this creates an additional driving force for the second reduction process. The concerted transfer of protons and electrons is commonly denoted as proton-coupled electron transfer.

Due to this so-called proton-coupled electron transfer (PCET), the overall reaction scheme of quinones turns out to be complex in aqueous solutions: the combination of three redox as well as in each case three protonation states yields a total number of 9 potential species, which are described by the 9-membered square scheme (see Scheme 5). In this scheme, horizontal pathways correspond to electron transfers, whereas vertical pathways represent protonation reactions. Because of the minimum proton activity, merely electron transfers and thus a horizontal movement across the scheme is observed in alkaline aqueous solutions. For acidic solutions on the other hand, a multitude of reaction pathways are to be considered, comprising varying sequences of proton and electron transfer.

In light of this, there is a general debate if the PCET of quinones is to be described as a stepwise or a concerted pathway. With respect to the homogeneous reactions, it was recently reported that the PCET of quinones is in fact a complicated mix of concerted and stepwise pathways at intermediate pH.[169] Nonetheless, in buffered or sufficiently acidic media – i.e. at low pH values − protonation and deprotonation may be considered to occur at equilibrium, assuming a fast and diffusion-controlled rate of the reaction.[170] On this assumption, the ratio of different protonation states of each redox state will be constant at a given pH, which implies that the reaction rate is solely determined by the kinetic limitations of the electron transfer.[171] Based on this prerequisite, the involved protonation states are grouped and the redox reaction can be described by a simple two-electron transfer with an apparent equilibrium potential E_{app} and an apparent rate constant k_{app}.[172]

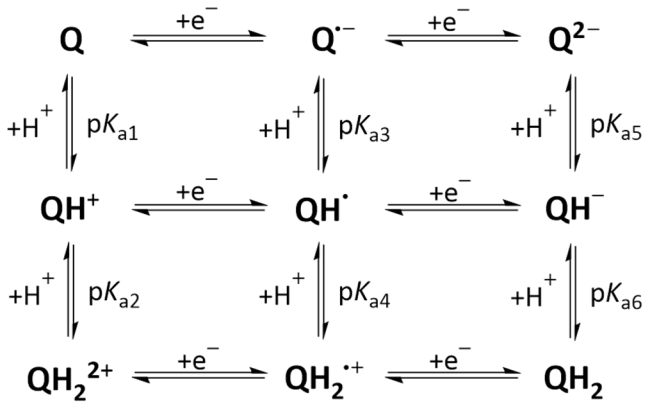

Scheme 5: The nine-membered square scheme describes the potential reaction pathways of quinones during reduction. The pathways or reaction sequences are determined by the acid dissociation constants of the involved species and the actual pH value of the solution. Horizontal pathways represent the transfer of electrons, whereas the transfer of protons is illustrated as vertical movement across the scheme.

However, it is important to note that the overall kinetics of the charge transfer are affected by the reaction pathway along the square scheme, which may vary as a function of the applied conditions: k_{app} and E_{app} highly depend on the acid dissociation constants (pK_a) of the individual species as well as the pH value of the solution. Hence, different sequences of protonation (chemical step C) and electron transfer (denoted as E) are postulated for different pH regions: to give an example, besides the solely electron-based EE process in highly alkaline solutions, an EECC process is found for anthraquinone-2,6-disulfonate (AQDS) around pH 10. Between pH 4 and 7 an alternating ECEC mechanism is dominant, which in turn switches to an CECE sequence at very low proton activities (pH ≈ 1).[42] These results coincide with the studies of Laviron[171] and Vetter[173], which focused on the reaction sequence of benzoquinone (BQ).

This reaction sequence may in fact largely affect the observed kinetics of the occurring redox process, which primarily refers to pH regions featuring an alternating transfer of electrons and protons. For instance, considering a reduction at intermediate pH values (ECEC), the first electron transfer (E_1) is followed by a protonation of the reduction product $Q^{\bullet -}$, which generates the protonated semiquinone radical $QH^{\bullet}$. Interestingly, this species is more oxidizing than the initial compound Q prior to the first electron transfer, which is why the original order of both events as seen in aprotic solvents is reversed. This alteration in the order of redox events is commonly denoted as potential-inversion. In this situation E_2 is more positive than E_1 and the redox reaction occurs at a new mean equilibrium potential E_{app}, which is positively shifted with regard to E_1. This implies that the two otherwise sequential electron transfers take place simultaneously as manifested by a single cathodic and anodic wave in the experiment. One would assume that this concerted charge transfer results in a highly driven process.[82,174] However, as a matter of fact, wide peak-to-peak separations are observed

between the cathodic and anodic current response in CVs for a high degree of potential inversion, implying slow charge transfer kinetics.[166] This contradictory behavior may be explained by means of the significant shift of the equilibrium potential evoked by the protonation of the reduced species $Q^{\bullet-}$: to allow for a reaction at equilibrium, current has to flow significantly prior to the actual potential E_1 of the first electron transfer, which de facto initiates the whole process. However, the intrinsic electron transfer rates of quinones are insufficient to ensure this, which eventually manifests as the high overpotentials observed in the CV.[156] This behavior is taken into account by equation (9), which correlates the degree of potential inversion ($E_1 - E_2$) with the apparent kinetics of the reaction:

$$k_{app} = k_r \exp\left[\frac{F}{4RT}\left(E_1 - E_2\right)\right] \tag{9}$$

Here, k_r is the actual kinetic rate constant of the occurring electron transfer, which declines with an increasing degree of potential inversion as expressed by k_{app}.[172] In order to achieve fast charge transfer kinetics, it would be necessary to diminish the relative potential difference between the individual electron transfers ($E_1 - E_2$). More precisely, it may be favorable to thermodynamically stabilize the semiquinone intermediate species, which effectively corresponds to a positive shift of E_1 relative to E_2. The stability of $Q^{\bullet-}$ can be quantified by means of the equilibrium constant K_c of the comproportionation reaction between Q and QH_2 (equation 10).[175] Returning to the initial argument, the equilibrium constant directly correlates with the degree of potential inversion, which is given by equation (11):

$$Q + QH_2 \rightleftharpoons 2Q^{\bullet-} + 2H^+ \tag{10}$$

$$\log K_c = \log \frac{\left[Q^{\bullet-}\right]^2 \left[H^+\right]^2}{\left[Q\right]\left[QH_2\right]} = \frac{F}{RT}\left(E_1 - E_2\right) \tag{11}$$

Conclusively, a stabilization of the semiquinone intermediate – i.e. a positive shift of the first charge transfer E_1 – corresponds to a decreased extent of potential inversion and, by implication, improved charge transfer kinetics. To accomplish this, a number of measures has been identified. Besides the aforementioned effect of ion-pairing caused by cationic additives[165,166], distinct structural motifs have

been reported to contribute to the stability of $Q^{\bullet -}$: to give an example, the addition of fused benzene rings to already existing quinone structures was identified to have a beneficial impact on the charge delocalization within the semiquinone and consequently its stability.[176] Furthermore, a significant increase of K_c was corroborated with respect to the addition of electron withdrawing substituents, which eventually promotes fast charge transfer kinetics in the case of strong potential inversion.[175–177] It is to be noted that this was alternatively accomplished by a nitrogen-based heterocyclic modification of the quinone base structure within the framework of this thesis. This approach will be discussed as part of the discussion in section 2.

Pourbaix diagrams

Given the fact that protons may take part in the redox reactions of quinones, the equilibrium potential of the charge transfer consequently varies as a function of the applied pH value. The potential of the reversible reduction process involving the uptake of *h* protons and *n* electrons

$$\mathrm{Q} + h\,\mathrm{H^+} + n\,\mathrm{e^-} \rightleftharpoons \mathrm{QH}_h^{(h-n)+} \tag{12}$$

thus may be described by the Nernst equation (13) as follows:

$$E_{\mathrm{exp}} = E^{0'}\left(\mathrm{Q/QH_2}\right) - \frac{RT}{nF}\ln\frac{\left[\mathrm{QH}_h^{(h-n)+}\right]}{\left[Q\right]\left[\mathrm{H^+}\right]^h} \tag{13}$$

Subsequently, the logarithmic term can be further modified to yield equation (14), where $E^{0'}$ (Q/QH_2) is the formal potential of the reduction of the quinone, which is altered as a function of the proton activity as measured by E_{exp}. As the pH value of an aqueous solution is defined as the negative decadic logarithm of the proton activity [H^+], the associated term can be replaced as described by equation (15),

$$E_{\mathrm{exp}} = E^{0'}\left(\mathrm{Q/QH_2}\right) + \frac{RT}{nF}\ln\left[\mathrm{H^+}\right]^h - \frac{RT}{nF}\ln\frac{\left[\mathrm{QH}_h^{(h-n)+}\right]}{\left[Q\right]} \tag{14}$$

$$E_{\mathrm{exp}} = E^{0'}\left(\mathrm{Q/QH_2}\right) - 2.303\frac{hRT}{nF}\mathrm{pH} - \frac{RT}{nF}\ln\frac{\left[\mathrm{QH}_h^{(h-n)+}\right]}{\left[Q\right]} \tag{15}$$

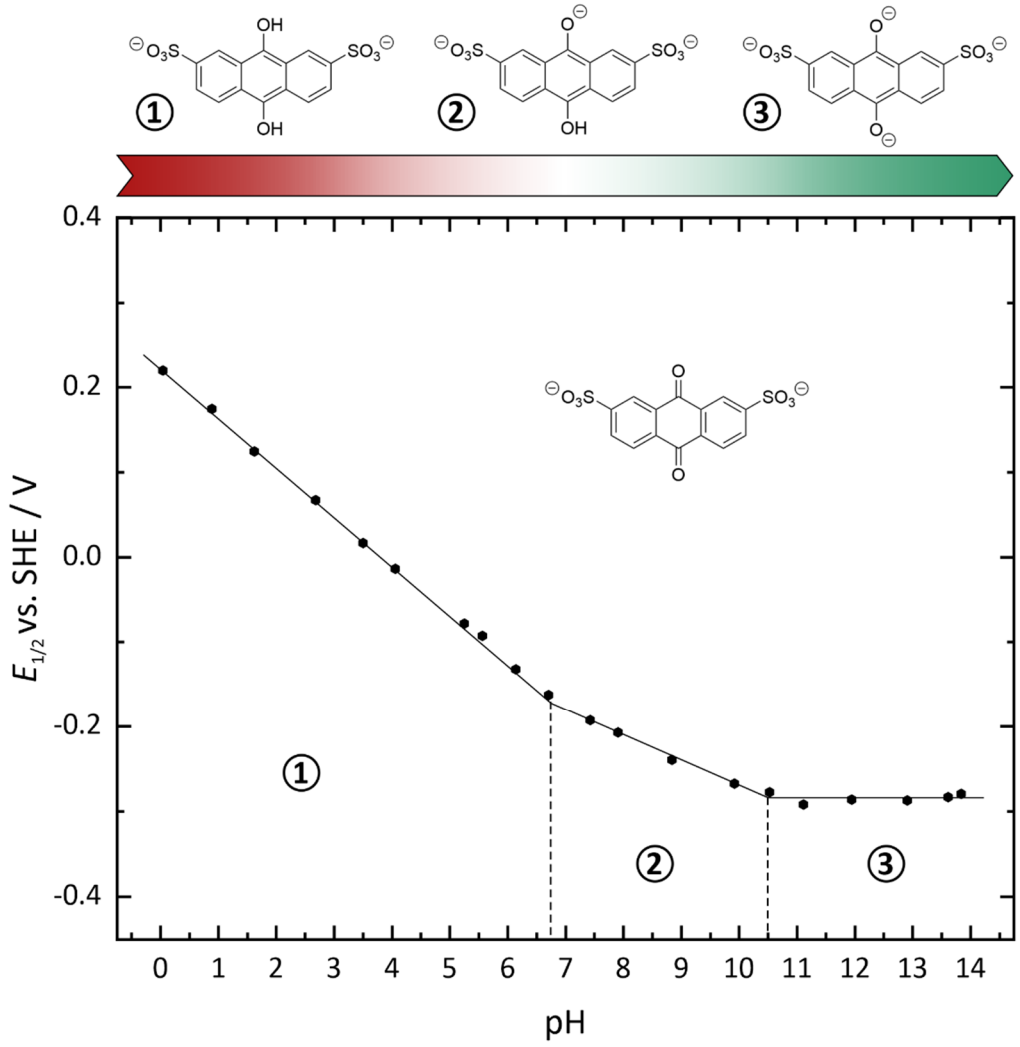

Figure 6: Pourbaix diagram of AQDS. The pH dependent voltammetric analysis of the 2,7-disulfonate AQ derivative reveals three domains of varying slopes *m*. This implies a divergent ratio of transferred electrons and protons ($2e^-/2H^+$: m_{theo} = 59 mV/pH; $2e^-/1H^+$: m_{theo} = 29 mV/pH; $2e^-$: m_{theo} = 0 mV/pH). Consequently, the acid dissociation constants of the variously protonated species can be derived from the intersection of the three domains ($pK_{a1} \approx 6.75$; $pK_{a2} \approx 10.5$).

which then explicitly describes the relation between the measured potential of the reaction and the applied pH value.[178] In this light, it becomes apparent that the relation between E_{exp} and the applied pH value is not consistent, but rather depends on the ratio of transferred protons *h* and electrons *n*. In this context, Pourbaix diagrams represent an effective presentation format to illustrate such correlations and the resulting domains associated with species of varying protonation states. As opposed to the compound class of phenols, the oxidation and reduction products of quinones are stable on the timescale of CV experiments, which is why reliable values can be obtained for the pH-dependent equilibrium potentials.[179] To give an example, the Pourbaix diagram of AQDS (Figure 6) is divided into three domains, which correspond to a $2e^-/2H^+$ (pH < 6.75), a $2e^-/1H^+$ (6.75 < pH < 10.5) and a $2e^-$ (pH > 10.5) reaction. In accordance with equation (15) a slope of 59, 29 and 0 mV pH^{-1} respectively is yielded for these domains, whose intersections correspond to the pK_a values of the

related species. Conclusively, due to the favorable illustration of varying reaction mechanisms and significant quantities such as pK_a values, Pourbaix diagrams are considered as a useful tool for the investigation of PCET reactions.

1.3.2 Structure-property-relationships

To achieve a high cell voltage for RFBs as well as for any other battery system, the potential difference between the reactants located at the anode and cathode needs to be as large as possible. Whereas inorganic active materials such as vanadium generally exhibit invariant potentials[180], the wide design space of quinonoid structure motifs delivers access to a multitude of design opportunities. The reactivity or rather electron affinity of organic reactants is determined by the energy of their lowest unoccupied molecular orbital (LUMO).[159] By implication, the electronic properties of quinones are directly correlated with their structural design, which makes this compound class highly adaptable for an application within specific potential ranges and media. The direct relationship between the half-wave potentials E_{hw} of organic reactants in polarographic experiments and their LUMO energy was first established by A. Maccoll[181]:

$$E_{hw} = -E_{m+1} + C \qquad (16)$$

In this equation, C describes the difference in solvation energies of the neutral molecule and its radical anion, whereas $-E_{m+1}$ corresponds to the negative of the LUMO energy. On the assumption that C is constant, the differences in half-wave potentials for a series of varying quinones thus should be solely given by $-\Delta E_{m+1}$. Peover was the first one to experimentally demonstrate this interrelation for the first of the two occuring electron transfers on the basis of a selection of unsubstituted quinone species in acetonitrile.[182] As part of this study, he also corroborated that the same orbital (LUMO) is associated with the first as well as the second electron transfer. However, a less predictable behavior was found for the overall redox potentials in protic solvents as well as substituted quinones in general. This was attributed to the contribution of other factors such as hydrogen bonding and complications induced by the varying pK_a values of different species.[183,184] Consequently, a precise quantitative prediction for the impact of specific substituents is not trivial under such conditions. Nevertheless, the electron density – i.e. the energy level of the LUMO − is to be considered as a decisive factor to adapt the redox potential of quinone compounds.

In that context, it should be noted that a change in electron density may arise from mesomeric as well as inductive effects of substituents.[185] The inductive effect describes the donation (+I) or acception (−I) of electron density through the sigma (σ) bonds of the molecule, which is generally governed by the relative electronegativity of the bonded atoms. For instance, methyl groups ($-CH_3$) are commonly considered electron donating, while highly electronegative substituents such as halogens (−F, −Cl, −Br) act as electron density acceptors. Mesomeric or resonance effects on the other hand describe the delocalization of electron pairs in conjugated systems: for instance, substituents such as hydroxyl (−OH), alkoxy (−OR) or amino groups ($-NH_2$) contribute to the electron density of a π-bonded system by donating their available lone-pairs (+M). Conversely, moieties like carbonyl ($R_2-C=O$), nitro ($-NO_2$) and sulfonic acid ($-SO_3H$) are known to decrease the electron density of the conjugated system by accepting electron pairs from it (−M).[186] By means of illustration, both effects are depicted in Scheme 6. For the most part, the two phenomena are opposing each other: considering a −OH moiety, the electron withdrawing character of oxygen (−I) on the one hand and the availability of lone electron pairs (+M) on the other hand simultaneously allows for negative inductive as well as positive mesomeric effects. Interestingly, the incorporation of hydroxyl moieties was generally found to decrease the redox potential of quinones in aqueous solution, emphasizing the electron donating character of –OH after all.[39] Which of both effects predominates eventually depends on the relative electronegativity of the associated atoms and the efficiency of the overlap between the *p* orbitals of the respective substituent and the conjugated system. In this regard, the extent of interaction may be determined by the relative position of functional groups and the specific geometry of the resulting resonance structures.[187] As a general rule, for $-NH_2$ and −OR moieties resonance commonly predominates induction, whereas inductive effects have a stronger impact in the case of halogens.[188]

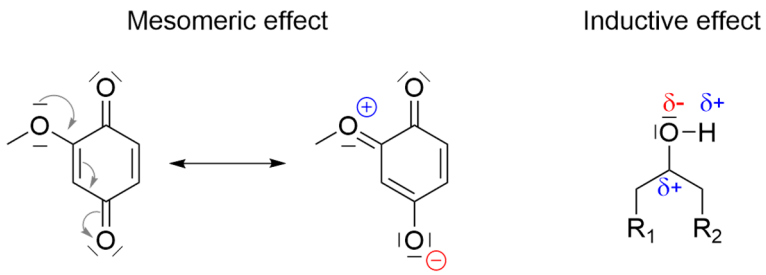

Scheme 6: Schematic illustration of mesomeric and inductive effects of functional groups. For a better understanding, electron lone pairs are included. Whereas single bonded substituents equipped with electron lone pairs such as –OMe commonly act as electron donors (+M), double bonded substituents such as $R_2-C=O$ tend to withdraw electron density via resonance (−M). The impact of mesomeric effects is mainly determined by the degree of orbital overlap, whereas inductive effects are generally governed by the relative electronegativity of the associated binding partners. For instance, hydroxyl oxygen acts as an inductive electron acceptor due to its high intrinsic electronegativity, thus effectively decreasing the electron density of the attached system R_1/R_2.

In consequence of the complex interplay between hydrogen bonding, protonation, mesomeric and inductive effects, the exact prediction of redox potentials of organic reactants presents a challenging endeavor. However, due to the ever-increasing processing power of modern computers, more and more of these factors can be accounted for in theoretical calculations, namely DFT calculations. In the past ten years, powerful models supported by experimental results have been elaborated to effectively describe the structure-property relationships of quinones.[189–194] In accordance with the LUMO energy theory established by Maccoll (equation 16), electron donating substituents such as −OH, $-CH_3$ and –OR groups were found to increase the electron density of quinones, thus decreasing the redox potential compared to the base compound. On the other hand, electron withdrawing functional groups such as carboxyl (−COOH), sulfonic ($-SO_3H$) and phosphonic acid moieties ($-PO_3H_2$) had the opposite effect, shifting the redox potential to more positive values.[32] Furthermore, with respect to the energy density of ORFBs, the presence of hydrophilic substituents such as −OH, $-SO_3H$ and $-PO_3H_2$ was identified as an effective measure to promote the water solubility of quinones.[152]

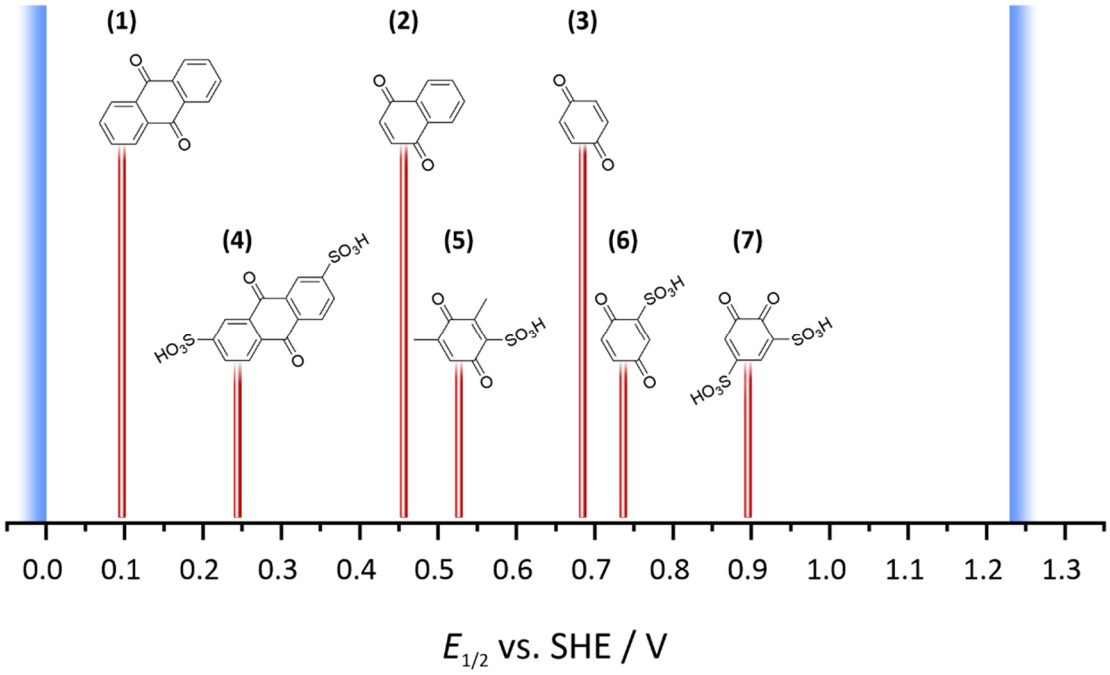

Figure 7: Overview of the reduction potentials of selected quinone base structures and substitution patterns: (1) AQ, (2) NQ, (3) BQ, (4) AQDS, (5) 1,4-benzoquinone-2,6-dimethyl-3-sulfonic acid[48], (6) 1,2-benzoquinone-2-sulfonic acid and (7) 1,2-benzoquinone-3,5-disulfonic acid. Apart from compound (5), all displayed compounds were analyzed as part of this thesis. The blue boundaries illustrate the ESW of water.

Nonetheless, it is important to note that the impact of such substituents on the overall electron density of an organic compound is limited. The intrinsic electron density of the base compound eventually dictates the approximate operable potential range, which can be further fleshed out by means of peripheral substituents.[189] Consequently, intrinsically electron-rich quinonoid compounds

such as AQs are considered as suitable base structures for anolyte active materials, whereas it may be more facile to derive high-potential catholyte compounds from BQs. In order to illustrate the structure-property relationships of quinones, a selection of varying quinone derivatives and their associated reduction potentials is displayed in Figure 7.

1.3.3 Degradation mechanisms

The structural integrity of active materials poses a crucial factor to achieve stable cycling performances and a high calendar life for energy storage devices. Whereas metal-based redox couples such as iron, chromium and vanadium are characterized by a commonly strict electrochemical conversion, organic reactants such as quinones may be prone to specific side reactions during cycling. As predefined by the vast research field of organic chemistry, a multitude of side reaction mechanisms may be conceived.[195,196] However, under the conditions present in ORFBs the number of plausible reaction pathways diminishes to a more limited selection.[197] Due to the aromatic nature of the reduced hydroquinone form, those mechanisms primarily concern the oxidized form, which is an α, β-unsaturated ketone that acts as an electrophile. Consequently, nucleophilic addition poses one of the major degradation pathways of quinones. In general, two different region-chemistries are to be distinguished, namely the 1,2- and 1,4-addition. The predominant mechanism of the two is determined by the nature and compatibility of nucleophile and electrophile. In this context, a distinction is made between so-called soft and hard reactants with regard to their respective polarizability: nucleophiles and electrophiles containing atoms of small dimensions and high electronegativity are commonly denoted as hard reactants, whereas soft reactants are rather based on comparatively large and mostly uncharged atoms.[198]

This concept of hard and soft reactants can also be transferred to the molecular orbital model: the “hardness” of reactants increases together with a rising energy of the empty, electrophilic orbitals (LUMO) and a decreasing energy of the filled, nucleophilic orbitals, also denoted as highest occupied molecular orbitals (HOMO). For the “softness” of reactants, the exact opposite is true.[199] In general, hard nucleophiles prefer to react with hard electrophiles, while soft nucleophiles by contrast mostly interact with soft electrophiles. This is due to the varying forms of interaction, which mediate the reaction between the two reaction partners. In accordance with the frontier molecular orbital analysis[200], hard-hard interactions are governed primarily by electrostatic attractions between positive and negative charges, whereas soft-soft interactions predominantly depend on the orbital overlap between the HOMO of the nucleophile and the LUMO of the electrophile.

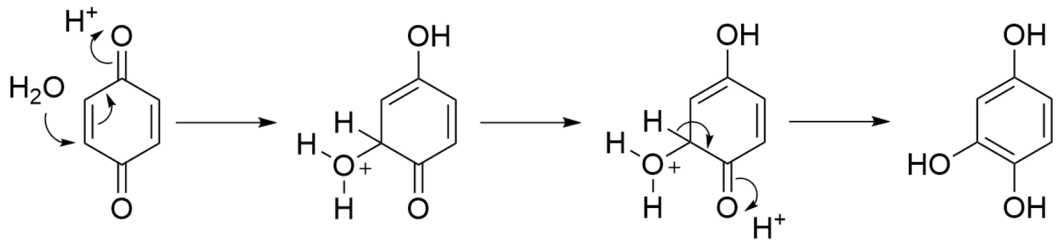

Scheme 7: Schematic illustration of the nucleophilic attack of quinones by water. The so-called conjugate or 1,4-addition, also often denoted as Michael addition, eventually results in the addition of a hydroxyl moiety. Furthermore, the formerly oxidized quinone is chemically transformed into the reduced hydroquinone state.

To return to the quinone system, α, β-unsaturated carbonyl compounds exhibit two electrophilic sites, which both are potentially prone to be attacked by nucleophiles. The carbonyl group features a high positive partial charge on the carbonyl carbon, which may promote a 1,2-addition with hard nucleophiles such as water or hydroxyl ions. Due to its large orbital character, the conjugated site between the α and β carbon on the other hand is to be considered as a soft electrophile, which is likely to react with soft nucleophiles like alkenes or thiols in a 1,4-addition reaction. This reaction is also denoted as conjugate addition, since it is associated with the withdrawal of electrons via resonance effects (see Scheme 7). For the special scenario of a carbanion acting as the nucleophile, the reaction is referred to as Michael addition.[195] However, in recent years it was used synonymous with the 1,4-addition of water within the context of quinonoid ORFBs. As described earlier, from the standpoint of frontier molecular orbital analysis, a 1,2-addition of water should be more likely in the case of α, β-unsaturated carbonyl compounds as quinones. Nonetheless, the nucleophilic addition of water and hydroxyl ions may in fact occur according to the conjugated pathway in aqueous solution, albeit at a slow rate, as supported by the given literature.[44,47,48,201] This may be explained by the large abundancy of both reagents in an ORFB environment in contrast to the otherwise preferred soft nucleophiles. This argument is further supported by the studies conducted as part of this thesis, which will be discussed in more detail in section 2.3.

Along with the undesired addition of substituents to unsubstituted sites, nucleophilic substitution of already present functional groups is one of the most common degradation modes of organic active materials. In this reaction, electron withdrawing substituents are commonly exchanged by nucleophilic species such as water, hydroxide ions or even reduced molecules of the used active species.[202,203] With respect to quinone compounds, various scenarios of this undesired degradation mechanism have been reported to date. Some of these are the hydrolysis of halogenoquinones in alkaline media[204], the acid-catalyzed proto-desulfonation of sulfonated BQ derivatives[49] and the alkyl chain cleavage of carboxylated AQs[43]. As already mentioned in context with the structure-property relationships of quinones, the introduction of new functional groups as well as the replacement of already present ones is known to affect the charge transfer characteristics of organic active species. The electron

affinity as well as the solubility of the attacked reactant may be altered drastically, which in turn might have a negative impact on the overall battery performance.[205]

Consequently, a multitude of potential degradation pathways have to be taken into consideration for the design of active material structures as well as the choice of solvent. Besides the described major nucleophilic degradation pathways, further modes comprising epoxidation[206,207], tautomerization[44], anthrone formation[208,209] and polymerization[210,211] of quinone active species have been reported. However, due to their comparatively marginal impact on the long-term performance of ORFBs, the reader is referred to the given specialized literature for more information.[212]

1.4 Performance-relevant key quantities (Publication I)

The performance of an ORFB is defined by the amount of energy that can be stored at a time as well as its power output during application. Both properties are strongly dependent on various physicochemical parameters.

The energy density W_d of a given system is defined as the product of its specific capacity C_s and the voltage between its two half-cells U:

$$W_d = C_s U \tag{17}$$

C_s in turn describes the charge that can be stored in a specific mass or volume of the electrolyte:

$$C_s = \frac{m n F}{M V} = \frac{c_0 m F}{M} \tag{18}$$

Here, m is the mass of the electrochemically active material, n is the number of electrons, F is the Faraday constant, M is the molar mass and V is the volume of the electrolyte. In consequence, the energy density of an ORFB is finally determined by the concentration of active material c_0, the number of electrons n associated with its redox process and – with respect to the cell voltage U – the difference between the redox potentials E_0 of the applied anolyte and catholyte active materials.[205]

The areal power density P_d on the other hand is influenced by the active surface area A, which is commonly defined as the effective area of the separator, and the inner resistance R_i of the cell.[7,213] This resistance comprises several contributions such as the electronic resistance of the electrolyte R_{el}, the charge transfer resistance of the anodic and cathodic processes R_{ct} as well as the mass transport resistance R_{mass}:

$$P_d = \frac{P}{A} = \frac{UI}{A} = \frac{I^2 R_i}{A} = \frac{(U_0 - IR_{el} - IR_{ct} - IR_{mass})}{A} \quad (19)$$

Thus, the power output of RFBs largely benefits from fast charge transfer kinetics and fast diffusion of active material, which is expressed by high kinetic rate constants k_0 and diffusion coefficients D. Conclusively, E_0, c_0, D and k_0 are to be considered as crucial factors for the performance of RFBs.[7]

As part of this thesis, an overview over these performance-relevant quantities was prepared and published in the journal *Chemie Ingenieur Technik*. This work outlines the parameters with the highest impact on the performance of RFBs, their interrelation and pitfalls in their determination. The overview is substantiated by experimental results, which illustrate the impact of the nature and pH value of the solvent on the electrochemical characteristics of quinone redox compounds. The manuscript was written by the author of this thesis and edited by one co-author.

J. D. Hofmann, D. Schröder, Which Parameter Is Governing for Aqueous Redox Flow Batteries with Organic Active Material? *Chemie Ingenieur Technik* **2019**, *91* (6), 786–794.

Which Parameter is Governing for Aqueous Redox Flow Batteries with Organic Active Material?

Jonas D. Hofmann[1,2] and Daniel Schröder[1,2,*]

DOI: 10.1002/cite.201800162

A multitude of factors contribute to the performance of redox flow batteries with organic active material. In this work, experimental and theoretical methods are elucidated to give information about the most important of these: redox potential, kinetic rate constant, diffusion constant, and solubility. They are found to be highly interdependent – especially for different solvents. By implication, novel organic active materials have to be analyzed jointly by chemists, materials scientists, and by reaction and process engineers to propel the redox flow battery as future energy storage device.

Keywords: Electrochemical performance, Energy storage, Quinones, Redox flow batteries, Voltammetry

Received: September 12, 2018; *revised:* February 18, 2019; *accepted:* February 27, 2019

1 Introduction

In view of the worldwide increasing demand for energy, redox flow batteries (RFBs) are seen as one future energy storage technology. They appeal with high efficiency, conceivably low cost for scale-up, and promising cycle life; besides, capacity and power density can be scaled independently [1]. Next to the state-of-the-art active material vanadium, organic active materials such as (2,2,6,6-tetramethylpiperidin-1-yl)oxyl (TEMPO), viologen, and quinone species have caught attention in research and development [2 – 8]. Especially quinones, which may be utilized from abundant resources like waste products from pulp processing, are of high economic interest [9 – 11].

A schematic of an RFB based on aqueous electrolytes with organic active material (ORFB) is shown in Fig. 1. An ORFB comprises of two electrodes and two tanks, which store the solvent including the redox-active material, i.e., the liquid electrolyte. The electrolyte used at the anode is called anolyte and the electrolyte supplied at the cathode is called catholyte. During operation, both electrolytes are pumped into the anode and cathode compartment, where the respective electrochemical reactions take place at the porous carbon felt current collectors. Anode and cathode are separated spatially by an ion-selective membrane (ISM), such as Nafion®, to allow for charge balancing.

In the past decade, the performance of ORFBs was increased significantly: starting with 9,10-anthraquinone-2,7-disulfonic acid (AQDS), Aziz and co-workers [12, 15] applied different quinone derivatives as anolyte-active material using aqueous sulfuric acid as solvent (open circuit voltage up to 0.94 V; power density around 1 W cm^{-2} at 90 % state of charge; bromine-based catholyte). Yang et al. [16] further combined AQDS as anolyte and 1,2-benzoquinone-3,5-disulfonic acid (BQDS) as catholyte to demonstrate the feasibility of an all-organic aqueous RFB (open circuit voltage of around 0.75 V; power density of 0.055 W cm^{-2}). Moreover, several concepts of alkaline ORFBs were reported. In these studies, derivatives of quinones [13, 17] as well as alloxazines [18] were applied together with ferricyanide/ferrocyanide to obtain theoretical open circuit voltages of up to 1.34 V.

To be economically competitive with established battery systems and to meet the system capital cost target of 150 $ per kWh [19], further improvements of cell voltage, energy density, and cycling stability are obligatory. To address these issues, many recent studies focus on the structure property relations of quinonoid compounds [20 – 25]. These studies demonstrate that the properties of quinonoid active materials can be modified as needed. For instance, the redox potential can be shifted in negative direction by electron-donating groups added to the redox-active species, while electron-withdrawing groups can evoke the opposite – a highly promising way to shape the overall cell potential by structurally modifying the active molecule. Furthermore, adding hydrophilic groups, such as sulfonic or phosphonic acid moieties, increases the solubility in aqueous solutions, which is beneficial to achieve higher energy densities.

The most important material properties and operating parameters for ORFBs are often investigated separately. To estimate the sole impact of one of the various intertwined parameters on ORFB performance is, however, not always straightforward. In this overview, the crucial parameters –

[1]Jonas D. Hofmann, Dr.-Ing. Daniel Schröder
daniel.schroeder@phys.chemie.uni-giessen.de
Justus Liebig University Giessen, Institute of Physical Chemistry, Heinrich-Buff-Ring 17, 35392 Giessen, Germany.
[2]Jonas D. Hofmann, Dr.-Ing. Daniel Schröder
Justus Liebig University Giessen, Center for Materials Research (LaMa), Heinrich-Buff-Ring 16, 35392 Giessen, Germany.

Chemie Ingenieur Technik Review

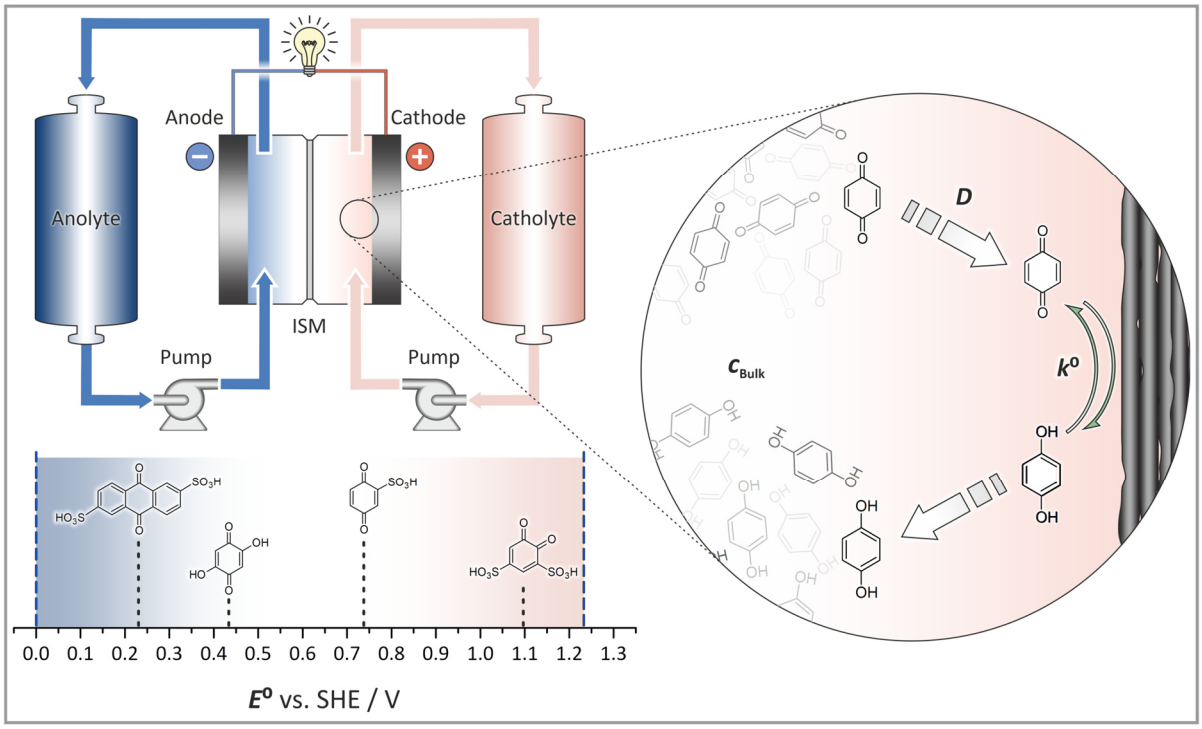

Figure 1. Schematic of a redox flow battery based on aqueous electrolytes with organic active material. It comprises two tanks for electrolyte solutions (the anolyte and the catholyte), which are pumped into the anode and cathode chamber of the battery. An ion-selective membrane (ISM) spatially separates anode and cathode and ensures ion transport. The parameters that govern the performance of the battery are the organic active material properties such as the redox potential E^0 vs. standard hydrogen electrode (SHE), bulk concentration c_{Bulk}, diffusion coefficient D, and the kinetic rate constant k^0. The depicted scale bar shows redox potentials of typical quinonoid organic molecules measured in 1 M sulfuric acid. From left to right: 9,10-anthraquinone-2,6-disulfonic acid (AQDS); 2,5-dihydroxy-1,4-benzoquinone; 1,4-benzoquinone-2-sulfonic acid; 1,2-benzoquinone-3,5-disulfonic acid (BQDS) [12 – 14].

as well as how to determine them – are highlighted one by one. In addition, their impact on the overall ORFB performance is discussed. This will help to draw conclusions for upscaling from the molecule level to the electrode interface level up to the electrode level – bridging the gap between the fundamental understanding of transport properties and electrode kinetics to the engineering of RFBs.

2 Governing Parameters for Redox Flow Battery Performance

In general, the performance of ORFBs is governed by four parameters, which are highlighted in Fig. 1: (1) the redox potential, the kinetic key figures (2) diffusion coefficient and (3) kinetic rate constant for the reaction at the electrode interface as well as (4) the solubility of the active material molecule in the solvent. In the following, these four essential parameters for ORFBs are described, an overview of the methods used for their investigation is given, and their contribution to the performance of ORFBs is assessed.

2.1 Redox Potential

Although power and capacity can be scaled independently by changing the size of the electrolyte tanks and the reaction chambers of an RFB, its energy density still needs to meet cost limits. Reasonably abundant and high-performing active materials have to be selected for the anolyte as well as for the catholyte. To achieve high cell voltages, the difference between the redox potential of both active materials needs to be as high as possible (Fig. 1). Thereby, the electrochemical stability window of water has to be kept in mind; the reactants' redox potentials should lie within the potential range of 0 to 1.23 V vs. standard hydrogen electrode (SHE) to prevent hydrogen or oxygen evolution reactions. To expand the accessible potential range, it is possible to take advantage of kinetic effects such as the hydrogen and oxygen evolution overvoltage on carbon electrodes [26, 27].

There are numerous voltammetric techniques available to determine potentials at which organic active materials are reduced or oxidized, with cyclic voltammetry (CV) being the most common one. For this method, the potential is swept continuously beyond the redox potential of the active material. The occurring charge transfer and consumption of

active material then results in a concentration gradient near the electrode surface. The concentration gradient evokes a current that rises with the proceeding potential sweep. Shortly after the scan passes the formal redox potential $E^{0'}$, the gradient and, therefore, the measured current reaches its maximum. This is followed by a relaxation of the diffusion layer and a decrease of the current, consequently [28, 29]. The resulting peak shape, e.g., as depicted in Fig. 2, is characteristic for cyclic voltammograms of diffusion-based redox reactions and can be used to extract its specific potential [30]. To close the cycle, the scan direction is inverted, which also reverts the charge transfer and generates another current peak. On the assumption that all of the associated reactants exhibit similar diffusion coefficients, the mean value of both peaks then poses a good approximation to the formal redox potential $E^{0'}$ [31]. Conclusively, CV enables a straightforward and direct comparison of different active materials and their redox potentials.

As opposed to this, density functional theory (DFT)-based calculations constitute a convenient theoretical approach to determine redox potentials of specific molecule structures. This technique considers the difference in Gibbs free energy of the reduction in solution to predict the associated potentials. As an integral part of investigations regarding the structure property relations of ORFB active materials it has been frequently used in recent publications [22, 32].

In general, electron-rich compounds are needed as anolyte for ORFBs, which implies a low redox potential (see the left hand side of the scale in Fig. 1). Since anthraquinones possess two aromatic rings that provide high electron density, they inherently exhibit low redox potentials of about 0.077 V vs. SHE [33] at a pH value of 0, which makes them a promising anolyte base structure. Several derivatives, such as AQDS, were already investigated in full-cell applications [15, 16, 20].

In contrast, excluding the electron-donating rings from the base structure results in electron-poor compounds for the right-hand side of the potential scale that may be used as catholyte active materials. BQDS, e.g., exhibits a very high formal redox potential of 1.1 V vs. SHE in 1 M sulfuric acid [14]. For this derivative, the intrinsically high redox potential of the benzoquinone base structure was shifted even further in positive direction. This is a result of the added sulfonic acid substituents and the orientation of the carbonyl group redox centers, which was changed from para to ortho [34, 35]. Nonetheless, for anolyte as well as for catholyte active materials, further structural improvements are necessary to minimize the unused potential range and to increase the cell voltage of ORFBs in the end.

2.2 Diffusion Coefficient

The diffusion of the active material towards the electrode plays an equally important role for the performance that can be attained in a full cell: for fast mass transport, especially in highly porous media such as the carbon felts used as current collectors in ORFBs, a high diffusion coefficient for transport of the organic reactants in the solvent is obligatory. To ensure a high power output, the molecules need to get to and away from the electrode as fast as possible to undergo charge transfer.

A multitude of methods can be used to determine the diffusion coefficient, albeit not all of the available techniques are universally applicable. For example, in the case of CV at macroelectrodes, the correction of faradaic currents for capacitive effects – especially for the reversal scan – is not unambiguous. Therefore, system properties that theoretically may be determined by the evaluation of peak heights of cyclic voltammograms would be afflicted with high measurement uncertainty [36]. One way to reduce the impact of the occurring double-layer capacitance during potential sweep is to utilize an ultramicroelectrode as the interfacial capacitance diminishes with decreasing electrode radius. This effect is very beneficial in particular for chronoamperometry (CA) measurements, which belong to the group of potential step techniques: a potential step is applied to the system, which electrochemically activates and consumes the reactant on the electrode surface. The resulting concentration gradient drives a current flow that decreases as the thickness of the diffusion layer changes with time. This correlation is described by the Cottrel equation (Eq. (1)), which can be solved for the diffusion coefficient, consequently [37 – 39]:

$$i(t) = \frac{nFAcD^{1/2}}{\pi^{1/2}t^{1/2}} \tag{1}$$

Here $i(t)$ is the current in A, n is the number of transferred electrons, A is the geometric area of the working electrode in cm^2, c is the concentration of the electrochemically active species in $mol\,cm^{-3}$, D is the diffusion coefficient in cm^2s^{-1} and t is the passed time in s.

Nonetheless, there are more established techniques to determine D, which are based on forced convection of the electrolyte. For these so-called hydrodynamic methods, the electrode moves with respect to the solution. In the case of rotating disc electrodes (RDEs), the electrode can be rotated at specific rates, which enables voltammetric measurements under steady-state conditions [36]. Ultimately, capacitive effects and natural convection can be minimized, which leads to more accurate and reproducible diffusion coefficients than for transient current techniques in quiescent solutions such as CV or CA. The most common form of hydrodynamic voltammetry combines linear sweep voltammetry (LSV) with an RDE. For this kind of measurement, the potential is swept linearly at different rotation rates of the working electrode. For each rotation rate, one limiting current is determined. The deviation of the resulting limiting currents is a consequence of the change in diffusion layer width. Considering the Levich equation (Eq. (2)) [40],

a plot of the measured limiting currents versus the square root of the associated rotation rates then yields a slope, which can be used to determine D.

$$i_{lim} = 0.62nFAD^{2/3}\omega^{1/2}\nu^{-1/6}c \quad (2)$$

Here, i_{lim} is the limiting current in A, ω is the angular velocity in rad s^{-1}, ν is the kinematic viscosity of the solution in cm^2s^{-1}, and the other parameters are as denoted before. The active species of the well-studied all-vanadium RFB, e.g., exhibit values for D within the range of 1.4 to $5.7 \cdot 10^{-6}$ cm^2s^{-1} in aqueous solutions of sulfuric acid [41]. These values may serve as a benchmark for upcoming organic active materials. Most of the diffusion coefficients reported in the literature for organic anolyte as well as catholyte active materials match up to these values [6, 8, 13, 42]. The majority of the relevant base structures intrinsically feature diffusion coefficients that are able to compete with the established vanadium species, which then also applies for their functionalized derivatives since changes to the base structure would impact overall diffusion insignificantly. Therefore, it should be noted at this point that the current focus of investigation could be rather on the improvement of the other three governing parameters presented in this work.

2.3 Kinetic Rate Constant

The heterogeneous kinetic rate constant k^0 for the reaction of the organic redox-active material at the electrode interface has a significant impact on ORFB performance. In combination with the diffusion coefficient it determines the mean retention time of the reactant in the electrochemical double layer before the charge transfer is completed. Therefore, high rate constants promote a fast cell reaction and allow for high current densities that can be drawn from the cell without raising overpotentials that may affect the depth of discharge as well as cell performance and stability in a wider sense.

There are several approaches based on different electrochemical techniques to determine the heterogeneous electron transfer rate constant k^0 of an occurring redox reaction. Similar to the quantities mentioned before some of these approaches involve CV measurements. For example, Nicholson and Shain proposed a voltammetric method [43], which benefits from the progressive transition from reversible to irreversible charge transfer behavior depending on the applied potential scan rate. The corresponding potential difference between anodic and cathodic peak can be compared with a working curve, which then yields the rate constant for the system of interest. A similar approach was proposed later by Rüssel et al. [44].

However, similar to the determination of diffusion coefficients described above, hydrodynamic measurements may be used to determine k^0 as an alternative to transient current methods. After a linear potential sweep at different rotation rates, the data can be evaluated further to extract the exchange current density and the heterogeneous rate constant according to the Koutecký-Levich and Tafel equation [40, 45].

Organic active materials generally exhibit high kinetic rate constants, which stand for very fast charge transfer reactions: values of up to $7.2 \cdot 10^{-3}$ cm s^{-1} were reported for anthraquinone derivatives, which may be related to low reorganization energies that are required for the aromatic π system [12, 32]. This allows to surpass the rate constant of a large number of inorganic redox couples by several orders of magnitude [41]. Even quinonoid compounds with less extensive aromatic systems, such as benzoquinones, still exhibit rate constants of around 10^{-4} cm s^{-1} [42], which still match up with already established systems (compare with $3.0 \cdot 10^{-7}$ cm s^{-1} for VO_2^+/VO^{2+} [41]). Overall, these values imply fast kinetics that enable high current densities in the absence of major voltage losses. Preserving this advantage against inorganic or nonaqueous systems may be very beneficial for the commercial launch of ORFBs.

2.4 Solubility of Active Material

To fulfill the economical requirements and to be competitive with more established energy storage systems, ORFBs need to exhibit sufficient energy and power densities. Therefore, the amount of active species that can be stored per volume unit of the electrolyte solution and converted at a time plays a major role to achieve these goals. The maximum active material concentration is a decisive factor for the overall performance of ORFBs. For instance, together with k^0, the amount of active substance transported per volume of electrolyte determines the maximum current density that can be withdrawn from the cell at a certain pump rate without provoking reactant depletion and voltage losses. Besides some of the aforementioned electrochemical methods, ultraviolet-visible (UV-vis) spectroscopy, making use of the concentration-dependent absorbance of a solution [46, 47], is a well-suited technique to determine the maximum concentration of an organic active material in a certain solvent.

It should be noted that measures to increase the reactant solubility by structural modification of the base molecule also affect a multitude of other parameters: starting from the blank anthraquinone, which is nearly insoluble in water (0.006 g L^{-1}) [33], hydrophilic substituents, e.g., sulfonic or phosphonic acid groups, can be utilized to increase the solvation free energy ΔG^0_{solv} considerably [22]. Nevertheless, for AQDS and its sulfonic acid derivatives, this also implicates a positive redox potential shift of about 50 mV per moiety [20]. In the case of low-potential anolyte active materials this would mean a decrease of the cell voltage in return for the increased solubility. Furthermore, hydrophilic substituents – depending on their position relative to the

carbonyl group redox centers – may also have a detrimental impact on the charge transfer kinetics caused by intramolecular hydrogen bonding interactions [14]. As a result of the enhanced polarity, the interaction between solvent and active material as well as the individual molecules also increases, which in turn negatively affects the diffusion of reactants. These implications of structural functionalization need to be considered in any case. Organic reactants such as AQDS already exhibit a reasonable solubility of up to $1\,mol\,L^{-1}$ in aqueous solutions combined with promising cycling performances [16]. However, it should be kept in mind that such high active material concentrations and, as a consequence thereof, increased intermolecular interactions may prevent that the complete charge can be retained during cycling [48]. Furthermore, it should be noted that the solubility of the active material also depends on the present temperature in the system. Whereas low temperatures are commonly detrimental for the maximum solubility of the active material, elevated temperatures may not only promote solvation but might also lead to decomposition and to precipitation of solid material as in the case of vanadium [49 – 51]. To overcome these limitations, it may be necessary to apply measures for temperature control or to modify the solvent composition [52].

Conclusively, the maximum active material concentration has a very strong impact on other key parameters and, thus, on the overall ORFB performance. For applications that demand high peak currents, high active material concentrations are obligatory. However, from an economical point of view, the reactant solubility does hardly affect the costs per kWh, which is why already existing compounds like AQDS still remain competitive with higher concentrated systems in economic terms. In fact, with about $50\,\$\,kWh^{-1}$, the estimated capital costs of aqueous electrolytes based on quinones and other organic active materials amount to less than one third of the cost of an all-vanadium electrolyte [53].

2.5 Solvent-Related Effects on the Governing Parameters and Their Determination

Apart from the active material structure, the used solvent and its associated features pose a versatile tool to optimize the properties and performance of an ORFB electrolyte. As will be described in the following section, solvent characteristics such as polarity, acidity as well as viscosity dictate the complexation, charge transfer behavior, and mobility of the active material in solution [54]. To emphasize this observation, own work on the impact of the applied solvent and concomitant pH value on the governing parameters as well as the pitfalls of their investigation are presented.

As a general rule, the proton activity or pH value of a solution both directly and indirectly affects a multitude of parameters relevant for the performance of a full cell. In alkaline media, the high pH value promotes the deprotonation of protic moieties, which increases the overall solubility in aqueous environments. On the other hand, in acidic media (low pH values), protons directly take part in the redox reaction of quinones, which in line with the Nernst equation affects the redox potential of the molecule. The contribution of protons in the occurring redox reaction furthermore has an immediate effect on the charge transfer kinetics of quinonoid electroactive molecules. In aprotic as well as alkaline aqueous solutions, quinones solely undergo a subsequent two-electron transfer to form the dianion as final product [54, 55]. However, when a structure-specific proton activity (pK_a value) is attained, the electron transfer is being accompanied by additional protonation reactions, which implicates a so-called potential inversion [56]. The potential inversion implies that an originally occurring stepwise two-electron transfer will proceed as a simultaneous two-electron transfer. In the case of quinone reduction this results in the following. In the first step, the quinone is reduced to the semiquinone anion radical. If an excess of protons is available in acidic solution, the semiquinone anion radical accepts a proton from the acidic solution. The now protonated compound is much easier to be reduced further than the quinone in its initial state. Hence, the associated current for the resulting simultaneous two-electron transfer is observed at one single potential value, whereas the original stepwise two-electron transfer in the absence of potential inversion would be observed at two separate redox potentials [57].

For extensive aromatic systems such as anthraquinones, this effect is very beneficial since it boosts the charge transfer kinetics, making it a fast and highly driven process. As opposed to this trend, the overall reaction rate for smaller quinone compounds, such as benzoquinones, may even decrease due to potential inversion. This decrease may be attributed to their comparably confined aromatic system, which does not allow for an efficient charge delocalization and, hence, stabilization of the intermediate semiquinone radical (for further information see also [58 – 60]). Consequently, the complex structure and solvent specific interplay of the governing parameters has to be taken into account regarding the overall full-cell performance.

As already implied, the charge transfer characteristics of quinones are dominated by the transfer of two electrons. As a matter of fact, analyzing CV data for more than one electron transfer is not always straightforward because multiple processes occur simultaneously, making it difficult to extract the parameters of interest. This issue will be pointed out on the basis of own measurements. All methods and parameters used for the experiments are as previously reported by Hofmann et al. [32]. Fig. 2 shows cyclic voltammograms of the methoxy-substituted 2,3-diaza-anthraquinone (DAQ) measured in different media. DAQs in line with other quinones undergo a two-electron transfer during reduction [55].

For redox reactions comprising multiple electron transfers, two distinct scenarios may be valid: the case of subse-

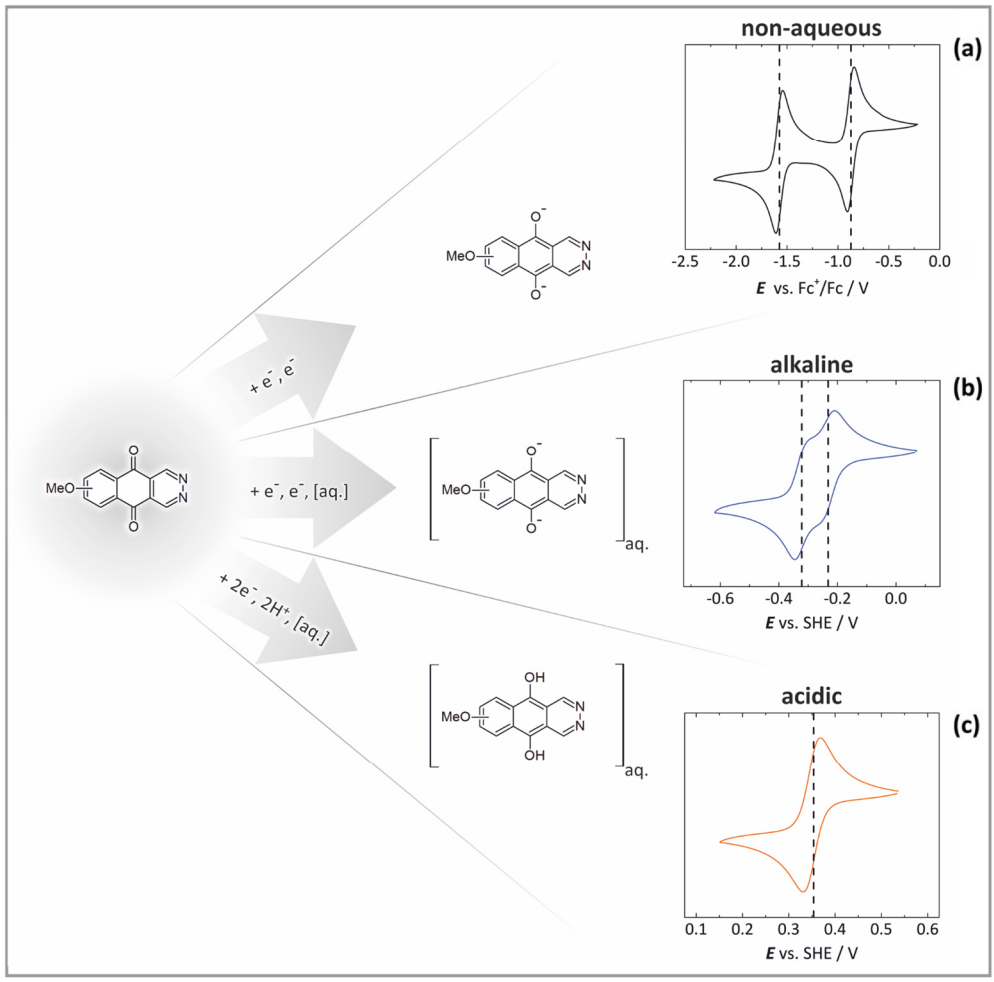

Figure 2. Impact of nature and pH value of the applied solvent on the charge transfer characteristics of the molecule class of diaza-anthraquinones introduced recently by Hofmann et al. [32]: cyclic voltammograms of 0.5 mM methoxy-substituted 2,3-diaza-anthraquinone in a) 0.1 M tetrabutylammonium hexafluorophosphate/acetonitrile, b) 1 M KOH, and c) 2 M H_2SO_4. As illustrated by the varying current responses, the applied solvent dictates complexation, redox chemistry and consequently the charge transfer behavior of the active material.

quent charge transfer and the case of highly driven simultaneous charge transfer. To begin with, it is assumed that both electron transfers occur at potentials well separated from each other. As soon as there is a chance to apply sufficiently positive or negative potentials to ensure full depletion of the substrate on the electrode surface, the electron transfers and the associated oxidation states can be investigated independently. As depicted in Fig. 2a, this holds true for DAQs in nonaqueous solvents where the two distinct electron transfers are separated by more than 700 mV. With respect to electrostatic effects, this seems reasonable, since it takes a certain activation energy to add another electron to a molecule that is already negatively biased after the first reduction [57]. Due to the clear separation of both processes, the relevant quantities can be determined by an individual evaluation of the two subsequent single-electron transfers using techniques such as CV, CA, or LSV (RDE) [58].

For the second scenario, it is assumed that a simultaneous charge transfer takes place. Thus, the number of transferred electrons takes on an integer value of two in the equations relying on the aforementioned experimental methods. Thus, the relevant quantities of the investigated species can unequivocally be determined here as well [36, 61]. This case holds for the reduction of DAQs in acidic aqueous environment (Fig. 2c). Due to hydrogen bonding effects and protonation-driven potential inversion, the two individual processes seen in Fig. 2a converge. As a result, only a single wave with a peak separation close to the theoretical value of 29 mV – postulated by the Nernst equation for a two-electron process – can be attained. On the assumption of fast

protonation equilibria and a low stability of potential intermediates, the two-electron transfer is considered to be highly driven and simultaneous [59, 62].

Under certain conditions, multiple charge transfers do not meet the requirements for a simultaneous process nor is a clear distinction between the individual transfers feasible. This holds, e.g., for the redox reaction of DAQs in alkaline solution. As depicted in Fig. 2b, despite the stabilization induced by hydrogen bonding, the two individual waves do not merge fully, which is due to the absence of protonation in alkaline environment. As a consequence, relevant quantities of the associated processes, such as exact redox potentials and kinetic rate constants, cannot be accessed any longer by the aforementioned conventional experimental methods.

Nevertheless, to extract relevant kinetic information out of the given low overpotential regime, digital simulation might be applied. Software such as Digisim® (BASi) or DigiElch® (Gamry Instruments) enables the simulation of current responses emanating from different charge transfer scenarios: individual chemical and electronic processes that may occur during a potential scan can be combined to reconstruct the characteristics seen in the experiment. Extended versions of these programs allow for least-squares fitting of single measurements and the extraction of kinetic information by nonlinear regression algorithms taking into account several measurements under varied conditions. Commonly, there is a huge number of parameters that need to be determined at a time, which emphasizes the significance of experimental values to support the results attained by simulation. Especially in the case of multiple electron transfers in combination with proton transfer reactions, it remains difficult to unambiguously fit voltammograms to a specific set of parameters [63, 64]. Conclusively, electrochemical simulation software is considered to be a versatile tool to analyze complex charge transfer scenarios albeit it remains crucial to check the validity of the applied model assumptions on the basis of experimental results.

3 Conclusions

In this work, it was shown that redox potential, kinetic rate constant, diffusion coefficient, and solubility are highly complex measures and are particularly intertwined for redox flow batteries with organic active material. Apart from that, a multitude of experimental and theoretical methods exist for determination of these parameters. It is always challenging to identify in each case, which parameter is the governing one for the performance of energy systems with novel redox-active materials – especially if various solvents might be applicable and are of interest in view of cost efficiency. In the end, it becomes evident that in combination with a specific active material structure, the nature of the applied solvent impacts the overall ORFB performance the most, since it can have a great impact on basically all of the presented key properties/parameters. Consequently, further compatible and high-performing combinations of molecule structure and solvent have to be investigated to increase the performance and economic viability of ORFBs. By and large, much effort is needed in future research and development for organic chemists, materials scientists as well as for chemical engineers to propel the redox flow battery as promising device for future energy conversion and storage.

The authors gratefully acknowledge financial support by BMEL (Federal Ministry of Food and Agriculture) within the project FOREST (22403116) and by Fonds der Chemischen Industrie within Material Cost Allowances, and thank Daniel Stock for fruitful discussions.

Jonas D. Hofmann received his master's degree in material science from the Justus-Liebig University Giessen. There, he is currently a PhD candidate at the Institute of Physical Chemistry under the supervision of Prof. Jürgen Janek and Dr.-Ing. Daniel Schröder. His research interests include aqueous redox-flow batteries and the characterization of sustainable organic active materials to increase their energy efficiency and cycling stability for stationary energy storage applications.

Daniel Schröder is a process engineer and received his education at the Otto-von-Guericke University Magdeburg and the Max Planck Institute for Dynamics of Complex Technical Systems in Magdeburg. In 2015, he received his PhD in process engineering from TU Braunschweig, working on secondary zinc-oxygen batteries. Afterwards, he joined the Institute of Physical Chemistry at Justus-Liebig University Giessen as junior group leader. His research group focuses on fundamental understanding and improving of redox-flow batteries, as well as lithium-, sodium-, and zinc-based next-generation batteries by using model-based and operando techniques.

Symbols used

A	[cm^2]	geometric area
c	[mol cm^{-3}]	concentration of the electrochemically active species
c_{Bulk}	[mol L^{-1}]	bulk active material concentration
D	[$cm^2 s^{-1}$]	diffusion coefficient
E^0	[V]	redox potential
$E^{0'}$	[V]	formal redox potential
F	[C mol^{-1}]	Faraday constant
$i(t)$	[A]	Cottrell current
i_{lim}	[A]	hydrodynamic limiting current
k^0	[cm s^{-1}]	kinetic rate constant
n	[–]	number of transferred electrons
t	[s]	time

Greek symbols

ν	[$cm^2 s^{-1}$]	kinematic viscosity
ω	[rad s^{-1}]	angular velocity

Abbreviations

AQDS	9,10-anthraquinone-2,7-disulfonic acid
BQDS	1,2-benzoquinone-3,5-disulfonic acid
CA	chronoamperometry
CV	cyclic voltammetry
DAQ	diaza-anthraquinone
DFT	density functional theory
ISM	ion-selective membrane
LSV	linear sweep voltammetry
ORFB	redox flow battery based on aqueous electrolytes with organic active material
RDE	rotating disc electrode
RFB	redox flow battery
SHE	standard hydrogen electrode
TEMPO	(2,2,6,6-tetramethylpiperidin-1-yl)oxyl
UV-vis	ultraviolet-visible

References

[1] R. Ye, D. Henkensmeier, S. J. Yoon, Z. Huang, D. K. Kim, Z. Chang, S. Kim, R. Chen, *J. Electrochem. Energy Convers. Storage* **2017**, *15 (1)*, 010801. DOI: https://doi.org/10.1115/1.4037248

[2] X. Wei, W. Duan, J. Huang, L. Zhang, B. Li, D. Reed, W. Xu, V. Sprenkle, W. Wang, *ACS Energy Lett.* **2016**, *1 (4)*, 705 – 711. DOI: https://doi.org/10.1021/acsenergylett.6b00255

[3] D. Schmidt, B. Häupler, C. Friebe, M. D. Hager, U. S. Schubert, *Polymer* **2015**, *68*, 321 – 327. DOI: https://doi.org/10.1016/j.polymer.2015.05.028

[4] E. J. Son, J. H. Kim, K. Kim, C. B. Park, *J. Mater. Chem. A* **2016**, *4 (29)*, 11179 – 11202. DOI: https://doi.org/10.1039/C6TA03123D

[5] P. Leung, A. A. Shah, L. Sanz, C. Flox, J. R. Morante, Q. Xu, M. R. Mohamed, C. Ponce de León, F. C. Walsh, *J. Power Sources* **2017**, *360*, 243 – 283. DOI: https://doi.org/10.1016/j.jpowsour.2017.05.057

[6] T. Janoschka, N. Martin, M. D. Hager, U. S. Schubert, *Angew. Chem., Int. Ed.* **2016**, *55 (46)*, 14427 – 14430. DOI: https://doi.org/10.1002/anie.201606472

[7] T. Liu, X. Wei, Z. Nie, V. Sprenkle, W. Wang, *Adv. Energy Mater.* **2016**, *6 (3)*, 1501449. DOI: https://doi.org/10.1002/aenm.201501449

[8] B. Hu, C. DeBruler, Z. Rhodes, T. L. Liu, *J. Am. Chem. Soc.* **2017**, *139 (3)*, 1207 – 1214. DOI: https://doi.org/10.1021/jacs.6b10984

[9] J. J. Bozell, *Top. Curr. Chem.* **2014**, *353*, 229 – 255. DOI: https://10.1007/128_2014_535

[10] H. Zhu, L. Wang, Y. Chen, G. Li, H. Li, Y. Tang, P. Wan, *RSC Adv.* **2014**, *4 (56)*, 29917 – 29924. DOI: https://doi.org/10.1039/C4RA03793F

[11] C. Awungacha Lekelefac, N. Busse, M. Herrenbauer, P. Czermak, *Int. J. Photoenergy* **2015**, *2015*, 137634. DOI: https://doi.org/10.1155/2015/137634

[12] B. Huskinson, M. P. Marshak, C. Suh, S. Er, M. R. Gerhardt, C. J. Galvin, X. Chen, A. Aspuru-Guzik, R. G. Gordon, M. J. Aziz, *Nature* **2014**, *505 (7482)*, 195 – 198. DOI: https://doi.org/10.1038/nature12909

[13] Q. Chen, M. R. Gerhardt, L. Hartle, M. J. Aziz, *J. Electrochem. Soc.* **2016**, *163 (1)*, A5010 – A5013. DOI: https://doi.org/10.1149/2.0021601jes

[14] B. Yang, L. Hoober-Burkhardt, S. Krishnamoorthy, A. Murali, G. K. S. Prakash, S. R. Narayanan, *J. Electrochem. Soc.* **2016**, *163 (7)*, A1442 – A1449. DOI: https://doi.org/10.1149/2.1371607jes

[15] K. Lin et al., *Science* **2015**, *349 (6255)*, 1529 – 1532. DOI: https://doi.org/10.1126/science.aab3033

[16] Z. Yang, L. Tong, D. P. Tabor, E. S. Beh, M.-A. Goulet, D. De Porcellinis, A. Aspuru-Guzik, R. G. Gordon, M. J. Aziz, *Adv. Energy Mater.* **2018**, *8 (8)*, 1702056. DOI: https://doi.org/10.1002/aenm.201702056

[17] K. Lin, R. Gómez-Bombarelli, E. S. Beh, L. Tong, Q. Chen, A. Valle, A. Aspuru-Guzik, M. J. Aziz, R. G. Gordon, *Nat. Energy* **2016**, *1 (9)*, 16102. DOI: https://doi.org/10.1038/nenergy.2016.102

[18] *Grid Energy Storage*, U.S. Department of Energy, Washington, D.C. **2013**. www.energy.gov/sites/prod/files/2014/09/f18/Grid%20Energy%20Storage%20December%202013.pdf

[19] M. R. Gerhardt, L. Tong, R. Gómez-Bombarelli, Q. Chen, M. P. Marshak, C. J. Galvin, A. Aspuru-Guzik, R. G. Gordon, M. J. Aziz, *Adv. Energy Mater.* **2017**, *7 (8)*, 1601488. DOI: https://doi.org/10.1002/aenm.201601488

[20] M. T. Huynh, C. W. Anson, A. C. Cavell, S. S. Stahl, S. Hammes-Schiffer, *J. Am. Chem. Soc.* **2016**, *138 (49)*, 15903 – 15910. DOI: https://doi.org/10.1021/jacs.6b05797

[21] S. Er, C. Suh, M. P. Marshak, A. Aspuru-Guzik, *Chem. Sci.* **2015**, *6 (2)*, 885 – 893. DOI: https://doi.org/10.1039/C4SC03030C

[22] Y. Ding, Y. Li, G. Yu, *Chem* **2016**, *1 (5)*, 790 – 801. DOI: https://doi.org/10.1016/j.chempr.2016.09.004

[23] J. E. Bachman, L. A. Curtiss, R. S. Assary, *J. Phys. Chem. A* **2014**, *118 (38)*, 8852 – 8860. DOI: https://doi.org/10.1021/jp5060777

[24] S. D. Pineda Flores, G. C. Martin-Noble, R. L. Phillips, J. Schrier, *J. Phys. Chem. C* **2015**, *119 (38)*, 21800 – 21809. DOI: https://doi.org/10.1021/acs.jpcc.5b05346

[25] B. Yang, L. Hoober-Burkhardt, F. Wang, G. K. S. Prakash, S. R. Narayanan, *J. Electrochem. Soc.* **2014**, *161 (9)*, A1371 – A1380. DOI: https://doi.org/10.1149/2.1001409jes

[26] Z. Yang, J. Zhang, M. C. W. Kintner-Meyer, X. Lu, D. Choi, J. P. Lemmon, J. Liu, *Chem. Rev.* **2011**, *111 (5)*, 3577 – 3613. DOI: https://doi.org/10.1021/cr100290v

[27] J. Noack, N. Roznyatovskaya, T. Herr, P. Fischer, *Angew. Chem., Int. Ed.* **2015**, *54 (34)*, 9776 – 9809. DOI: https://doi.org/10.1002/anie.201410823

[28] B. Speiser, *Chem. Unserer Zeit* **1981**, *15 (1)*, 21 – 26. DOI: https://doi.org/10.1002/ciuz.19810150105
[29] B. Speiser, *Chem. Unserer Zeit* **1981**, *15 (2)*, 62 – 67. DOI: https://doi.org/10.1002/ciuz.19810150206
[30] N. Elgrishi, K. J. Rountree, B. D. McCarthy, E. S. Rountree, T. T. Eisenhart, J. L. Dempsey, *J. Chem. Educ.* **2018**, *95 (2)*, 197 – 206. DOI: https://doi.org/10.1021/acs.jchemed.7b00361
[31] F. Scholz, *Electroanalytical Methods: Guide to Experiments and Applications*, Springer, Heidelberg **2009**.
[32] J. D. Hofmann, F. L. Pfanschilling, N. Krawczyk, P. Geigle, L. Hong, S. Schmalisch, H. A. Wegner, D. Mollenhauer, J. Janek, D. Schröder, *Chem. Mater.* **2018**, *30 (3)*, 762 – 774. DOI: https://doi.org/10.1021/acs.chemmater.7b04220
[33] J. Revenga, F. Rodríguez, J. Tijero, *J. Electrochem. Soc.* **1994**, *141 (2)*, 330 – 333. DOI: https://doi.org/10.1149/1.2054725
[34] X.-Q. Zhu, C.-H. Wang, *J. Org. Chem.* **2010**, *75 (15)*, 5037 – 5047. DOI: https://doi.org/10.1021/jo100735s
[35] S. Gottis, A.-L. Barrès, F. Dolhem, P. Poizot, *ACS Appl. Mater. Interfaces* **2014**, *6 (14)*, 10870 – 10876. DOI: https://doi.org/10.1021/am405470p
[36] A. J. Bard, L. R. Faulkner, *Electrochemical Methods: Fundamentals and Applications*, John Wiley & Sons, New York **2000**.
[37] C. G. Zoski, *Handbook of Electrochemistry*, Elsevier, Amsterdam **2007**.
[38] C. H. Hamann, *Elektrochemie*, Wiley-VCH, Weinheim **2005**.
[39] J. E. Baur, R. M. Wightman, *J. Electroanal. Chem. Interfacial Electrochem.* **1991**, *305 (1)*, 73 – 81. DOI: https://doi.org/10.1016/0022-0728(91)85203-2
[40] V. G. Levich, *Physicochemical Hydrodynamics*, Prentice-Hall, Englewood Cliffs, NJ **1962**.
[41] A. Z. Weber, M. M. Mench, J. P. Meyers, P. N. Ross, J. T. Gostick, Q. Liu, *J. Appl. Electrochem.* **2011**, *41 (10)*, 1137 – 1164. DOI: https://doi.org/10.1007/s10800-011-0348-2
[42] L. Hoober-Burkhardt, S. Krishnamoorthy, B. Yang, A. Murali, A. Nirmalchandar, G. K. S. Prakash, S. R. Narayanan, *J. Electrochem. Soc.* **2017**, *164 (4)*, A600 – A607. DOI: https://doi.org/10.1149/2.0351704jes
[43] R. S. Nicholson, *Anal. Chem.* **1965**, *37 (11)*, 1351 – 1355. DOI: https://doi.org/10.1021/ac60230a016
[44] C. Rüssel, W. Jaenicke, *Electrochim. Acta* **1982**, *27 (12)*, 1745 – 1750. DOI: https://doi.org/10.1016/0013-4686(82)80173-4
[45] J. Tafel, *Z. Phys. Chem.* **1905**, *50A*, 641.
[46] P. Atkins, J. de Paula, *Atkins' Physical Chemistry*, Oxford University Press, Oxford **2010**.
[47] L. Tong, Q. Chen, A. A. Wong, R. Gómez-Bombarelli, A. Aspuru-Guzik, R. G. Gordon, M. J. Aziz, *Phys. Chem. Chem. Phys.* **2017**, *19 (47)*, 31684 – 31691. DOI: https://doi.org/10.1039/C7CP05881K
[48] T. J. Carney, S. J. Collins, J. S. Moore, F. R. Brushett, *Chem. Mater.* **2017**, *29 (11)*, 4801 – 4810. DOI: https://doi.org/10.1021/acs.chemmater.7b00616
[49] M. Skyllas-Kazacos, *J. Power Sources* **2003**, *124 (1)*, 299 – 302. DOI: https://doi.org/10.1016/S0378-7753(03)00621-9
[50] F. Rahman, M. Skyllas-Kazacos, *J. Power Sources* **2009**, *189 (2)*, 1212 – 1219. DOI: https://doi.org/10.1016/j.jpowsour.2008.12.113
[51] F. Rahman, M. Skyllas-Kazacos, *J. Power Sources* **1998**, *72 (2)*, 105 – 110. DOI: https://doi.org/10.1016/S0378-7753(97)02692-X
[52] L. Li, S. Kim, W. Wang, M. Vijayakumar, Z. Nie, B. Chen, J. Zhang, G. Xia, J. Hu, G. Graff, M. J. Aziz, *Adv. Energy Mater.* **2011**, *1 (3)*, 394 – 400. DOI: https://doi.org/10.1002/aenm.201100008
[53] D. G. Kwabi, K. Lin, Y. Ji, E. F. Kerr, M.-A. Goulet, D. De Porcellinis, D. P. Tabor, D. A. Pollack, A. Aspuru-Guzik, R. G. Gordon, M. J. Aziz, *Joule* **2018**, *2 (9)*, P1894 – P1906. DOI: https://doi.org/10.1016/j.joule.2018.07.005
[54] N. Gupta, H. Linschitz, *J. Am. Chem. Soc.* **1997**, *119 (27)*, 6384 – 6391. DOI: https://doi.org/10.1021/ja970028j
[55] P. S. Guin, S. Das, P. C. Mandal, *Int. J. Electrochem.* **2011**, *2011*, 816202. DOI: https://doi.org/10.4061/2011/816202
[56] D. H. Evans, *Chem. Rev.* **2008**, *108 (7)*, 2113 – 2144. DOI: https://doi.org/10.1021/cr068066l
[57] M. Quan, D. Sanchez, M. F. Wasylkiw, D. K. Smith, *J. Am. Chem. Soc.* **2007**, *129 (42)*, 12847 – 12856. DOI: https://doi.org/10.1021/ja0743083
[58] Y.-R. Kim, R. S. Kim, S. K. Kang, M. G. Choi, H. Y. Kim, D. Cho, J. Y. Lee, S.-K. Chang, T. D. Chung, *J. Am. Chem. Soc.* **2013**, *135 (50)*, 18957 – 18967. DOI: https://doi.org/10.1021/ja410406e
[59] R. S. Kim, T. D. Chung, *Bull. Korean Chem. Soc.* **2014**, *35 (11)*, 3143 – 3155. DOI: https://doi.org/10.5012/bkcs.2014.35.11.3143
[60] A. E. Alegría, M. López, N. Guevara, *J. Chem. Soc., Faraday Trans.* **1996**, *92 (24)*, 4965 – 4968. DOI: https://doi.org/10.1039/FT9969204965
[61] R. G. Compton, C. E. Banks, *Understanding Voltammetry*, Imperial College Press, London **2010**.
[62] J. R. T. Johnsson Wass, E. Ahlberg, I. Panas, D. J. Schiffrin, *J. Phys. Chem. A* **2006**, *110 (5)*, 2005 – 2020. DOI: https://doi.org/10.1021/jp055414z
[63] C. Batchelor-McAuley, B. R. Kozub, D. Menshykau, R. G. Compton, *J. Phys. Chem. C* **2011**, *115 (3)*, 714 – 718. DOI: https://doi.org/10.1021/jp1096585
[64] C. Costentin, M. Robert, J.-M. Savéant, *Chem. Rev.* **2010**, *110 (12)*, PR1 – PR40. DOI: https://doi.org/10.1021/cr100038y

1.5 State of the art and potential limits of quinone active materials in ORFBs

As implied earlier, the research field of aqueous redox flow batteries based on quinonoid active materials is a quite recent one. The associated research gained attraction not until the pioneering work of Yang *et al*.[50] and Huskinson *et al*.[39] in the year 2014. Both research groups presented the approach of an anthraquinone-based electrolyte for the low-potential side of a redox flow battery. The derivative, commonly abbreviated as AQDS, was equipped with two sulfonic acid moieties to improve the solubility in aqueous solution. Yang *et al*. further utilized a quinone-based catholyte, capitalizing on ORFBs completely based on quinonoid active materials – an approach that should be pursued exclusively by this working group in the following years. Other research groups primarily focused on the use of quinone derivatives as anolyte active materials. Several studies were published with regard to basic[40,41,43,214], acidic[34,215,216] and also neutral aqueous solution[36,37,217–219]. Great improvements have been reported considering the resilience against detrimental side reactions such as nucleophilic substitution or Michael addition. However, these efforts solely relate to the comparably electron-rich quinone species, which were applied as anolyte active materials. The range of applied catholyte active materials is considerably limited to the highly hazardous bromine and rather bulky metal-based coordination compounds such as ferrocene or ferrocyanide. The reason for this lies in the overall susceptibility of organic compounds against nucleophilic side reactions: these processes can be excluded easier in the case of intrinsically more electron-rich compounds such as the primarily used homocyclic AQ derivatives.[44] Consequently, the hardest task on the way to all-quinone ORFBs will be to identify structural motifs that combine a high electron affinity with a high cycling stability.

The theoretical framework for the design of potential catholyte active materials was already revealed by a large number of studies focusing on the computational as well as experimental analysis of the structure-property relationship of quinones.[189–191,193] These studies focused on the impact of the nature and position of specific substituents on the redox potential as well as the water solubility of varying quinone base structures. The observed trends were found to be well-reflected by experimental results.[32,220] Electron-withdrawing functional groups such as nitro, sulfonic and phosphonic acid groups shift the redox potential to more positive values, enabling the design of promising high-potential materials. Relating back to the work of Yang *et al*., different BQ species were investigated as potential catholyte active materials, including 1,2-benzoquinone-3,5-disulfonic acid (BQDS) and the electrochemically more stable DHDMBS (3,6-dihydroxy-2,4-dimethylbenzenesulfonic acid).[47–49]

However, all of the so far proposed quinonoid catholyte materials failed to offer high redox potentials with a high cycling stability.[7,46] Since regular quinones – despite the opportunities given by the addition of specific functional groups – are struggling to fulfill these requirements, different

structural motifs are obligatory. In that respect, heterocyclic alternatives to the established quinone base structures may offer opportunities to create novel quinonoid active materials towards efficient and sustainable energy storage.

2 Results and Discussion

At the beginning of this PhD project, only a small number of quinone species was applied successfully as the active material of ORFBs.[39,50] This proof of concept motivated further research aiming to improve the energy density of ORFBs on the basis of different structural motifs. In this context, the redox potential as well as the solubility of quinone active species were identified as significant key properties. Consequently, combined experimental and computational studies investigated the structure-property-relationships of different quinone species.[189,190,193] The reported structures were limited to homocyclic quinonoid base structures such as AQs, NQs and BQs, which were altered by the addition of peripheral substituents. This approach allowed for an adjustment of the general properties determined by the respective base structure. However, the influence of the peripheral substituents is limited with respect to the tailoring of active species with specific electrochemical properties. The design of alternative base structures on the other hand is a promising approach to deliver access to novel active materials with vastly different properties, since the characteristics of an organic active species are predominantly defined by its backbone.

In this light, novel quinone base structures were developed and characterized as part of the joint project FOREST (Future Organic Electrolyte for Energy Storage) funded by the BMEL (Federal Ministry of Food and Agriculture). The methods for the synthesis of these compounds were developed at the Institute of Organic Chemistry at the Justus Liebig University Giessen within the research group of Professor Wegner. The concepts and methods for the physico- and electrochemical characterization of the resulting structural motifs were developed by the author of this work within the research group of Professor Janek at the Institute of Physical Chemistry at the Justus Liebig University Giessen. In this context, the results presented in the following section constitute the basis of this thesis. These results comprise two scientific publications elucidating the design and characterization of nitrogen-based quinone analogues as well as further investigations on the reduction mechanism of diaza-quinones in different solvents.

2.1 Publication II: Quest for Organic Active Materials for Redox Flow Batteries: 2,3-Diaza-anthraquinones and Their Electrochemical Properties

This publication introduces the compound class of DAAQs as possible active species for ORFBs. To gain a fundamental understanding of their structure-property relationships, three derivatives were investigated at varying pH values. Performance-relevant quantities – such as redox potential, diffusion coefficient and kinetic rate constant – were determined by means of cyclic voltammetry and hydrodynamic measurements.

In acidic solution, the results revealed a distinct positive potential shift of about 300 mV for DAAQs compared to their homocyclic analogues. In alkaline solution an extraordinary charge transfer behavior was observed: a graduation of the commonly concerted two electron transfers implies an increased stabilization of the intermediate semiquinone species as compared to homocyclic AQs. Besides, all the investigated derivatives were found to exhibit competitive diffusion coefficients and kinetic rate constants, implying the applicability of DAAQs with respect to fast energy conversion in ORFBs. As a proof of concept, the investigated derivatives were further subjected to full-cell measurements. In addition, a DFT-based model was established to theoretically describe the structure-property relationships of DAAQs. Conclusively, the electro- and physicochemical properties of the heterocyclic DAAQs were thoroughly investigated, revealing their beneficial properties for stationary storage applications.

The concepts and experiments of the electrochemical characterization of DAAQs for this publication were developed by the author of this thesis under the supervision of D. Schröder and J. Janek. The paper was written by the first author and edited by the nine co-authors. The full-cell experiments were conducted by F. L. Pfanschilling under my supervision. The synthetic methods of the investigated diaza-anthraquinone derivatives were developed by the research group of H. A. Wegner. The compounds were synthesized by L. Hong and S. Schmalisch. D. Mollenhauer and S. Schwan contributed the DFT calculations on the redox potentials of the investigated active materials. H. A. Wegner, N. Krawczyk and P. Geigle contributed to the scientific discussions. Reprinted with permission from *Chemistry of Materials*.

J. D. Hofmann, F. L. Pfanschilling, N. Krawczyk, P. Geigle, L. Hong, S. Schmalisch, H. A. Wegner, D. Mollenhauer, J. Janek, D. Schröder, Quest for Organic Active Materials for Redox Flow Batteries: 2,3-Diaza-Anthraquinones and Their Electrochemical Properties. *Chem. Mater.*, **2018**, *30* (3), 762–774.

CHEMISTRY OF MATERIALS
Cite This: Chem. Mater. 2018, 30, 762−774
Article
pubs.acs.org/cm

Quest for Organic Active Materials for Redox Flow Batteries: 2,3-Diaza-anthraquinones and Their Electrochemical Properties

Jonas D. Hofmann,[†] Felix L. Pfanschilling,[†] Nastaran Krawczyk,[‡] Peter Geigle,[‡] Longcheng Hong,[§] Sebastian Schmalisch,[§] Hermann A. Wegner,[§,∥] Doreen Mollenhauer,[†,∥] Jürgen Janek,*[,†,∥] and Daniel Schröder*[,†,∥]

[†]Institute of Physical Chemistry, Justus Liebig University Giessen, Heinrich-Buff-Ring 17, 35392 Giessen, Germany
[‡]CMBlu Projekt AG, Industriestraße 19, 63755 Alzenau, Germany
[§]Institute of Organic Chemistry, Justus Liebig University Giessen, Heinrich-Buff-Ring 17, 35392 Giessen, Germany
[∥]Center for Materials Research, Justus Liebig University Giessen, Heinrich-Buff-Ring 16, 35392 Giessen, Germany

Supporting Information

ABSTRACT: To be competitive with other electrically rechargeable large scale energy storage, the range of active materials for redox flow batteries is currently expanded by organic compounds—this holds especially for the redox active material class of quinones that can be derived from naturally abundant resources at low cost. Here we propose the modified quinone 2,3-diaza-anthracenedione, and two of its derivatives, as a promising active material for aqueous redox flow batteries. We systematically study the electrochemical performance (redox potentials, rate constants, diffusion coefficients) for these three compounds at different pH values experimentally and complement the results with density functional calculations: A positive redox potential shift of about 300 mV is achieved by the incorporation of a diaza moiety into the anthraquinone base structure. Our experiments at low pH show that the addition of a methoxy group to the base structure of the 2,3-diaza-anthracenedione strongly increases the electrochemical stability in aqueous acidic media—although the impact of the conjugate base is not clear yet. Furthermore, a functionalization with two hydroxyl groups evokes a negative redox potential shift of 54 mV in acidic and 264 mV in alkaline solution. This demonstrates that this novel class of compounds is very versatile and can be tailor-made for use as active material in redox flow batteries—either in alkaline or acidic media. The 2,3-diaza-anthracenediones presented in this study were used as anolyte active materials in a full redox flow cell as a proof of concept; best cycling stability was achieved with 2,3-diaza-anthracenediones functionalized with a methoxy group as active material. Transferring our findings to other quinone base structures, such as naphthoquinones, could lead to even better performing catholyte and anolyte active materials for future redox flow batteries with organic active material.

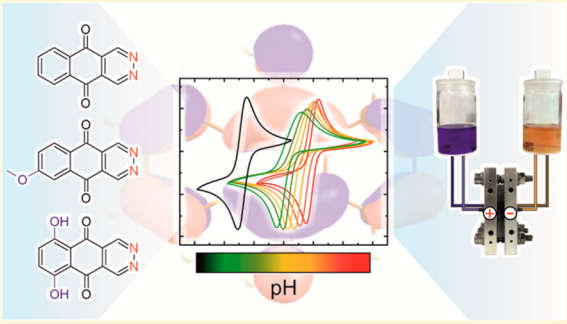

INTRODUCTION

Aromatic organic compounds constitute a great source of potentially low-cost active materials for energy storage applications and especially for redox flow batteries (RFBs)[1−6] due to their promising electrochemical properties and high abundance in natural resources. Consequently, many recent publications have focused on a highly promising class of aromatic compounds for electrochemical applications—quinones.[7−12]

Primarily, 9,10-anthraquinone-2,7-disulfonic acid (AQDS) is considered as the redox active aromatic model compound suitable for low-cost and efficient RFB application.[13] AQDS undergoes a kinetically fast two-electron transfer that is accompanied by a transfer of two protons—provided that sufficient proton activity is guaranteed. Aziz et al. applied AQDS and other quinone derivatives as anolyte active material in acidic[1,8,11] as well as alkaline[12] aqueous electrolytes. Yang et al. proposed an all-organic RFB based on quinonoid active materials with 1,2-benzoquinone-3,5-disulfonic acid as catholyte.[9] Despite these efforts, most of these RFBs show relatively poor cycling stability, and improvable cell voltages and energy densities, mainly arising from low active material concentrations.

To meet these challenges, several computational and experimental studies were conducted regarding the influence of structural functionalization on the redox potential and solubility of quinone compounds (e.g., by Er et al.).[14−16] Their results prove that the incorporation of electron-withdrawing

Received: October 6, 2017
Revised: January 25, 2018
Published: January 25, 2018

DOI: 10.1021/acs.chemmater.7b04220
Chem. Mater. 2018, 30, 762−774

substituents, such as $-NO_2$, $-COOCH_3$, or $-CN$, leads to stronger oxidants, which increase the resultant redox potentials, thereby making them well-suited as catholyte active materials. Conversely, electron-donating groups, such as $-NH_2$, $-OH$, and $-OCH_3$, can produce weaker oxidants, decreasing their redox potential, and making them well-suited as anolyte active materials. Additionally, a functionalization with hydrophilic substituents, such as phosphoric or sulfonic groups, increases the water solubility of the compounds, resulting in a higher energy density of the entire RFB cell.[17]

Going further, Wegner et al. modified the anthraquinone (AQ) base structure by incorporating two adjacent nitrogen atoms into the aromatic system.[18] Starting from alternatively substituted 1,4-naphtoquinones, a wide range of 2,3-diaza-anthracenediones, also called diaza-anthraquinones (DAAQs), can be synthesized—affording a great opportunity for the investigation of the structure−property relationships of diaza-based quinone compounds for RFBs. Previously utilized solely for pharmacological applications (e.g., cancer treatment[19,20]), this class of compounds may be a promising supplement to homocyclic quinone derivatives for energy storage applications.

To evaluate their potential as active materials for energy storage applications, we conducted a systematic analysis of the base structure 2,3-diaza-9,10-anthracenedione (DAD) and two differently substituted derivatives of it [DAD(MeO) = 2,3-diaza-6-methoxy-anthracene-9,10-dione; DADdi(OH) = 2,3-diaza-5,8-dihydroxy-anthracene-9,10-dione]. Initially, we characterized the electrochemical properties and assessed the impact of specific structural functionalizations on the resultant electrochemically active material properties by means of experimental investigation and density functional theory (DFT) calculations. Finally, we show full-cell RFB tests with these compounds, thereby highlighting the potential of DAAQs as redox compounds in future energy storage applications.

EXPERIMENTAL SECTION

Chemicals. Potassium ferrocyanide and potassium ferricyanide were purchased from Sigma-Aldrich and used as received as catholyte active material in the full-cell measurements. Concentrated sulfuric acid was also purchased from Sigma-Aldrich and diluted with deionized water to gain solutions with a concentration of 2 mol/L. For the measurements in hydrochloric acid we used 1 M HCl by ORG Laborchemie. The 1 M KOH was purchased from Grüssing Chemicals and used as received. For the analytical measurements in nonaqueous electrolytes, a combination of acetonitrile and tetrabutylammonium hexafluorophosphate ($TBAPF_6$) was used of which both components were purchased from Sigma-Aldrich. Before the measurement, acetonitrile was dried by molecular sieves, and $TBAPF_6$ was dried in a vacuum oven at 100 °C for 24 h.

In the search for a promising catholyte active material, different DAAQs were investigated in half-cell as well as in full-cell measurements. These compounds were synthesized by a novel synthesis route based on the use of a bidentate bisborane Lewis acid catalyst enabling an inverse electron-demand Diels−Alder (IEDDA) reaction with 1,2,4,5-tetrazine. The procedure was described in detail by Hong et al.[21]

All reagents and solvents for synthesis were obtained from Sigma-Aldrich, Acros, TCI, or Alfa Aesar and were used as received unless otherwise stated. 6-Methoxy-1,4-naphtoquinone[22] and 1,2,4,5-tetrazine[23] were prepared according to literature procedures whereas tetrazine has additionally been purified via sublimation. Technical grade solvents for extraction and column chromatography were bulb-to-bulb distilled prior to usage. Air-sensitive reactions were set up using dry glassware in a glovebox, or just flushed by nitrogen or argon.

Synthesis of Diaza-anthraquinones. 2,3-Diaza-9,10-anthracenedione (DAD), 2,3-diaza-5,8-dihydroxy-anthracene-9,10-dione (DADdi(OH)), and 2,3-diaza-6-methoxy-anthracene-9,10-dione (DAD(MeO)) were synthesized according to Wegner's method.[21] The synthesis of 2,3-diaza-6-methoxy-anthracene-9,10-dione DAD-(MeO) was modified by using an air-stable version of the catalyst via complexation of the bidentate Lewis acid catalyst with pyridazine.

METHODS

Cyclic Voltammetry. For aqueous electrolytes a three-electrode setup comprising an AUTOLAB PGSTAT 204 potentiostat, an aqueous Ag/AgCl reference electrode (3 M KCl filling solution) from Metrohm, and a Pt sheet counter electrode were used for the half-cell measurements via cyclic voltammetry. The working electrode, which we also used for the RDE studies, was a 3 mm diameter glassy carbon disk electrode (Metrohm). Before each measurement, the glassy carbon working electrode was polished with alumina paste (1 μm particle diameter, ALS) and rinsed with deionized water. The procedure then was repeated with another alumina paste (0.05 μm particle diameter, ALS). The electrolyte solution was degassed by a constant argon flow for 1 h before the measurement was started. The diaza compounds were tested in alkaline as well as in acidic aqueous solutions at different scan rates ranging from 1 to 0.01 V/s. The measured currents were normalized by means of the electrode surface area, the active material concentration, and the scan rate so that electrode kinetics and potential side reactions could be compared directly.

For the cyclic voltammetry (CV) measurements in acetonitrile, we utilized a Microcell HC (rhd instruments) instrument with a 5 mm glassy carbon working electrode and a Pt counter electrode. The voltammograms were measured versus a $Ag/AgNO_3$ reference electrode (10 mM $AgNO_3$, 10 mM Crypt[2.2.2], 0.5 M $Bu_4N[CLO_4]$ in acetonitrile; by rhd instruments). Tetrabutylammonium hexafluorophosphate ($TBAPF_6$) was used as the conducting salt. Acetonitrile was dried by adding activated 0.3 nm molecular sieves at least 48 h prior to use.

To apply a background correction, all CV measurements were repeated under the exclusion of active material. The resulting background currents then were subtracted from the data we received for the measurement with solvent, active material, and conducting salt. The uncompensated resistance of the half-cell setup was determined by the positive feedback method and compensated during CV measurements.

RDE Studies. Similar to the aforementioned CV measurements the glassy carbon rotating disc electrode (RDE) was polished to a mirror shine before the measurement was started. The voltage was linearly swept between two potentials with a scan rate of 10 mV/s. The range of the scanned potential interval was selected depending on the redox potential of the investigated compound. During the linear potential sweep the electrode was rotated at 200−3000 rpm. The maximum currents were then plotted versus the square root of the rotation rate (ω) according to the Levich equation:

$$i_{lim} = 0.62nFAD^{2/3}\omega^{1/2}\nu^{-1/6}C_0 \quad (1)$$

Here, i_{lim} is the limiting current, n is the number of transferred electrons, ω is the angular velocity in rad/s, ν is the kinematic viscosity of the solution in cm^2/s, and c_0 is the concentration of the electrochemically active species in mol/cm^3. From the slope of the fit we were able to determine the diffusion coefficient D of the investigated compound.

Full-Cell Measurements. The setup for the full-cell experiments comprised a pump (Ismatec Reglo analog), two glass containers for the electrolytes (100 mL each, equipped with a stirring bar), the electrochemical converter, tubing, and a gas washing bottle filled with water to moisturize the argon that was used for purging the two glass containers during operation. This was necessary to get rid of oxygen dissolved in the electrolytes and to prevent solvent evaporation by the continuous stream of argon. The pumping speed of anolyte and catholyte was 29.6 mL/min per half cell. As an additional protection against unwanted air-oxidation, a custom-built acryl glass lid was used

DOI: 10.1021/acs.chemmater.7b04220
Chem. Mater. 2018, 30, 762−774

to cover the entire setup. The interior of this box was purged with nitrogen.

The electrochemical cell itself consisted of two identical half cells. They comprised an outer shell alumina plate with an inlet and outlet for the electrolytes, a SIGRACELL TF6 bipolar plate from SGL Carbon as current collector, and a polyethylene distance holder. The distance holder was provided with a cavity where the actual electrode material, a piece of carbon felt (SIGRACELL GFA 6 EA), was placed. An NM 212 Nafion membrane (effective area = 5.8 mm^2), purchased from Quintech, was used to separate the two half-cells and to ensure ion transport. Rubber gaskets were applied to prevent leakage, and the entire system was firmly screwed together before the measurement.

When used as received, the carbon felts showed a hydrophobic behavior. For this reason, the carbon felts were heat-treated before use in order to create hydrophilic groups by air-oxidation. After 24 h at 400 °C in air, the carbon felts were able to soak up water. The increased wettability led to a decrease of the overall cell resistance from 2 Ω to about 0.4 Ω, obtained by impedance measurement (Figure S8).

The galvanostatic cycling experiments were conducted with an SP-150 potentiostat from BioLogic. In the case of DAD and DAD(MeO) a constant charge/discharge current of 15 mA was applied to the cell until a certain cutoff voltage was reached. Due to their very similar redox potentials, both compounds were cycled between 0.8 and 0.2 V. For the cell based on DADdi(OH), the cutoff voltage for the discharge process had to be set to a higher value of 1 V, which arises from its more negative redox potential relative to DAD and DAD(MeO). When the threshold voltage was reached, the discharge process, limited by a cutoff voltage of 0.6 V, was started. For the full-cell cycling experiments an active material concentration of 0.5 mM was applied, which is in accordance with the half-cell measurements that were conducted. For DAD(MeO) and DADdi(OH) 20 mL of electrolyte was used, while for DAD the total volume amounted to 30 mL. The diaza-anthraquinones were cycled together with the well-studied redox couple $[FeII(CN)_6]^{4-}/[FeIII(CN)_6]^{3-}$ as the catholyte active material, which had been previously used in similar experiments.[12] For this study it was deployed in excess amounts of 5 equiv in relation to the anolyte active material to exclude any limitations emanating from this part of the cell.

DATA EVALUATION AND CALCULATIONS

Diffusion Coefficient D and Half-Wave Potential $E_{1/2}$. To evaluate the influence of different substituents on the charge transfer characteristics of the diaza compounds, the half-wave potential $E_{1/2}$ was calculated as the mean value of the cathodic and the anodic peak potentials assuming that the reduced and the oxidized form of the compound have identical diffusion coefficients. The diffusion coefficients of the active compounds were determined based on the CVs using the Randles–Sevcik equation[24]

$$i_p = 0.4463nFAc_0\left(\frac{nF\nu D}{RT}\right)^{1/2} \quad (2)$$

where i_p is the peak current in A, c_0 is the concentration of active material in mol/cm^3, n is the number of transferred electrons, F is the Faraday constant (96 485 C/mol), A is the geometric area of the working electrode in cm^2, ν is the CV scan rate in V/s, D is the diffusion coefficient in cm^2/s, R is the universal gas constant (8.314 J/(K mol)), and T is the temperature in K.

Evaluation of Rate Constant. To calculate the heterogeneous electron transfer rate constant k^0 we evaluated the cathodic current response of the presented diaza compounds, which is depicted in the CVs measured in acidic aqueous solution (see Figure 1). According to the Tafel equation a linearly fitted plot of $\log(i)$ versus the applied overpotential η

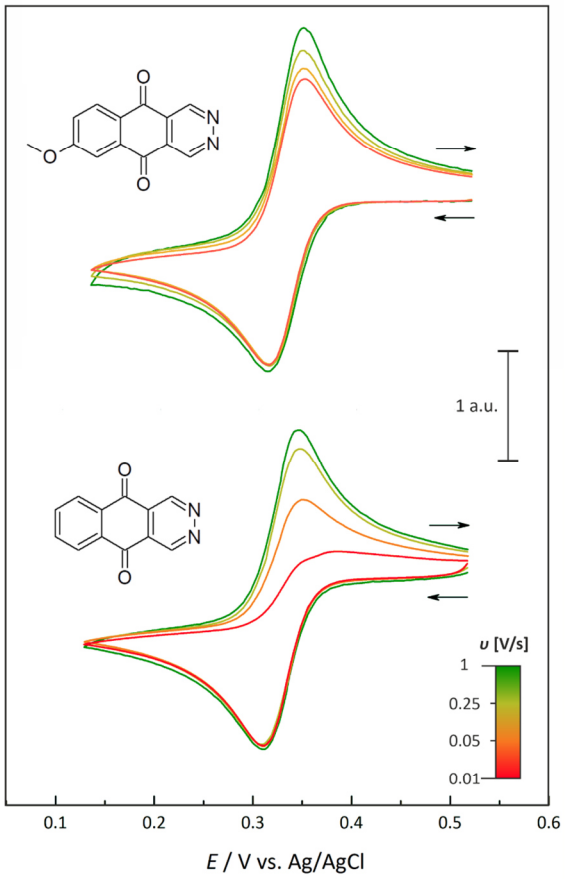

Figure 1. Influence of a methoxy group on the electrochemical stability of aromatic diaza compounds under acidic conditions. Measurements were conducted in an aqueous 2 M H_2SO_4 solution. Both CVs of the diaza compounds DAD and DAD(MeO) are normalized to the active material concentration of 0.5 mM and the square root of the applied scan rates (1, 0.25, 0.05, and 0.01 V/s) according to the Randles–Sevcik equation. Hence, the ordinate is displayed in arbitrary units (a.u.). DAD undergoes a decrease of the anodic peak current density proportional to the lowering of the applied scan rate, which might be due to a side reaction of the reduced species that is generated in the cathodic half cycle. For DAD(MeO), the reversibility of the occurring charge transfer is distinctly enhanced, especially at low scan rates, which is indicated by a peak current ratio close to unity. This is related to the incorporation of the methoxy group into the quinonoid molecular structure.

(see the SI, Figure S6) yields an ordinate intercept that equals the log of the exchange current i_0 (with α as transmission coefficient):

$$\log(i) = \log(i_0) + \frac{\alpha nF\eta}{2.303RT} \quad (3)$$

The current and potential values used for this plot were extracted from the descending part of the CV at a scan rate of 0.025 V/s. By transferring the determined value for i_0 to eq 4 the heterogeneous rate constant can be calculated:

$$i_0 = k^0nFAc_0 \quad (4)$$

DOI: 10.1021/acs.chemmater.7b04220
Chem. Mater. 2018, 30, 762–774

Density Functional Calculations. DFT calculations for the determination of DAAQ reduction potentials were performed using the Gaussian 09[25] software package. Structure optimizations, calculation of the energetics, and the computation of the zero-point energy, thermal correction, and entropy contribution to evaluate the Gibbs free energy at 298 K were done using the BP86 density functional (generalized gradient approximation) in an unrestricted manner and in combination with the dispersion correction D3 of Grimme with a Becke−Johnson damping.[26−29] Furthermore, a density fitting was applied to expedite the calculations. All elements were characterized in an all-electron description employing the correlation consistent valence aug-cc-pVDZ Dunning-type basis set.[30] Applying the larger basis set aug-cc-pVTZ resulted in negligible structural changes and potential variations smaller than 0.02 V. The simulation of solvent effects (water) was done via the polarizable continuum model (PCM).[31] Frequency calculations confirmed all calculated structures to be minima structures.

The calculation of the redox potential was done using a thermodynamic cycle.[32] Thereby, the Gibbs free energy of the electron was chosen to be 37 meV at 298 K based on Fermi−Dirac statistics.[33] The reduction of quinone to hydroquinone is a two-electron and two-proton process at low pH values (see Figure S1), which was also confirmed for the reduction of functionalized 9,10-anthraquinones to 9,10-anthrahydroquinones by Huskinson et al.[1,34] Due to the similarity of the DAAQ molecules under investigation to 9,10-anthraquinones, we assumed the reduction of the different molecules as a two-electron two-proton process in a single-step reaction for the low pH value of 0:

$$\mathrm{DAAQ} + 2\mathrm{e}^- + 2\mathrm{H}^+ \leftrightarrow \mathrm{DAAQH_2} \tag{5}$$

This results in the generation of the reduced and protonated form of the diaza-anthraquinone, $DAAQH_2$. Motivated by the elevated basicity of phthalazine (pK_a = 3.5), which is a six-membered heterocycle with a close resemblance to the investigated DAAQs, we additionally calculated reduction potentials for the case of a single protonation of the diaza moiety at low pH values.[35] For the solvation free energy of the protons, we used a value of $\Delta G^0_{solv}(H^+) = -1098.9$ kJ/mol.[33,36] For pH values above 12, Revenga et al. determined the reduction of 9,10-anthraquinone as a two-electron process in a single step to the corresponding dianion.[37] Because of the close structural resemblance we can transfer this model to the presented DAAQs. We assume the reduction of the molecules for pH 14 to take place as a two-electron process in a single step, yielding the dianion $DAAQ^{2-}$ of the diaza-anthraquinone:

$$\mathrm{DAAQ} + 2\mathrm{e}^- \leftrightarrow \mathrm{DAAQ}^{2-} \tag{6}$$

However, there is an important detail that needs to be considered: Since the incorporation of the diaza moiety results in a higher overall proton affinity of DAAQs in comparison with AQs (pK_{a1} = 9, pK_{a2} = 12.05), their carbonyl moieties may also be easier to protonate.[37,38] Therefore, we additionally investigated the reduction of DAAQs to the corresponding one-fold protonated monoanions in the case of DAD and DAD(MeO) and the trianion for DADdi(OH) at high pH value.

The reduction potential of the molecule in solution was calculated using the following equation:

$$E_{calc} = -\frac{\Delta G_{rxn}}{nF} - E_{SHE} \tag{7}$$

Therein, ΔG_{rxn} is the difference in Gibbs free energy of the reduction in solution, and the other quantities are as denoted before. The reduction potential is computed with respect to a standard hydrogen reference electrode (SHE) with an absolute potential of 4.28 V.[39,40] Thus, all redox potentials are reported versus SHE. Furthermore, we assumed that the diffusion coefficients of the oxidized and reduced species are very similar. The calculated reduction potentials are dependent on the used density functional, for which the accuracy might change with the type of the molecular system under consideration. For example, the calculation of the reduction potential of DAD at pH 14 using the B3LYP-D3/aug-cc-pVDZ level of theory leads to a potential shift of −0.179 V.[41] Furthermore, the calculated reduction potentials depend on the chosen value for the reference electrode and $\Delta G^0_{solv}(H^+)$.[33]

The initial structure for the structure optimization of DAD was generated by modifying the 9,10-anthraquinone molecule. All other structures were generated from the optimized DAD molecule. For the protonated carbonyl groups of the reduced diaza compounds $DADH_2$ and $DAD(MeO)H_2$ at a pH value of zero, different structures are obtained, depending on the orientation of the hydrogen atoms. For $DADH_2$, a structure with both hydrogen atoms orientated away from the diaza moiety was slightly energetically preferred (by 11 and 36 meV), while for $DAD(MeO)H_2$, the structure with a mixed hydrogen atom orientation was more favorable (by 2 and 25 meV). As a result, these configurations were used to calculate the reduction potential. Due to the additional hydroxyl groups of DADdi(OH), several possible hydrogen orientations can be obtained. We calculated three different structures for DADdi(OH), whereby the one with hydrogen atoms oriented toward the carbonyl groups is preferred by 417 meV (compared to a mixed hydrogen atom orientation) or 848 meV (compared to two hydrogen atoms oriented away from the carbonyl group). Furthermore, seven different $DADdi(OH)H_2$ structures were computed that differ by 72−390 meV from the energetically preferred structure, where all hydrogen atoms are orientated away from the diaza moiety. Accordingly, this structure was used for the calculation of the reduction potential. As stated before, for low pH values we also considered the case of a proton added to the diaza moiety of the energetically preferred structures. In addition, the reduction potential of AQ was calculated at the same level of theory.

At pH 14 we considered different protonation states of the hydroxyl groups. As a result, we additionally calculated the state of one protonated hydroxyl moiety, i.e., the monoanion, to occur for DAD and DAD(MeO), and the tri- and tetra-anion for DADdi(OH).

■ RESULTS AND DISCUSSION

Electrochemical Behavior of Diaza-anthraquinones. We systematically investigated three DAAQ compounds as candidates for active materials in RFBs (see Figure 3 for the molecular structures): the diaza-anthraquinone core structure DAD without any functionalization, the methoxyl-substituted analogue, abbreviated as DAD(MeO), and DADdi(OH), which was augmented by two hydroxyl groups in close proximity to the carbonyl groups of the AQ backbone.

To gain insight into the associated electrochemical properties, DAD, DAD(MeO), and DADdi(OH) were investigated in

DOI: 10.1021/acs.chemmater.7b04220
Chem. Mater. 2018, 30, 762−774

different solutions. The DAAQ compounds were first investigated in aqueous solutions, where the pH was varied to determine the influence of protonation on the electrochemical behavior. Additional measurements were also conducted in acetonitrile as an aprotic, nonaqueous solvent to better resolve the electron transfer steps in the cyclic voltammograms recorded (see the SI).

Reversibility in Acidic Media. Applying cyclic voltammetry to the parent diaza compound DAD under acidic conditions at high scan rates yields fully reversible charge transfer (Figure 1). DAD is reduced to its hydroquinonoid form, via the consumption of two electrons and two protons, and then directly reoxidized in the backward scan at a half-wave potential $E_{1/2}$ of 0.328 V versus Ag/AgCl. This is evidenced by a single, well-defined cathodic and anodic wave for which both are separated by 35 mV, which is close to the theoretical value for peak separation (according to the Nernst equation for a two-electron transfer process: ΔE_{pp} = 29.5 mV at 298.15 K).

This result is in good agreement with the general charge transfer characteristics of quinones when proton donors are present.[34,42] In comparison to the well-investigated AQDS, DAD exhibits a positive shift of 300 mV in its redox potential caused by the incorporation of the diaza moiety (Figure S2). Different from DAD, AQDS features peripheral functionalization in terms of two sulfonic acid groups, which impedes a direct comparison of both compounds. Nevertheless, according to Er et al., such functional groups, in the aforementioned positions, have a negligible influence on the redox properties. Thus, the positive potential shift arises solely from the modification of the DAD core structure, which is consistent with related reports.[43,44] Referring to the work of Gerhardt et al., the two sulfonic acid groups should even contribute to an overall positive potential shift of approximately 50 mV for AQDS compared to unsubstituted AQ, which further emphasizes the distinct positive potential shift caused by the herein introduced diaza-functionalization.[8] This effect could be particularly beneficial in the case of naphtho- or benzoquinones, which intrinsically exhibit more positive redox potentials, as compared with AQ compounds. An additional positive potential shift, induced by incorporating a diaza group, could serve as a versatile method to increase the energy density of full-cell RFBs.

Applying scan rates of less than 1 V/s affects the CV curve obtained for DAD, as the anodic peak current density decreases from high to low scan rates, resulting ultimately in an almost completely irreversible process at 0.01 V/s. This phenomenon is accompanied by the generation of red crystals on the electrode surface, which may indicate a polymerization or precipitation process. As this coloring is especially seen at low scan rates, we assume that an unstable species is being formed during reduction of DAD, which then may undergo a comparably slow side reaction. The direct interaction among the reduced species, as well as an interaction of reduced molecules and the bulk material,[13] cannot be excluded and further analysis is required to gain more insight.

Impact of the Diaza Moiety. Nitrogen substitution can reduce the electron density in aromatic mono- and oligoazines, given that N atoms are more electronegative than C atoms. However, the lone-pair of electrons can also interact due to an electron-donating resonance effect.[45] As a more positive redox potential is observed for DAD than for AQDS, it is likely that the electron-withdrawing effect is dominant in the present case.

However, the redox potential is not the only quantity that is being affected by the presence of the two adjacent N atoms within the aromatic structure: The incorporation of N atoms leads to heterocycles with notably increased gas phase basicities,[46,47] which also holds true for the aqueous phase.[45] This implies that the nitrogen substitution increases the proton affinity for the class of DAAQs. Their extended π-system also contributes by inducing an electron-donating effect. Keeping in mind that the reduction/oxidation of carbonyl groups is intended during RFB operation, the reducing half cycle introduces two hydroxyl moieties into the molecular structure. These groups can also act as electron donators, increasing the proton affinity even more.[38,48]

Therefore, it may be possible that, next to the desired protonation during electrochemical reduction of the carbonyl group, a protonation of the diaza moiety could take place at low pH. In the unlikely event that the diaza moiety would be protonated, the reduced ionic species that is formed could then undergo side reactions during the course of cathodic and the following anodic potential scan, giving a possible explanation for the observed crystal formation. A similar behavior was already reported for benzoquinone, which is able to form different associates with its reduced hydroquinone form depending on their respective molar ratio.[49] The study by Valero et al. furthermore explains that by the addition of conducting salts with specific stoichiometry a crystalline complex can be formed due to electrostatic stabilization, which is in accordance with the aforementioned generation of red crystals observed in our experiments. Although the parameters in this study—such as the used solvent—deviate from the ones used for our experiments, there are still indications that the supporting electrolyte plays a key role in the precipitation mechanism of unwanted side products in the case of DAAQ. Especially in view of the fact that we conducted measurements in aqueous solutions of 1 M hydrochloric acid without crystal formation (see Figure S12), it should be noted that there are more factors promoting this side reaction—such as the nature of the conjugated base of the used supporting electrolyte. Although the exact mechanism of the side reaction remains unclear, there are strong indications that the red crystals are formed due to the specific interaction of DAAQs and sulfuric acid, which will be the subject of future studies.

Enhancing Stability and Redox Potential by Substitution. In contrast, the addition of a methoxy moiety to the backbone of the DAAQ leads to a clearly improved reversibility of the charge transfer. DAD(MeO) remains stable during the CV measurements at both high and low scan rates (Figure 1). A direct comparison of anodically and cathodically transferred charge (see Figure S13) provides more evidence for this observation: For DAD(MeO) we observe a constant ratio of 0.9 throughout the entire range of investigated scan rates. For DAD this only applies to a high scan rate of 1 V/s; in the case of low scan rates (0.01 V/s) only small ratios of down to 0.56 were calculated.

For DAD(MeO) we observe that the CV characteristics at high scan rates differ slightly from the ones obtained at low scan rates. Thus, we assume that a small portion of the species may adsorb at the electrochemically active area of the working electrode. In view of the fact that the displayed currents have been normalized to the square root of the scan rate, which only applies for processes that are governed by diffusion, the normalization supposedly cannot account for these current contributions (see also Figure 2). The charge ratio, however,

DOI: 10.1021/acs.chemmater.7b04220
Chem. Mater. 2018, 30, 762−774

remained constant. Ultimately, the charge retention of DAD was significantly increased by the incorporation of a methoxy group.

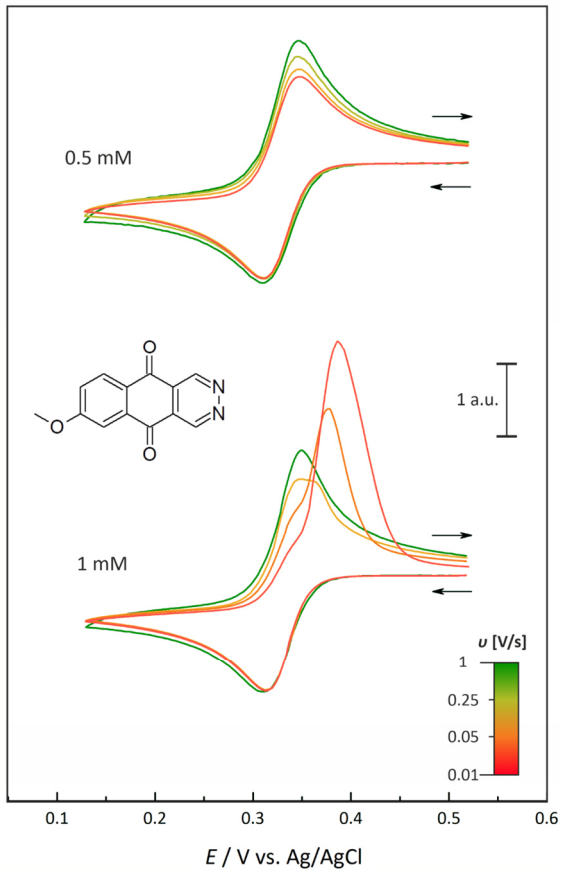

Figure 2. Influence of active material concentrations on the charge transfer characteristics of DAD(MeO) in acidic media. Both insets depict normalized CVs of different active material concentrations in 2 M H_2SO_4 at several scan rates. Hence, the ordinate is displayed in arbitrary units. At an active material concentration of 0.5 mM, the ratio of cathodically and anodically transferred charge remains nearly unity over the depicted scan rates of 1, 0.25, 0.05, and 0.025 V/s. When the concentration is increased to 1 mM, unity of the ratios can only be attained at high scan rates. Lowering the scan rate leads to a decrease of the anodically transferred charge. From 0.1 V/s on, a second process, which emerges from 0.36 V vs Ag/AgCl and shifts in a positive direction with decreasing scan rate, starts to dominate the charge transfer characteristics. This process exhibits a nonlinear relation of peak current and the square root of the applied scan rate. This suggests the contribution of an adsorbed species, implying the involvement of a precipitation process at higher concentrations similar to the one observed in the case of DAD.

Furthermore, the formation of crystals on the working electrode due to potential side effects was not observed for DAD(MeO), as it was for DAD under the same conditions. This enhanced stability of DAD(MeO) against precipitation could either be attributed to a steric hindrance or an electronic stabilization of the molecular structure by the added methoxy group.

Nevertheless, as seen in Figure 2, the concentration dependent charge transfer behavior gives rise to the idea that, particularly at higher active material concentrations, a polymolecular reaction takes place at the electrode surface. Lowering the scan rate initially leads to a decrease of the anodic peak current, which is followed by the onset of another process that seems to originate from a side reaction. As the process exhibits a nonlinear dependence on the peak current by the square root of the applied scan rate, this is likely the contribution of an adsorbed or precipitated species. Nevertheless, even though electrode passivation was observed at low scan rates by increasing the active material concentration, it was less pronounced than in the case of DAD.

Comproportionation reactions can take place when the oxidized and the reduced species of a quinone are present in solution. This usually yields two semiquinone radicals.[50] These semiquinone molecules are highly redox active and may even form superoxide or hydrogen peroxide.[51,52] The generation of this highly reactive radical species may cause the degradation of active material in vicinity of the electrode surface, resulting possibly in the formation of a passivating layer. Given that methoxy groups have often been reported to stabilize radicals,[53−55] the enhanced reversibility of DAD(MeO) can be attributed to this property. However, as mentioned above, the association of reduced active material close to the electrode surface and pristine bulk material combined with a stabilization by the supporting electrolyte could be the cause for crystal formation.

Augmenting the base structure by two hydroxyl groups in close vicinity to the carbonyl moiety has no beneficial effect on the compound's stability in acidic aqueous solution. Only a small anodic charge can be retained after reducing DADdi(OH) at low scan rates (Figure 3). Instead, the redox potential was shifted to more negative values by 54 mV, relative to DAD, which further highlights the potential for improvement of the electrochemical properties of DAAQs. Furthermore, the incorporation of the two hydrophilic hydroxyl groups into the otherwise hydrophobic molecule structure was expected to contribute to an increased water solubility of the compound. Based on the findings presented herein, this trend could not be verified.[15,16] In general, the presented DAAQs exhibited a low solubility of 1−2 mM in 2 M H_2SO_4 and a slightly decreased solubility of about 1 mM in 1 M KOH. Further studies are needed to clarify whether this feature is attributed to the diaza moiety, for instance due to an increase in intermolecular interactions, and how the water solubility can be increased.

Overall, the results at low pH prove that the methoxy group strongly increases the electrochemical stability of diaza compounds in acidic media. In the presence of proton donors, a combination of protecting and electron-donating/electron-withdrawing groups may be the key to meeting the demands for high specific energy storage in RFBs.

Reversibility in Alkaline Media. Figure 3 displays a direct comparison of the CVs obtained for each diaza compound in alkaline aqueous solution. All depicted CVs indicate that full electrochemical reversibility was attained by changing the electrolyte, avoiding the aforementioned protonation reaction in acidic media. As it is already the case for acidic solutions, the half-wave potentials of DAD and DAD(MeO) do not vary significantly from each other at high pH values.

Another feature of the displayed CVs is the peak splitting that is observed for DAD and DAD(MeO): while a slight graduation of the peak currents is already observed for DAD,

DOI: 10.1021/acs.chemmater.7b04220
Chem. Mater. 2018, 30, 762−774

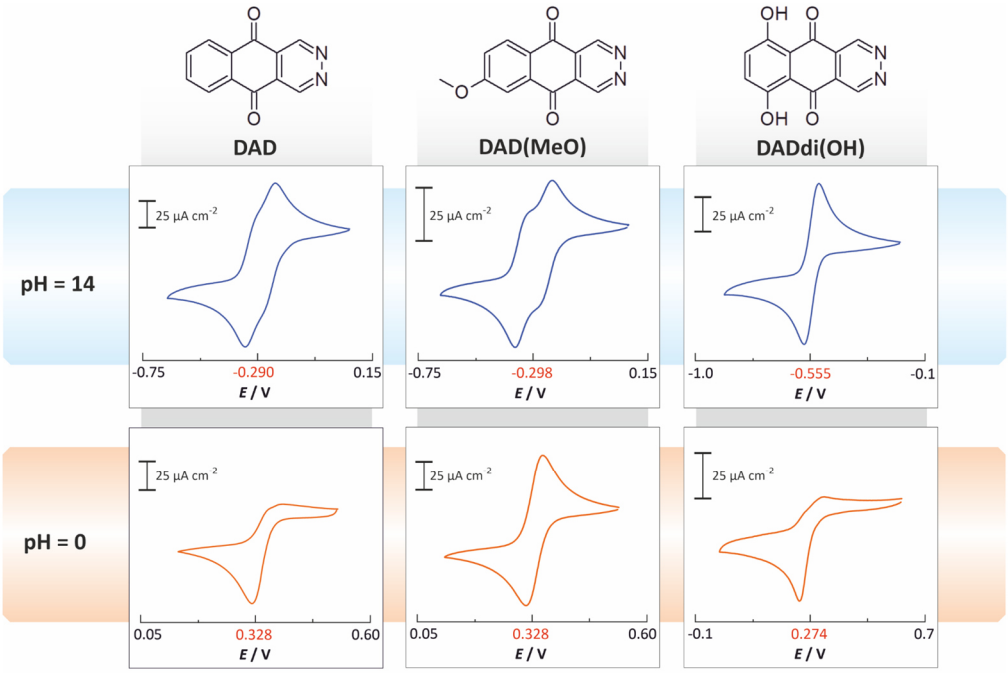

Figure 3. Comparison of the charge transfer characteristics of the three investigated diaza-anthraquinones, all cell potentials recorded vs Ag/AgCl. The measurements were conducted under alkaline (1 M KOH; pH = 14) and acidic (2 M H_2SO_4; for the sake of simplicity we assumed that pH = 0) conditions and an active material concentration of 0.5 mM. Reversible charge transfer is observed for all three molecules in alkaline solution. DAD and DAD(MeO) undergo a two-electron charge transfer at nearly identical redox potentials whereas DADdi(OH) is reduced at a more negative potential. For the first two compounds a peak separation can be observed, which is not the case for DADdi(OH). In acidic solution, a nearly reversible charge transfer is only observed for DAD(MeO). Compared to the other compounds DADdi(OH) exhibits a redox potential that is 54 mV lower, which is a result of the structure functionalization with two hydroxyl groups. The overall good reversibility in alkaline solution suggests that the full-cell cycling at high pH values is beneficial. Because of the unexpectedly strong negative redox potential shift under these conditions, the highest theoretical cell voltage should be attained by using DADdi(OH) as the anolyte active material.

the peak splitting becomes even more pronounced with DAD(MeO). This behavior is highly unusual for quinonoid species in aqueous solution and has only been reported in a few publications for different base structures.[56,57] In these studies, peak splitting was achieved by stabilizing the semiquinone radical species; cation species, compatible with the semiquinone structure, were added to form ion pairs. In our experiments peak splitting is independent of the chosen cation size. It can be observed to the same extent when using two different cations—either Na^+ or K^+. Besides aqueous NaOH and KOH solutions, no other additives were used thus far.

Concerning the presented diaza compounds, we suggest that peak splitting is solely correlated to the modification of the base AQ structure. Compared to homocyclic AQs, the cation semiquinone radical is presumably further stabilized during the electrochemical reaction at the electrode surface due to an increased electron-donating resonance effect provided by the free electron pairs of nitrogen. On the other hand, the stability of the anion semiquinone radical may benefit from the electron-withdrawing nature of nitrogen. Thus, the charge transfer characteristics of DAD and especially DAD(MeO) mirror the presumed increase in peak splitting caused by a thermodynamically stabilized semiquinone radical.

Measurements conducted in acetonitrile, under the exclusion of hydrogen bonding and protonation effects, further support this assumption. It is reported that, in aprotic organic solvents, two electrons are being transferred stepwise during the redox process of quinones.[58] A direct comparison of CVs of regular quinones and the presented DAAQs reveals an increased separation between the peaks of the two associated electron transfers in the latter case (see the SI, Figure S3). This fact also supports the assumption that the semiquinone is being stabilized to a greater extent by the incorporation of nitrogen into the aromatic system. As a consequence, the redox potential of the first reduction process becomes more positive relative to the potential at which the dianion is being formed.

Going back to alkaline aqueous systems one would expect the two voltammetric waves to merge as a result of hydrogen bonding interaction between the dianion and the surrounding water molecules.[59] However, the heterocyclic structure presumably leads to an increased potential difference between the two charge transfers so that the impact of hydrogen bonding interactions is not sufficient to close this gap. Hence, the two voltammetric waves do not merge as expected and as it is well-known for aqueous solutions of quinones in general. For DAD and DAD(MeO) this only seems to be the case in the presence of proton donors that can cause a potential inversion for good measure.

In contrast, DADdi(OH) exhibits a notably different behavior. Here, no peak splitting is observed in the CVs, although, like DAD and DAD(MeO), it features a reversible charge transfer. This may be attributed to the functionalization in the form of two hydroxyl groups, which increases the possibility for hydrogen bonding interactions between the

DOI: 10.1021/acs.chemmater.7b04220
Chem. Mater. 2018, 30, 762−774

Table 1. Kinetic and Electrochemical Quantities of the Investigated Diaza Compounds Determined with CV Measurements and Density Functional Calculations[a] (UPB86-D3/aug-cc-pVDZ with PCM)

			$E_{1/2}$ (pH = 0) [V vs SHE]		$E_{1/2}$ (pH = 14) [V vs SHE]	
compound	D [cm^2/s]	k^0 [cm/s]	experimental	DFT	experimental	DFT
DAD	3.78×10^{-6}	1.131×10^{-3}	0.538	0.590 (0.328)	−0.081	−0.448
DAD(MeO)	4.12×10^{-6}	1.201×10^{-3}	0.538	0.551 (0.295)	−0.088	−0.505
DADdi(OH)	1.61×10^{-6}	6.848×10^{-4}	0.484	0.345 (0.073)	−0.345	−1.804 (−0.439)
AQ			0.077[37]	0.120	−0.534[37]	−0.915

[a]The reduction potential at pH = 0 was calculated under the assumption of a protonated diaza group. For comparison, the value for an unprotonated diaza group is given in brackets. The reduction potentials at pH = 14 were calculated for different protonation states of the hydroxyl groups and can be found in detail in the Supporting Information (Table T2). The values depicted in this table refer to the completely deprotonated forms of the reduced compounds. For DADdi(OH) we added a value in brackets that relates to the state of one protonated hydroxyl group.

DADdi(OH) species and water as the solvent. Eventually, the structural modification could have a positive impact on the coordination of the dianion species by water molecules leading to an increased stabilization toward the semiquinone and the merging of both voltammetric waves. Moreover, the structural modification of DADdi(OH) seems to have a distinct effect on the compound's mean half-wave potential. With a value of $E_{1/2}$ = −555 mV versus Ag/AgCl, DADdi(OH) offers a notably lower half-wave potential than expected, based on the potential shift of −54 mV observed for acidic solutions and theoretical approximations.[15,16] In alkaline solution, it undercuts the other two molecular structures by more than 250 mV. With regard to the cell voltage achievable for RFBs with DAAQs, this feature makes DADdi(OH) better suited for the application as anolyte relative to the other diaza compounds investigated in this work. Unfortunately, this derivative shows slower electrode kinetics, illustrated by an increased peak separation, which can be observed especially at high scan rates (Figure S4).

The remarkably low $E_{1/2}$ for DADdi(OH) is most likely due to the two hydroxyl groups being present in the deprotonated form at the applied pH of 14. These moieties have an intrinsically positive inductive effect, causing a negative redox potential shift in the modified compound. This trend was verified by our experiments for high pH values. Here we obtained an $E_{1/2}$ which for DADdi(OH) is 264 mV more negative than for DAD (see Table 1). On top of that, their deprotonation at high pH and the resulting generation of free electron pairs, located at the oxygen atoms in close vicinity to the carbonyl groups, may suggest an additional increase of electron density within the aromatic system. This is also reflected by our experimental results, attesting a negative potential shift from pH 0 to 14 that is 210 mV greater for DADdi(OH) than it is for DAD, which does not feature any hydroxyl groups (Table 1). In total, these effects may explain the explicit decrease of $E_{1/2}$ for the material class of DAAQs and especially DADdi(OH) in alkaline solution.

As novel active materials for RFBs need to meet the set cost targets[60] in order to be an alternative for nuclear or fossil-fueled power supplies, the observed trend for $E_{1/2}$ by modifying the structure of diaza compounds is highly promising: a higher potential difference between anolyte and catholyte directly causes lower cell stack costs, which is simply achieved by structural optimizations of the redox active molecule.

Electron Transfer Kinetics for Diaza-anthraquinones. For a more comprehensive understanding of their electrochemical properties, the diffusion coefficient D and the standard heterogeneous rate constant k^0 of the DAAQs were determined from the Randles−Sevcik equation (Figure S5) and the Tafel plot.[61,62]

The necessary data for the Tafel Plot (Figure S6) were gathered from the descending part of the cathodic peak, depicted in the CVs in Figure 1. For these investigations only the CVs measured at low pH were considered since a clear distinction of the two-electron transfer processes was not feasible at high pH. The calculations have been conducted under the assumption that a highly driven and concerted two-electron transfer is taking place. As can be seen from Table 1, the determined values for D and k^0 for DAAQs are within the same order of magnitude for comparable quinonoid compounds (e.g., AQDS).[1] DAD(MeO) exhibits the highest diffusion coefficient and heterogeneous rate constant, directly followed by DAD. For DAD(MeO) the diffusion coefficient, which was determined according to the Randles−Sevcik equation, could be verified by hydrodynamic measurements since electrode passivation does not occur for this compound under the applied conditions (see Figure S7).

If we assume that the methoxy group increases the hydrodynamic radius of the diffusing molecule, the enhanced diffusion coefficient is counterintuitive, as compared to DAD. A more beneficial coordination by surrounding solvent molecules, on the other hand, may provide an advantage by increasing the mobility of the solvation complex. In both cases, we determined k^0 to lie within an order of magnitude of 10^{-3} cm/s, which indicates fast electron transfer kinetics. For DADdi(OH), D and k^0 are much smaller, representing the slowest kinetics of the three compounds, which was already indicated by the increasing peak separation at elevated scan rates (see Figure S4). This might be explained by the hydroxyl groups in close vicinity to the carbonyl moieties, causing intramolecular interactions that lead up to a hampered charge transfer behavior as reported by Yang et al.[63] The concomitant polarity of the molecule could also be responsible for a stronger interaction with the water dipoles in the electrolyte solution, resulting in the observed decrease of D.

Density Functional Calculations on DAAQ Reduction Potentials as Well as DAAQ Geometric and Electronic Structure. For a deeper understanding of the electrochemical behavior of DAAQs, DFT calculations were performed. In our theoretical approach, we calculated the geometric and electronic structure of single DAAQ molecules under the assumption of different protonation states in aqueous solvent. Based on these results, we calculated theoretical reduction potentials to further comprehend the experimental outcomes. The associated computational details are described in the experimental section.

For low pH values the calculated reduction potentials of the investigated DAAQs are in good agreement with our experimental results (see Table 1). For DAD and DAD(MeO)

DOI: 10.1021/acs.chemmater.7b04220
Chem. Mater. 2018, 30, 762−774

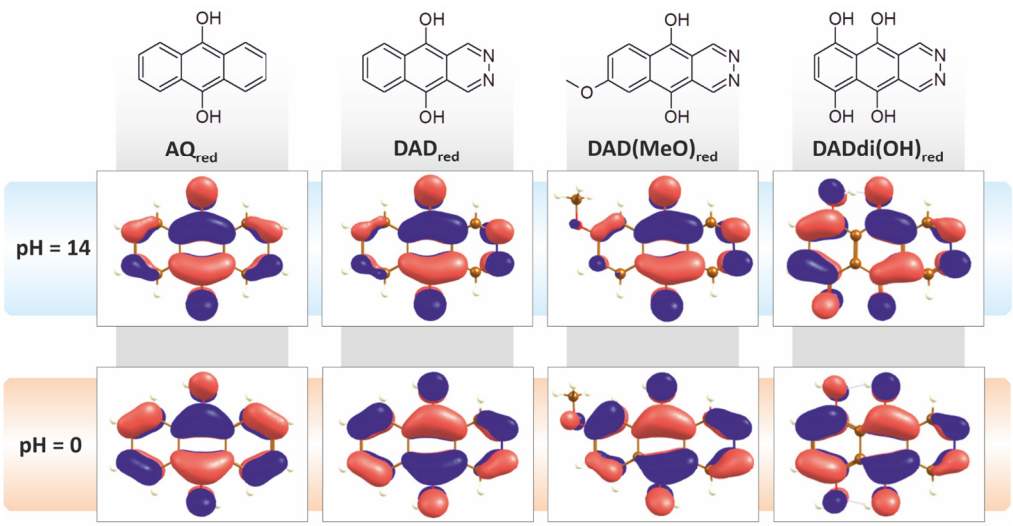

Figure 4. Highest occupied molecular orbital of the reduced molecules anthraquinone (AQ), 2,3-diaza-9,10-anthracenedione (DAD), 2,3-diaza-6-methoxy-anthracene-9,10-dione (DAD(MeO)), and 2,3-diaza-5,8-dihydroxy-anthracene-9,10-dione (DADdi(OH)) at the pH values of 14 and 0 calculated by density functional theory (UPB86/aug-cc-pVDZ with PCM). The highest occupied molecular orbitals of the reduced DAAQ molecules resemble the ones of the reduced AQ, especially at low pH values. For DAD(MeO) and DADdi(OH) there are additional antibonding contributions of the C−O bonds of the methoxy or hydroxyl substituents.

the reduction potentials are close together, which is also reflected by our experimental observations. The fact that the reduction potential of DAD(MeO) is more negative compared to that of DAD in our calculations may be attributed to the weakly electron-donating character of methoxy moieties, which is not reflected in our measurements, but was previously described in other DFT studies.[15] We were also able to reproduce the negative potential shift evoked by the two hydroxyl groups of DADdi(OH) in a precise manner with DFT. Furthermore, as a result of the diaza-functionalization we generally observed a strong positive potential shift of DAAQs compared to unsubstituted AQ. Since the diaza-functionalization also increases the compound's proton affinity, we additionally discussed the case of a protonated diaza moiety. Both scenarios very well describe the relative potential variations as a function of different DAAQ substitutions. We even attained a great accordance with our absolute experimental values assuming a protonated diaza moiety. Overall the calculated reduction potentials do not vary more than 0.140 V (DADdi(OH)) from the potentials observed in our experiments.

For high pH values the calculated potentials strongly differ depending on the distinct protonation states we considered for the hydroxyl moieties present before (DADdi(OH)) and after electrochemical reduction (see the SI, Table T2). According to Revenga et al., for AQ at pH values above 12 the formation of a dianion can be assumed, since no proton transfer is involved.[37] Accordingly, for the completely deprotonated reduction products of DAD, DAD(MeO), and AQ we calculated reasonable values that—as in the case of low pH—reproduce the structure dependent trend specified by our experimental results. However, for these molecules we observed a larger offset of up to 0.400 V between DFT calculation and our practical results compared to low pH values.

At high pH, DADdi(OH) poses the most complex case of the presented DFT calculations. Because of its two intrinsic hydroxyl groups, there is a high number of protonation sites that need to be considered (see Table T2). To begin with, we assumed a completely deprotonated molecule before and after the two-electron transfer reduction process. With respect to the pK_a values of the similar compound 1,4-dihydroxy-anthracene-9,10-dione (pK_{a1} = 9.5; pK_{a2} = 11.18) this assumption seems reasonable.[64] For this scenario we obtained a reduction potential that is distinctly more negative than in the case of the other investigated compounds. Although the calculated negative potential shift is more pronounced than expected, the observed trend is still in accordance with our experiments.

Furthermore, DADdi(OH) requires a more differentiated consideration: Mukherjee et al. reported very high acid constants for the dissociation of the third and fourth hydroxyl group (pK_{a3} = 13; $pK_{a4} \gg 14$) of the closely related reduced form of 1,4-dihydroxy-2-sulfonate-anthracene-9,10-dione.[65] In addition they postulated that the sulfonic acid group of their molecule lowers the semiquinone's pK_a. It is to be noted that the here-presented 2,3-diaza-5,8-dihydroxy-anthracene-9,10-dione does not feature a sulfonic acid group. Therefore, transferring the idea by Mukherjee et al. to DADdi(OH) gives strong indications that a protonation should be considered for this DAAQ during the course of reduction despite the strongly alkaline environment. This can be further substantiated by the fact that in alkaline solution no peak splitting can be observed for DADdi(OH) as opposed to DAD and DAD(MeO), which may be a result of protonation and a concomitant potential inversion. Besides, the sluggish charge transfer kinetics depicted in Figure S4 may also result from an equilibrium potential shift caused by protonation or intramolecular hydrogen bonding effects.[59,63] Assuming a two-electron−one-proton transfer leads up to a calculated reduction potential of −0.439 V versus SHE, which agrees well with its experimental counterpart, but does not reflect the general trend observed for DAD, DAD(MeO), and AQ.

DOI: 10.1021/acs.chemmater.7b04220
Chem. Mater. 2018, 30, 762−774

Overall, the presented DFT calculations demonstrate that there are many parameters that need to be taken into account to make reliable predictions concerning DAAQ reduction potentials. Especially for high-throughput computational screening, quantities such as pK_a values and the resulting different protonation states of the investigated molecules are crucial to attain a good alignment with experimental results. Especially for calculations regarding complex molecule states, such as the reduced state of DADdi(OH) at high pH value, further studies are needed. However, even though a conclusive validation of the applied model has yet to be performed, our calculations pose a promising starting point for further calculations on DAAQ reduction potentials.

The highest occupied molecular orbital (HOMO) of the reduced molecules, which corresponds to the lowest unoccupied molecular orbital (LUMO) of the unreduced molecules, can be used to visualize the qualitative bond length changes during reduction (see Figure 4). The displayed orbital contributions with bonding character indicate bond shortening, whereas orbital contributions with antibonding character lead up to bond elongation. The HOMOs of the reduced DAAQ molecules are very similar to the HOMOs of anthraquinone (AQ), whereby a slightly better agreement could be attained at low pH values.

The reduction of the DAAQs at low pH results in a strong elongation of the quinone C−O bond and the neighboring C−C bond toward the diaza moiety. The corresponding C−C bond away from the diaza group is less elongated. The diaza N−N bond length increases for all DAAQs comparable to the corresponding C−C bond. The absolute bond length changes for DAD and DAD(MeO) are closer to each other than to DADdi(OH). Similar qualitative bond length changes occur for the reduction at high pH value, but in general, the absolute values of bond length changes are smaller. An exception is the bond elongation of the N−N bond of the diaza moiety as well as the corresponding C−C bond, which turns out to be larger than at low pH values.

The HOMOs of the reduced DAD(MeO) and DADdi(OH) include an additional antibonding contribution from the C−O bonds of the methoxy or hydroxyl substituents. The smaller C−O bond elongation of the methoxy group for low compared to high pH values indicates slightly higher stability of this bond at low pH values. See Table T1 in the Supporting Information for a more detailed overview of the calculated bond length alterations.

■ CONCLUSIONS

We systematically investigated three DAAQ compounds as potential active materials for RFBs. For aqueous solutions, a positive redox potential shift of about 300 mV can be achieved through the incorporation of a diaza moiety into the AQ base structure, which, combined with the subsequent structural functionalization, provides a great opportunity for increasing the achievable energy density of quinone-based RFBs.

For a comprehensive understanding of the electrochemical properties, the compounds were studied in different solvents—both experimentally and with density functional calculations. Investigations at low pH proved that the addition of a methoxy group strongly increases the electrochemical stability of diaza compounds in aqueous acidic media. Furthermore, the functionalization with two hydroxyl groups in close vicinity to the carbonyl group resulted in a negative redox potential shift of 54 mV for acidic and 264 mV for alkaline solutions. These results demonstrate that this novel class of compounds is highly versatile and can be tailor-made for use as active material in RFBs.

For the CV measurements in alkaline aqueous solutions, a reversible charge transfer behavior is observed for all of the three molecular structures. At high pH a splitting of the cathodic and anodic voltammetric wave occurs for DAD and DAD(MeO). This characteristic is highly unusual for quinonoid compounds in aqueous solution and has only been reported in a few publications. The functionalization with a methoxy moiety intensifies this effect, and we assume that it—as well as the diaza group—stabilizes the semiquinone radical, thereby leading to an increased potential difference between the two individual electron transfers. This is also reflected by the aforementioned increase in electrochemical stability of DAD(MeO) at low pH. Additionally, for DADdi(OH), a remarkably low redox potential of −0.555 V versus Ag/AgCl was achieved, which even undercuts established anolyte active materials such as AQDS.

Furthermore, our DFT calculations reveal further trends regarding the reduction potentials of differently substituted DAAQs that are in good agreement with our experimental results. Especially for the scenario of strongly acidic conditions we calculated reduction potentials that reflect the structure dependent trend specified by our experimental results. For high pH values a greater offset from the experimental potentials was obtained while at least maintaining a qualitative conformity. The redox potential shifts evoked by the incorporation of a diaza moiety as well as a change in pH value could also be reproduced with great accordance to the experimental outcomes.

Moreover, our theoretical considerations give useful indications about whether a DAAQs species is likely to be in a protonated state or not. Besides, the geometric and electronic structures of DAAQs were illustrated, indicating bond length changes during reduction that allow to estimate relative stability.

The DAAQs presented in this study were also used as anolyte active materials in a full RFB as proof of concept. Based on the findings of the half-cell experiments, galvanostatic cycling experiments were conducted in alkaline solution, which ensured electrochemical reversibility. In these measurements we were able to demonstrate that a suitable structural functionalization can be a useful tool to manipulate the electrochemical characteristics of DAAQ-based RFBs. While we observed the highest Coulombic efficiencies for DAD(MeO) as anolyte active material, as a result of the dihydroxy-functionalization we attained the highest cell voltages for RFBs based on DADdi(OH).

In general, low active material solubilities and long-term stability issues of DAAQs need to be addressed in future studies to be competitive with established quinonoid active materials on the full-cell scale. However, we present a class of compounds that is very versatile, which gives reason to believe that the aforementioned challenges can be overcome by further structural optimization.

Since a higher potential difference between anolyte and catholyte reduces cell stack costs for RFBs, diaza-based quinonoid compounds serve as a promising material class for custom-tailored active materials. As the diaza moiety leads to a strong positive redox potential shift, DAAQs and above all diaza-naphtoquinones should be taken into consideration as catholyte active materials. Especially for naphthoquinones,

DOI: 10.1021/acs.chemmater.7b04220
Chem. Mater. 2018, 30, 762−774

which intrinsically exhibit higher redox potentials relative to anthraquinones, the distinct positive potential shift could be highly beneficial in terms of high cell voltages and energy densities. With this in mind, the diaza-based structural modification, in combination with protecting groups (e.g., −MeO) and electron-withdrawing groups (e.g., $-NO_2$), could lead to promising organic active materials to meet the high specific energy storage demands in RFBs.

■ ASSOCIATED CONTENT

Supporting Information

The Supporting Information is available free of charge on the ACS Publications website at DOI: 10.1021/acs.chemmater.7b04220.

Additional electrochemistry data, SEM images, impedance data, and DFT calculations (PDF)

■ AUTHOR INFORMATION

Corresponding Authors

*E-mail: juergen.janek@phys.chemie.uni-giessen.de.
*E-mail: daniel.schroeder@phys.chemie.uni-giessen.de.

ORCID

Hermann A. Wegner: 0000-0001-7260-6018
Daniel Schröder: 0000-0002-2198-0218

Notes

The authors declare no competing financial interest.

■ ACKNOWLEDGMENTS

The project was supported by the CMBlu AG. H.A.W., J.J., and D.S. gratefully acknowledge financial support by BMEL (Federal Ministry of Food and Agriculture) within the project FOREST (22403116), and by the CMBlu AG.

■ REFERENCES

(1) Huskinson, B.; Marshak, M. P.; Suh, C.; Er, S.; Gerhardt, M. R.; Galvin, C. J.; Chen, X.; Aspuru-Guzik, A.; Gordon, R. G.; Aziz, M. J. A Metal-Free Organic-Inorganic Aqueous Flow Battery. *Nature* **2014**, *505*, 195−198.

(2) Lin, K.; Gómez-Bombarelli, R.; Beh, E. S.; Tong, L.; Chen, Q.; Valle, A.; Aspuru-Guzik, A.; Aziz, M. J.; Gordon, R. G. A Redox-Flow Battery with an Alloxazine-Based Organic Electrolyte. *Nat. Energy* **2016**, *1*, 16102.

(3) Wei, X.; Pan, W.; Duan, W.; Hollas, A.; Yang, Z.; Li, B.; Nie, Z.; Liu, J.; Reed, D.; Wang, W.; et al. Materials and Systems for Organic Redox Flow Batteries: Status and Challenges. *ACS Energy Lett.* **2017**, *2*, 2187−2204.

(4) Liu, T.; Wei, X.; Nie, Z.; Sprenkle, V.; Wang, W. A Total Organic Aqueous Redox Flow Battery Employing a Low Cost and Sustainable Methyl Viologen Anolyte and 4-HO-TEMPO Catholyte. *Adv. Energy Mater.* **2016**, *6*, 1501449.

(5) Schmidt, D.; Häupler, B.; Friebe, C.; Hager, M. D.; Schubert, U. S. Synthesis and Characterization of New Redox-Active Polymers Based on 10-(1,3-Dithiol-2-Ylidene)Anthracen-9(10H)-One Derivatives. *Polymer* **2015**, *68*, 321−327.

(6) Duan, W.; Huang, J.; Kowalski, J. A.; Shkrob, I. A.; Vijayakumar, M.; Walter, E.; Pan, B.; Yang, Z.; Milshtein, J. D.; Li, B.; et al. Wine-Dark Sea" in an Organic Flow Battery: Storing Negative Charge in 2,1,3-Benzothiadiazole Radicals Leads to Improved Cyclability. *ACS Energy Lett.* **2017**, *2*, 1156−1161.

(7) Hoober-Burkhardt, L.; Krishnamoorthy, S.; Yang, B.; Murali, A.; Nirmalchandar, A.; Prakash, G. K. S.; Narayanan, S. R. A New Michael-Reaction-Resistant Benzoquinone for Aqueous Organic Redox Flow Batteries. *J. Electrochem. Soc.* **2017**, *164*, A600−A607.

(8) Gerhardt, M. R.; Tong, L.; Gómez-Bombarelli, R.; Chen, Q.; Marshak, M. P.; Galvin, C. J.; Aspuru-Guzik, A.; Gordon, R. G.; Aziz, M. J. Anthraquinone Derivatives in Aqueous Flow Batteries. *Adv. Energy Mater.* **2017**, *7*, 1601488.

(9) Yang, B.; Hoober-Burkhardt, L.; Krishnamoorthy, S.; Murali, A.; Prakash, G. K. S.; Narayanan, S. R. High-Performance Aqueous Organic Flow Battery with Quinone-Based Redox Couples at Both Electrodes. *J. Electrochem. Soc.* **2016**, *163*, A1442−A1449.

(10) Potash, R. A.; McKone, J. R.; Conte, S.; Abruña, H. D. On the Benefits of a Symmetric Redox Flow Battery. *J. Electrochem. Soc.* **2016**, *163*, A338−A344.

(11) Chen, Q.; Gerhardt, M. R.; Hartle, L.; Aziz, M. J. A Quinone-Bromide Flow Battery with 1 W/Cm2 Power Density. *J. Electrochem. Soc.* **2016**, *163*, A5010−A5013.

(12) Lin, K.; Chen, Q.; Gerhardt, M. R.; Tong, L.; Kim, S. B.; Eisenach, L.; Valle, A. W.; Hardee, D.; Gordon, R. G.; Aziz, M. J.; et al. Alkaline Quinone Flow Battery. *Science* **2015**, *349*, 1529−1532.

(13) Carney, T. J.; Collins, S. J.; Moore, J. S.; Brushett, F. R. Concentration-Dependent Dimerization of Anthraquinone Disulfonic Acid and Its Impact on Charge Storage. *Chem. Mater.* **2017**, *29*, 4801−4810.

(14) Huynh, M. T.; Anson, C. W.; Cavell, A. C.; Stahl, S. S.; Hammes-Schiffer, S. Quinone 1 E− and 2 E−/2 H+ Reduction Potentials: Identification and Analysis of Deviations from Systematic Scaling Relationships. *J. Am. Chem. Soc.* **2016**, *138*, 15903−15910.

(15) Er, S.; Suh, C.; Marshak, M. P.; Aspuru-Guzik, A. Computational Design of Molecules for an All-Quinone Redox Flow Battery. *Chem. Sci.* **2015**, *6*, 885−893.

(16) Pineda Flores, S. D.; Martin-Noble, G. C.; Phillips, R. L.; Schrier, J. Bio-Inspired Electroactive Organic Molecules for Aqueous Redox Flow Batteries. 1. Thiophenoquinones. *J. Phys. Chem. C* **2015**, *119*, 21800−21809.

(17) Son, E. J.; Kim, J. H.; Kim, K.; Park, C. B. Quinone and Its Derivatives for Energy Harvesting and Storage Materials. *J. Mater. Chem. A* **2016**, *4*, 11179−11202.

(18) Schweighauser, L.; Bodoky, I.; Kessler, S. N.; Häussinger, D.; Donsbach, C.; Wegner, H. A. Bidentate Lewis Acid Catalyzed Domino Diels−Alder Reaction of Phthalazine for the Synthesis of Bridged Oligocyclic Tetrahydronaphthalenes. *Org. Lett.* **2016**, *18*, 1330−1333.

(19) De Isabella, P.; Palumbo, M.; Sissi, C.; Carenini, N.; Capranico, G.; Menta, E.; Oliva, A.; Spinelli, S.; Krapcho, A. P.; Giuliani, F. C.; et al. Physicochemical Properties, Cytotoxic Activity and Topoisomerase Ii Inhibition of 2,3-Diaza-Anthracenediones. *Biochem. Pharmacol.* **1997**, *53*, 161−169.

(20) Krapcho, A. P.; Maresch, M. J.; Hacker, M. P.; Menta, E.; Oliva, A.; Giuliani, F. C.; Spinelli, S. Aza and Diaza Bioisosteric Anthracene-9,10-Diones as Antitumor Agents. *Acta Biochim. Polym.* **1995**, *42* (4), 427−432.

(21) Hong, L.; Ahles, S.; Strauss, M. A.; Logemann, C.; Wegner, H. A. Synthesis of 2,3-Diaza-Anthraquinones via the Bidentate Lewis Acid Catalysed Inverse Electron-Demand Diels−Alder (IEDDA) Reaction. *Org. Chem. Front.* **2017**, *4*, 871−875.

(22) Ren, J.; Lu, L.; Xu, J.; Yu, T.; Zeng, B.-B. Selective Oxidation of 1-Tetralones to 1,2-Naphthoquinones with IBX and to 1,4-Naphthoquinones with Oxone® and 2-Iodobenzoic Acid. *Synthesis* **2015**, *47*, 2270−2280.

(23) Domasevitch, K. V.; Gural'skiy, I. A.; Solntsev, P. V.; Rusanov, E. B.; Krautscheid, H.; Howard, J. A. K.; Chernega, A. N. 4,4′-Bipyridazine: A New Twist for the Synthesis of Coordination Polymers. *Dalton Trans.* **2007**, No. 29, 3140−3148.

(24) Hamann, C. H. *Elektrochemie; Auflage: 4. vollst. überarb. u. aktualis. Auflage*; Wiley-VCH Verlag GmbH & Co. KGaA: Weinheim, 2005.

(25) Frisch, M. J.; Trucks, G. W.; Schlegel, H. B.; Scuseria, G. E.; Robb, M. A.; Cheeseman, J. R.; Scalmani, G.; Barone, V.; Mennucci, B.; Petersson, G. A.; Nakatsuji, H.; Caricato, M.; Li, X.; Hratchian, H. P.; Izmaylov, A. F.; Bloino, J.; Zheng, G.; Sonnenberg, J. L.; Hada, M.; Ehara, M.; Toyota, K.; Fukuda, R.; Hasegawa, J.; Ishida, M.; Nakajima, T.; Honda, Y.; Kitao, O.; Nakai, H.; Vreven, T.; Montgomery, J. A., Jr.;

DOI: 10.1021/acs.chemmater.7b04220
Chem. Mater. 2018, 30, 762−774

Peralta, J. E.; Ogliaro, F.; Bearpark, M.; Heyd, J. J.; Brothers, E.; Kudin, K. N.; Staroverov, V. N.; Kobayashi, R.; Normand, J.; Raghavachari, K.; Rendell, A.; Burant, J. C.; Iyengar, S. S.; Tomasi, J.; Cossi, M.; Rega, N.; Millam, J. M.; Klene, M.; Knox, J. E.; Cross, J. B.; Bakken, V.; Adamo, C.; Jaramillo, J.; Gomperts, R.; Stratmann, R. E.; Yazyev, O.; Austin, A. J.; Cammi, R.; Pomelli, C.; Ochterski, J. W.; Martin, R. L.; Morokuma, K.; Zakrzewski, V. G.; Voth, G. A.; Salvador, P.; Dannenberg, J. J.; Dapprich, S.; Daniels, A. D.; Farkas, O.; Foresman, J. B.; Ortiz, J. V.; Cioslowski, J.; Fox, D. J. *Gaussian 09*, revision A.01; Gaussian, Inc.: Wallingford, CT, 2009.

(26) Becke, A. D. Density-Functional Exchange-Energy Approximation with Correct Asymptotic Behavior. *Phys. Rev. A: At., Mol., Opt. Phys.* **1988**, *38*, 3098−3100.

(27) Perdew, J. P.; Yue, W. Accurate and Simple Density Functional for the Electronic Exchange Energy: Generalized Gradient Approximation. *Phys. Rev. B: Condens. Matter Mater. Phys.* **1986**, *33*, 8800−8802.

(28) Grimme, S.; Antony, J.; Ehrlich, S.; Krieg, H. A Consistent and Accurate Ab Initio Parametrization of Density Functional Dispersion Correction (DFT-D) for the 94 Elements H-Pu. *J. Chem. Phys.* **2010**, *132*, 154104.

(29) Grimme, S.; Ehrlich, S.; Goerigk, L. Effect of the Damping Function in Dispersion Corrected Density Functional Theory. *J. Comput. Chem.* **2011**, *32*, 1456−1465.

(30) Kendall, R. A.; Dunning, T. H.; Harrison, R. J. Electron Affinities of the First-row Atoms Revisited. Systematic Basis Sets and Wave Functions. *J. Chem. Phys.* **1992**, *96*, 6796−6806.

(31) Tomasi, J.; Mennucci, B.; Cammi, R. Quantum Mechanical Continuum Solvation Models. *Chem. Rev.* **2005**, *105*, 2999−3094.

(32) Kim, H.; Goodson, T.; Zimmerman, P. M. Achieving Accurate Reduction Potential Predictions for Anthraquinones in Water and Aprotic Solvents: Effects of Inter- and Intramolecular H-Bonding and Ion Pairing. *J. Phys. Chem. C* **2016**, *120*, 22235−22247.

(33) Ho, J.; Coote, M. L.; Cramer, C. J.; Truhlar, D. G. Theoretical Calculation of Reduction Potentials. *Org. Electrochem.* **2012**, *5*, 229−259.

(34) Guin, P. S.; Das, S.; Mandal, P. C. Electrochemical Reduction of Quinones in Different Media: A Review. *Int. J. Electrochem.* **2011**, *2011*, e816202-1−e816202-22.

(35) Castle, R. N. *Condensed Pyridazines Including Cinnolines and Phthalazines*; John Wiley & Sons, 2009.

(36) Fawcett, W. R. The Ionic Work Function and Its Role in Estimating Absolute Electrode Potentials. *Langmuir* **2008**, *24*, 9868−9875.

(37) Revenga, J.; Rodríguez, F.; Tijero, J. Study of the Redox Behavior of Anthraquinone in Aqueous Medium. *J. Electrochem. Soc.* **1994**, *141*, 330−333.

(38) Raczyńska, E. D.; Gal, J.-F.; Maria, P.-C. Gas-Phase Basicity of Aromatic Azines: A Short Review on Structural Effects. *Int. J. Mass Spectrom.* **2017**, *418*, 130−139.

(39) Isse, A. A.; Gennaro, A. Absolute Potential of the Standard Hydrogen Electrode and the Problem of Interconversion of Potentials in Different Solvents. *J. Phys. Chem. B* **2010**, *114*, 7894−7899.

(40) Kelly, C. P.; Cramer, C. J.; Truhlar, D. G. Aqueous Solvation Free Energies of Ions and Ion-Water Clusters Based on an Accurate Value for the Absolute Aqueous Solvation Free Energy of the Proton. *J. Phys. Chem. B* **2006**, *110*, 16066−16081.

(41) Becke, A. D. Density-Functional Thermochemistry. III. The Role of Exact Exchange. *J. Chem. Phys.* **1993**, *98*, 5648−5652.

(42) Kim, R. S.; Chung, T. D. The Electrochemical Reaction Mechanism and Applications of Quinones. *Bull. Korean Chem. Soc.* **2014**, *35*, 3143−3155.

(43) Wang, Z.; Li, A.; Gou, L.; Ren, J.; Zhai, G. Computational Electrochemistry Study of Derivatives of Anthraquinone and Phenanthraquinone Analogues: The Substitution Effect. *RSC Adv.* **2016**, *6*, 89827−89835.

(44) Zhao, Q.; Zhu, Z.; Chen, J. Molecular Engineering with Organic Carbonyl Electrode Materials for Advanced Stationary and Redox Flow Rechargeable Batteries. *Adv. Mater.* **2017**, *29*, 1607007.

(45) Aue, D. H.; Webb, H. M.; Davidson, W. R.; Toure, P.; Hopkins, H. P.; Moulik, S. P.; Jahagirdar, D. V. Relationships between the Thermodynamics of Protonation in the Gas and Aqueous Phase for 2-, 3-, and 4- Substituted Pyridines. *J. Am. Chem. Soc.* **1991**, *113*, 1770−1780.

(46) Hunter, E. P. L.; Lias, S. G. Evaluated Gas Phase Basicities and Proton Affinities of Molecules: An Update. *J. Phys. Chem. Ref. Data* **1998**, *27*, 413−656.

(47) Wiseman, A.; Sims, L. A.; Snead, R.; Gronert, S.; Maclagan, R. G. A. R.; Meot-Ner, M. Protonation Energies of 1−5-Ring Polycyclic Aromatic Nitrogen Heterocyclics: Comparing Experiment and Theory. *J. Phys. Chem. A* **2015**, *119*, 118−126.

(48) Maclagan, R. G. A. R.; Gronert, S.; Meot-Ner, M. Protonated Polycyclic Aromatic Nitrogen Heterocyclics: Proton Affinities, Polarizabilities, and Atomic and Ring Charges of 1−5-Ring Ions. *J. Phys. Chem. A* **2015**, *119*, 127−139.

(49) Gamboa-Valero, N.; Astudillo, P. D.; González-Fuentes, M. A.; Leyva, M. A.; Rosales-Hoz, M.; de, J.; González, F. J. Hydrogen Bonding Complexes in the Quinone-Hydroquinone System and the Transition to a Reversible Two-Electron Transfer Mechanism. *Electrochim. Acta* **2016**, *188*, 602−610.

(50) Song, Y.; Buettner, G. R. Thermodynamic and Kinetic Considerations for the Reaction of Semiquinone Radicals to Form Superoxide and Hydrogen Peroxide. *Free Radical Biol. Med.* **2010**, *49*, 919−962.

(51) Bolton, J. L.; Trush, M. A.; Penning, T. M.; Dryhurst, G.; Monks, T. J. Role of Quinones in Toxicology. *Chem. Res. Toxicol.* **2000**, *13*, 135−160.

(52) Armitage, B.; Yu, C.; Devadoss, C.; Schuster, G. B. Cationic Anthraquinone Derivatives as Catalytic DNA Photonucleases - Mechanisms for DNA-Damage and Quinone Recycling. *J. Am. Chem. Soc.* **1994**, *116*, 9847−9859.

(53) Cain, E. N.; Solly, R. K. Radical Stabilization Energies in Esters..Beta.-Carbomethoxy Group from Kinetics of the Thermal Isomerization of 1-Chloro-4-Carbomethoxybicyclo[2.2.0]Hexane in the Liquid Phase. *J. Am. Chem. Soc.* **1973**, *95*, 4791−4796.

(54) Mathew, S.; Abraham, T. E.; Zakaria, Z. A. Reactivity of Phenolic Compounds towards Free Radicals under in Vitro Conditions. *J. Food Sci. Technol.* **2015**, *52*, 5790−5798.

(55) Velkov, Z. A.; Kolev, M. K.; Tadjer, A. V. Modeling and Statistical Analysis of DPPH Scavenging Activity of Phenolics. *Collect. Czech. Chem. Commun.* **2007**, *72*, 1461−1471.

(56) Li, Q.; Batchelor-McAuley, C.; Lawrence, N. S.; Hartshorne, R. S.; Compton, R. G. Electrolyte Tuning of Electrode Potentials: The One Electron vs. Two Electron Reduction of Anthraquinone-2-Sulfonate in Aqueous Media. *Chem. Commun.* **2011**, *47*, 11426−11428.

(57) Kim, Y.-R.; Kim, R. S.; Kang, S. K.; Choi, M. G.; Kim, H. Y.; Cho, D.; Lee, J. Y.; Chang, S.-K.; Chung, T. D. Modulation of Quinone PCET Reaction by Ca2+ Ion Captured by Calix[4]Quinone in Water. *J. Am. Chem. Soc.* **2013**, *135*, 18957−18967.

(58) Gupta, N.; Linschitz, H. Hydrogen-Bonding and Protonation Effects in Electrochemistry of Quinones in Aprotic Solvents. *J. Am. Chem. Soc.* **1997**, *119*, 6384−6391.

(59) Quan, M.; Sanchez, D.; Wasylkiw, M. F.; Smith, D. K. Voltammetry of Quinones in Unbuffered Aqueous Solution: Reassessing the Roles of Proton Transfer and Hydrogen Bonding in the Aqueous Electrochemistry of Quinones. *J. Am. Chem. Soc.* **2007**, *129*, 12847−12856.

(60) DOE Office of Electricity Delivery & Energy Reliability. Program Planning Document on Energy Storage, 2011.

(61) Bard, A. J.; Faulkner, L. R. *Electrochemical Methods: Fundamentals and Applications*; Wiley, 2000.

(62) Muhammad, H.; Tahiri, I. A.; Muhammad, M.; Masood, Z.; Versiani, M. A.; Khaliq, O.; Latif, M.; Hanif, M. A Comprehensive Heterogeneous Electron Transfer Rate Constant Evaluation of Dissolved Oxygen in DMSO at Glassy Carbon Electrode Measured by Different Electrochemical Methods. *J. Electroanal. Chem.* **2016**, *775*, 157−162.

DOI: 10.1021/acs.chemmater.7b04220
Chem. Mater. 2018, 30, 762−774

(63) Yang, B.; Hoober-Burkhardt, L.; Wang, F.; Prakash, G. K. S.; Narayanan, S. R. An Inexpensive Aqueous Flow Battery for Large-Scale Electrical Energy Storage Based on Water-Soluble Organic Redox Couples. *J. Electrochem. Soc.* **2014**, *161*, A1371−A1380.
(64) Armarego, W. L. F. *Purification of Laboratory Chemicals*; Butterworth-Heinemann, 2017.
(65) Mukherjee, T.; Land, E. J.; Swallow, A. J.; Guyan, P. M.; Bruce, J. M. Successive Addition of Electrons to Sodium Quinizarin-2- and −6-Sulphonate in Aqueous Solution. a Pulse and γ-Radiolysis Study. *J. Chem. Soc., Faraday Trans. 1* **1988**, *84*, 2855−2873.

DOI: 10.1021/acs.chemmater.7b04220
Chem. Mater. 2018, 30, 762−774

2.2 Elucidating the impact of the nature and pH value of the solvent on the charge transfer characteristics of diaza-quinones

Publication II revealed several peculiarities with regard to the electrochemical properties of DAAQs compared to their homocyclic analogues. Besides the observed increase of the redox potential, the nitrogen-based functionalization most notably affected the charge transfer characteristics of the investigated derivatives. This is particularly evident for measurements in alkaline solution, which revealed an extraordinary separation of the two commonly simultaneous electron transfers observed for the reduction of quinones in aqueous solution. To gain a deeper understanding of their charge transfer behavior, the DAAQs were systematically studied with regard to the impact of the nature and pH value of the applied solvent. For that purpose, voltammetric measurements were conducted in aqueous solutions of varying pH value as well as in aprotic, organic solvents. Whereas the pH-dependent measurements of publication II were limited to scenarios of high (pH = 0) and low acidity (pH = 14), the pH value was adjusted incrementally in this case, enabling the construction of a Pourbaix diagram. As the charge transfer behavior of quinonoid compounds is known to be affected by protonation and hydrogen bonding, these measurements were complemented by experiments in acetonitrile as an aprotic, non-hydrogen bonding solvent to mitigate or even eliminate effects of this sort.

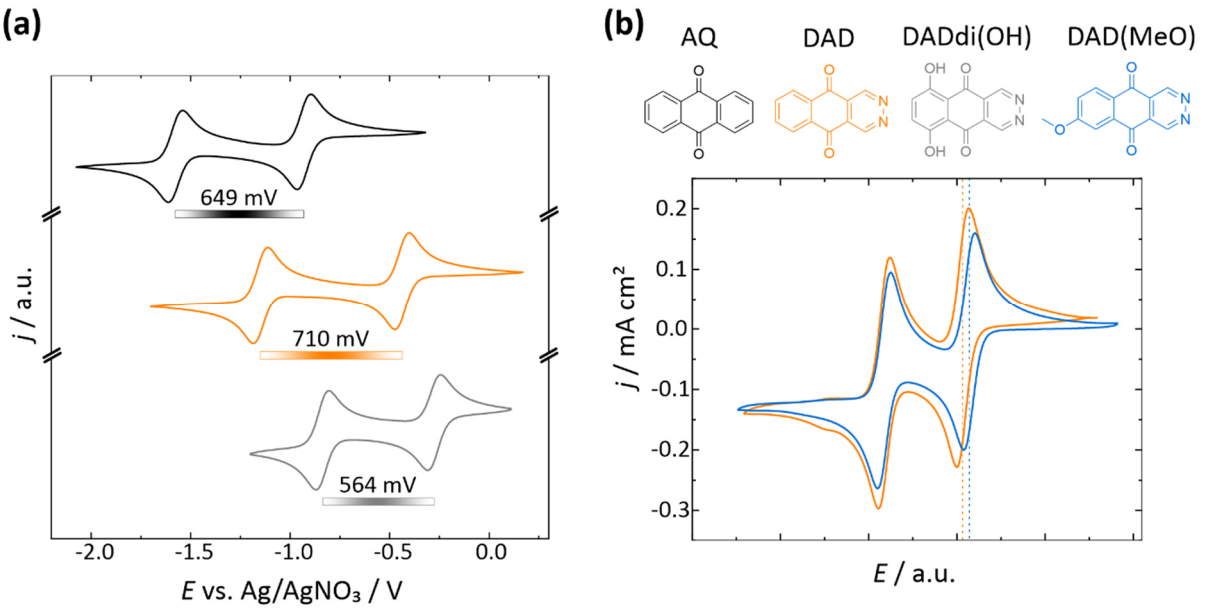

Figure 8: Voltammetric overview of varying quinone compounds. (a) Comparison of reduction potentials and relative potential differences ΔE_p between the two subsequent electron transfers of AQ, DAD and DADdi(OH) in acetonitrile. (b) Comparison of the ΔE_p of DAD and DAD(MeO). For the sake of clarity, *E* was shifted to match the potentials of the reduction process at more negative potentials for both CVs.

As described in publication II, a separation of the two occurring charge transfer steps, formerly described as peak splitting, is observed for some DAAQs in alkaline aqueous media as a result of a stabilized semiquinone intermediate. This theory was corroborated by a direct comparison of the CVs of the unmodified DAAQ base structure and its homocyclic AQ analogue in a nonaqueous solvent. To substantiate these results, the experiment was repeated subsequently under optimized conditions as thoroughly dried electrolyte components. As depicted in Figure 8(a), the stabilizing effect of the incorporated nitrogen evokes a positive potential shift of the first reduction process and thus manifests in an increased relative potential difference between the two occurring charge transfers. For DAD, this turns out to be 60 mV larger as compared to the regular AQ species.

An even more pronounced peak splitting was observed in the case of DAD(MeO), which was associated with the radical-stabilizing effect of methoxy groups. Indeed, the increased graduation observed in alkaline solution is corroborated by comparative measurements in acetonitrile as depicted in Figure 8(b). With regard to valence band theory, this stabilizing effect is to be associated with the interaction between the radical center and the nonbonding electron pairs of oxygen provided by the methoxy group.[221] Since the methoxy moiety enables an extended delocalization of the radical and hence an increased resonance energy, the intermediate is thermodynamically stabilized. This manifests in a positive potential shift of the first peak at more positive potentials in the CV. Furthermore, it is substantiated by the similar reduction potentials of DAD and DAD(MeO) − especially with regard to acidic solution − despite the well-known positive mesomeric effect of the methoxy moiety. By implication, the anticipated electron-donating effect of the methoxy group may be compensated by the positive shift due to resonance stabilization.

Interestingly, no peak splitting at all is observed for DADdi(OH) in alkaline solution. As already indicated in section 1.3.1, this may be explained by the additional influence of intramolecular hydrogen bonding, which emanates from the hydroxyl substituents added to the structure in close vicinity to the characteristic hydroxyl/carbonyl groups. The same effect leads to allegedly contradictory results for CV measurements in acetonitrile: in spite of the commonly electron donating effect of the incorporated hydroxyl moieties, a positive potential shift is observed as compared to the unfunctionalized base structure DAD (see Figure 5). Furthermore, the relative potential difference of the subsequent electron transfers is clearly reduced as a result of this effect. It is to be expected that this also translates to the measurements in aqueous media, which consequently feature a single reduction and oxidation peak.

The impact of hydrogen bonding and protonation adds another layer of complexity for measurements in aqueous solution, which go beyond the intrinsic factors given by the specific structure of the derivatives. In order to resolve the charge transfer behavior of DAAQs as a function of

these effects, voltammetric measurements were carried out under incremental variation of the pH value of the electrolyte. Subsequently, a Pourbaix diagram was created by means of the formal potentials extracted from these measurements. This form of presentation illustrates the interplay of protonation and electron transfer on the basis of pH dependent potential shifts according to the theoretical framework given in section 1.3.2. Intersections between areas of different slopes are to be interpreted as the dissociation constants (pK_a) of the associated protonation states.

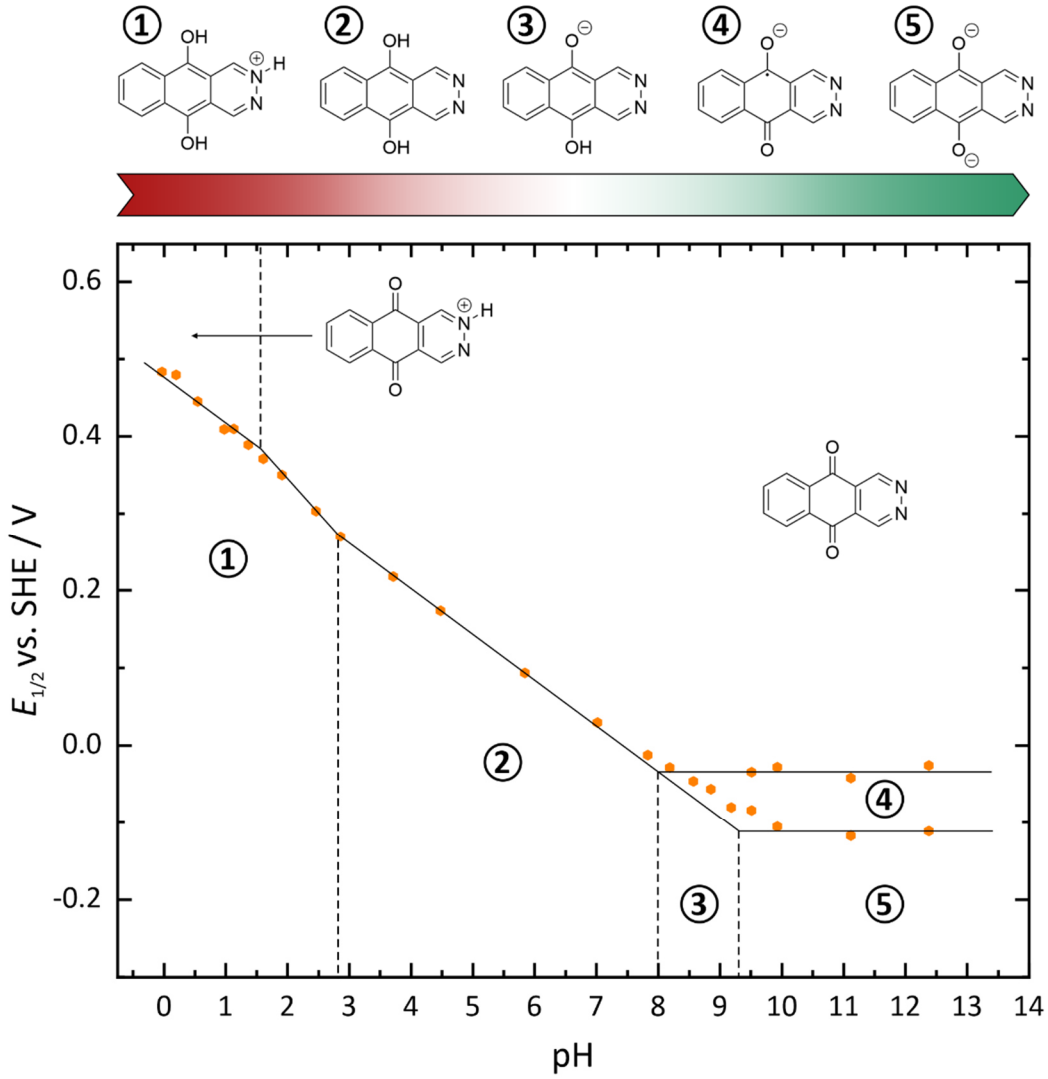

Figure 9: Pourbaix diagram of the unfunctionalized diaza-anthraquinone DAD. A pH-dependent voltammetric analysis reveals three domains of varying slopes. Below pH = 1.5 the educt is present in a protonated state, resulting in a $2e^-/2H^+$ reduction (m_{theo} = 59 mV/pH). Between pH = 1.5 and pH = 2.85, the diaza-moiety is protonated in the course of the occurring reduction, resulting in a $2e^-/3H^+$ process (m_{theo} = 89 mV/pH), followed by another $2e^-/2H^+$ reaction sequence. The semiquinone anion radical $Q^{\bullet -}$ is protonated up to a pH value of 8. From this point, the second voltammetric wave associated with the formation of QH^- shifts further on according to a $1e^-/1H^+$ process. By implication, the peak splitting priorly observed for DAD at high pH values increases up to a pH value of 9.4, which marks the formation of the dianion Q^{2-} in the absence of protonation. Consequently, the potential of the two individual electron transfers remains constant for pH values beyond that.

It becomes evident that the Pourbaix diagram of DAAQs in Figure 9 features a number of peculiar features as compared to the homocyclic AQDS (compare Figure 6). This primarily applies to the extreme regions of the pH scale: whereas the area between pH = 2.85 and pH = 8 exhibits a slope of about 59 mV/pH − representing a $2e^-/2H^+$ transfer as already encountered for AQDS − extraordinary characteristics are observed at pH values below and above that range. Originating from pH = 8, the graduation of the two individual electron transfers increases together with the pH value of the solution. Unlike the semiquinone intermediate ($pK_a \approx 8$), a protonation of the dianion Q^{2-} as the final reduction product occurs up to pH ≈ 9.4. This results in a slope of 59 mV/pH ($1e^-/1H^+$) and eventually the distinct peak splitting as observed in publication II. Beyond a pH value of 9.4, the potential of both individual electron transfers remains constant, since protonation is not further involved in the reduction process. Regarding the area below pH = 2.85, the slope clearly increases as compared to the intermediate pH region. This suggests that the ratio of transferred electrons and protons changes in favor of the latter. The determined slope of 84 mV/pH indicates a $3H^+/2e^-$ transfer, which is associated with a theoretical slope of 89 mV/pH. The pK_a value of 3.47[222] for phthalazine as a reference compound legitimates this assumption of an additional protonation of the diaza-moiety in the course of DAAQ reduction. The situation changes once more going to even more acidic conditions below pH = 1.5: as indicated by the reduced slope, DAD is presumably present in its protonated form even prior to reduction. However, the experimentally determined slope of 71 mV/pH slightly surpasses the anticipated value of 59 mV/pH for a $2e^-/2H^+$ process. Anyway, there is strong indication that DAAQs undergo an additional protonation process at low pH values compared to homocyclic AQs. The resulting cationic form of the protonated active material may become relevant for RFBs based on proton-conducting membranes. However, the implications for the crossover behavior of DAAQs are yet to be investigated.

Nevertheless, DAAQs may also be applied as effective at less acidic pH values: as stated earlier, the reaction sequence of AQs is determined by an alternating electron and proton transfer at pH values below 7 (see section 1.3.1 for more detailed information). A reaction sequence of this sort is commonly accompanied by a high degree of potential inversion, which according to equation (9) leads to sluggish overall charge transfer kinetics.[36,37,42,218] Now with regard to DAAQs, the diaza-induced stabilization of the semiquinone intermediate should diminish the degree of potential inversion in this pH region, thus positively affecting the apparent rate constant k_{app}. Ultimately, this effect should translate to low peak separations ΔE_p during CV.[166] For the purpose of a conclusive evaluation of the overall charge transfer kinetics of DAAQs in the neutral to acidic pH region, the voltammetric measurements conducted as part of the Pourbaix analysis will be consulted. As illustrated in Figure 10, DAD indeed features a considerably low and constant peak separation across the investigated pH range, which even applies

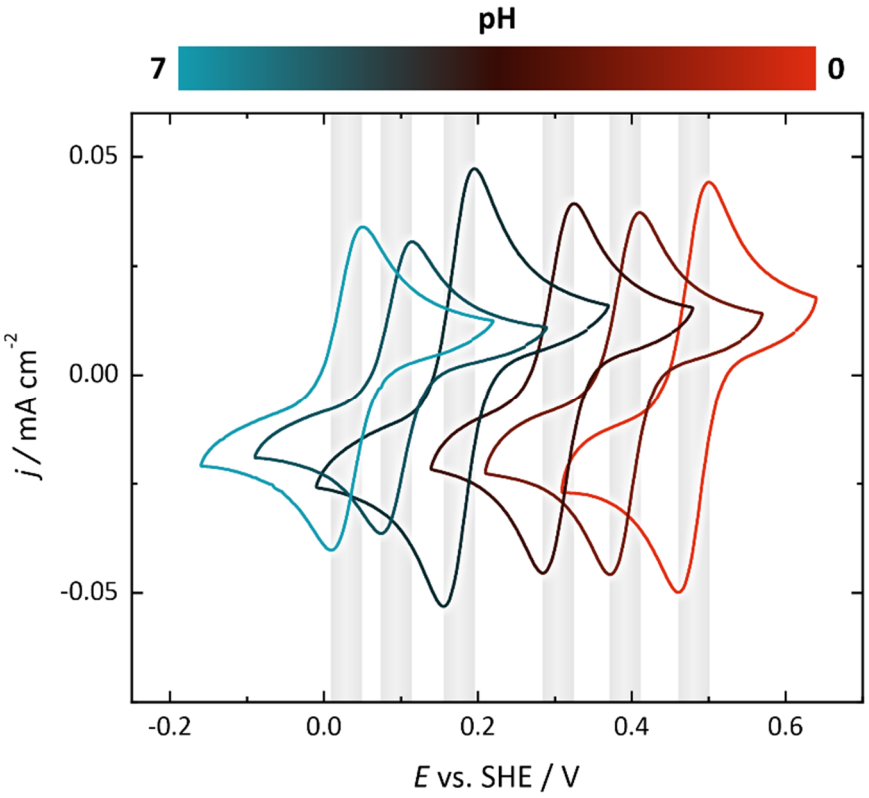

Figure 10: Voltammetric evaluation of the charge transfer kinetics of DAAQs in the pH range between 0 and 7 by means of ΔE_p. The grey highlights mark a potential interval of 40 mV, which is maintained across the investigated pH range.

to the potentially problematic alternating reaction sequences. In fact, the measured ΔE_p of about 40 mV comes very close to the value of 30 mV anticipated for an ideal two-electron transfer.[82] By implication, electron transfer occurs at solely marginal overpotentials with respect to the associated equilibrium potential. Conclusively, DAAQs offer fast charge transfer kinetics unaffected by the respective reaction sequence. This allows for an efficient application across a large range of pH values and thus poses a major advantage over homocyclic analogues, which may be negatively affected by the consequences of potential inversion.

Experimental:

The investigated active materials were provided by the research group Wegner (Institute of Organic Chemistry, JLU Giessen). The voltammetric measurements in acetonitrile and aqueous solutions were conducted according to the procedure described in publication II.[167] To allow for measurements at distinct pH values, buffered aqueous solutions up to an ionic strength of 0.2 mol L^{-1} were prepared. The buffer components (H_3PO_4, KH_2PO_4, K_2HPO_4, K_3PO_4, $KHSO_4$, K_2SO_4, NH_4Cl, $C_4H_6O_4$) were purchased from Sigma Aldrich and used as received. The setup for measurements in nonaqueous solvents comprised a glassy carbon working electrode (Ø = 5 mm), a Pt sheet counter electrode, a $Ag/AgNO_3$ reference electrode and about 3 mL of electrolyte. The aqueous setup

comprised a glassy carbon working electrode (Ø = 3 mm), a Pt sheet counter electrode, a Ag/AgCl (3M KCl) reference electrode and 20 mL of electrolyte. The buffered aqueous solutions were prepared and measured by Felix Kerner under my supervision as part of the B.Sc. thesis “Characterizing organic active materials for aqueous redox flow batteries at various pH values”.[223]

2.3 Publication III: Tailoring Dihydroxyphthalazines to Enable their Stable and Efficient Use in the Catholyte of Aqueous Redox Flow Batteries

Based on the promising properties of DAAQs revealed in publication II, the following research aimed to further capitalize on the benefits of the nitrogen-based functionalization of homocyclic quinones. As outlined earlier, the number of quinonoid high-potential active materials is sincerely limited as a result of the associated challenges regarding the susceptibility versus nucleophilic side reactions. The aim was to transfer the concept to an intrinsically electron-poor species to obtain capable catholyte active materials, since a distinct relative increase of the redox potential is achieved for diaza-modified compounds. The NQ base structure was identified as a suitable template yielding the novel compound class of dihydroxyphthalazines, which was thoroughly investigated in this publication.

Three dihydroxyphthalazine derivatives featuring varying substitution patterns were characterized according to different methods comprising cyclic voltammetry in quiescent solution as well as hydrodynamic measurements using a rotating disc electrode. In consequence of their heterocyclic structure, dihydroxyphthalazines are able to compete with BQ species, which are considered as state of the art quinonoid catholyte materials. The results reveal that the high redox potentials achieved for this compound class are complemented by fast charge transfer kinetics. Besides, vulnerable sites of the DHP base structure were identified and blocked by methyl substituents to address the general susceptibility of catholyte active materials versus nucleophilic side reactions. The modified structure exhibited a high stability during exhaustive electrolysis, clearly surpassing the performance of established BQ species. The improved cycling stability was supported by ^{1}H NMR measurements. In order to further improve upon the beneficial properties of DHPs, DFT calculations were performed focusing on the design of desirable structural motifs for future research. Thereby, a number of structures with increased redox potentials as well as increased water solubility were outlined to propel research in this field. With this publication, the compound class of dihydroxyphthalazines is introduced as a capable high-potential active species, filling an existing gap regarding stable quinonoid catholyte active materials for ORFBs.

The concepts and experiments of this publication were developed by the author of this thesis under the supervision of D. Schröder and J. Janek. The paper was written by the first author and edited by the seven co-authors. The synthetic methods of the investigated dihydroxyphthalazines were developed by the research group of H. A. Wegner. S. Schmalisch synthesized the DHP derivatives and further assisted with the evaluation of the conducted ^{1}H NMR measurements. D. Mollenhauer and S. Schwan contributed the DFT calculations on the redox potentials of the investigated active materials. H. A. Wegner and L. Hong contributed to the scientific discussions.

J. D. Hofmann, S. Schmalisch, S. Schwan, L. Hong, H. A. Wegner, D. Mollenhauer, J. Janek, D. Schröder, Tailoring Dihydroxyphthalazines to Enable Their Stable and Efficient Use in the Catholyte of Aqueous Redox Flow Batteries. *Chem. Mater.* **2020**, *32* (8), 3427–3438.

CHEMISTRY OF MATERIALS

pubs.acs.org/cm Article

Tailoring Dihydroxyphthalazines to Enable Their Stable and Efficient Use in the Catholyte of Aqueous Redox Flow Batteries

Jonas D. Hofmann, Sebastian Schmalisch, Sebastian Schwan, Longcheng Hong, Hermann A. Wegner, Doreen Mollenhauer, Jürgen Janek,* and Daniel Schröder*

Cite This: https://dx.doi.org/10.1021/acs.chemmater.9b05077 Read Online

ACCESS | Metrics & More | Article Recommendations | Supporting Information

ABSTRACT: To enable cost-efficient stationary energy storage, organic active materials are the subject of current investigations with regard to their application in aqueous redox flow batteries. Especially quinones with their beneficial electrochemical properties and natural abundance pose a promising class of compounds for this challenging endeavor. Yet, there are not many active materials available for the catholyte side to realize solely quinone-based systems. Herein we introduce the novel hydroquinone 5,8-dihydroxy-2,3-phthalazine together with two of its derivatives and propose it as a promising active material for the catholyte side of aqueous redox flow batteries. We systematically investigate the electrochemical properties as well as the structure−property relationship of this class of compounds. The unmodified dihydroxyphthalazine exhibits a favorably high redox potential of 796 mV vs SHE in acidic solution that is competitive with benzoquinone compounds. Moreover, the introduced dihydroxyphthalazines feature a high electron transfer rate surpassing benzoquinone species by almost one order of magnitude. With regard to stable cycling performance, we further achieved a high resilience against detrimental side reactions such as Michael addition by adding methyl substituents to the base structure. Our experimental findings are supported and extended by theoretical considerations in terms of density functional theory calculations. With this combined approach we outline further promising dihydroxyphthalazine-based materials with regard to performance-relevant quantities like redox potential, cycling stability, and water solubility. This study aims to propel further research in the field of quinone-based active materials for the catholyte of future aqueous redox flow batteries.

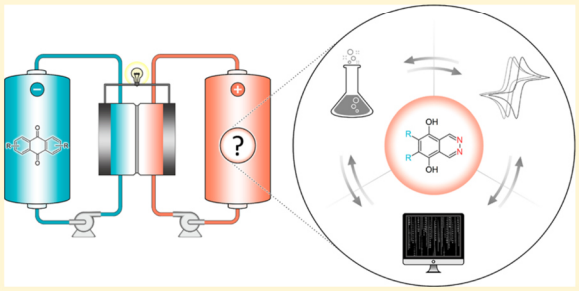

INTRODUCTION

Aromatic organic compounds constitute a promising class of materials to meet the requirements for safe and cost-efficient stationary electrochemical energy storage. Especially quinones, which may be derived from abundant resources such as lignin, have attracted interest in both research and industry. Due to their fast charge transfer kinetics and tunable redox potentials, many recent publications have investigated the structure−property relationship of quinonoid compounds and their application in redox flow batteries (RFBs): quinones undergo a fast two-electron transfer in aqueous solution, which is characterized by high charge transfer rate constants. Especially in acidic solution the charge transfer is considered to be very fast and simultaneous as a consequence of fast protonation, which occurs while the molecule is reduced.[1,2] Starting with the studies by Huskinson et al.[3] and Yang et al.[4] in 2014, various quinone derivatives have been investigated in acidic as well as alkaline aqueous solution and are applied successfully in RFBs.[5−8] Usually, quinones are employed as anolyte active materials, due to their high electron density and, hence, low redox potentials.[9,10] In spite of this trend, Yang et al. originally proposed an aqueous RFB that is completely based on quinone active materials, namely, 9,10-anthraquinone-2,7-disulfonic acid (AQDS) as anolyte and 1,2-benzoquinone-3,5-disulfonic acid (BQDS) as catholyte.[4]

Due to the highly electrophilic character of BQDS, it is prone to grave side reactions, namely, the Michael addition, which yields poor capacity retention.[11,12] To overcome the side reactions, an alternative structure was introduced—the so-called 3,6-dihydroxy-2,4-dimethylbenzenesulfonic acid (DHDMBS). DHDMBS alleviated the affinity toward nucleophilic attacks by blocking some of the potential attack sites with methyl groups.[13] However, despite this progress, all quinone-based RFBs proposed still suffer from insufficient cycling stability.

To address these shortcomings, the structure−property relationship of a multitude of different quinone-based derivatives was investigated in detail by computational as well

Received: December 9, 2019
Revised: March 27, 2020
Published: March 27, 2020

as experimental methods.[8,14−17] In this context, high-throughput computational screening approaches by means of density functional theory (DFT) calculations proved to be a powerful tool for a successful *in silico* design of candidates for redox flow batteries.[15,17−19] In these studies, electron-donating groups such as hydroxyl, methyl, and methoxy moieties were found to mainly increase the electron density of the base structure of the active material, yielding decreased redox potentials compared to the base compound. On the other hand, electron-withdrawing functional groups such as nitro, sulfonic, and phosphonic acid groups had the opposite effect, shifting the redox potential to more positive values. In addition, the presence of hydrophilic substituents such as hydroxyl, sulfonic, and phosphonic acid promotes the compounds solubility in water and hence may be very beneficial for the achievable energy density of the RFB.[15] These trends derived from computational analysis are in fact well-reflected by experimental studies of quinonoid compounds.[20−22]

Most of the studies covering the structure−property relationship of quinones focus on substitution strategies for already known quinone base structures such as anthra- (AQ) or benzoquinone (BQ). Yet, only a few studies aimed to modify the quinone base structure itself[23−25] and even fewer treated the subject within the context of aqueous redox flow batteries.[26,27]

In an earlier study we highlighted the impact of incorporating nitrogen into the anthraquinone base structure, introducing 2,3-diaza-9,10-anthraquinones as novel group of active materials for aqueous RFBs.[28] As a result of the electron withdrawing character of the incorporated nitrogen, the compound redox potential was shifted by approximately 460 mV into the positive direction compared to the homocyclic anthraquinone.[29] Thus, we demonstrated that it is also possible to tune the properties of quinone compounds for an application in RFBs by altering their base structure, which may potentially be transferred to quinone-based catholyte materials as well.

However, to enable the high redox potentials needed for the catholyte side it is necessary to start with base structures that by nature exhibit a lower electron density: in this work, we consequently transfer the method of functionalizing the base structure with diaza moieties to naphthoquinones, introducing dihydroxyphthalazines (DHP) as a novel class of active materials for the catholyte side of fully quinone-based aqueous RFBs. We systematically investigate the structure−property relationship of the base structure 5,8-dihydroxy-2,3-phthalazine (DHP) and its two derivatives with different substitution patterns ($DHP(Me)_2$ = 5,8-dihydroxy-6,7-dimethyl-2,3-phthalazine; DHP(MeO) = 5,8-dihydroxy-6-methoxy-2,3-phthalazine). We determine performance-relevant quantities such as diffusion coefficients, kinetic rate constants, and redox potentials of the compounds. Furthermore, we demonstrate the improved cycling stability of DHPs over BQDS in a side-by-side comparison based on exhaustive electrolysis.[30]

In order to increase the redox potential of DHPs and to gain information about the effect of specific substitution patterns, we further conducted density functional theory (DFT) calculations with dispersion correction. In combination with our experimental results, we propose promising DHP target structures as potential candidates of the DHPs as the catholyte active material for future RFBs.

■ EXPERIMENTAL SECTION

Chemicals. The disodium salt monohydrate (97%) of the hydroquinone form of BQDS (4,5-dihydroxy-1,3-benzenedisulfonic acid, in the following used synonymously) as well as 1,4-dihydroxybenzene (TraceCERT), 1,2-dihydroxybenzene (≥99%), and 1,4-dihydroxynaphthalene (≥97%) were purchased from Sigma-Aldrich and used as received. Concentrated sulfuric acid was also purchased from Sigma-Aldrich and diluted with deionized water to gain solutions with a concentration of 1 mol/L. The air-stable bidentate boron Lewis acid catalyst (pyridazine complex of 5,10-dimethyl-5,10-dihydroboranthrene) was prepared according to a procedure introduced by Hong et al.[31]

Synthesis and Chemical Characterization of Dihydroxyphthalazines. *General Information.* All reagents from abcr, Alfa-Aesar, Fluorochem, Merck, Sigma-Aldrich, TCI, and VWR were used as received or bulb-to-bulb distilled before usage. Dry solvents were obtained from ACROS/Fisher-Scientific with the AcroSeal cap and used without purification. Degassed solvents were obtained via freeze-bump-thaw cycling.

Water sensitive reactions were conducted with dried glassware. Drying was performed with a heat gun under an argon atmosphere. For particularly water sensitive reactions multiple heating/flushing cycles were conducted. The same applies for air sensitive reactions, which were set up in a nitrogen-filled glovebox or in a fume hood with nitrogen as protective gas. Pressure-demanding reactions were conducted in glass pressure tubes.

Chemical Characterization. After synthesis the resulting products were chromatographically purified and analyzed for their specific structure and mass via NMR analysis as well as mass spectrometry. For preparative column chromatography 60 M silica gel (0.063 nm−0.200 nm) or flash silica gel (0.04 nm−0.063 nm) from Machery-Nagel was used. For thin layer chromatography POLYGRAM SILG/UV_{254} polyester sheets precoated with silica gel 60 and a fluorescent indicator were applied. Detection occurred via UV light at 254 or 365 nm with a GAMAG UV-light cabinet or via development with potassium permanganate, iodine, or phosphomolybdic acid.

NMR spectra of ^{1}H and ^{13}C were measured on Bruker Avance II 200 MHz Microbay, Bruker Avance II 400 MHz, Bruker Avance III 400 MHz HD, and Bruker Avance III HD 600 MHz spectrometers. The last two spectrometers were used for two-dimensional spectra. Deuterated solvents were purchased from Eurisotop and Deutero and used without purification. Chemical shifts are reported in ppm (parts per million) with respect to the signal of the used solvent given in brackets. Coupling constants are given in Hertz (Hz), and signals are reported as s = singlet, d = doublet, and m = multiplet.

To determine the exact mass of the synthesized products electrospray ionization mass spectra and high-resolution mass spectra were measured on an ESI-MS Bruker Mikro-TOF and on an ESI-MS Finnigan LCQ−DUO.

1,2,4,5-Tetrazine. Cold hydrazine hydrate (100 mL, 2.00 mol, 2.78 equiv) was added to solid formamidinium acetate (77.9 g, 726 mmol, 1.00 equiv) for 10 min at 0 °C while stirring in a 1 L flask. The clear solution formed initially solidified after 5−8 min of stirring and was left for 1 h. Afterward ice water (50 mL) was added, and the mixture was stirred for an additional hour in an ice bath. The solid was filtered with suction via a Büchner funnel and dehydrated to the extent possible by pressing. The solid was dissolved in cold glacial acetic acid (250 mL), and $NaNO_2$ (25.8 g, 374 mmol, 0.510 equiv) was added in small portions for 2 h at 0 °C (ice bath) while stirring. After an additional 1.5 h of stirring, the mixture was precooled to −18 °C (cooling is necessary for high yield), and ice water (375 mL) was added subsequently. The solution was extracted with 2 × 5 × 200 mL (2 × 1 L separatory funnels were used at the same time) of cold CH_2Cl_2. The combined extracts were washed with a solution of saturated $NaHCO_3$ (830 mL) and water (664 mL) and then dried overnight over $CaCl_2$ in a refrigerator. The red-violet solution was gently evaporated to a volume of 30−40 mL by distilling the solvent from a 500 mL flask through a 30 cm Vigreux column. The residual liquid was transferred into a Schlenk tube, and the remaining solvent was evaporated under reduced pressure (−40 °C, 0.90 mbar). The residual solid was sublimed at rt and 1.00 mbar directly on a cooling finger (−40 °C, acetone/liquid N_2) yielding the pure product as deep-red and very volatile crystals (3.5 g, 12%).

^{1}H NMR (200 MHz, chloroform-*d*) δ 10.40 (s, 1H).

https://dx.doi.org/10.1021/acs.chemmater.9b05077
Chem. Mater. XXXX, XXX, XXX−XXX

The synthesis of tetrazine was conducted according to Domasevitch et al.[32] Analytical data are in accordance with literature data.

2,3-Dimethyl-1,4-benzoquinone. 2,3-Dimethyl-1,4-hydroquinone (2.10 g, 15.2 mL, 1.00 equiv) was suspended in a mixture of acetonitrile (30 mL) and water (15 mL). While stirring the mixture at rt, tetrabutylammonium bromide (247 mg, 760 μmol, 5.00 mol %) and Oxone (5.61 g, 9.12 mmol, 0.600 equiv) were added. The color of the mixture turned from brown to dark brown, and a precipitate was formed. After about 45 min the reaction mixture was diluted with ethyl acetate (100 mL) and water (100 mL). The obtained organic phase was washed with water (75 mL) and brine (75 mL) before the solvent was removed under reduced pressure. The crude product was recrystallized from hot cyclohexane. After filtration, 2,3-dimethyl-1,4-benzoquinone was obtained as a yellow solid (800 mg, 39%).

^{1}H NMR (400 MHz, chloroform-*d*) δ 6.71 (s, 1H), 2.02 (s, 3H).

^{13}C NMR (101 MHz, chloroform-*d*) δ 187.5, 141.4, 136.4, 12.3.

MP: 57.6 °C (lit. 55−57 °C).

Analytical data are in accordance with the literature.[33]

5,8-Dihydroxy-2,3-phthalazine (DHP). A dried, nitrogen filled Schlenk tube equipped with a stirring bar was charged with the air-stable bidentate Lewis acid catalyst (42.6 mg, 150 μmol, 5.00 mol %), benzoquinone (360 mg, 3.00 mol, 1.00 equiv), and tetrazine (948 mg, 11.5 mmol, 3.50 equiv) under a nitrogen atmosphere. Subsequently, benzotrifluoride (23 mL) was added. The reaction mixture was heated to 55 °C while stirring, then sealed under a nitrogen atmosphere, and finally stirred at 110 °C overnight. After cooling the mixture down, the solvent and excess tetrazine were removed via a liquid nitrogen-filled cooling trap under vacuum. Solid residues were dissolved/suspended in a 1:1 mixture of DCM/MeOH and adsorbed on silica. After purification via column chromatography (150 g silica, DCM/MeOH 8:2), 5,8-dihydroxy-phthalazine was obtained as a dark green solid (505 mg, 94%).

^{1}H NMR (400 MHz, DMSO-d_6) δ 10.27 (s, 2H), 9.57 (s, 2H), 7.16 (s, 2H).

^{13}C NMR (101 MHz, DMSO-d_6) δ 145.4, 144.9, 116.4, 116.3.

HRMS (ESI-MS) m/z calculated $[C_8H_6N_2O_2]^+$: $[H]^+$ 163.0502; found: 163.0502.

MP: >300 °C (decomposition).

5,8-Dihydroxy-6,7-dimethyl-2,3-phthalazine DHP(Me)$_2$. A dried, nitrogen filled Schlenk tube equipped with a stirring bar was charged with the air-stable bidentate Lewis acid catalyst (14.2 mg, 50.0 μmol, 5.00 mol %), freshly recrystallized (from cyclohexane) 2,3-dimethyl-benzoquinone (136 mg, 1.00 mol, 1.00 equiv), and tetrazine (287 mg, 3.50 mmol, 3.50 equiv) under nitrogen atmosphere. Subsequently, benzotrifluoride (6 mL) was added. The reaction mixture was heated to 55 °C while stirring, then sealed under nitrogen atmosphere, and finally stirred at 110 °C overnight. After cooling the mixture down, the solvent and excess tetrazine were removed via a liquid nitrogen-filled cooling trap under vacuum. Solid residues were dried under vacuum, dissolved in MeOH/DCM, and adsorbed on silica for chromatography. After purification via column chromatography (75 g silica, DCM/MeOH 8:2) 6,7-dimethyl-5,8-dihydroxyphthalazine was obtained as a yellow-brown solid (168 mg, 88%).

^{1}H NMR (400 MHz, DMSO-d_6) δ 9.62 (s, 2H), 9.33 (s, 2H), 2.33 (s, 6H).

^{13}C NMR (101 MHz, DMSO-d_6) δ 146.0, 142.9, 129.5, 116.1, 13.9.

HRMS (ESI-MS) m/z calculated $[C_{10}H_{10}N_2O_2]^+$: $[H]^+$ 191.0815; found: 191.0818.

EA: (%) for $C_{10}H_{10}N_2O_2$: calculated C, 63.15; H, 5.30; N, 14.73; found C 61.58; H, 5.02; N, 15.49.

MP: >300 °C (decomposition).

5,8-Dihydroxy-6-methoxy-2,3-phthalazine DHP(MeO). A dried, nitrogen filled Schlenk tube equipped with a stirring bar was charged with the air-stable bidentate Lewis acid catalyst (21.3 mg, 75.0 μmol, 10.0 mol %), 2-methoxy-1,4-benzoquinone (105 mg, 750 μmol, 1.00 equiv), and tetrazine (308 mg, 3.75 mmol, 5.00 equiv) under nitrogen atmosphere. Afterward, benzotrifluoride (6 mL) was added. The reaction mixture was heated to 55 °C while stirring, then sealed under a nitrogen atmosphere, and finally stirred at 110 °C overnight. After cooling the mixture down, the solvent and excess tetrazine were removed via a liquid nitrogen-filled cooling trap under vacuum. Solid residues were dissolved/suspended in a 1:1 mixture of DCM/MeOH and adsorbed on silica. After purification via column chromatography (75g silica, DCM/MeOH 8:2−7:3) 2,3-dihydroxy-6-methoxyphthalazine was obtained as a solid. Further recrystallization/heating from $CHCl_3$/MeOH (9:1) resulted in a brown-yellow solid as the final product (33 mg, 23%).

^{1}H NMR (400 MHz, DMSO-d_6) δ 10.61 (s, 1H), 9.53 (d, J = 1.4 Hz, 1H), 9.41 (d, J = 1.4 Hz, 1H), 9.36 (s, 1H), 7.14 (s, 1H), 3.92 (s, 3H).

^{13}C NMR (101 MHz, DMSO-d_6) δ 149.0, 147.3, 145.5, 145.03,132.01, 116.8, 110.5, 103.9, 56.3.

HRMS (ESI-MS) m/z calculated for $[C_9H_8N_2O_2]^+$: $[H]$+ 163.0502 ; found: 163.0503.

MP: >300 °C (decomposition).

2,3-Diazanaphthoquinone (DNQ). $NaIO_4$ (56.1 mg, 263 μmol, 1.05 equiv) was added to a suspension of 5,8-dihydroxyphthalazine (40.5 mg, 250 μmol, 1.00 equiv) in water (1 mL). The resulting reaction mixture was stirred for 45 min. Then, water was removed under reduced pressure, and the solid residue was dissolved/suspended in DCM (ultrasonic was used to increase solubility). The mixture was filtered through a cotton and sand plug in a Pasteur pipet. Volatile compounds were removed under vacuum. The product 2,3-diazanaphthoquinone was obtained as a dark red solid (16 mg, 40%). Besides this approach, alternative routes were investigated for the synthesis of DNQ. The associated conditions and results are given in Figure S1.

^{1}H NMR (400 MHz, DMSO-d_6) δ 9.73 (s, 2H), 7.24 (s, 2H).

^{13}C NMR (101 MHz, DMSO-d_6) δ 184.7, 145.9, 138.3, 124.4.

HRMS (ESI-MS) m/z calculated for $[C_8H_4N_2O_2]^+$: $[Na]^+$ 183.0165; found: 183.0166.

MP: >300 °C (decomposition) Analytical data are in accordance with literature data.[34]

5,6-Dihydroxyphthalazine. Phthalazine acetonide (101 mg, 500 μmol, 1.00 equiv) was dissolved in ethanol (1 mL) before adding 12 drops of HCl (conc.). Afterward the reaction mixture was heated to reflux for 3 h. After cooling down, volatile compounds were removed under reduced pressure. After washing with $CHCl_3$, the pure product was obtained as a yellow solid (53 mg, 62%).

^{1}H NMR (400 MHz, DMSO-d_6) δ 9.97 (s, 1H), 9.91 (s, 1H), 8.04−7.93 (m, 1H).

^{13}C NMR (101 MHz, DMSO-d_6) δ 153.1, 149.3, 147.7, 141.6, 127.3, 122.9, 120.5, 118.9.

HRMS (ESI-MS) m/z calculated $[C_8H_6N_2O_2]^+$: $[H]^+$ 163.0502; found: 163.0502.

MP: >300 °C (decomposition)

Methods. *Cyclic voltammetry.* For the half-cell measurements via cyclic voltammetry (CV), a three-electrode setup comprising an AUTOLAB PGSTAT 128N potentiostat, an aqueous Ag/AgCl reference electrode (3M KCl filling solution), and a Pt sheet counter electrode from Metrohm was used. Prior to each measurement, the glassy carbon working electrode with a disc diameter of 3 mm was polished with alumina paste (1 and 0.05 μm particle diameter, ALS) and rinsed with deionized water. Before the measurement was started, the electrolyte (overall volume of 30 mL) was purged by a constant flow of argon for 30 min. The different active materials were investigated in acidic aqueous solutions at different scan rates ranging from 1.00 V/s to 0.01 V/s.

To quantify the electron affinity of the studied active materials we determined the midpoint potential $E_{1/2}$ as mean potential value of the resulting anodic (E_{pc}) and cathodic (E_{pa}) peaks. Assuming that reduced and oxidized species exhibit equal diffusion coefficients, $E_{1/2}$ can be used as an approximation for the formal potential $E^{0\prime}$ in the case of reversible redox reactions. It should be noted that formal potentials are conditional constants that refer to conditions different from the standard conditions (compare standard redox potential E_0). Nonetheless, the formal potential allows for a straightforward and direct comparison of different active materials as long as the strictly defined experimental conditions such as electrolyte composition and reactant concentration are maintained.[35]

https://dx.doi.org/10.1021/acs.chemmater.9b05077
Chem. Mater. XXXX, XXX, XXX−XXX

To extract the faradaic current response, all half-cell measurements were repeated under the exclusion of active material. The obtained capacitive currents were then subtracted from the data received for the complete electrolyte comprising solvent, active material, and conducting salt (if needed). The uncompensated resistance of the half-cell setup was determined according to the positive feedback method and compensated by 85% during voltammetric measurements.

Rotating Disc Electrode Studies. As in the case of the aforementioned CV measurements, the glassy carbon rotating disc electrode (RDE) was polished to mirror shine prior to the actual measurement. For the RDE studies the voltage was linearly swept in a potential interval, which was selected according to the redox potential of the investigated compound. The potential was swept with a scan rate of 10 mV/s while rotating the electrode at discrete values between 200 and 3000 rpm. To yield the diffusion coefficient D of the active species the resulting maximum currents were plotted versus the square root of the applied rotation rate (ω) according to the Levich equation:

$$I_{\mathrm{lim}} = 0.62zFAD^{2/3}\omega^{1/2}\nu^{-1/6}c_0 \tag{1}$$

Here I_{lim} is the limiting current, z is the number of transferred electrons, F is the Faraday constant (96485.33 A s mol^{-1}), A is the electrode surface area in cm^2, ω is the angular velocity in rad s^{-1}, ν is the kinematic viscosity of the solution in cm^2 s^{-1}, and c_0 is the concentration of the electrochemically active species in mol cm^{-3}. Since the other quantities are known, the diffusion coefficient D (cm^2 s^{-1}) is determined from the slope of the applied linear regression.

The limiting currents obtained at certain overpotentials then are plotted versus $\omega^{-1/2}$. According to the Koutecký–Levich eq 3 the intercept determined by linear regression yields the reciprocal of the kinetic current I_k in the absence of mass transport limitations:

$$\frac{1}{I_{\mathrm{lim}}} = \frac{1}{I_k} + \frac{1}{0.62zFAD^{2/3}\omega^{1/2}\nu^{-1/6}c_0} \tag{2}$$

Subsequently the exchange current I_0 is obtained by a plot of log (I_k) versus the associated overpotentials η, which is described by the Tafel equation:

$$\eta = \frac{2.303RT}{\alpha zF}\log(I_k) - \log(I_0) \tag{3}$$

The intercept of a linear regression yields I_0, whereas the charge transfer coefficient α can be extracted from the slope of the fit. The obtained exchange current is then inserted into eq 4 to finally calculate the rate constant k_0:

$$k_0 = \frac{I_0}{zFAc_0} \tag{4}$$

Exhaustive Electrolysis. To assess the electrochemical stability of the investigated active materials and to determine the number of transferred electrons per molecule, we conducted bulk electrolysis experiments, herein also referred to as exhaustive electrolysis.[30] The setup used comprises two electrode compartments, which are separated by a Nafion membrane to allow for charge compensation and to prevent active material crossover at the same time. The electrolyte used in the working electrode compartment contained a defined amount of active material (1 mM concentration at a total volume of 30 mL), which was omitted in the counter electrode compartment. To ensure fast active material conversion we utilized a graphite felt working electrode with high surface area (Sigracell GFA6 EA; SGL Carbon) and an Ag/AgCl reference electrode (3 M KCl filling solution; Metrohm) for potential control. In the second compartment, a Pt sheet served as the counter electrode. To electrochemically convert the dissolved active material a constant voltage well beyond the redox potential of the associated species was applied (for detailed information see the SI) while the solution was constantly stirred. According to Faraday's law the number z of transferred electrons per molecule then could be extracted based on the charge Q gained from the employed molar amount of substance n:

$$Q = nzF \tag{5}$$

Computational Details. We utilized DFT calculations applying the Gaussian09 software package to determine the redox potentials of the DHP derivatives.[36] For all structure optimizations and energetic calculations we employed the generalized gradient approximation density functional PBE in an unrestricted manner together with the Grimme dispersion correction D3 and a Becke–Johnson damping.[37−39] All elements were described by an all-electron correlation consistent valence double-zeta basis set with augmented diffuse functions (aug-cc-pVDZ).[40] Solvent effects were taken into account by a polarizable continuum model (PCM) using the ε_r value of water.[41] To evaluate the Gibbs free energy at 298 K we computed the zero-point vibrational energy and thermal corrections as well as entropy contributions.

Due to the structural similarity of the DHP derivatives to quinones and diaza-anthraquinones, the reduction process was assumed to take place as a simultaneous two-electron, two-proton transfer at a low pH value of 0:[42]

$$\mathrm{DHP} + 2\mathrm{e}^- + 2\mathrm{H}^+ \leftrightarrow \mathrm{DHPH_2} \tag{6}$$

According to eq 7 the redox potential consequently was calculated by means of the Gibbs free energy ΔG_{red} of the reduction in solution, which yields the reduced and protonated form of DHP, $DHPH_2$:

$$E_{\mathrm{calc}} = -\frac{\Delta G_{\mathrm{red}}}{nF} - E_{\mathrm{SHE}} \tag{7}$$

To reflect the impact of protonation we considered the solvation free energy of protons with a value of $\Delta G_{\mathrm{solv}}(\mathrm{H}^+) = -1112.5$ kJ mol^{-1}.[43] The redox potential was calculated with respect to the standard hydrogen reference electrode (SHE) by employing an absolute value of 4.28 V for E_{SHE}.[43] In addition, E_{calc} was computed by considering the Gibbs free energy of an electron as well as employing different values for $\Delta G_{\mathrm{solv}}(\mathrm{H}^+)$ or E_{SHE}. However, only marginal shifts were observed for the absolute potential values, and the qualitative trends are not influenced. The reduction potential also depends on the applied density functional. For instance, distinctly larger deviations from experimental potentials were observed when the GGA functional BP86 and the hybrid functionals B3LYP or PBE0 with a dispersion correction D3 were applied alternatively: as a consequence, the E_{calc} values obtained for DHP, $DHP(Me)_2$, and DHP(OMe) are on average 0.119 to 0.128 V higher compared to the values obtained with PBE-D3.[44−48]

Regarding the redox potentials computed at a PBE-D3/aug-cc-pVDZ(PCM) level of theory a low mean absolute deviation (MAD) of 30 mV is obtained with respect to experimentally determined values of $E_{1/2}$. Despite such relatively small values, the limitations of the simple polarizable continuum model can lead to larger MADs. In this context, for DFT(PCM) calculations the computation of 19 two-electron, two-proton reduction potentials of anthraquinone derivatives at low pH value resulted in a MAD of 37 mV for 16 redox reactions and 194 mV for the remaining 3 redox reactions compared to experimental values.[49] In the latter case, anthraquinone derivatives with ether groups have been identified to require extended models such as those represented by QM/MM approaches including explicit water molecules to form hydrogen bonds for a reliable prediction of reduction potentials. Conclusively, along this study and the benchmark of this work at a PBE-D3/aug-cc-pVDZ(PCM) level of theory, we assume a MAD of 30 mV to 194 mV for the calculated redox potentials at low pH value. However, it is to be expected that the lower boundary of the MAD applies for most of the considered redox reactions.

To obtain reliable redox potentials the pK_a values and the associated protonation states of the investigated molecules also have to be considered. With respect to the pK_a values of phthalazine (3.5)[50] and phthalimide (9),[51] we assume the diaza and imide moieties to be protonated at a pH value of 0. For the phosphonic acid moiety we considered different protonation states (pK_{a1} ≈ 1−2, pK_{a2} ≈ 5−7)[52] and the deprotonated state for the sulfonic acid moiety (pK_a < 0).[53]

The calculated redox potentials reported in this work refer to the structurally optimized conformers of the molecules that exhibit the lowest energies. Thus, in the cases of DHP, DHP(MeO), and $DHP(Me)_2$, the position of the hydroxyl hydrogen was varied to

https://dx.doi.org/10.1021/acs.chemmater.9b05077
Chem. Mater. XXXX, XXX, XXX−XXX

investigate the influence on the computed E_{calc}. For these derivatives, the conformer featuring hydroxyl hydrogens pointing away from the diaza moiety turned out to be the energetically preferred one. For the scenario of both hydrogens pointing toward the diaza moiety (135 mV to 290 mV) or a mixed orientation (98 mV to 104 mV), distinctly higher energies and redox potentials were yielded. Interestingly, for DHP(SO_2Me)(Me) a mixed orientation of hydroxyl hydrogens is preferred since the energetically less favorable interactions between the hydroxyl hydrogen and the $-SO_2$Me moiety are avoided. In summary, apart from scenarios of competing interactions that required further conformer stabilization, we computed E_{calc} on the basis of DHP conformers with the hydroxyl hydrogens oriented away from the diaza moiety. All optimized structures have been confirmed to be minima by frequency calculations.

The reactivity or stability of the molecules has been estimated by considering the deviation from the ring planarity by measurement of dihedral angles. In this context, calculations with the MP2 algorithm and population calculations with an introduced ring distortion along the lowest ring out-of-plane vibrations conducted by Zhigalko et al. revealed the possibility of nonplanar geometries for naphthalene.[54] They estimated the degree of nonplanarity by dihedral angles in the range of about ±17° at room temperature in conjunction with a variation in energy of up to 2 kcal mol^{-1}. An analysis of 868 naphthalene derivatives of the Cambridge Crystal Structure Database supported their observation. In order to estimate the energetic variation due to ring planarity distortion of DHP derivatives, we replaced the substituents of the DHP derivatives with hydrogen atoms and calculated the relative energy of the distorted DHP with respect to the planar DHP.

Considering the relative energies of the DHP moieties of DHP derivatives compared to planar DHP in the context of the study from Zhigalko et al. with regard to naphthalene derivatives, two conclusions can be made. First, the energy variation caused by ring distortion is larger for DHP derivatives than for naphthalene derivatives. And second, considering the energy variation of distorted DHP moieties in the context of naphthalene derivatives, no crystal structures (and thus stable structures) should be found for large dihedral angles within the DHP moieties. Thus, the distorted ring structure gives evidence for a reduced stability or higher reactivity of the molecule compared to planar DHP.

■ RESULTS AND DISCUSSION

Comparing the Electrochemical Properties of DHPs and Hydrobenzoquinones. We first focused on the experimental investigation of the structure−property relationship of different DHP derivatives. First, we analyzed the dihydroxy-phthalazine base structure DHP without further functionalization. Second, the compound DHP(MeO), which features an additional methoxy group, was the subject of our investigation. Third, the compound DHP$(Me)_2$, which was functionalized with two methyl groups in between the characteristic ketone/hydroxyl moieties of the quinonoid backbone, was synthesized and tested.

As a measure of performance, we determined physicochemical key quantities such as the diffusion coefficient, the charge transfer rate constant, and the redox potential of each active material. To shed light on the electrochemical properties of DHPs we compared the aforementioned performance measures with the ones obtained for BQDS and DHDMBS, since they are considered as the benchmark quinonoid active materials for the catholyte of aqueous RFBs. To allow for a direct comparison of the associated base structures we complemented our studies with the unsubstituted hydrobenzoquinone (HBQ) in *para*-configuration (1,4-dihydroxybenzene) as well as in *ortho*-configuration (1,2-dihydroxybenzene).

The compounds were investigated in aqueous 1 M sulfuric acid (H_2SO_4) by cyclic voltammetry (CV) in quiescent solution and by hydrodynamic measurements using a rotating disc electrode (RDE) during linear potential sweep. By means of eq 1 and 2, the hydrodynamic measurements were used to determine the diffusion coefficients and charge transfer rate constants of the studied active materials (see Figure S2). The diffusion coefficients of all the compounds covered in this work lie within the same order of magnitude of 10^{-6} cm^2/s, which is in the same range as for comparable organic active materials.[55−58] The obtained values are listed in Table 1.

Table 1. Overview of the Physicochemical Key Quantities of Different BQ and DHP Derivatives Determined in 1 M H_2SO_4

compound	D [cm^2 s^{-1}]	k_0 [cm s^{-1}]	$E_{1/2}$ vs SHE [V]
para-HBQ	7.1×10^{-6}	6.7×10^{-4}	0.683
ortho-HBQ	7.8×10^{-6}	4.2×10^{-4}	0.782
BQDS	5.2×10^{-6}	2.2×10^{-4}	0.895
DHDMBS[13]	4.1×10^{-6}	1.3×10^{-4}	0.522
DHP	5.4×10^{-6}	1.6×10^{-3}	0.796
DHP$(Me)_2$	3.3×10^{-6}	1.8×10^{-3}	0.691
DHP(MeO)	2.1×10^{-6}	1.2×10^{-3}	0.722

CV was used to determine the midpoint potentials $E_{1/2}$ and the overall charge transfer characteristic of the investigated compounds. As can be seen in Figure 1b, BQDS features a comparably high midpoint potential of 895 mV vs SHE under acidic conditions (1 M H_2SO_4). Due to the intrinsically low electron density within the benzoquinone base structure, it exhibits a highly oxidizing character. The electron density is further decreased by the two electron-withdrawing groups incorporated, i.e., the sulfonic acid groups.[20] In addition, BQDS benefits from the *ortho*-configuration of its intrinsic carbonyl/hydroxyl groups, which further increases the redox potential to more positive values.[59,60]

On the downside, BQDS (see Figure 1b) shows a large peak-to-peak separation of 204 mV. This large peak-to-peak separation implies sluggish charge transfer kinetics, i.e., high overvoltages are needed to evoke a current flow. For energy storage applications high overpotentials and slow kinetics are detrimental, since the overall cell efficiency suffers from the resulting voltage losses. In other studies, even higher values of up to 490 mV were reported for the peak-to-peak separation.[4,61] The same trend applies for DHDMBS, which in contrast to BQDS is a *para*-quinone equipped with only a single sulfonic acid moiety and two methyl substituents. Consequently, the midpoint potential decreases by about 360 mV[13] compared to BQDS.

The DHP base structure shows $E_{1/2}$ = 796 mV vs SHE, which is 342 mV higher than for the homocyclic analogue, 1,4-hydronaphthoquinone (see the SI; Figure S3a). The higher potential is caused by the intrinsic electron affinity resulting from the additional diaza-moiety incorporated. In line with previous studies the redox potential of DHP shifts to more positive values as a consequence of the electron-withdrawing character of nitrogen.[28]

Although being not as high as the value of $E_{1/2}$ for BQDS, the positive potential of the DHP base structure yet indicates that the class of DHPs is able to compete with the class of benzoquinones. Thus, DHPs may well be candidates for the preparation of the catholyte in RFBs. The results obtained for DHP should rather be compared to the base structure of BQDS, which is the unsubstituted HBQ: the electron affinity of BQDS is

https://dx.doi.org/10.1021/acs.chemmater.9b05077
Chem. Mater. XXXX, XXX, XXX−XXX

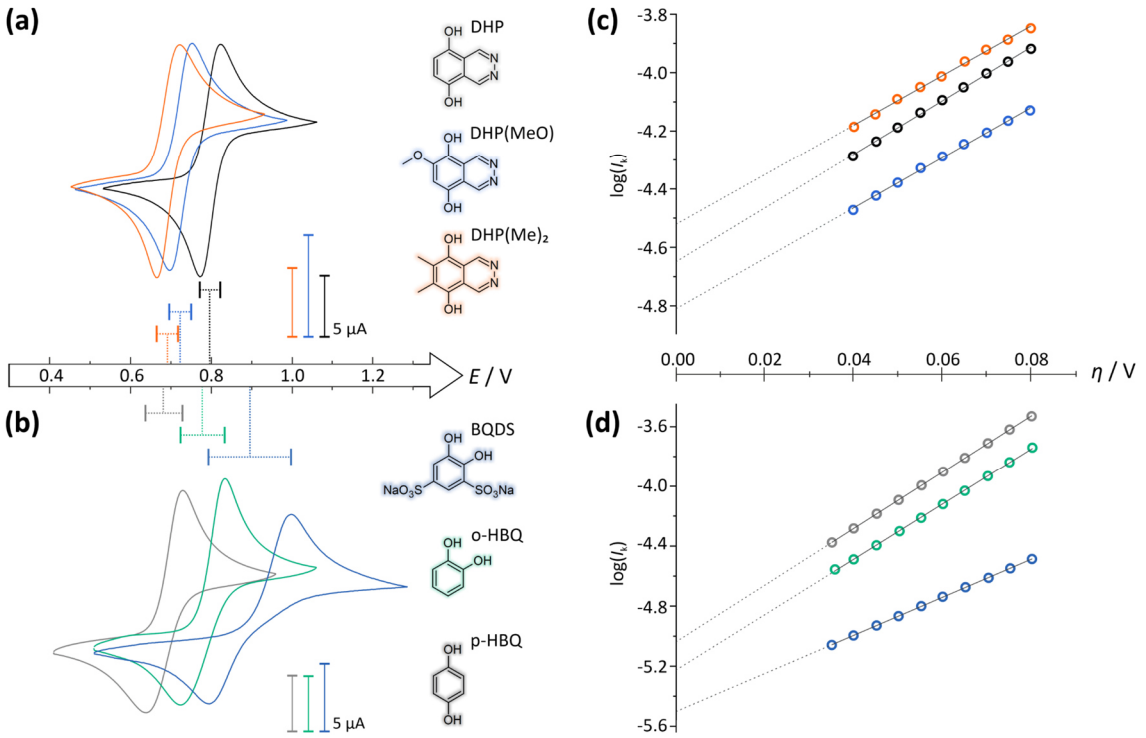

Figure 1. Electrochemical characterization of dihydroxyphthalazine and hydrobenzoquinone molecules in aqueous solution. Cyclic voltammograms of different DHP (a) and HBQ derivatives including BQDS (b) were measured in 1 M H_2SO_4 at a scan rate of 10 mV/s. Tafel plots of the investigated DHP (c) and HBQ (b) active materials. The underlying data were obtained by hydrodynamic RDE measurements (see Figure S2). The exchange current I_0 taken from the *y*-axis intercept (see Table T1 for discrete values) of (c) and (d) was used to calculate k_0 according to eq 4. The associated values are given in Table 1.

already altered by electron withdrawing sulfonic acid moieties, whereas DHP exhibits no peripheral functional groups. In fact, the unsubstituted *ortho*-benzoquinone features a midpoint potential of 782 mV vs SHE, which is slightly lower than the 796 mV measured for the unsubstituted DHP. The blank *para*-benzoquinone even undercuts this value by 113 mV (see Figure 1b).

Different to the HBQs, DHPs possess a more extensive aromatic system due to the attached heterocyclic ring. Especially in the case of combined proton and electron transfer this may be beneficial regarding the kinetics of the occurring charge transfer: the redox reaction of quinones is characterized by a transfer of two electrons which—depending on the proton activity—is accompanied by a transfer of up to two protons. When a quinone receives a proton after the first of the two electron transfers, the protonated intermediate is thermodynamically easier to reduce than the initial compound before the first electron and concomitant proton transfer. This goes along with a noticeable positive shift of the secondary redox potential associated with the protonated intermediate. If the order of both charge transfers is inverted, this effect is referred to as potential inversion.[62] Under specific conditions the potential inversion may result in a highly driven process that combines the transfer of two electrons, which otherwise would take place sequentially due to electrostatic repulsion.[63] However, for a large potential difference between both charge transfers—i.e., a strong inversion—the reaction rate constant k_0 is diminished, since a high overpotential is needed to evoke a current flow.[64] As a result, large peak-to-peak separations may be observed as in the case of BQDS and DHDMBS. Yet it should be taken into account that other factors such as intramolecular hydrogen bonding arising from attached sulfonic acid moieties may as well contribute to a decrease of k_0.[4] To increase the reaction rate it may be necessary to reduce the degree of potential inversion, which is achieved by adding a fused benzene ring or electron withdrawing substituents to the base structure.[65,66]

For the case of DHP both conditions are met since the additional heterocyclic ring contributes to the expansion of the aromatic system and further introduces electron withdrawing properties due to the nitrogen incorporated. Consequently, DHP shows a comparably low peak separation of only 45 mV (see Figure 1a), which yet indicates faster kinetics as compared with the rather confined aromatic system of BQDS: the charge transfer rate constant of the DHP derivatives—revealed by RDE measurements—is about one order of magnitude higher than for BQDS, DHDMBS, and the unsubstituted hydrobenzoquinone under the same conditions (compare Table 1). Besides, the diffusion-controlled nature of the redox reaction of DHPs was verified by means of scan rate dependent CV studies (see Figure S3c).

Enhanced Electrochemical Stability of DHP by Structure Functionalization. A major drawback of most organic active materials used in the catholyte is their predisposition toward side reactions—such as nucleophilic addition—due to their highly electrophilic character.[16] Quinones in aqueous solutions are likely to be attacked by nucleophiles such as OH^- or even the solvent water itself at free ring positions—especially if electron withdrawing groups such

https://dx.doi.org/10.1021/acs.chemmater.9b05077
Chem. Mater. XXXX, XXX, XXX−XXX

as sulfonic acid or carboxylic acid moieties are present. Although additions may also take place at substituted ring positions, this is less likely to occur due to steric reasons.[61] It is to be noted that oxidized quinones are more susceptible to such Michael addition than their reduced counterparts. This is due to the aromatic structure of reduced quinones, which allows for charge delocalization and, therefore, prevents nucleophilic attacks.

When the quinone moiety is attacked by water it is transformed into its hydroquinone state (see the SI, Scheme 1). As a consequence, the hydroquinone may subsequently be oxidized once again by transferring two electrons. In theory, this process may even take place several times in a sequence until a fully hydroxylated molecule is obtained. Since hydroxyl groups are highly electron donating, the final molecule would exhibit a distinctly lower redox potential than the initial compound.[15] This side reaction—with respect to stability and efficiency of the active material used in the catholyte of a RFB—can be seen as highly detrimental.[16]

The compound BQDS is well-known to undergo the Michael addition during cycling in aqueous RFBs: the intrinsically high electron affinity of the *ortho*-benzoquinone base structure and the free ring positions in close proximity to its two sulfonic acid groups constitute a high driving force for potential nucleophilic attacks.[11]

To quantify the susceptibility of BQDS toward the Michael addition and to make a comparison with the presented DHP derivatives, we conducted exhaustive electrolysis experiments. According to Faraday's law (see eq 5) the charge extracted from the electrolyte solution can be used to calculate the number of electrons transferred per molecule. Starting with the reduced form of BQDS it should in theory be possible to extract up to six electrons per molecule by complete oxidation: two electrons from the pristine compound and in total four electrons resulting from two possible Michael additions following the first oxidation. As displayed in Figure 2 by the end of the exhaustive electrolysis an average number of 5.82 electrons was transferred per molecule, which is very close to the anticipated, yet undesirable, number of six electrons. The deviation of 3% may be explained by impurities, which amount to 3.0% percent of the total mass (see Methods section).

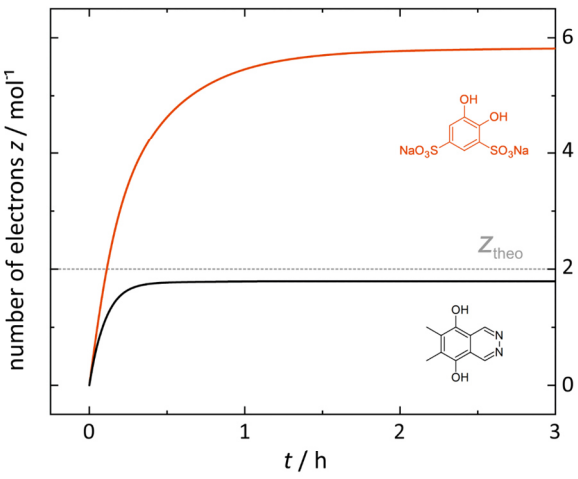

Figure 2. Exhaustive electrolysis of BQDS and DHP(Me)$_2$. The measurement was performed in 2 M HCl at an active material concentration of 1 mM. For the quinone compound a two-electron transfer is anticipated. For DHP(Me)$_2$ a complete oxidation takes place within the first 30 min of the experiment resulting in an average number of 1.79 electrons transferred per molecule. In the case of BQDS a final value is attained after about 2 h, which amounts to a total number of 5.82 electrons transferred.

The H NMR spectrum validates the distinct structural changes during full oxidation of the active material. However, the high number of different signals suggests that the degradation mechanism of BQDS may be more complex (see Figure S4d).

Considering the application of BQDS as active material for the catholyte of RFBs, the induced structural change is a serious constraint since not only its electron affinity but also its redox pattern may ultimately change from *ortho*- to *para*- configuration (see the SI, Scheme 1). According to our measurements, the potential drop solely related to the diverging redox pattern corresponds to a value of about 100 mV (see also Table 1 and Figure 1b). Taking both effects into account the potential decreases by 230 mV, which was revealed by CV measurements taken before and after electrolysis (see Figure S3b).

For the DHP base structure, we observed similar charge transfer characteristics during exhaustive electrolysis, which resulted in an average number of 5.78 transferred electrons per molecule (see Figure S4a). However, the transformation seems to take place much slower than for BQDS as indicated by the shallow slope of the number of electrons transferred with time before reaching the final value. Comparing the H NMR spectra of the pristine compound and the electrolysis product reveals that (as in the case of BQDS) the vacant sites in close vicinity of the carbonyl groups are prone to nucleophilic attacks (see Figure S4b).

To prevent such structural changes, one strategy is to block susceptible positions that may undergo the Michael addition. Thus, we introduced two methyl substituents to the DHP base compound to obtain DHP(Me)$_2$. If these measures to suppress the addition of water were successful, only a two-electron transfer should be observed during oxidation. As can be seen in Figure 2 the maximum amount of capacity was already attained after roughly half an hour. This shows that sluggish side reactions, which may retard complete charge extraction as in the case of DHP, are mitigated for DHP(Me)$_2$. Furthermore, the total value of transferred electrons per molecule was determined to be 1.79 for DHP(Me)$_2$. In fact, this observation is in very good agreement with the anticipated value derived from the utilized mass of active material and considering the substance purity of 92 ± 4% (determined by elemental analysis). Moreover, a direct comparison between the ^{1}H NMR spectra of the pristine and the fully oxidized compound (see Figure S4c) reveals that the structure of DHP(Me)$_2$ remains intact: solely the signals associated with the two hydroxyl moieties of the reduced form are absent after oxidation whereas apart from that all signals remain unchanged. It is to be noted that the increased stability of DHP(Me)$_2$ comes with a trade-off: due to the electron donating character of the methyl substituents the redox potential experiences a negative shift of 105 mV versus the unsubstituted DHP. Nevertheless, the approach to suppress the degradation of DHP by methyl-based structure functionalization proved to be very successful.

A similar approach was reported by Hoober-Burkhardt et al., who blocked empty sites of the benzoquinone base structure with methyl groups to obtain DHDBMS.[13] On the downside, the compound features a midpoint potential of only 522 mV versus SHE. This potential is surpassed by DHP(Me)$_2$ by a

https://dx.doi.org/10.1021/acs.chemmater.9b05077
Chem. Mater. XXXX, XXX, XXX−XXX

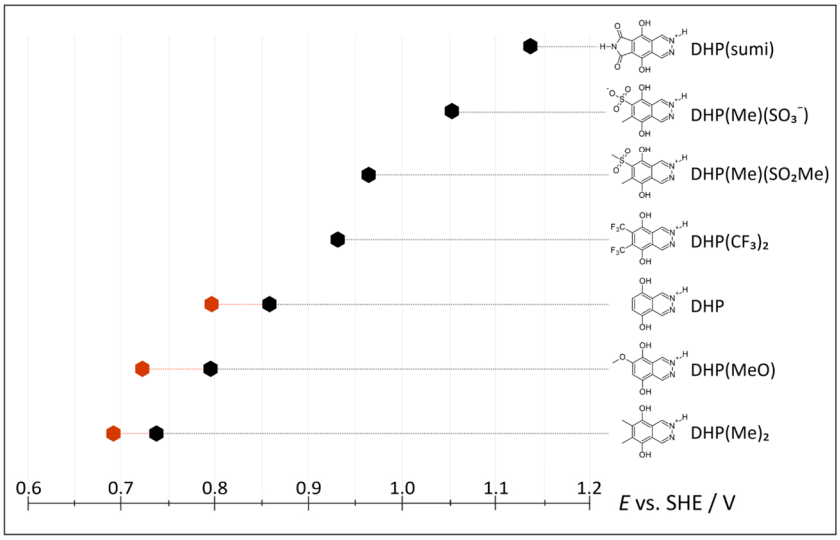

Figure 3. Overview of selected calculated E_{calc} (black symbols) and experimental $E_{1/2}$ values (red symbols) for different DHP substitution patterns at a pH value of 0. $E_{1/2}$ was determined in 1 M H_2SO_4 with an active material concentration of 1 mM. Taking into account the pK_a value of phthalazine (3.47), we assumed the diaza-moiety to be protonated under the applied conditions.[70]

considerable value of 190 mV, which further emphasizes the potential of the novel class of DHPs to be used as active material in the catholyte of aqueous RFBs.

Discussing Further Target Molecules by Means of DFT. The experimental results of our study concerning the structure−property relationship of the presented dihydroxyphthalazines yield promising insights for the properties relevant for electrochemical applications. Most of all, the high charge transfer rate constants and the stability of DHPs may be very beneficial for the design of stable catholyte active materials that allow for fast charge transfer at low voltage losses. Furthermore, the unsubstituted DHP exhibits an intrinsically high redox potential that surpasses the value of the *ortho*- and *para*-benzoquinone base structure. Our measures to stabilize DHPs against nucleophilic Michael additions by blocking the free sites of the quinone ring proved to be very successful as well. However, the structures presented in this work were not optimized for electron affinity and water solubility beyond that of the base structure.

To identify prospective target molecules that improve upon these quantities, we performed DFT-D3 calculations of different DHP substitution patterns. The selected level of theory of our calculations was compared to the experimental results obtained for DHP, DHP(Me)$_2$, and DHP(MeO): the experimentally determined values for $E_{1/2}$ and the calculated redox potentials E_{calc} (see Figure 3) are in good agreement within a MAD of 30 mV. The structure-related relative shifts of $E_{1/2}$ are reflected very well by the DFT-based values. Electron-donating moieties such as methyl and methoxy groups shift the redox potential to more negative values, whereas the sum of two methyl groups outweighs the impact of one methoxy group added to the structure. With regard to our calculations, the use of electron-withdrawing functional groups revealed the expected increase of redox potentials compared to DHP (see also Table T2). Considering the high degree of conformity between calculated and experimentally determined potential values, we assume to obtain reliable trends for E_{calc}. However, it is to be noted that, depending on the functional groups attached to DHP, a MAD of up to 194 mV may be possible due to the simple polarizable continuum model.

In order to identify distinct target molecules from the herein introduced class of active materials, we performed DFT-D3 calculations focusing on selected DHP derivatives: the aim was to achieve high electron affinities while also taking the synthetic accessibility of the associated substitution patterns into account. Thus, rather than considering the entirety of all possible substitution patterns—as in the case of a high-throughput computational screening—only 32 DHP derivatives were the subject of our DFT-D3 calculations. Starting from the base structure, we selected specific functional groups to reflect well-known trends to modify the electron affinity of the compounds while also considering the impact on water solubility. All of the investigated DHP derivatives are listed in Table T2 in the SI, together with their associated E_{calc}. In addition, we determine the dihedral angles of the DHP ring system to estimate the distortion from the planar arrangement for each derivative. We used these angles and the energetic variations evoked by the distortion of the DHP unit as an indicator for the stability of the substituted molecule compared to pristine DHP.

Since the effect of the incorporated functional groups is generally assumed to be cumulative, a complete substitution of the quinone ring is desirable in practical synthesis. As a side benefit, free sites are blocked as an effective measure to prevent potential nucleophilic side reactions such as Michael additions.

Accordingly, the computed redox potentials of four DHP compounds selected in line with the aforementioned requirements are shown in Figure 3 together with the experimentally investigated derivatives: the listed compounds are sorted in order of increasing redox potential, starting from DHP(Me)$_2$ as the least oxidizing compound. DHP(Me)$_2$ is followed by DHP(MeO) and the base structure DHP.

By adding two trifluoromethyl ($-CF_3$) substituents to DHP, compound DHP(CF$_3$)$_2$ is obtained. Since $-CF_3$ groups are highly electronegative, the overall electron density of the molecule decreases compared to the base structure. Hence, it can be observed that E_{calc} increases accordingly. This behavior is

https://dx.doi.org/10.1021/acs.chemmater.9b05077
Chem. Mater. XXXX, XXX, XXX−XXX

in line with the already reported trend obtained via high-throughput computational screening of anthraquinone species.[15] On the downside, a large deviation from an ideal planarity is obtained for the oxidized molecule. The maximum dihedral angle of 22° determined for the optimized structure corresponds to an energy increase of 4.0 kcal mol^{-1} of the DHP unit, which may imply a reduced stability compared to pristine DHP.

Furthermore, $-CF_3$ has been shown to decrease the solubility of anthraquinone derivatives, which combined with the merely slight increase in electron affinity rather limits the applicability of DHP$(CF_3)_2$ as a catholyte active material.

As an alternative, sulfonic acid ($-SO_3^-$) groups are well-known to feature electron-withdrawing properties while also being very hydrophilic.[20] Since from the synthetic point of view it may be difficult to add two $-SO_3^-$ groups in close vicinity to each other the substituent was combined with a methyl (−Me) moiety to obtain the compound DHP(Me)(SO_3^-). The sulfonic acid group serves to increase the solubility in water, and—as a result of its electron withdrawing character—the electron affinity of DHP, whereas −Me blocks the unsubstituted site of the quinone ring, which may be prone to nucleophilic attacks. Considering our experimental results (compare Figure 1a) as well as computational studies the methyl group should slightly lower the overall potential of the compound. With respect to our calculations this decrease yet is compensated by the considerable electron-withdrawing character of $-SO_3^-$. However, according to our calculations the molecule is distorted by up to 18° (energy of the DHP unit increases by 2.4 kcal mol^{-1}) from ideal planarity by placing both substituents in adjacent positions. As such high dihedral angles may indicate a lower stability compared to the base structure DHP, DHP(Me)-(SO_3^-) is not considered as an appropriate candidate for catholyte active materials.

As an alternative, we consider the methylsulfonyl group (SO_2Me), since it might be easier to synthesize.[67] For the resulting compound DHP(Me)(SO_2Me) a slight decrease of electron affinity is to be expected whereas at the same time it should maintain a high solubility in water. As a beneficial side effect, the distortion angle of the molecule decreases to a maximum dihedral angle of 5°, which may yield an increased stability compared to DHP(Me)(SO_3^-).

Along with other performance-relevant quantities of RFB active materials such as the redox potential and the maximum solubility, kinetic aspects need to be taken into account with regard to practical applications as well. For instance, intramolecular hydrogen-bonding interactions caused by substituents in close vicinity to the carbonyl groups of the quinone ring may be detrimental for the rate constant k_0 of the charge transfer.[4,68] As a consequence, $-SO_3^-$ or $-SO_2Me$ groups may not be the ideal choice for the design of the DHP-based catholyte active materials despite their highly electron-withdrawing and hydrophilic properties.

Thus, as an alternative approach we propose to substitute the DHP base structure with a succinimidyl moiety. In line with the concept of increasing the electron affinity of quinones by incorporating nitrogen—as demonstrated by DHP—the succinimidyl moiety features a heterocyclic structure. Beyond that, our calculations imply that the ring system of the derivative maintains a planar structure even after substituting DHP with a succinimidyl moiety.

The E_{calc} calculated for DHP(sumi) displays a high value of 1.137 V vs SHE. Furthermore, as indicated by the high water solubility of succinimide of 330 g/L, the succinimidyl moiety should be very beneficial for the hydrophilicity of DHP(sumi).[69] As a profitable side effect, the originally unsubstituted sites of DHP are blocked by the substituent, which should hinder potentially detrimental side reactions in these positions. In terms of hydrogen bonding effects succinimidyl may enable higher rate constants than $-SO_3^-$ or $-SO_2Me$ since the distance between hydrogen bond donor and acceptor turns out to be significantly larger (see Figure S5). Altogether, in view of our calculations, our experimental findings and existing knowledge in literature, DHP(sumi) may be a very promising active material for the catholyte side of aqueous redox flow batteries.

■ CONCLUSIONS

We herein introduce the material class of dihydroxyphthalazines as versatile redox-active molecules that exhibit beneficial electro- and physicochemical properties for the application in aqueous redox flow batteries. Our approach is to increase the electron affinity of homocyclic quinones by modifying the base structure of the quinone with nitrogen. The unsubstituted dihydroxyphthalazine base structure exhibits a high value of $E_{1/2}$ that exceeds the potential of the parental naphthoquinone by 342 mV. In fact, the dihydroxyphthalazine base structure even surmounts the potential of *para*- as well as *ortho*-benzoquinones, underlining its significance regarding the design of quinone-based active materials for the catholyte of aqueous redox flow batteries. In addition, the investigated dihydroxyphthalazine derivatives exhibit high diffusion coefficients as well as fast charge transfer kinetics that should allow for fast charge transfer at low voltage losses during application.

We further demonstrated that dihydroxyphthalazines can be functionalized to prevent parasitic side reactions such as the Michael addition (e.g., the nucleophilic addition of water). In the case of the methylated dihydroxyphthalazine this was accomplished by blocking the free sites in between the hydroxyl or, respectively, carbonyl moieties of the quinone ring with methyl groups. Both exhaustive electrolysis and H NMR measurements indicate the anticipated transfer of two electrons per molecule under the exclusion of Michael addition. We also report a considerable influence of the added electron-donating moieties (i.e., methyl and methoxy) on the electron affinity of the dihydroxyphthalazine base structure resulting in reduced midpoint potentials. Since we were able to identify the associated positions as vulnerable sites for nucleophilic attacks as well as positions with a high impact on $E_{1/2}$, we hope to stimulate further research on the structure−property relationship of DHPs focusing on these sites.

In order to extend these findings, we conducted DFT-D3 calculations of different substitution patterns of DHP aiming for increased electron affinities. Based on our theoretical considerations that were complemented by experimental results, we identified promising catholyte active materials. They were selected based on optimal values for the redox potential, the resilience against nucleophilic attacks, and the solubility in water. One compound (base structure substituted with a succinimidyl moiety) was identified to possess a favorably high redox potential above 1 V vs SHE. Judging by the high solubility in water of succinimide this compound should come along with a high hydrophilicity. In addition, hydrogen bonding effects that are critical for the kinetic rate constant are minimized.

Altogether, dihydroxyphthalazines pose a promising class of compounds for the design of tailor-made high-potential active materials for aqueous redox flow batteries. As dihydroxyph-

https://dx.doi.org/10.1021/acs.chemmater.9b05077
Chem. Mater. XXXX, XXX, XXX−XXX

thalazines are partially synthesized by organic precursors that may be derived from naturally abundant sources, this work may also lead to new routes to economic and sustainable energy storage. In combination with quinones operating at low potentials in the anolyte it may be possible to realize systems that enable stable cycling with fast charge transfer at high cell voltages to meet the high requirements of peak load leveling. On the basis of our experimental results and the design strategies given, we hope to propel further research in the field of quinone-based catholyte active materials for aqueous redox flow batteries.

■ ASSOCIATED CONTENT

Supporting Information

The Supporting Information is available free of charge at https://pubs.acs.org/doi/10.1021/acs.chemmater.9b05077.

Additional synthesis information; hydrodynamic analysis of active materials including a table with cumulated results; cyclic voltammograms of different quinone species; electrolysis data and ^{1}H NMR spectra; and DFT calculations (PDF)

■ AUTHOR INFORMATION

Corresponding Authors

Jürgen Janek − *Institute of Physical Chemistry and Center for Materials Research, Justus Liebig University Giessen, 35392 Giessen, Germany;* orcid.org/0000-0002-9221-4756; Email: juergen.janek@phys.chemie.uni-giessen.de

Daniel Schröder − *Institute of Physical Chemistry and Center for Materials Research, Justus Liebig University Giessen, 35392 Giessen, Germany;* orcid.org/0000-0002-2198-0218; Email: daniel.schroeder@phys.chemie.uni-giessen.de

Authors

Jonas D. Hofmann − *Institute of Physical Chemistry, Justus Liebig University Giessen, 35392 Giessen, Germany*

Sebastian Schmalisch − *Institute of Organic Chemistry, Justus Liebig University Giessen, 35392 Giessen, Germany*

Sebastian Schwan − *Institute of Physical Chemistry and Center for Materials Research, Justus Liebig University Giessen, 35392 Giessen, Germany*

Longcheng Hong − *Institute of Organic Chemistry, Justus Liebig University Giessen, 35392 Giessen, Germany*

Hermann A. Wegner − *Institute of Organic Chemistry and Center for Materials Research, Justus Liebig University Giessen, 35392 Giessen, Germany;* orcid.org/0000-0001-7260-6018

Doreen Mollenhauer − *Institute of Physical Chemistry and Center for Materials Research, Justus Liebig University Giessen, 35392 Giessen, Germany*

Complete contact information is available at: https://pubs.acs.org/10.1021/acs.chemmater.9b05077

Notes

The authors declare the following competing financial interest(s): J.D.H, S.S., L.H., H.W., J.J. and D.S. have filed for a patent on the synthesis and the use of DHPs in redox flow battery applications.

■ ACKNOWLEDGMENTS

S.S. and D.M. acknowledge the support by the administrators of the YACANA Cluster and the IT Centre (HRZ) of the Justus-Liebig University Giessen. H.W., J.J., and D.S. gratefully acknowledge financial support by BMEL (Federal Ministry of Food and Agriculture) within the project FOREST (22403116).

■ REFERENCES

(1) Quan, M.; Sanchez, D.; Wasylkiw, M. F.; Smith, D. K. Voltammetry of Quinones in Unbuffered Aqueous Solution: Reassessing the Roles of Proton Transfer and Hydrogen Bonding in the Aqueous Electrochemistry of Quinones. *J. Am. Chem. Soc.* **2007**, *129* (42), 12847−12856.

(2) Hofmann, J. D.; Schröder, D. Which Parameter Is Governing for Aqueous Redox Flow Batteries with Organic Active Material? *Chem. Ing. Tech.* **2019**, *91* (6), 786−794.

(3) Huskinson, B.; Marshak, M. P.; Suh, C.; Er, S.; Gerhardt, M. R.; Galvin, C. J.; Chen, X.; Aspuru-Guzik, A.; Gordon, R. G.; Aziz, M. J. A Metal-Free Organic-Inorganic Aqueous Flow Battery. *Nature* **2014**, *505* (7482), 195−198.

(4) Yang, B.; Hoober-Burkhardt, L.; Wang, F.; Surya Prakash, G. K.; Narayanan, S. R. An Inexpensive Aqueous Flow Battery for Large-Scale Electrical Energy Storage Based on Water-Soluble Organic Redox Couples. *J. Electrochem. Soc.* **2014**, *161* (9), A1371−A1380.

(5) Kwabi, D. G.; Lin, K.; Ji, Y.; Kerr, E. F.; Goulet, M.-A.; De Porcellinis, D.; Tabor, D. P.; Pollack, D. A.; Aspuru-Guzik, A.; Gordon, R. G.; Aziz, M. J. Alkaline Quinone Flow Battery with Long Lifetime at PH 12. *Joule* **2018**, *2*, 1894.

(6) Ji, Y.; Goulet, M.-A.; Pollack, D. A.; Kwabi, D. G.; Jin, S.; Porcellinis, D. D.; Kerr, E. F.; Gordon, R. G.; Aziz, M. J. A Phosphonate-Functionalized Quinone Redox Flow Battery at Near-Neutral PH with Record Capacity Retention Rate. *Adv. Energy Mater.* **2019**, *9* (12), 1900039.

(7) Yang, Z.; Tong, L.; Tabor, D. P.; Beh, E. S.; Goulet, M.-A.; De Porcellinis, D.; Aspuru-Guzik, A.; Gordon, R. G.; Aziz, M. J. Alkaline Benzoquinone Aqueous Flow Battery for Large-Scale Storage of Electrical Energy. *Adv. Energy Mater.* **2018**, *8* (8), 1702056.

(8) Tong, L.; Goulet, M.-A.; Tabor, D. P.; Kerr, E. F.; De Porcellinis, D.; Fell, E. M.; Aspuru-Guzik, A.; Gordon, R. G.; Aziz, M. J. Molecular Engineering of an Alkaline Naphthoquinone Flow Battery. *ACS Energy Letters* **2019**, *4* (8), 1880−1887.

(9) Lee, W.; Park, G.; Kwon, Y. Alkaline Aqueous Organic Redox Flow Batteries of High Energy and Power Densities Using Mixed Naphthoquinone Derivatives. *Chem. Eng. J.* **2020**, *386*, 123985.

(10) Lee, W.; Permatasari, A.; Kwon, B. W.; Kwon, Y. Performance Evaluation of Aqueous Organic Redox Flow Battery Using Anthraquinone-2,7-Disulfonic Acid Disodium Salt and Potassium Iodide Redox Couple. *Chem. Eng. J.* **2019**, *358*, 1438−1445.

(11) Yang, B.; Hoober-Burkhardt, L.; Krishnamoorthy, S.; Murali, A.; Prakash, G. K. S.; Narayanan, S. R. High-Performance Aqueous Organic Flow Battery with Quinone-Based Redox Couples at Both Electrodes. *J. Electrochem. Soc.* **2016**, *163* (7), A1442−A1449.

(12) Permatasari, A.; Lee, W.; Kwon, Y. Performance Improvement by Novel Activation Process Effect of Aqueous Organic Redox Flow Battery Using Tiron and Anthraquinone-2,7-Disulfonic Acid Redox Couple. *Chem. Eng. J.* **2020**, *383*, 123085.

(13) Hoober-Burkhardt, L.; Krishnamoorthy, S.; Yang, B.; Murali, A.; Nirmalchandar, A.; Prakash, G. K. S.; Narayanan, S. R. A New Michael-Reaction-Resistant Benzoquinone for Aqueous Organic Redox Flow Batteries. *J. Electrochem. Soc.* **2017**, *164* (4), A600−A607.

(14) Huynh, M. T.; Anson, C. W.; Cavell, A. C.; Stahl, S. S.; Hammes-Schiffer, S. Quinone 1 e− and 2 e−/2 H+ Reduction Potentials: Identification and Analysis of Deviations from Systematic Scaling Relationships. *J. Am. Chem. Soc.* **2016**, *138* (49), 15903−15910.

(15) Er, S.; Suh, C.; Marshak, M. P.; Aspuru-Guzik, A. Computational Design of Molecules for an All-Quinone Redox Flow Battery. *Chem. Sci.* **2015**, *6* (2), 885−893.

(16) Tabor, D. P.; Gómez-Bombarelli, R.; Tong, L.; Gordon, R. G.; Aziz, M. J.; Aspuru-Guzik, A. Theoretical and Experimental Investigation of the Stability Limits of Quinones in Aqueous Media: Implications for Organic Aqueous Redox Flow Batteries. *ChemRxiv*, 2018; DOI: 10.26434/chemrxiv.6990053.v2

(17) Bachman, J. E.; Curtiss, L. A.; Assary, R. S. Investigation of the Redox Chemistry of Anthraquinone Derivatives Using Density Functional Theory. *J. Phys. Chem. A* **2014**, *118* (38), 8852−8860.
(18) Assary, R. S.; Brushett, F. R.; Curtiss, L. A. Reduction Potential Predictions of Some Aromatic Nitrogen-Containing Molecules. *RSC Adv.* **2014**, *4* (101), 57442−57451.
(19) Cheng, L.; Assary, R. S.; Qu, X.; Jain, A.; Ong, S. P.; Rajput, N. N.; Persson, K.; Curtiss, L. A. Accelerating Electrolyte Discovery for Energy Storage with High-Throughput Screening. *J. Phys. Chem. Lett.* **2015**, *6* (2), 283−291.
(20) Gerhardt, M. R.; Tong, L.; Gómez-Bombarelli, R.; Chen, Q.; Marshak, M. P.; Galvin, C. J.; Aspuru-Guzik, A.; Gordon, R. G.; Aziz, M. J. Anthraquinone Derivatives in Aqueous Flow Batteries. *Adv. Energy Mater.* **2017**, *7* (8), 1601488.
(21) Carretero-González, J.; Castillo-Martínez, E.; Armand, M. Highly Water-Soluble Three-Redox State Organic Dyes as Bifunctional Analytes. *Energy Environ. Sci.* **2016**, *9* (11), 3521−3530.
(22) Lin, K.; Chen, Q.; Gerhardt, M. R.; Tong, L.; Kim, S. B.; Eisenach, L.; Valle, A. W.; Hardee, D.; Gordon, R. G.; Aziz, M. J.; Marshak, M. P. Alkaline Quinone Flow Battery. *Science* **2015**, *349* (6255), 1529−1532.
(23) Wang, Z.; Li, A.; Gou, L.; Ren, J.; Zhai, G. Computational Electrochemistry Study of Derivatives of Anthraquinone and Phenanthraquinone Analogues: The Substitution Effect. *RSC Adv.* **2016**, *6* (92), 89827−89835.
(24) Shimizu, A.; Tsujii, Y.; Kuramoto, H.; Nokami, T.; Inatomi, Y.; Hojo, N.; Yoshida, J. Nitrogen-Containing Polycyclic Quinones as Cathode Materials for Lithium-Ion Batteries with Increased Voltage. *Energy Technology* **2014**, *2* (2), 155−158.
(25) Liang, Y.; Zhang, P.; Yang, S.; Tao, Z.; Chen, J. Fused Heteroaromatic Organic Compounds for High-Power Electrodes of Rechargeable Lithium Batteries. *Adv. Energy Mater.* **2013**, *3* (5), 600−605.
(26) Hatakeyama-Sato, K.; Nagano, T.; Noguchi, S.; Sugai, Y.; Du, J.; Nishide, H.; Oyaizu, K. Hydrophilic Organic Redox-Active Polymer Nanoparticles for Higher Energy Density Flow Batteries. *ACS Appl. Polym. Mater.* **2019**, *1* (2), 188−196.
(27) Zhao, Q.; Zhu, Z.; Chen, J. Molecular Engineering with Organic Carbonyl Electrode Materials for Advanced Stationary and Redox Flow Rechargeable Batteries. *Adv. Mater.* **2017**, *29* (48), 1607007.
(28) Hofmann, J. D.; Pfanschilling, F. L.; Krawczyk, N.; Geigle, P.; Hong, L.; Schmalisch, S.; Wegner, H. A.; Mollenhauer, D.; Janek, J.; Schröder, D. Quest for Organic Active Materials for Redox Flow Batteries: 2,3-Diaza-Anthraquinones and Their Electrochemical Properties. *Chem. Mater.* **2018**, *30* (3), 762−774.
(29) Revenga, J.; Rodríguez, F.; Tijero, J. Study of the Redox Behavior of Anthraquinone in Aqueous Medium. *J. Electrochem. Soc.* **1994**, *141* (2), 330−333.
(30) Bard, A. J.; Faulkner, L. R. *Electrochemical Methods: Fundamentals and Applications*; Wiley: New York, 2000.
(31) Hong, L.; Ahles, S.; Heindl, A. H.; Tiétcha, G.; Petrov, A.; Lu, Z.; Logemann, C.; Wegner, H. A. An Air-Stable Bisboron Complex: A Practical Bidentate Lewis Acid Catalyst. *Beilstein J. Org. Chem.* **2018**, *14* (1), 618−625.
(32) Domasevitch, K. V.; Gural'skiy, I. A.; Solntsev, P. V.; Rusanov, E. B.; Krautscheid, H.; Howard, J. A. K.; Chernega, A. N. 4,4′-Bipyridazine: A New Twist for the Synthesis of Coordination Polymers. *Dalton Trans.* **2007**, No. 29, 3140−3148.
(33) Ali, M. H.; Welker, A.; York, C. A Facile and Selective Procedure for Oxidation of Hydroquinones Using Silica Gel Supported Catalytic Cerium(IV) Ammonium Nitrate. *Synthesis* **2015**, *47* (20), 3207−3211.
(34) Paige, M.; Kosturko, G.; Bulut, G.; Miessau, M.; Rahim, S.; Toretsky, J. A.; Brown, M. L.; Üren, A. Design, Synthesis and Biological Evaluation of Ezrin Inhibitors Targeting Metastatic Osteosarcoma. *Bioorg. Med. Chem.* **2014**, *22* (1), 478−487.
(35) Scholz, F. *Electroanalytical Methods: Guide to Experiments and Applications*; Springer Science & Business Media: New York, 2009.
(36) Frisch, M. J.; Trucks, G. W.; Schlegel, H. B.; Scuseria, G. E.; Robb, M. A.; Cheeseman, J. R.; Scalmani, G.; Barone, V.; Mennucci, B.; Petersson, G. A.; Nakatsuji, H.; Caricato, M.; Li, X.; Hratchian, H. P.; Izmaylov, A. F.; Bloino, J.; Zheng, G.; Sonnenberg, J. L.; Hada, M.; Ehara, M.; Toyota, K.; Fukuda, R.; Hasegawa, J.; Ishida, M.; Nakajima, T.; Honda, Y.; Kitao, O.; Nakai, H.; Vreven, T.; Montgomery, J. A., Jr.; Peralta, J. E.; Ogliaro, F.; Bearpark, M.; Heyd, J. J.; Brothers, E.; Kudin, K. N.; Staroverov, V. N.; Kobayashi, R.; Normand, J.; Raghavachari, K.; Rendell, A.; Burant, J. C.; Iyengar, S. S.; Tomasi, J.; Cossi, M.; Rega, N.; Millam, N. J.; Klene, M.; Knox, J. E.; Cross, J. B.; Bakken, V.; Adamo, C.; Jaramillo, J.; Gomperts, R.; Stratmann, R. E.; Yazyev, O.; Austin, A. J.; Cammi, R.; Pomelli, C.; Ochterski, J. W.; Martin, R. L.; Morokuma, K.; Zakrzewski, V. G.; Voth, G. A.; Salvador, P.; Dannenberg, J. J.; Dapprich, S.; Daniels, A. D.; Ö., Farkas; Foresman, J. B.; Ortiz, J. V.; Cioslowski, J.; Fox, D. J. *Gaussian 09*, revision A.01; Gaussian, Inc.: Wallingford, CT, 2009.
(37) Perdew, J. P.; Burke, K.; Ernzerhof, M. Generalized Gradient Approximation Made Simple. *Phys. Rev. Lett.* **1996**, *77* (18), 3865−3868.
(38) Grimme, S.; Antony, J.; Ehrlich, S.; Krieg, H. A Consistent and Accurate Ab Initio Parametrization of Density Functional Dispersion Correction (DFT-D) for the 94 Elements H-Pu. *J. Chem. Phys.* **2010**, *132* (15), 154104.
(39) Grimme, S.; Ehrlich, S.; Goerigk, L. Effect of the Damping Function in Dispersion Corrected Density Functional Theory. *J. Comput. Chem.* **2011**, *32* (7), 1456−1465.
(40) Kendall, R. A.; Dunning, T. H.; Harrison, R. J. Electron Affinities of the First-row Atoms Revisited. Systematic Basis Sets and Wave Functions. *J. Chem. Phys.* **1992**, *96* (9), 6796−6806.
(41) Tomasi, J.; Mennucci, B.; Cammi, R. Quantum Mechanical Continuum Solvation Models. *Chem. Rev.* **2005**, *105* (8), 2999−3094.
(42) Guin, P. S.; Das, S.; Mandal, P. C. Electrochemical Reduction of Quinones in Different Media: A Review. *Int. J. Electrochem.* **2011**, *2011*, 816202.
(43) Ho, J.; Coote, M. L.; Cramer, C. J.; Truhlar, D. G. Theoretical Calculation of Reduction Potentials. *Org. Electrochem.* **2015**, *5*, 229−259.
(44) Becke, A. D. Density-Functional Exchange-Energy Approximation with Correct Asymptotic Behavior. *Phys. Rev. A: At., Mol., Opt. Phys.* **1988**, *38* (6), 3098−3100.
(45) Perdew, J. P. Density-Functional Approximation for the Correlation Energy of the Inhomogeneous Electron Gas. *Phys. Rev. B: Condens. Matter Mater. Phys.* **1986**, *33* (12), 8822−8824.
(46) Adamo, C.; Barone, V. Toward Reliable Density Functional Methods without Adjustable Parameters: The PBE0Model. *J. Chem. Phys.* **1999**, *110* (13), 6158−6170.
(47) Lee, C.; Yang, W.; Parr, R. G. Development of the Colle-Salvetti Correlation-Energy Formula into a Functional of the Electron Density. *Phys. Rev. B: Condens. Matter Mater. Phys.* **1988**, *37* (2), 785−789.
(48) Stephens, P. J.; Devlin, F. J.; Chabalowski, C. F.; Frisch, M. J. Ab Initio Calculation of Vibrational Absorption and Circular Dichroism Spectra Using Density Functional Force Fields. *J. Phys. Chem.* **1994**, *98* (45), 11623−11627.
(49) Kim, H.; Goodson, T.; Zimmerman, P. M. Achieving Accurate Reduction Potential Predictions for Anthraquinones in Water and Aprotic Solvents: Effects of Inter- and Intramolecular H-Bonding and Ion Pairing. *J. Phys. Chem. C* **2016**, *120* (39), 22235−22247.
(50) Castle, R. N. *Condensed Pyridazines Including Cinnolines and Phthalazines*; John Wiley & Sons: New York, 2009.
(51) Fox, M. A.; Whitesell, J. K. *Organic Chemistry*, 3rd ed.; Jones and Bartlett Publishers: Sudbury, MA, 2004.
(52) Sevrain, C. M.; Berchel, M.; Couthon, H.; Jaffrès, P.-A. Phosphonic Acid: Preparation and Applications. *Beilstein J. Org. Chem.* **2017**, *13* (1), 2186−2213.
(53) Guthrie, J. P. Hydrolysis of Esters of Oxy Acids: PKa Values for Strong Acids; Brønsted Relationship for Attack of Water at Methyl; Free Energies of Hydrolysis of Esters of Oxy Acids; and a Linear Relationship between Free Energy of Hydrolysis and PKa Holding over a Range of 20 PK Units. *Can. J. Chem.* **1978**, *56* (17), 2342−2354.

https://dx.doi.org/10.1021/acs.chemmater.9b05077
Chem. Mater. XXXX, XXX, XXX−XXX

(54) Zhigalko, M. V.; Shishkin, O. V.; Gorb, L.; Leszczynski, J. Out-of-Plane Deformability of Aromatic Systems in Naphthalene, Anthracene and Phenanthrene. *J. Mol. Struct.* **2004**, *693* (1), 153−159.
(55) Chen, Q.; Gerhardt, M. R.; Hartle, L.; Aziz, M. J. A Quinone-Bromide Flow Battery with 1 W/Cm2 Power Density. *J. Electrochem. Soc.* **2016**, *163* (1), A5010−A5013.
(56) Hu, B.; DeBruler, C.; Rhodes, Z.; Liu, T. L. Long-Cycling Aqueous Organic Redox Flow Battery (AORFB) toward Sustainable and Safe Energy Storage. *J. Am. Chem. Soc.* **2017**, *139* (3), 1207−1214.
(57) Janoschka, T.; Martin, N.; Hager, M. D.; Schubert, U. S. An Aqueous Redox-Flow Battery with High Capacity and Power: The TEMPTMA/MV System. *Angew. Chem., Int. Ed.* **2016**, *55* (46), 14427−14430.
(58) Drazevic, E.; Szabo, C.; Konya, D.; Lund, T.; Wedege, K.; Bentien, A. Investigation of Tetramorpholinohydroquinone as a Potential Catholyte in a Flow Battery. *ACS Appl. Energy Mater.* **2019**, *2*, 4745.
(59) Zhu, X.-Q.; Wang, C.-H. Accurate Estimation of the One-Electron Reduction Potentials of Various Substituted Quinones in DMSO and CH3CN. *J. Org. Chem.* **2010**, *75* (15), 5037−5047.
(60) Gottis, S.; Barrès, A.-L.; Dolhem, F.; Poizot, P. Voltage Gain in Lithiated Enolate-Based Organic Cathode Materials by Isomeric Effect. *ACS Appl. Mater. Interfaces* **2014**, *6* (14), 10870−10876.
(61) Wedege, K.; Dražević, E.; Konya, D.; Bentien, A. Organic Redox Species in Aqueous Flow Batteries: Redox Potentials, Chemical Stability and Solubility. *Sci. Rep.* **2016**, *6*, 39101.
(62) Evans, D. H. One-Electron and Two-Electron Transfers in Electrochemistry and Homogeneous Solution Reactions. *Chem. Rev.* **2008**, *108* (7), 2113−2144.
(63) Batchelor-McAuley, C.; Compton, R. G. Voltammetry of Multi-Electron Electrode Processes of Organic Species. *J. Electroanal. Chem.* **2012**, *669*, 73−81.
(64) Kim, Y.-R.; Kim, R. S.; Kang, S. K.; Choi, M. G.; Kim, H. Y.; Cho, D.; Lee, J. Y.; Chang, S.-K.; Chung, T. D. Modulation of Quinone PCET Reaction by Ca2+ Ion Captured by Calix[4]Quinone in Water. *J. Am. Chem. Soc.* **2013**, *135* (50), 18957−18967.
(65) Alegría, A. E.; López, M.; Guevara, N. Thermodynamics of Semiquinone Disproportionation in Aqueous Buffer. *J. Chem. Soc., Faraday Trans.* **1996**, *92* (24), 4965−4968.
(66) Bishop, C. A.; Tong, L. K. J. Equilibria of Substituted Semiquinones at High PH. *J. Am. Chem. Soc.* **1965**, *87* (3), 501−505.
(67) Hong, L.; Ahles, S.; Strauss, M. A.; Logemann, C.; Wegner, H. A. Synthesis of 2,3-Diaza-Anthraquinones via the Bidentate Lewis Acid Catalysed Inverse Electron-Demand Diels−Alder (IEDDA) Reaction. *Org. Chem. Front.* **2017**, *4* (5), 871−875.
(68) Kim, R. S.; Park, W.; Hong, H.; Chung, T. D.; Kim, S. Quinone Electrochemistry Altered by Local Hydrophobic Environment and Hydrogen Bonding Interactions. *Electrochem. Commun.* **2014**, *41*, 39−43.
(69) *GESTIS database: succinimide*. http://gestis.itrust.de/nxt/gateway.dll/gestis_de/040260.xml?f=templates$fn=default.htm$3.0 (accessed Aug. 5, 2019).
(70) Chesseman, G. W. H.; Cookson, R. F. *Condensed Pyrazines*; John Wiley & Sons: New York, 2009.

https://dx.doi.org/10.1021/acs.chemmater.9b05077
Chem. Mater. XXXX, XXX, XXX−XXX

3 Conclusions and Outlook

In this PhD project, nitrogen-modified quinone analogues were introduced as potent active species. These open up attractive design opportunities for organic active materials used in ORFBs. It was demonstrated that diaza-quinones feature unique properties, which are very beneficial for energy storage applications. In the context of this thesis, these characteristics were thoroughly investigated by means of various electrochemical and analytical techniques. Based on the gained results, the structural motif of diaza-quinones was developed and refined to obtain stable and efficient active materials for ORFBs.

At the beginning of this project, only a few studies focusing on the structure-property relationships of quinone compounds for ORFBs had been published. The studies revealed nowadays well-known trends considering the impact of peripheral functionalization on the properties of established base structures such as AQs, NQs and BQs. In this work, however, the base structure itself was altered in order to further expand upon the existing knowledge on the structure-property relationships of quinonoid compounds. To investigate the impact and potential benefit of a heterocyclic structure with regard to ORFBs, the performance-relevant parameters of DAAQs were fully characterized. The results revealed competitive charge transfer kinetics and diffusion coefficients, which were complemented by remarkable electrochemical features: the nitrogen-based modification was found to increase the electron affinity of the associated compound, which translates to a distinct positive shift of its redox potential of about 300 mV. Additionally, varying substitution patterns opened up opportunities to further adjust the electrochemical properties of the base compound: two incorporated hydroxyl moieties resulted in a negative shift of the redox potential by 54 mV in acidic and 264 mV in alkaline aqueous solution. Besides, the cycling stability of DAAQs was clearly increased in acidic solution by adding a methoxy moiety to the base structure. The measurements in alkaline solution further indicated a stabilization of the DAAQ semiquinone anion radical as compared to commonly used homocyclic quinone analogues.

These findings were substantiated by subsequent studies under optimized anhydrous conditions, which revealed a stabilization of the semiquinone intermediate. This manifests in an increased potential difference between the two occurring charge transfers, surpassing the homocyclic AQ by 60 mV. This peculiarity holds great opportunities, especially for the charge transfer kinetics of quinones under the influence of protonation (see section 1.3.1). Indeed, complementary voltammetric studies of DAAQs yielded negligible overpotentials across a pH range from 0 to 7. For commonly used homocyclic quinone species, this range is prone to a high degree of potential inversion and thus worse kinetics. Consequently, the diaza-modified derivatives offer kinetic advantages in the case of

protonation, which renders this compound class more flexible with regard to optimizations of the pH value of ORFB systems.

Beyond that, the pH dependent voltammetric studies were carried out up to a pH of 14. This resulted in a comprehensive analysis of diaza-quinones across the full pH range. The interplay of electron and proton transfer was resolved by a Pourbaix analysis, yielding the pK_a values of varying protonation states. Thus, a deeper understanding of specific features of DAAQs – such as the observed peak splitting in alkaline solution as well as an additional state of protonation at pH values below 3 – was gained. Overall, the electrochemical characteristics of this new class of compounds were thoroughly elucidated, emphasizing the versatile character of diaza-functionalized quinones in general as well as their excellent applicability as an active material in ORFBs.

In order to further capitalize on the unique features of diaza-quinones, the focus of this thesis was subsequently strengthened on the design of capable active species for the catholyte side of ORFBs. Previous results showed an increased redox potential of diaza-quinones compared to their homocyclic analogues. Consequently, the concept was transferred to intrinsically more electron-deficient structural motifs, introducing the naphthoquinone-based class of DHPs. In fact, the unsubstituted DHP base structure exhibits a high redox potential of 796 mV vs. SHE, which is 282 mV more positive in 1M H_2SO_4 than the unsubstituted DAAQ investigated priorly. More importantly, this value even surpasses the redox potential of any of the established homocyclic base structures of quinones, including BQs. In addition, a comprehensive characterization revealed superior charge transfer kinetics of DHPs, outperforming BQs by one order of magnitude.

The resilience of the organic active material against detrimental side reactions poses another essential factor to enable high efficiencies during ORFB operation. This issue was addressed in terms of a structural modification of the blank DHP. To prevent the conjugate addition of water, the base structure was augmented by two methyl moieties in this work. A combined approach of exhaustive oxidative electrolysis and a structural elucidation by ^{1}H NMR analysis demonstrated the desired electrochemical oxidation of the methylated DHP without nucleophilic side reactions.

To gain a further understanding of the structure-property relationships of DHPs, a total of three varying derivatives was experimentally characterized according to different voltammetric methods. As in the case of homocyclic quinones, the redox potential could be lowered systematically by incorporating electron-donating methoxy and methyl groups. Overall, the free sites in between the characteristic hydroxyl, or respectively, carbonyl moieties were identified as positions with a distinct impact on the redox potential as well as the stability of DHPs. Based on these findings, structural motifs were outlined in order to further improve upon the promising properties of diaza-quinones in terms

of energy and power density. In this context, substitution patterns with increased redox potential and water solubility were defined by means of DFT calculations to propel further research in this field.

Conclusively, this thesis provides insightful information on the structure-property relationships of nitrogen-based heterocyclic quinones. This fundamental understanding of the physico- and electrochemical characteristics of diaza-quinones, which is supported by experimental results and theoretical considerations, provides valuable guidance for the design of high-performing quinonoid active materials for ORFBs. This particularly applies to the high-potential side of the battery, which is restrained by problems associated with the highly electrophilic nature of the active material. Besides this central purpose, the gained knowledge may also contribute to the progress of related research areas focusing on organic compounds as part of energy storage concepts. For instance DHPs in particular may pose favorable n-type organic electrode materials due to their high intrinsic redox potential, enabling high working potentials of up to 3 V vs. Li^+/Li.[224,225] Furthermore, the design strategies presented in this work may also contribute to the development of redox mediators for metal-ion batteries, fuel cells or dye-sensitized solar cells because of the favorable charge transfer characteristics.[226–229]

Nevertheless, this work first and foremost lays the foundation for the further development of quinone-based ORFBs while also revealing future tasks to leverage this promising technology:

- This work provides useful design strategies to optimize the electrochemical performance of quinonoid active materials for ORFBs. The focus was put on the beneficial replacement of two adjacent ring carbons by nitrogen, resulting in distinct improvements of electrochemical key quantities. However, adjustments of relative atom positions within the structure may allow for further optimization. For instance, switching to an ortho-configuration of the characteristic carbonyl moieties is expected to increase E^0 due to an increased degree of coordination between the two carbonyl oxygens and the incoming cation/proton.[230] A similar effect was reported for the placement of nitrogen in β-position relative to the carbonyl group.[231] Consequently, the potential of the structural motif of diaza-quinones is not fully exhausted yet and may be improved further to create even more elaborated structures with superior performance.
- The main emphasis of this work was to elucidate the structure-property relationships of diaza-quinones in different media and their structural refinement. However, it is imperative to evaluate a multitude of intertwined factors in order to enable a high cycling performance of ORFBs. These factors are directly affected by the choice of solvent and comprise the achievable cell potential, membrane resistance as well as redox kinetics, solubility and

crossover of the applied active material. The results gained in this work provide guidance on how to optimize the performance of diaza-quinones as a function of the nature and pH value of the used solvent. However, further studies will be necessary to define optimal operating conditions in order to fully capitalize on the beneficial properties of this promising compound class at system level. In this context, the revealed additional protonation state at low pH values and its implications for the interaction between the resulting cationic species and the applied membrane material should be taken into consideration for future studies as well.

- The electrode material of ORFBs is a decisive factor in the process of energy conversion as it mediates the charge transfer between the external circuit and the dissolved active species. Hence, electrode design provides a considerable development potential with respect to morphological and surface chemical optimization. Whereas sulfonic acid groups and comparable moieties capable of hydrogen-bonding were generally found to be detrimental for the kinetics of the occurring charge transfer[50], recent reports indicate that kinetic disadvantages of this sort may be compensated by a clever design of electrode materials.[232] Therefore, future work should be committed to the investigation and refinement of varying electrode concepts.
- Due to the comparably low solubility of the investigated diaza-quinone derivatives, potential concentration-dependent effects could not be accounted for in this work. However, as soon as higher concentrations of active material can be realized – e.g. according to the design strategies proposed in publication III – it will be essential to investigate their actual existence and extent. For instance, the viscosity of the electrolyte may be significantly altered at elevated concentrations, thus affecting the overall efficiency at system level. Besides, in this work the solvent was investigated as the main motive for nucleophilic side reactions. Yet, considering high concentrations of active species, a nucleophilic attack originating from the reduced form of the active material may be considered as well.

4 References

(1) Yang, Z.; Zhang, J.; Kintner-Meyer, M. C. W.; Lu, X.; Choi, D.; Lemmon, J. P.; Liu, J. Electrochemical Energy Storage for Green Grid. *Chem. Rev.* **2011**, *111* (5), 3577–3613. https://doi.org/10.1021/cr100290v.

(2) Chen, H.; Cong, T. N.; Yang, W.; Tan, C.; Li, Y.; Ding, Y. Progress in Electrical Energy Storage System: A Critical Review. *Progress in Natural Science* **2009**, *19* (3), 291–312. https://doi.org/10.1016/j.pnsc.2008.07.014.

(3) Placke, T.; Kloepsch, R.; Dühnen, S.; Winter, M. A. Lithium Ion, Lithium Metal, and Alternative Rechargeable Battery Technologies: The Odyssey for High Energy Density. *Journal of Solid State Electrochemistry* **2017**, *21*, 1939–1964. https://doi.org/10.1007/s10008-017-3610-7.

(4) Adelhelm, P.; Hartmann, P.; Bender, C. L.; Busche, M.; Eufinger, C.; Janek, J. From Lithium to Sodium: Cell Chemistry of Room Temperature Sodium–Air and Sodium–Sulfur Batteries. *Beilstein Journal of Nanotechnology* **2015**, *6*, 1016–1055. https://doi.org/10.3762/bjnano.6.105.

(5) Weber, A. Z.; Mench, M. M.; Meyers, J. P.; Ross, P. N.; Gostick, J. T.; Liu, Q. Redox Flow Batteries: A Review. *J. Appl. Electrochem.* **2011**, *41* (10), 1137–1164. https://doi.org/10.1007/s10800-011-0348-2.

(6) Budischak, C.; Sewell, D.; Thomson, H.; Mach, L.; Veron, D. E.; Kempton, W. Cost-Minimized Combinations of Wind Power, Solar Power and Electrochemical Storage, Powering the Grid up to 99.9% of the Time. *Journal of Power Sources* **2013**, *225*, 60–74. https://doi.org/10.1016/j.jpowsour.2012.09.054.

(7) Luo, J.; Hu, B.; Hu, M.; Zhao, Y.; Liu, T. L. Status and Prospects of Organic Redox Flow Batteries toward Sustainable Energy Storage. *ACS Energy Lett.* **2019**, *4* (9), 2220–2240. https://doi.org/10.1021/acsenergylett.9b01332.

(8) Thaller, L. H. Electrically Rechargeable Redox Flow Cells; August 26, 1974 - August 30, 1974, 1974.

(9) Thaller, L. H. Electrically Rechargeable REDOX Flow Cell. US3996064A, December 7, 1976.

(10) Thaller, L. H. *Redox Flow Cell Energy Storage Systems*; 1979.

(11) Skyllas-Kazacos, M.; Rychick, M.; Robins, R. All-Vanadium Redox Battery. US4786567A, November 22, 1988.

(12) Skyllas-Kazacos, M.; Rychcik, M.; Robins, R. G.; Fane, A. G.; Green, M. A. New All-Vanadium Redox Flow Cell. *J. Electrochem. Soc.* **1986**, *133* (5), 1057–1058. https://doi.org/10.1149/1.2108706.

(13) Skyllas-Kazacos, M.; Grossmith, F. Efficient Vanadium Redox Flow Cell. *J. Electrochem. Soc.* **1987**, *134* (12), 2950–2953. https://doi.org/10.1149/1.2100321.

(14) Skyllas-Kazacos, M.; Kazacos, G.; Poon, G.; Verseema, H. Recent Advances with UNSW Vanadium-Based Redox Flow Batteries. *Int. J. Energy Res.* **2010**, *34* (2), 182–189. https://doi.org/10.1002/er.1658.

(15) Steeley, W. *VRB Energy Storage for Voltage Stabilization*; 2005.

(16) Tsekouras, G. J.; Anastasopoulos, C. A.; Kontargyri, V. T.; Kanellos, F. D.; Karanasiou, I. S.; Salis, A. D.; Mastorakis, N. E. A Demand Side Management Program of Vanadium Redox Energy

Storage System for an Interconnected Power System. In *ENVIRONMENTAL EDUCATION*; 2008; pp 94–100.

(17) Shigematsu, T. Redox Flow Battery for Energy Storage. *SEI technical review* **2011**, *73* (7), 13.

(18) Alotto, P.; Guarnieri, M.; Moro, F. Redox Flow Batteries for the Storage of Renewable Energy: A Review. *Renewable and Sustainable Energy Reviews* **2014**, *29*, 325–335. https://doi.org/10.1016/j.rser.2013.08.001.

(19) VisBlue website https://visblue.com/product.html (accessed Nov 18, 2019).

(20) VoltStorage website https://voltstorage.com/en/voltstorage-smart-home-battery/ (accessed Nov 18, 2019).

(21) Vanadium Price https://www.vanadiumprice.com/ (accessed Nov 19, 2019).

(22) Skyllas-Kazacos, M. Performance Improvements and Cost Considerations of the Vanadium Redox Flow Battery. *ECS Trans.* **2019**, *89* (1), 29–45. https://doi.org/10.1149/08901.0029ecst.

(23) Lithium Price http://www.metalary.com/lithium-price/ (accessed Nov 18, 2019).

(24) Lin, K.; Gómez-Bombarelli, R.; Beh, E. S.; Tong, L.; Chen, Q.; Valle, A.; Aspuru-Guzik, A.; Aziz, M. J.; Gordon, R. G. A Redox-Flow Battery with an Alloxazine-Based Organic Electrolyte. *Nat. Energy* **2016**, *1* (9), 16102. https://doi.org/10.1038/nenergy.2016.102.

(25) Wei, X.; Pan, W.; Duan, W.; Hollas, A.; Yang, Z.; Li, B.; Nie, Z.; Liu, J.; Reed, D.; Wang, W.; Sprenkle, V. Materials and Systems for Organic Redox Flow Batteries: Status and Challenges. *ACS Energy Lett.* **2017**, *2* (9), 2187–2204. https://doi.org/10.1021/acsenergylett.7b00650.

(26) Liu, T.; Wei, X.; Nie, Z.; Sprenkle, V.; Wang, W. A Total Organic Aqueous Redox Flow Battery Employing a Low Cost and Sustainable Methyl Viologen Anolyte and 4-HO-TEMPO Catholyte. *Adv. Energy Mater.* **2016**, *6* (3), 1501449. https://doi.org/10.1002/aenm.201501449.

(27) Schmidt, D.; Häupler, B.; Friebe, C.; Hager, M. D.; Schubert, U. S. Synthesis and Characterization of New Redox-Active Polymers Based on 10-(1,3-Dithiol-2-Ylidene)Anthracen-9(10H)-One Derivatives. *Polymer* **2015**, *68*, 321–327. https://doi.org/10.1016/j.polymer.2015.05.028.

(28) Duan, W.; Huang, J.; Kowalski, J. A.; Shkrob, I. A.; Vijayakumar, M.; Walter, E.; Pan, B.; Yang, Z.; Milshtein, J. D.; Li, B.; Liao, C.; Zhang, Z.; Wang, W.; Liu, J.; Moore, J. S.; Brushett, F. R.; Zhang, L.; Wei, X. "Wine-Dark Sea" in an Organic Flow Battery: Storing Negative Charge in 2,1,3-Benzothiadiazole Radicals Leads to Improved Cyclability. *ACS Energy Lett.* **2017**, *2* (5), 1156–1161. https://doi.org/10.1021/acsenergylett.7b00261.

(29) Bozell, J. J. Approaches to the Selective Catalytic Conversion of Lignin: A Grand Challenge for Biorefinery Development. *Top. Curr. Chem.* **2014**, *353*, 229–255. https://doi.org/10.1007/128_2014_535.

(30) Zhu, H.; Wang, L.; Chen, Y.; Li, G.; Li, H.; Tang, Y.; Wan, P. Electrochemical Depolymerization of Lignin into Renewable Aromatic Compounds in a Non-Diaphragm Electrolytic Cell. *RSC Adv.* **2014**, *4* (56), 29917–29924. https://doi.org/10.1039/C4RA03793F.

(31) Awungacha Lekelefac, C.; Busse, N.; Herrenbauer, M.; Czermak, P. Photocatalytic Based Degradation Processes of Lignin Derivatives. *Int. J. Photoenergy* **2015**, *2015*, 18.

(32) Gerhardt, M. R.; Tong, L.; Gómez-Bombarelli, R.; Chen, Q.; Marshak, M. P.; Galvin, C. J.; Aspuru-Guzik, A.; Gordon, R. G.; Aziz, M. J. Anthraquinone Derivatives in Aqueous Flow Batteries. *Adv. Energy Mater.* **2017**, *7* (8), 1601488. https://doi.org/10.1002/aenm.201601488.

(33) Potash, R. A.; McKone, J. R.; Conte, S.; Abruña, H. D. On the Benefits of a Symmetric Redox Flow Battery. *J. Electrochem. Soc.* **2016**, *163* (3), A338–A344. https://doi.org/10.1149/2.0971602jes.

(34) Chen, Q.; Gerhardt, M. R.; Hartle, L.; Aziz, M. J. A Quinone-Bromide Flow Battery with 1 W/Cm2 Power Density. *J. Electrochem. Soc.* **2016**, *163* (1), A5010–A5013. https://doi.org/10.1149/2.0021601jes.

(35) Lin, K.; Chen, Q.; Gerhardt, M. R.; Tong, L.; Kim, S. B.; Eisenach, L.; Valle, A. W.; Hardee, D.; Gordon, R. G.; Aziz, M. J.; Marshak, M. P. Alkaline Quinone Flow Battery. *Science* **2015**, *349* (6255), 1529–1532. https://doi.org/10.1126/science.aab3033.

(36) Hu, B.; Luo, J.; Hu, M.; Yuan, B.; Liu, T. L. A PH-Neutral, Metal-Free Aqueous Organic Redox Flow Battery Employing an Ammonium Anthraquinone Anolyte. *Angewandte Chemie International Edition* **2019**, *58* (46), 16629–16636. https://doi.org/10.1002/anie.201907934.

(37) Ji, Y.; Goulet, M.-A.; Pollack, D. A.; Kwabi, D. G.; Jin, S.; Porcellinis, D. D.; Kerr, E. F.; Gordon, R. G.; Aziz, M. J. A Phosphonate-Functionalized Quinone Redox Flow Battery at Near-Neutral PH with Record Capacity Retention Rate. *Advanced Energy Materials* **2019**, *9* (12), 1900039. https://doi.org/10.1002/aenm.201900039.

(38) Tong, L.; Jing, Y.; Gordon, R. G.; Aziz, M. J. Symmetric All-Quinone Aqueous Battery. *ACS Appl. Energy Mater.* **2019**, *2* (6), 4016–4021. https://doi.org/10.1021/acsaem.9b00691.

(39) Huskinson, B.; Marshak, M. P.; Suh, C.; Er, S.; Gerhardt, M. R.; Galvin, C. J.; Chen, X.; Aspuru-Guzik, A.; Gordon, R. G.; Aziz, M. J. A Metal-Free Organic-Inorganic Aqueous Flow Battery. *Nature* **2014**, *505* (7482), 195–198. https://doi.org/10.1038/nature12909.

(40) Tong, L.; Goulet, M.-A.; Tabor, D. P.; Kerr, E. F.; De Porcellinis, D.; Fell, E. M.; Aspuru-Guzik, A.; Gordon, R. G.; Aziz, M. J. Molecular Engineering of an Alkaline Naphthoquinone Flow Battery. *ACS Energy Letters* **2019**, *4* (8), 1880–1887.

(41) Yang Zhengjin; Tong Liuchuan; Tabor Daniel P.; Beh Eugene S.; Goulet Marc-Antoni; Porcellinis Diana; Aspuru-Guzik Alán; Gordon Roy G.; Aziz Michael J. Alkaline Benzoquinone Aqueous Flow Battery for Large-Scale Storage of Electrical Energy. *Adv. Energy Mater.* **2018**, *8* (8), 1702056. https://doi.org/10.1002/aenm.201702056.

(42) Batchelor-McAuley, C.; Li, Q.; Dapin, S. M.; Compton, R. G. Voltammetric Characterization of DNA Intercalators across the Full PH Range: Anthraquinone-2,6-Disulfonate and Anthraquinone-2-Sulfonate. *J. Phys. Chem. B* **2010**, *114* (11), 4094–4100. https://doi.org/10.1021/jp1008187.

(43) Kwabi, D. G.; Lin, K.; Ji, Y.; Kerr, E. F.; Goulet, M.-A.; De Porcellinis, D.; Tabor, D. P.; Pollack, D. A.; Aspuru-Guzik, A.; Gordon, R. G.; Aziz, M. J. Alkaline Quinone Flow Battery with Long Lifetime at PH 12. *Joule* **2018**. https://doi.org/10.1016/j.joule.2018.07.005.

(44) Tabor, D. P.; Gómez-Bombarelli, R.; Tong, L.; Gordon, R. G.; Aziz, M. J.; Aspuru-Guzik, A. Theoretical and Experimental Investigation of the Stability Limits of Quinones in Aqueous Media: Implications for Organic Aqueous Redox Flow Batteries. *ChemRxiv: 10.26434/chemrxiv. 6990053. v2* **2018**.

(45) Goulet, M.-A.; Aziz, M. J. Flow Battery Molecular Reactant Stability Determined by Symmetric Cell Cycling Methods. *J. Electrochem. Soc.* **2018**, *165* (7), A1466–A1477. https://doi.org/10.1149/2.0891807jes.

(46) Drazevic, E.; Szabo, C.; Konya, D.; Lund, T.; Wedege, K.; Bentien, A. Investigation of Tetramorpholinohydroquinone as a Potential Catholyte in a Flow Battery. *ACS Appl. Energy Mater.* **2019**. https://doi.org/10.1021/acsaem.9b00351.

(47) Yang, B.; Hoober-Burkhardt, L.; Krishnamoorthy, S.; Murali, A.; Prakash, G. K. S.; Narayanan, S. R. High-Performance Aqueous Organic Flow Battery with Quinone-Based Redox Couples at Both Electrodes. *J. Electrochem. Soc.* **2016**, *163* (7), A1442–A1449. https://doi.org/10.1149/2.1371607jes.

(48) Hoober-Burkhardt, L.; Krishnamoorthy, S.; Yang, B.; Murali, A.; Nirmalchandar, A.; Prakash, G. K. S.; Narayanan, S. R. A New Michael-Reaction-Resistant Benzoquinone for Aqueous Organic Redox Flow Batteries. *J. Electrochem. Soc.* **2017**, *164* (4), A600–A607. https://doi.org/10.1149/2.0351704jes.

(49) Murali, A.; Nirmalchandar, A.; Krishnamoorthy, S.; Hoober-Burkhardt, L.; Yang, B.; Soloveichik, G.; Prakash, G. K. S.; Narayanan, S. R. Understanding and Mitigating Capacity Fade in Aqueous Organic Redox Flow Batteries. *J. Electrochem. Soc.* **2018**, *165* (7), A1193–A1203. https://doi.org/10.1149/2.0161807jes.

(50) Yang, B.; Hoober-Burkhardt, L.; Wang, F.; Prakash, G. K. S.; Narayanan, S. R. An Inexpensive Aqueous Flow Battery for Large-Scale Electrical Energy Storage Based on Water-Soluble Organic Redox Couples. *J. Electrochem. Soc.* **2014**, *161* (9), A1371–A1380. https://doi.org/10.1149/2.1001409jes.

(51) Kangro, D. W. A Method for Storing Electrical Energy. DE914264C, June 28, 1954.

(52) Kangro, W.; Pieper, H. Zur frage der speicherung von elektrischer energie in flüssigkeiten. *Electrochimica Acta* **1962**, *7* (4), 435–448. https://doi.org/10.1016/0013-4686(62)80032-2.

(53) Rahman, F.; Skyllas-Kazacos, M. Solubility of Vanadyl Sulfate in Concentrated Sulfuric Acid Solutions. *Journal of Power Sources* **1998**, *72* (2), 105–110. https://doi.org/10.1016/S0378-7753(97)02692-X.

(54) Rahman, F.; Skyllas-Kazacos, M. Vanadium Redox Battery: Positive Half-Cell Electrolyte Studies. *Journal of Power Sources* **2009**, *189* (2), 1212–1219. https://doi.org/10.1016/j.jpowsour.2008.12.113.

(55) Li, L.; Kim, S.; Wang, W.; Vijayakumar, M.; Nie, Z.; Chen, B.; Zhang, J.; Xia, G.; Hu, J.; Graff, G.; Liu, J.; Yang, Z. A Stable Vanadium Redox-Flow Battery with High Energy Density for Large-Scale Energy Storage. *Advanced Energy Materials* **2011**, *1* (3), 394–400. https://doi.org/10.1002/aenm.201100008.

(56) Agar, E.; Knehr, K. W.; Chen, D.; Hickner, M. A.; Kumbur, E. C. Species Transport Mechanisms Governing Capacity Loss in Vanadium Flow Batteries: Comparing Nafion® and Sulfonated Radel Membranes. *Electrochimica Acta* **2013**, *98*, 66–74. https://doi.org/10.1016/j.electacta.2013.03.030.

(57) Eifert, L.; Banerjee, R.; Jusys, Z.; Zeis, R. Characterization of Carbon Felt Electrodes for Vanadium Redox Flow Batteries: Impact of Treatment Methods. *J. Electrochem. Soc.* **2018**, *165* (11), A2577–A2586. https://doi.org/10.1149/2.0531811jes.

(58) Gong, K.; Fang, Q.; Gu, S.; Li, S. F. Y.; Yan, Y. Nonaqueous Redox-Flow Batteries: Organic Solvents, Supporting Electrolytes, and Redox Pairs. *Energy Environ. Sci.* **2015**, *8* (12), 3515–3530. https://doi.org/10.1039/C5EE02341F.

(59) Skyllas-Kazacos, M. Novel Vanadium Chloride/Polyhalide Redox Flow Battery. *Journal of Power Sources* **2003**, *124* (1), 299–302. https://doi.org/10.1016/S0378-7753(03)00621-9.

(60) Noack, J.; Roznyatovskaya, N.; Herr, T.; Fischer, P. The Chemistry of Redox-Flow Batteries. *Angew. Chem. Int. Ed.* **2015**, *54* (34), 9776–9809. https://doi.org/10.1002/anie.201410823.

(61) Dunn, B.; Kamath, H.; Tarascon, J.-M. Electrical Energy Storage for the Grid: A Battery of Choices. *Science* **2011**, *334* (6058), 928–935. https://doi.org/10.1126/science.1212741.

(62) Arenas, L. F.; Loh, A.; Trudgeon, D. P.; Li, X.; Ponce de León, C.; Walsh, F. C. The Characteristics and Performance of Hybrid Redox Flow Batteries with Zinc Negative Electrodes for Energy Storage. *Renewable and Sustainable Energy Reviews* **2018**, *90*, 992–1016. https://doi.org/10.1016/j.rser.2018.03.016.

(63) Ulaganathan, M.; Suresh, S.; Mariyappan, K.; Periasamy, P.; Pitchai, R. New Zinc–Vanadium (Zn–V) Hybrid Redox Flow Battery: High-Voltage and Energy-Efficient Advanced Energy Storage System. *ACS Sustainable Chem. Eng.* **2019**, *7* (6), 6053–6060. https://doi.org/10.1021/acssuschemeng.8b06194.

(64) Bard, A. J.; Parsons, R.; Jordan, J. *Standard Potentials in Aqueous Solution*; CRC Press, 1985.

(65) Zhang, J.; Jiang, G.; Xu, P.; Kashkooli, A. G.; Mousavi, M.; Yu, A.; Chen, Z. An All-Aqueous Redox Flow Battery with Unprecedented Energy Density. *Energy Environ. Sci.* **2018**, *11* (8), 2010–2015. https://doi.org/10.1039/C8EE00686E.

(66) Xie, C.; Liu, Y.; Lu, W.; Zhang, H.; Li, X. Highly Stable Zinc–Iodine Single Flow Batteries with Super High Energy Density for Stationary Energy Storage. *Energy Environ. Sci.* **2019**, *12* (6), 1834–1839. https://doi.org/10.1039/C8EE02825G.

(67) Yeo, R. S.; Chin, D.-T. A Hydrogen-Bromine Cell for Energy Storage Applications. *J. Electrochem. Soc.* **1980**, *127* (3), 549. https://doi.org/10.1149/1.2129710.

(68) Gileadi, E.; Srinivasan, S.; Salzano, F. J.; Braun, C.; Beaufrere, A.; Gottesfeld, S.; Nuttall, L. J.; Laconti, A. B. An Electrochemically Regenerative Hydrogen—Chlorine Energy Storage System for Electric Utilities. *Journal of Power Sources* **1977**, *2* (2), 191–200. https://doi.org/10.1016/0378-7753(77)80019-0.

(69) Thomassen, M.; Sandnes, E.; Børresen, B.; Tunold, R. Evaluation of Concepts for Hydrogen – Chlorine Fuel Cells. *J Appl Electrochem* **2006**, *36* (7), 813–819. https://doi.org/10.1007/s10800-006-9140-0.

(70) Kosek, J. A.; Laconti, A. B. Advanced Hydrogen Electrode for a Hydrogen-Bromine Battery. *Journal of Power Sources* **1988**, *22* (3), 293–300. https://doi.org/10.1016/0378-7753(88)80024-7.

(71) Goor-Dar, M.; Travitsky, N.; Peled, E. Study of Hydrogen Redox Reactions on Platinum Nanoparticles in Concentrated HBr Solutions. *Journal of Power Sources* **2012**, *197*, 111–115. https://doi.org/10.1016/j.jpowsour.2011.09.044.

(72) Ferro, S.; Battisti, A. D. The Bromine Electrode. Part I: Adsorption Phenomena at Polycrystalline Platinum Electrodes. *Journal of Applied Electrochemistry* **2004**, *34* (10), 981–987. https://doi.org/10.1023/B:JACH.0000042666.25746.e6.

(73) Duduta, M.; Ho, B.; Wood, V. C.; Limthongkul, P.; Brunini, V. E.; Carter, W. C.; Chiang, Y.-M. Semi-Solid Lithium Rechargeable Flow Battery. *Advanced Energy Materials* **2011**, *1* (4), 511–516. https://doi.org/10.1002/aenm.201100152.

(74) Qi, Z.; Koenig, G. M. Review Article: Flow Battery Systems with Solid Electroactive Materials. *Journal of Vacuum Science & Technology B* **2017**, *35* (4), 040801. https://doi.org/10.1116/1.4983210.

(75) Soloveichik, G. L. Flow Batteries: Current Status and Trends. *Chem. Rev.* **2015**, *115* (20), 11533–11558. https://doi.org/10.1021/cr500720t.

(76) Chakrabarti, M. H.; Brandon, N. P.; Hajimolana, S. A.; Tariq, F.; Yufit, V.; Hashim, M. A.; Hussain, M. A.; Low, C. T. J.; Aravind, P. V. Application of Carbon Materials in Redox Flow Batteries. *Journal of Power Sources* **2014**, *253*, 150–166. https://doi.org/10.1016/j.jpowsour.2013.12.038.

(77) Merle, G.; Wessling, M.; Nijmeijer, K. Anion Exchange Membranes for Alkaline Fuel Cells: A Review. *Journal of Membrane Science* **2011**, *377* (1–2), 1–35. https://doi.org/10.1016/j.memsci.2011.04.043.

(78) Chen, H.; Cong, G.; Lu, Y.-C. Recent Progress in Organic Redox Flow Batteries: Active Materials, Electrolytes and Membranes. *Journal of Energy Chemistry* **2018**. https://doi.org/10.1016/j.jechem.2018.02.009.

(79) Ke, X.; Prahl, J. M.; Alexander, J. I. D.; Wainright, J. S.; Zawodzinski, T. A.; Savinell, R. F. Rechargeable Redox Flow Batteries: Flow Fields, Stacks and Design Considerations. *Chem. Soc. Rev.* **2018**, *47* (23), 8721–8743. https://doi.org/10.1039/C8CS00072G.

(80) Parasuraman, A.; Lim, T. M.; Menictas, C.; Skyllas-Kazacos, M. Review of Material Research and Development for Vanadium Redox Flow Battery Applications. *Electrochimica Acta* **2013**, *101*, 27–40. https://doi.org/10.1016/j.electacta.2012.09.067.

(81) Ke, X.; Alexander, J. I. D.; Prahl, J. M.; Savinell, R. F. Flow Distribution and Maximum Current Density Studies in Redox Flow Batteries with a Single Passage of the Serpentine Flow Channel. *Journal of Power Sources* **2014**, *270*, 646–657. https://doi.org/10.1016/j.jpowsour.2014.07.155.

(82) Bard, A. J.; Faulkner, L. R. *Electrochemical Methods: Fundamentals and Applications*; Wiley: New York, 2000.

(83) Milshtein, J. D.; Tenny, K. M.; Barton, J. L.; Drake, J.; Darling, R. M.; Brushett, F. R. Quantifying Mass Transfer Rates in Redox Flow Batteries. *J. Electrochem. Soc.* **2017**, *164* (11), E3265. https://doi.org/10.1149/2.0201711jes.

(84) Pletcher, D.; Wills, R. A Novel Flow Battery: A Lead Acid Battery Based on an Electrolyte with Soluble Lead(II). *Phys. Chem. Chem. Phys.* **2004**, *6* (8), 1779–1785. https://doi.org/10.1039/B401116C.

(85) Dullien, F. A. L. *Porous Media: Fluid Transport and Pore Structure*; Academic Press, 2012.

(86) Carta, R.; Palmas, S.; Polcaro, A. M.; Tola, G. Behaviour of a Carbon Felt Flow by Electrodes Part I: Mass Transfer Characteristics. *J Appl Electrochem* **1991**, *21* (9), 793–798. https://doi.org/10.1007/BF01402816.

(87) Bamford, C. H.; Tipper†, C. F. H.; Compton, R. G. *Electrode Kinetics: Principles and Methodology*; Elsevier, 1986.

(88) Torres, L. M.; Gil, A. F.; Galicia, L.; González, I. Understanding the Difference between Inner- and Outer-Sphere Mechanisms: An Electrochemical Experiment. *J. Chem. Educ.* **1996**, *73* (8), 808. https://doi.org/10.1021/ed073p808.

(89) Bard, A. J. Inner-Sphere Heterogeneous Electrode Reactions. Electrocatalysis and Photocatalysis: The Challenge. *J. Am. Chem. Soc.* **2010**, *132* (22), 7559–7567. https://doi.org/10.1021/ja101578m.

(90) Pratt, H. D.; Hudak, N. S.; Fang, X.; Anderson, T. M. A Polyoxometalate Flow Battery. *Journal of Power Sources* **2013**, *236*, 259–264. https://doi.org/10.1016/j.jpowsour.2013.02.056.

(91) Bourke, A.; Miller, M. A.; Lynch, R. P.; Wainright, J. S.; Savinell, R. F.; Buckley, D. N. Effect of Cathodic and Anodic Treatments of Carbon on the Electrode Kinetics of VIV/VV Oxidation-Reduction. *J. Electrochem. Soc.* **2015**, *162* (8), A1547–A1555. https://doi.org/10.1149/2.0671508jes.

(92) Sum, E.; Skyllas-Kazacos, M. A Study of the V(II)/V(III) Redox Couple for Redox Flow Cell Applications. *Journal of Power Sources* **1985**, *15* (2), 179–190. https://doi.org/10.1016/0378-7753(85)80071-9.

(93) Sun, B.; Skyllas-Kazacos, M. Chemical Modification of Graphite Electrode Materials for Vanadium Redox Flow Battery Application—Part II. Acid Treatments. *Electrochimica Acta* **1992**, *37* (13), 2459–2465. https://doi.org/10.1016/0013-4686(92)87084-D.

(94) Shao, Y.; Wang, X.; Engelhard, M.; Wang, C.; Dai, S.; Liu, J.; Yang, Z.; Lin, Y. Nitrogen-Doped Mesoporous Carbon for Energy Storage in Vanadium Redox Flow Batteries. *Journal of Power Sources* **2010**, *195* (13), 4375–4379. https://doi.org/10.1016/j.jpowsour.2010.01.015.

(95) Lu, Y.; Goodenough, J. B.; Kim, Y. Aqueous Cathode for Next-Generation Alkali-Ion Batteries. *J. Am. Chem. Soc.* **2011**, *133* (15), 5756–5759. https://doi.org/10.1021/ja201118f.

(96) Doris, S. E.; Ward, A. L.; Baskin, A.; Frischmann, P. D.; Gavvalapalli, N.; Chénard, E.; Sevov, C. S.; Prendergast, D.; Moore, J. S.; Helms, B. A. Macromolecular Design Strategies for Preventing Active-Material Crossover in Non-Aqueous All-Organic Redox-Flow Batteries. *Angewandte Chemie International Edition* **2017**, *56* (6), 1595–1599. https://doi.org/10.1002/anie.201610582.

(97) Hendriks, K. H.; Robinson, S. G.; Braten, M. N.; Sevov, C. S.; Helms, B. A.; Sigman, M. S.; Minteer, S. D.; Sanford, M. S. High-Performance Oligomeric Catholytes for Effective Macromolecular Separation in Nonaqueous Redox Flow Batteries. *ACS Cent Sci* **2018**, *4* (2), 189–196. https://doi.org/10.1021/acscentsci.7b00544.

(98) Zhang, H.; Zhang, H.; Li, X.; Mai, Z.; Zhang, J. Nanofiltration (NF) Membranes: The next Generation Separators for All Vanadium Redox Flow Batteries (VRBs)? *Energy Environ. Sci.* **2011**, *4* (5), 1676–1679. https://doi.org/10.1039/C1EE01117K.

(99) Xu, W.; Li, X.; Cao, J.; Yuan, Z.; Zhang, H. Morphology and Performance of Poly(Ether Sulfone)/Sulfonated Poly(Ether Ether Ketone) Blend Porous Membranes for Vanadium Flow Battery Application. *RSC Adv.* **2014**, *4* (76), 40400–40406. https://doi.org/10.1039/C4RA05083E.

(100) Wei, W.; Zhang, H.; Li, X.; Zhang, H.; Li, Y.; Vankelecom, I. Hydrophobic Asymmetric Ultrafiltration PVDF Membranes: An Alternative Separator for VFB with Excellent Stability. *Phys. Chem. Chem. Phys.* **2013**, *15* (6), 1766–1771. https://doi.org/10.1039/C2CP43761A.

(101) Janoschka, T.; Martin, N.; Martin, U.; Friebe, C.; Morgenstern, S.; Hiller, H.; Hager, M. D.; Schubert, U. S. An Aqueous, Polymer-Based Redox-Flow Battery Using Non-Corrosive, Safe, and Low-Cost Materials. *Nature* **2015**, *527* (7576), 78–81. https://doi.org/10.1038/nature15746.

(102) Zhao, Q.; Zhu, Z.; Chen, J. Molecular Engineering with Organic Carbonyl Electrode Materials for Advanced Stationary and Redox Flow Rechargeable Batteries. *Adv. Mater.* **2017**, *29* (48), 1607007. https://doi.org/10.1002/adma.201607007.

(103) Burgess, M.; Chénard, E.; Hernández-Burgos, K.; Nagarjuna, G.; Assary, R. S.; Hui, J.; Moore, J. S.; Rodríguez-López, J. Impact of Backbone Tether Length and Structure on the Electrochemical Performance of Viologen Redox Active Polymers. *Chem. Mater.* **2016**, *28* (20), 7362–7374. https://doi.org/10.1021/acs.chemmater.6b02825.

(104) Li, X.; Zhang, H.; Mai, Z.; Zhang, H.; Vankelecom, I. Ion Exchange Membranes for Vanadium Redox Flow Battery (VRB) Applications. *Energy Environ. Sci.* **2011**, *4* (4), 1147–1160. https://doi.org/10.1039/C0EE00770F.

(105) Mauritz, K. A.; Moore, R. B. State of Understanding of Nafion. *Chem. Rev.* **2004**, *104* (10), 4535–4586. https://doi.org/10.1021/cr0207123.

(106) Schmidt-Rohr, K.; Chen, Q. Parallel Cylindrical Water Nanochannels in Nafion Fuel-Cell Membranes. *Nat Mater* **2008**, *7* (1), 75–83. https://doi.org/10.1038/nmat2074.

(107) Wiley, D.; Fimbres Weihs, G. Electroosmotic Drag in Membranes. In *Encyclopedia of Membranes*; Drioli, E., Giorno, L., Eds.; Springer: Berlin, Heidelberg, 2016; pp 653–654. https://doi.org/10.1007/978-3-662-44324-8_2078.

(108) Sauter, F. Thermodynamics of Irreversible Processes, von S. R. de Groot. North-Holland Publishing Comp., Amsterdam 1951. 242 S., F. 17.50. *Angewandte Chemie* **1951**, *63* (23–24), 582–583. https://doi.org/10.1002/ange.19510632318.

(109) Ren, X.; Gottesfeld, S. Electro-Osmotic Drag of Water in Poly(Perfluorosulfonic Acid) Membranes. *J. Electrochem. Soc.* **2001**, *148* (1), A87–A93. https://doi.org/10.1149/1.1344521.

(110) Xi, J.; Wu, Z.; Qiu, X.; Chen, L. Nafion/SiO2 Hybrid Membrane for Vanadium Redox Flow Battery. *Journal of Power Sources* **2007**, *166* (2), 531–536. https://doi.org/10.1016/j.jpowsour.2007.01.069.

(111) Teng, X.; Zhao, Y.; Xi, J.; Wu, Z.; Qiu, X.; Chen, L. Nafion/Organic Silica Modified TiO2 Composite Membrane for Vanadium Redox Flow Battery via in Situ Sol–Gel Reactions. *Journal of Membrane Science* **2009**, *341* (1), 149–154. https://doi.org/10.1016/j.memsci.2009.05.051.

(112) Sang, S.; Wu, Q.; Huang, K. Preparation of Zirconium Phosphate (ZrP)/Nafion1135 Composite Membrane and H+/VO2+ Transfer Property Investigation. *Journal of Membrane Science* **2007**, *305* (1), 118–124. https://doi.org/10.1016/j.memsci.2007.07.041.

(113) Chakrabarti, M. H.; Dryfe, R. A. W.; Roberts, E. P. L. Evaluation of Electrolytes for Redox Flow Battery Applications. *Electrochimica Acta* **2007**, *52* (5), 2189–2195. https://doi.org/10.1016/j.electacta.2006.08.052.

(114) Liu, Q.; Sleightholme, A. E. S.; Shinkle, A. A.; Li, Y.; Thompson, L. T. Non-Aqueous Vanadium Acetylacetonate Electrolyte for Redox Flow Batteries. *Electrochemistry Communications* **2009**, *11* (12), 2312–2315. https://doi.org/10.1016/j.elecom.2009.10.006.

(115) Kim, H.; Yoon, T.; Jang, J.; Mun, J.; Park, H.; Ryu, J. H.; Oh, S. M. A Tetradentate Ni(II) Complex Cation as a Single Redox Couple for Non-Aqueous Flow Batteries. *Journal of Power Sources* **2015**, *283*, 300–304. https://doi.org/10.1016/j.jpowsour.2015.02.083.

(116) Cabrera, P. J.; Yang, X.; Suttil, J. A.; Hawthorne, K. L.; Brooner, R. E. M.; Sanford, M. S.; Thompson, L. T. Complexes Containing Redox Noninnocent Ligands for Symmetric, Multielectron Transfer Nonaqueous Redox Flow Batteries. *J. Phys. Chem. C* **2015**, *119* (28), 15882–15889. https://doi.org/10.1021/acs.jpcc.5b03582.

(117) Duan, W.; Vemuri, R. S.; Milshtein, J. D.; Laramie, S.; Dmello, R. D.; Huang, J.; Zhang, L.; Hu, D.; Vijayakumar, M.; Wang, W.; Liu, J.; Darling, R. M.; Thompson, L.; Smith, K.; Moore, J. S.; Brushett, F. R.; Wei, X. A Symmetric Organic-Based Nonaqueous Redox Flow Battery and Its State of Charge Diagnostics by FTIR. *J. Mater. Chem. A* **2016**, *4* (15), 5448–5456. https://doi.org/10.1039/C6TA01177B.

(118) Hagemann, T.; Winsberg, J.; Häupler, B.; Janoschka, T.; Gruber, J. J.; Wild, A.; Schubert, U. S. A Bipolar Nitronyl Nitroxide Small Molecule for an All-Organic Symmetric Redox-Flow Battery. *NPG Asia Materials* **2017**, *9* (1), e340–e340. https://doi.org/10.1038/am.2016.195.

(119) Winsberg, J.; Stolze, C.; Muench, S.; Liedl, F.; Hager, M. D.; Schubert, U. S. TEMPO/Phenazine Combi-Molecule: A Redox-Active Material for Symmetric Aqueous Redox-Flow Batteries. *ACS Energy Lett.* **2016**, *1* (5), 976–980. https://doi.org/10.1021/acsenergylett.6b00413.

(120) Zuman, P. *Substituent Effects in Organic Polarography*; Springer US, 1967. https://doi.org/10.1007/978-1-4684-8661-2.

(121) Fornari, R. P.; Mesta, M.; Hjelm, J.; Vegge, T.; de Silva, P. Molecular Engineering Strategies for Symmetric Aqueous Organic Redox Flow Batteries. *ACS Materials Lett.* **2020**, *2* (3), 239–246. https://doi.org/10.1021/acsmaterialslett.0c00028.

(122) Chen, R. Toward High-Voltage, Energy-Dense, and Durable Aqueous Organic Redox Flow Batteries: Role of the Supporting Electrolytes. *ChemElectroChem* **2019**, *6* (3), 603–612. https://doi.org/10.1002/celc.201801505.

(123) Chakrabarti, M. H.; Mjalli, F. S.; AlNashef, I. M.; Hashim, Mohd. A.; Hussain, Mohd. A.; Bahadori, L.; Low, C. T. J. Prospects of Applying Ionic Liquids and Deep Eutectic Solvents for Renewable Energy Storage by Means of Redox Flow Batteries. *Renewable and Sustainable Energy Reviews* **2014**, *30*, 254–270. https://doi.org/10.1016/j.rser.2013.10.004.

(124) Pratt, H. D.; Leonard, J. C.; Steele, L. A. M.; Staiger, C. L.; Anderson, T. M. Copper Ionic Liquids: Examining the Role of the Anion in Determining Physical and Electrochemical Properties. *Inorganica Chimica Acta* **2013**, *396*, 78–83. https://doi.org/10.1016/j.ica.2012.10.005.

(125) Berman, M. Advances in Materials for Ionic Liquid Flow Batteries https://www.osti.gov/servlets/purl/1364828 (accessed Jan 20, 2020).

(126) Zhang, Y.; Ye, R.; Henkensmeier, D.; Hempelmann, R.; Chen, R. "Water-in-Ionic Liquid" Solutions towards Wide Electrochemical Stability Windows for Aqueous Rechargeable Batteries. *Electrochimica Acta* **2018**, *263*, 47–52. https://doi.org/10.1016/j.electacta.2018.01.050.

(127) Chen, R.; Hempelmann, R. Ionic Liquid-Mediated Aqueous Redox Flow Batteries for High Voltage Applications. *Electrochemistry Communications* **2016**, *70*, 56–59. https://doi.org/10.1016/j.elecom.2016.07.003.

(128) Ejigu, A.; Greatorex-Davies, P. A.; Walsh, D. A. Room Temperature Ionic Liquid Electrolytes for Redox Flow Batteries. *Electrochemistry Communications* **2015**, *54*, 55–59. https://doi.org/10.1016/j.elecom.2015.01.016.

(129) Mamantov, G. A Brief Introduction to Electrochemistry in Molten Salts and Chloroaluminate Melts. In *Molten Salt Chemistry: An Introduction and Selected Applications*; Mamantov, G., Marassi, R., Eds.; NATO ASI Series; Springer Netherlands: Dordrecht, 1987; pp 259–270. https://doi.org/10.1007/978-94-009-3863-2_12.

(130) Chen, R.; Bresser, D.; Saraf, M.; Gerlach, P.; Balducci, A.; Kunz, S.; Schröder, D.; Passerini, S.; Chen, J. A Comparative Review of Electrolytes for Organic Material-Based Energy Storage Devices Employing Solid Electrodes and Redox Fluids. *ChemSusChem n/a* (n/a). https://doi.org/10.1002/cssc.201903382.

(131) Zoski, C. G. *Handbook of Electrochemistry*; Elsevier Science & Technology: Amsterdam ; Boston, 2007.

(132) Denison, J. T.; Ramsey, J. B. The Free Energy, Enthalpy and Entropy of Dissociation of Some Perchlorates in Ethylene Chloride and Ethylidene Chloride. *J. Am. Chem. Soc.* **1955**, *77* (9), 2615–2621. https://doi.org/10.1021/ja01614a085.

(133) Izutsu, K. *Electrochemistry in Nonaqueous Solutions*; John Wiley & Sons, 2009.

(134) Shin, S.-H.; Yun, S.-H.; Moon, S.-H. A Review of Current Developments in Non-Aqueous Redox Flow Batteries: Characterization of Their Membranes for Design Perspective. *RSC Adv.* **2013**, *3* (24), 9095–9116. https://doi.org/10.1039/C3RA00115F.

(135) Zhang, H.; Li, X.; Zhang, J. *Redox Flow Batteries: Fundamentals and Applications*; CRC Press, 2017.

(136) Zhang, D.; Lan, H.; Li, Y. The Application of a Non-Aqueous Bis(Acetylacetone)Ethylenediamine Cobalt Electrolyte in Redox Flow Battery. *Journal of Power Sources* **2012**, *217*, 199–203. https://doi.org/10.1016/j.jpowsour.2012.06.038.

(137) Wei, X.; Xu, W.; Huang, J.; Zhang, L.; Walter, E.; Lawrence, C.; Vijayakumar, M.; Henderson, W. A.; Liu, T.; Cosimbescu, L.; Li, B.; Sprenkle, V.; Wang, W. Radical Compatibility with Nonaqueous Electrolytes and Its Impact on an All-Organic Redox Flow Battery. *Angew. Chem. Int. Ed.* **2015**, *54* (30), 8684–8687. https://doi.org/10.1002/anie.201501443.

(138) Metzger, J. O. Lösungsmittelfreie organische Synthesen. *Angewandte Chemie* **1998**, *110* (21), 3145–3148. https://doi.org/10.1002/(SICI)1521-3757(19981102)110:21<3145::AID-ANGE3145>3.0.CO;2-U.

(139) Henschler, D. Occupational Toxicants. Critical Data Evaluation for MAK Values and Classification of Carcinogens. Volume 1. *VCH, NEW YORK, NY(USA). 1991.* **1991**.

(140) McNaught, A. D.; Wilkinson, A. *Compendium of Chemical Terminology: Iupac Recommendations: Gold Book*, Subsequent.; IUPAC International Union of Pure and Applied Chem: Oxford England ; Malden, MA, USA, 1997.

(141) Long, J.; Xu, Y.; Wang, T.; Yuan, Z.; Shu, R.; Zhang, Q.; Ma, L. Efficient Base-Catalyzed Decomposition and in Situ Hydrogenolysis Process for Lignin Depolymerization and Char Elimination. *Applied Energy* **2015**, *141*, 70–79. https://doi.org/10.1016/j.apenergy.2014.12.025.

(142) Bryan, C. C. Manufacture of Vanillin from Lignin. US2692291A, October 19, 1954.

(143) Bjørsvik, H.-R.; Minisci, F. Fine Chemicals from Lignosulfonates. 1. Synthesis of Vanillin by Oxidation of Lignosulfonates. *Org. Process Res. Dev.* **1999**, *3* (5), 330–340. https://doi.org/10.1021/op9900028.

(144) Schmitt, D.; Regenbrecht, C.; Hartmer, M.; Stecker, F.; Waldvogel, S. R. Highly Selective Generation of Vanillin by Anodic Degradation of Lignin: A Combined Approach of Electrochemistry and Product Isolation by Adsorption. *Beilstein J. Org. Chem.* **2015**, *11* (1), 473–480. https://doi.org/10.3762/bjoc.11.53.

(145) Zirbes, M.; Schmitt, D.; Beiser, N.; Pitton, D.; Hoffmann, T.; Waldvogel, S. R. Anodic Degradation of Lignin at Active Transition Metal-Based Alloys and Performance-Enhanced Anodes. *ChemElectroChem* **2019**, *6* (1), 155–161. https://doi.org/10.1002/celc.201801218.

(146) Li, Y.; Liu, W.; Wu, M.; Yi, Z.; Zhang, J. Oxidation of 2,3,5-Trimethylphenol to 2,3,5-Trimethylbenzoquinone with Aqueous Hydrogen Peroxide in the Presence of Spinel CuCo2O4. *Journal of Molecular Catalysis A: Chemical* **2007**, *261* (1), 73–78. https://doi.org/10.1016/j.molcata.2006.07.067.

(147) Wróblewska, A. Water as the Solvent for the Process of Phenol Hydroxylation over the Ti-MWW Catalyst. *Reac Kinet Mech Cat* **2013**, *108* (2), 491–505. https://doi.org/10.1007/s11144-012-0517-2.

(148) Parker, V. D. The Hydroquinone–Quinone Redox Behaviour in Acetonitrile. *J. Chem. Soc. D* **1969**, *0* (13), 716–717. https://doi.org/10.1039/C29690000716.

(149) Patai, S. *The Chemistry of the Quinonoid Compounds*; Wiley: London, 1974.

(150) Sartori, G.; Maggi, R. *Advances in Friedel-Crafts Acylation Reactions: Catalytic and Green Processes*; CRC Press, 2009.

(151) Pan, F.; Wang, Q. Redox Species of Redox Flow Batteries: A Review. *Molecules* **2015**, *20* (11), 20499–20517. https://doi.org/10.3390/molecules201119711.

(152) Son, E. J.; Kim, J. H.; Kim, K.; Park, C. B. Quinone and Its Derivatives for Energy Harvesting and Storage Materials. *J. Mater. Chem. A* **2016**, *4* (29), 11179–11202. https://doi.org/10.1039/C6TA03123D.

(153) Kim, R. S.; Chung, T. D. The Electrochemical Reaction Mechanism and Applications of Quinones. *Bull. Korean Chem. Soc.* **2014**, *35* (11), 3143–3155. https://doi.org/10.5012/bkcs.2014.35.11.3143.

(154) Gómez, M.; González, F. J.; González, I. Intra and Intermolecular Hydrogen Bonding Effects in the Electrochemical Reduction of α-Phenolic-Naphthoquinones. *Journal of Electroanalytical Chemistry* **2005**, *578* (2), 193–202. https://doi.org/10.1016/j.jelechem.2004.12.036.

(155) Eggins, B. R.; Chambers, J. Q. Proton Effects in the Electrochemistry of the Quinone Hydroquinone System in Aprotic Solvents. *J. Electrochem. Soc.* **1970**, *117* (2), 186–192. https://doi.org/10.1149/1.2407462.

(156) Quan, M.; Sanchez, D.; Wasylkiw, M. F.; Smith, D. K. Voltammetry of Quinones in Unbuffered Aqueous Solution: Reassessing the Roles of Proton Transfer and Hydrogen Bonding in the Aqueous Electrochemistry of Quinones. *J. Am. Chem. Soc.* **2007**, *129* (42), 12847–12856. https://doi.org/10.1021/ja0743083.

(157) Gupta, N.; Linschitz, H. Hydrogen-Bonding and Protonation Effects in Electrochemistry of Quinones in Aprotic Solvents. *J. Am. Chem. Soc.* **1997**, *119* (27), 6384–6391. https://doi.org/10.1021/ja970028j.

(158) Ashnagar, A.; Bruce, J. M.; Dutton, P. L.; Prince, R. C. One- and Two-Electron Reduction of Hydroxy-1,4-Naphthoquinones and Hydroxy-9,10-Anthraquinones. The Role of Internal Hydrogen Bonding and Its Bearing on the Redox Chemistry of the Anthracycline Antitumour Quinones. *Biochim. Biophys. Acta* **1984**, *801* (3), 351–359. https://doi.org/10.1016/0304-4165(84)90138-7.

(159) Aguilar-Martínez, M.; Macías-Ruvalcaba, N. A.; Bautista-Martínez, J. A.; Gómez, M.; González, F. J.; González, I. Review: Hydrogen Bond and Protonation as Modifying Factors of the Quinone Reactivity. *Current Organic Chemistry* **2004**, *8* (17), 1721–1738. https://doi.org/10.2174/1385272043369548.

(160) Wilford, J. H.; Archer, M. D. Solvent Effects on the Redox Potentials of Benzoquinone. *Journal of Electroanalytical Chemistry and Interfacial Electrochemistry* **1985**, *190* (1), 271–277. https://doi.org/10.1016/0022-0728(85)80094-2.

(161) Hayano, S.; Fujihira, M. The Effect of Water on the Reduction Potentials of Some Aromatic Compounds in the DMF-Water System. *BCSJ* **1971**, *44* (8), 2051–2055. https://doi.org/10.1246/bcsj.44.2051.

(162) Jeffrey, G. A. *An Introduction to Hydrogen Bonding*; Oxford University Press, 1997.

(163) Del Bene, J. E. Ab Initio Molecular Orbital Study of the Structures and Energies of Neutral and Charged Bimolecular Complexes of Water with the Hydrides AHn (A= Nitrogen, Oxygen, Fluorine, Phosphorus, Sulfur, and Chlorine). *The Journal of Physical Chemistry* **1988**, *92* (10), 2874–2880.

(164) Furman, N. H.; Stone, K. A Polarographic Study of Certain Anthraquinones1. *Journal of the American Chemical Society* **1948**, *70* (9), 3055–3061.

(165) Li, Q.; Batchelor-McAuley, C.; Lawrence, N. S.; Hartshorne, R. S.; Compton, R. G. Electrolyte Tuning of Electrode Potentials: The One Electron vs. Two Electron Reduction of Anthraquinone-2-Sulfonate in Aqueous Media. *Chem. Commun.* **2011**, *47* (41), 11426–11428. https://doi.org/10.1039/C1CC14191K.

(166) Kim, Y.-R.; Kim, R. S.; Kang, S. K.; Choi, M. G.; Kim, H. Y.; Cho, D.; Lee, J. Y.; Chang, S.-K.; Chung, T. D. Modulation of Quinone PCET Reaction by Ca2+ Ion Captured by Calix[4]Quinone in Water. *J. Am. Chem. Soc.* **2013**, *135* (50), 18957–18967. https://doi.org/10.1021/ja410406e.

(167) Hofmann, J. D.; Pfanschilling, F. L.; Krawczyk, N.; Geigle, P.; Hong, L.; Schmalisch, S.; Wegner, H. A.; Mollenhauer, D.; Janek, J.; Schröder, D. Quest for Organic Active Materials for Redox Flow Batteries: 2,3-Diaza-Anthraquinones and Their Electrochemical Properties. *Chem. Mater.* **2018**, *30* (3), 762–774. https://doi.org/10.1021/acs.chemmater.7b04220.

(168) Guin, P. S.; Das, S.; Mandal, P. Electrochemical Reduction of Sodium 1, 4-Dihydroxy-9, 10-Anthraquinone-2-Sulphonate in Aqueous and Aqueous Dimethyl Formamide Mixed Solvent: A Cyclic Voltammetric Study. *Int. J. Electrochem. Sci* **2008**, *3* (9), 1016–1028.

(169) Song, N.; Gagliardi, C. J.; Binstead, R. A.; Zhang, M.-T.; Thorp, H.; Meyer, T. J. Role of Proton-Coupled Electron Transfer in the Redox Interconversion between Benzoquinone and Hydroquinone. *J. Am. Chem. Soc.* **2012**, *134* (45), 18538–18541. https://doi.org/10.1021/ja308700t.

(170) Eigen, M. Kinetics of Proton Transfer Processes. *Discuss. Faraday Soc.* **1965**, *39* (0), 7–15. https://doi.org/10.1039/DF9653900007.

(171) Laviron, E. Electrochemical Reactions with Protonations at Equilibrium: Part X. The Kinetics of the p-Benzoquinone/Hydroquinone Couple on a Platinum Electrode. *Journal of Electroanalytical Chemistry and Interfacial Electrochemistry* **1984**, *164* (2), 213–227. https://doi.org/10.1016/S0022-0728(84)80207-7.

(172) Costentin, C. Electrochemical Approach to the Mechanistic Study of Proton-Coupled Electron Transfer. *Chem. Rev.* **2008**, *108* (7), 2145–2179. https://doi.org/10.1021/cr068065t.

(173) Vetter, K. J. Überspannung und Kinetik der Chinhydronelektrode. *Zeitschrift für Elektrochemie, Berichte der Bunsengesellschaft für physikalische Chemie* **1952**, *56* (8), 797–806. https://doi.org/10.1002/bbpc.19520560823.

(174) Evans, D. H. One-Electron and Two-Electron Transfers in Electrochemistry and Homogeneous Solution Reactions. *Chem. Rev.* **2008**, *108* (7), 2113–2144. https://doi.org/10.1021/cr068066l.

(175) Roginsky, V. A.; Pisarenko, L. M.; Bors, W.; Michel, C. The Kinetics and Thermodynamics of Quinone–Semiquinone–Hydroquinone Systems under Physiological Conditions. *J. Chem. Soc., Perkin Trans. 2* **1999**, No. 4, 871–876. https://doi.org/10.1039/A807650B.

(176) Alegría, A. E.; López, M.; Guevara, N. Thermodynamics of Semiquinone Disproportionation in Aqueous Buffer. *J. Chem. Soc., Faraday Trans.* **1996**, *92* (24), 4965–4968. https://doi.org/10.1039/FT9969204965.

(177) Bishop, C. A.; Tong, L. K. J. Equilibria of Substituted Semiquinones at High PH. *J. Am. Chem. Soc.* **1965**, *87* (3), 501–505. https://doi.org/10.1021/ja01081a018.

(178) Compton, R. G.; Banks, C. E. *Understanding Voltammetry*; World Scientific Publishing Company, 2010.

(179) Bailey, S. I.; Ritchie, I. M.; Hewgill, F. R. The Construction and Use of Potential–PH Diagrams in Organic Oxidation–Reduction Reactions. *J. Chem. Soc., Perkin Trans. 2* **1983**, No. 5, 645–652. https://doi.org/10.1039/P29830000645.

(180) Wang, W.; Luo, Q.; Li, B.; Wei, X.; Li, L.; Yang, Z. Recent Progress in Redox Flow Battery Research and Development. *Adv. Funct. Mater.* **2013**, *23* (8), 970–986. https://doi.org/10.1002/adfm.201200694.

(181) Maccoll, A. Reduction Potentials of Conjugated Systems. *Nature* **1949**, *163* (4135), 178–179. https://doi.org/10.1038/163178a0.

(182) Peover, M. E. Electron Affinities of Quinones : Correlation of One-Electron Redox Potentials with Quantum-Mechanical Calculation. *Nature* **1962**, *193* (4814), 475–476. https://doi.org/10.1038/193475a0.

(183) Chambers, J. Q. Electrochemistry of Quinones. In *Quinonoid Compounds (1974)*; John Wiley & Sons, Ltd, 2010; pp 737–791. https://doi.org/10.1002/9780470771303.ch3.

(184) Peover, M. E. A Polarographic Investigation into the Redox Behaviour of Quinones: The Roles of Electron Affinity and Solvent. *J. Chem. Soc.* **1962**, *0* (0), 4540–4549. https://doi.org/10.1039/JR9620004540.

(185) Wade, L. G. *Organic Chemistry*; Pearson, 2013.

(186) Vollhardt, K. P. C.; Shore, N. E. *Organic Chemistry: Structure and Function*, 2015th ed.; WH Freeman: New York, 2014.

(187) Sharma, G. S. D.; Eswaran, S. V. Substituent Effect of the Methoxy Group: A Matter of Give and Take. *Reson* **1997**, *2* (3), 73–75. https://doi.org/10.1007/BF02838971.

(188) Hepworth, J. D.; Waring, D. R.; Waring, M. J.; Waring, M. J. *Aromatic Chemistry*; Royal Society of Chemistry, 2002.

(189) Er, S.; Suh, C.; Marshak, M. P.; Aspuru-Guzik, A. Computational Design of Molecules for an All-Quinone Redox Flow Battery. *Chem. Sci.* **2015**, *6* (2), 885–893. https://doi.org/10.1039/C4SC03030C.

(190) Bachman, J. E.; Curtiss, L. A.; Assary, R. S. Investigation of the Redox Chemistry of Anthraquinone Derivatives Using Density Functional Theory. *J. Phys. Chem. A* **2014**, *118* (38), 8852–8860. https://doi.org/10.1021/jp5060777.

(191) Cheng, L.; Assary, R. S.; Qu, X.; Jain, A.; Ong, S. P.; Rajput, N. N.; Persson, K.; Curtiss, L. A. Accelerating Electrolyte Discovery for Energy Storage with High-Throughput Screening. *J. Phys. Chem. Lett.* **2015**, *6* (2), 283–291. https://doi.org/10.1021/jz502319n.

(192) Assary, R. S.; Brushett, F. R.; Curtiss, L. A. Reduction Potential Predictions of Some Aromatic Nitrogen-Containing Molecules. *RSC Adv.* **2014**, *4* (101), 57442–57451. https://doi.org/10.1039/C4RA08563A.

(193) Huynh, M. T.; Anson, C. W.; Cavell, A. C.; Stahl, S. S.; Hammes-Schiffer, S. Quinone 1 e– and 2 e–/2 H+ Reduction Potentials: Identification and Analysis of Deviations from Systematic Scaling Relationships. *J. Am. Chem. Soc.* **2016**, *138* (49), 15903–15910. https://doi.org/10.1021/jacs.6b05797.

(194) Pineda Flores, S. D.; Martin-Noble, G. C.; Phillips, R. L.; Schrier, J. Bio-Inspired Electroactive Organic Molecules for Aqueous Redox Flow Batteries. 1. Thiophenoquinones. *J. Phys. Chem. C* **2015**, *119* (38), 21800–21809. https://doi.org/10.1021/acs.jpcc.5b05346.

(195) Bruckner, R. *Advanced Organic Chemistry: Reaction Mechanisms*; Elsevier, 2001.

(196) Harmata, M.; Bruckner, R.; Wender, P. *Organic Mechanisms: Reactions, Stereochemistry and Synthesis*, 2010th ed.; Springer: Berlin, 2010.

(197) Wedege, K.; Dražević, E.; Konya, D.; Bentien, A. Organic Redox Species in Aqueous Flow Batteries: Redox Potentials, Chemical Stability and Solubility. *Sci. Rep.* **2016**, *6*, 39101. https://doi.org/10.1038/srep39101.

(198) Clayden, J.; Greeves, N.; Warren, S. *Organische Chemie*, 2nd ed.; Springer Spektrum, 2013.

(199) Anslyn, E. V.; Dougherty, D. A. *Modern Physical Organic Chemistry*; University Science Books, 2006.

(200) Fleming, I. *Frontier Orbitals and Organic Chemical Reactions*, 1. Auflage.; John Wiley & Sons: London, 1976.

(201) Tabor, D. P.; Gómez-Bombarelli, R.; Tong, L.; Gordon, R. G.; Aziz, M. J.; Aspuru-Guzik, A. Mapping the Frontiers of Quinone Stability in Aqueous Media: Implications for Organic Aqueous Redox Flow Batteries. *J. Mater. Chem. A* **2019**, *7* (20), 12833–12841. https://doi.org/10.1039/C9TA03219C.

(202) Hamlin, T. A.; Swart, M.; Bickelhaupt, F. M. Nucleophilic Substitution (SN2): Dependence on Nucleophile, Leaving Group, Central Atom, Substituents, and Solvent. *ChemPhysChem* **2018**, *19* (11), 1315–1330. https://doi.org/10.1002/cphc.201701363.

(203) Tandon, V. K.; Maurya, H. K. 'On Water': Unprecedented Nucleophilic Substitution and Addition Reactions with 1,4-Quinones in Aqueous Suspension. *Tetrahedron Letters* **2009**, *43* (50), 5896–5902. https://doi.org/10.1016/j.tetlet.2009.07.149.

(204) Kutyrev, A. A.; Moskva, V. V. Nucleophilic Reactions of Quinones. *Russ. Chem. Rev.* **1991**, *60* (1), 72. https://doi.org/10.1070/RC1991v060n01ABEH001032.

(205) Winsberg, J.; Hagemann, T.; Janoschka, T.; Hager, M. D.; Schubert, U. S. Redox-Flow Batteries: From Metals to Organic Redox-Active Materials. *Angew Chem Int Ed Engl* **2017**, *56* (3), 686–711. https://doi.org/10.1002/anie.201604925.

(206) Brunmark, A.; Cadenas, E. Redox and Addition Chemistry of Quinoid Compounds and Its Biological Implications. *Free Radical Biology and Medicine* **1989**, *7* (4), 435–477. https://doi.org/10.1016/0891-5849(89)90126-3.

(207) Brunmark, A.; Cadenas, E. Electronically Excited State Generation during the Reaction of P-Benzoquinone with H2O2: Relation to Product Formation: 2-OH- and 2,3-Epoxy-p-Benzoquinone the Effect of Glutathione. *Free Radical Biology and Medicine* **1987**, *3* (3), 169–180. https://doi.org/10.1016/0891-5849(87)90002-5.

(208) Matveev, V. V.; Isaenkov, V. E.; Belov, S. V.; Korneev, N. V. Study of Anthraquinone and Graphite Electrode Behaviour in Mixed Solvent Sulphuric Acid. In *New Promising Electrochemical Systems for Rechargeable Batteries*; Barsukov, V., Beck, F., Eds.; NATO ASI Series; Springer Netherlands: Dordrecht, 1996; pp 467–475. https://doi.org/10.1007/978-94-009-1643-2_35.

(209) Beck, F.; Heydecke, G. On the Mechanism of the Cathodic Reduction of Anthraquinone to Anthrone. *Berichte der Bunsengesellschaft für physikalische Chemie* **1987**, *91* (1), 37–43. https://doi.org/10.1002/bbpc.19870910109.

(210) Ragimov, A. V.; Mamedov, B. A.; Liogon'kii, B. I. The Alkali Initiated Polymerization of P-Benzoquinone. *Polymer Science U.S.S.R.* **1977**, *19* (11), 2922–2928. https://doi.org/10.1016/0032-3950(77)90312-4.

(211) Sabaa, M. W.; Madkour, T. M.; Yassin, A. A. Polymerization Products of P-Benzoquinone as Bound Antioxidants for Styrene-Butadiene Rubber: Part I—Preparation of Quinone Polymers. *Polymer Degradation and Stability* **1988**, *22* (3), 195–203. https://doi.org/10.1016/0141-3910(88)90010-9.

(212) Li, C.-J.; Chan, T.-H. *Comprehensive Organic Reactions in Aqueous Media*, 2.; Wiley-Interscience: Hoboken, N.J, 2007.

(213) Kurzweil, P.; Dietlmeier, O. K. *Elektrochemische Speicher: Superkondensatoren, Batterien, Elektrolyse-Wasserstoff, Rechtliche Grundlagen*; Springer-Verlag, 2016.

(214) Lin, K.; Chen, Q.; Gerhardt, M. R.; Tong, L.; Kim, S. B.; Eisenach, L.; Valle, A. W.; Hardee, D.; Gordon, R. G.; Aziz, M. J.; Marshak, M. P. Alkaline Quinone Flow Battery. *Science* **2015**, *349* (6255), 1529–1532. https://doi.org/10.1126/science.aab3033.

(215) Chen, Q.; Eisenach, L.; Aziz, M. J. Cycling Analysis of a Quinone-Bromide Redox Flow Battery. *J. Electrochem. Soc.* **2016**, *163* (1), A5057–A5063. https://doi.org/10.1149/2.0081601jes.

(216) Tong, L.; Chen, Q.; Wong, A. A.; Gómez-Bombarelli, R.; Aspuru-Guzik, A.; Gordon, R. G.; Aziz, M. J. UV-Vis Spectrophotometry of Quinone Flow Battery Electrolyte for in Situ Monitoring and Improved Electrochemical Modeling of Potential and Quinhydrone Formation. *Phys. Chem. Chem. Phys.* **2017**, *19* (47), 31684–31691. https://doi.org/10.1039/C7CP05881K.

(217) Beh, E. S.; De Porcellinis, D.; Gracia, R. L.; Xia, K. T.; Gordon, R. G.; Aziz, M. J. A Neutral PH Aqueous Organic–Organometallic Redox Flow Battery with Extremely High Capacity Retention. *ACS Energy Lett.* **2017**, *2* (3), 639–644. https://doi.org/10.1021/acsenergylett.7b00019.

(218) Lee, W.; Permatasari, A.; Kwon, Y. Neutral PH Aqueous Redox Flow Batteries Using Anthraquinone-Ferrocyanide Redox Couple. *J. Mater. Chem. C* **2020**. https://doi.org/10.1039/D0TC00640H.

(219) Hu, B.; DeBruler, C.; Rhodes, Z.; Liu, T. L. Long-Cycling Aqueous Organic Redox Flow Battery (AORFB) toward Sustainable and Safe Energy Storage. *J. Am. Chem. Soc.* **2017**, *139* (3), 1207–1214. https://doi.org/10.1021/jacs.6b10984.

(220) Carretero-González, J.; Castillo-Martínez, E.; Armand, M. Highly Water-Soluble Three-Redox State Organic Dyes as Bifunctional Analytes. *Energy & Environmental Science* **2016**, *9* (11), 3521–3530. https://doi.org/10.1039/C6EE01883A.

(221) Viehe, H. G.; Janousek, Z.; Merényi, R. *Substituent Effects in Radical Chemistry*; Springer Science & Business Media, 2012.

(222) Chesseman, G. W. H.; Cookson, R. F. *Condensed Pyrazines*; John Wiley & Sons: New York, 2009.

(223) Kerner, F. Characterizing Organic Active Materials for Aqueous Redox Flow Batteries at Various PH Values. Bachelor thesis, Justus Liebig University Giessen, 2019.

(224) Liang, Y.; Tao, Z.; Chen, J. Organic Electrode Materials for Rechargeable Lithium Batteries. *Advanced Energy Materials* **2012**, *2* (7), 742–769. https://doi.org/10.1002/aenm.201100795.

(225) Song, Z.; Zhou, H. Towards Sustainable and Versatile Energy Storage Devices: An Overview of Organic Electrode Materials. *Energy Environ. Sci.* **2013**, *6* (8), 2280–2301. https://doi.org/10.1039/C3EE40709H.

(226) Bergner, B. J.; Schürmann, A.; Peppler, K.; Garsuch, A.; Janek, J. TEMPO: A Mobile Catalyst for Rechargeable Li-O2 Batteries. *J. Am. Chem. Soc.* **2014**, *136* (42), 15054–15064. https://doi.org/10.1021/ja508400m.

(227) Preger, Y.; Gerken, J. B.; Biswas, S.; Anson, C. W.; Johnson, M. R.; Root, T. W.; Stahl, S. S. Quinone-Mediated Electrochemical O2 Reduction Accessing High Power Density with an Off-Electrode Co-N/C Catalyst. *Joule* **2018**, *2* (12), 2722–2731. https://doi.org/10.1016/j.joule.2018.09.010.

(228) O'Regan, B.; Grätzel, M. A Low-Cost, High-Efficiency Solar Cell Based on Dye-Sensitized Colloidal TiO 2 Films. *Nature* **1991**, *353* (6346), 737–740. https://doi.org/10.1038/353737a0.

(229) Feldt, S. M.; Gibson, E. A.; Gabrielsson, E.; Sun, L.; Boschloo, G.; Hagfeldt, A. Design of Organic Dyes and Cobalt Polypyridine Redox Mediators for High-Efficiency Dye-Sensitized Solar Cells. *J. Am. Chem. Soc.* **2010**, *132* (46), 16714–16724. https://doi.org/10.1021/ja1088869.

(230) Gottis, S.; Barrès, A.-L.; Dolhem, F.; Poizot, P. Voltage Gain in Lithiated Enolate-Based Organic Cathode Materials by Isomeric Effect. *ACS Appl. Mater. Interfaces* **2014**, *6* (14), 10870–10876. https://doi.org/10.1021/am405470p.

(231) Shimizu, A.; Tsujii, Y.; Kuramoto, H.; Nokami, T.; Inatomi, Y.; Hojo, N.; Yoshida, J. Nitrogen-Containing Polycyclic Quinones as Cathode Materials for Lithium-Ion Batteries with Increased Voltage. *Energy Technology* **2014**, *2* (2), 155–158. https://doi.org/10.1002/ente.201300148.

(232) Sedenho, G. C.; De Porcellinis, D.; Jing, Y.; Kerr, E.; Mejia-Mendoza, L. M.; Vazquez-Mayagoitia, Á.; Aspuru-Guzik, A.; Gordon, R. G.; Crespilho, F. N.; Aziz, M. J. Effect of Molecular Structure of Quinones and Carbon Electrode Surfaces on the Interfacial Electron Transfer Process. *ACS Appl. Energy Mater.* **2020**, *3* (2), 1933–1943. https://doi.org/10.1021/acsaem.9b02357.

5 Appendix

5.1 Supporting Information publication II

Supporting Information for

Quest for Organic Active Materials for Redox Flow Batteries: 2,3-Diaza-anthraquinones and their Electrochemical Properties

Jonas D. Hofmann[a], Felix L. Pfanschilling[a], Nastaran Krawczyk[b], Peter Geigle[b], Longcheng Hong[c], Sebastian Schmalisch[c], Hermann A. Wegner[c,d], Doreen Mollenhauer[a,d], Jürgen Janek[a,d*] and Daniel Schröder[a,d*]

[a] Institute of Physical Chemistry, Justus Liebig University Giessen, Heinrich-Buff-Ring 17, 35392 Giessen, Germany

[b] CMBlu Projekt AG, Industriestraße 19, 63755 Alzenau, Germany

[c] Institute of Organic Chemistry, Justus Liebig University Giessen, Heinrich-Buff-Ring 17, 35392 Giessen, Germany

[d] Center for Materials Research, Justus Liebig University Giessen, Heinrich-Buff-Ring 16, 35392 Giessen, Germany

* Corresponding Authors: Jürgen Janek, juergen.janek@phys.chemie.uni-giessen.de, Daniel Schröder, daniel.schroeder@phys.chemie.uni-giessen.de

Cyclic voltammetry

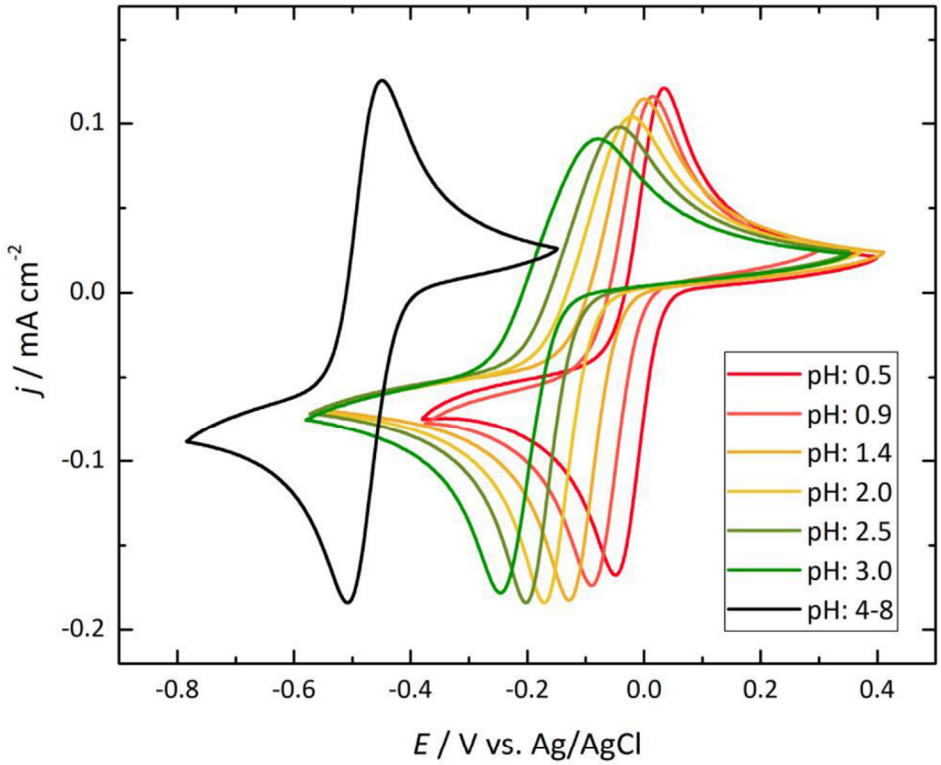

Figure S1: CVs of 1 mM AQDS in aqueous solution at a scan rate of 25 mV/s at different pH values. For the represented pH values different amounts of H_2SO_4 and KOH were added to the solution. Since no alteration can be observed for the redox potential of AQDS for pH values above 4, we assume that no protonation takes place in this pH range. Therefore, the reduction of AQDS solely is a two-electron process for unbuffered solutions at high pH values. For low pH values as 0.5 we observe a considerably more positive redox potential. This is a result of the concerted two-electron two-proton transfer of the AQDS redox reaction at pH values close to 0. For pH values in between these extreme cases the degree of protonation varies with proton activity, also affecting the redox potential.

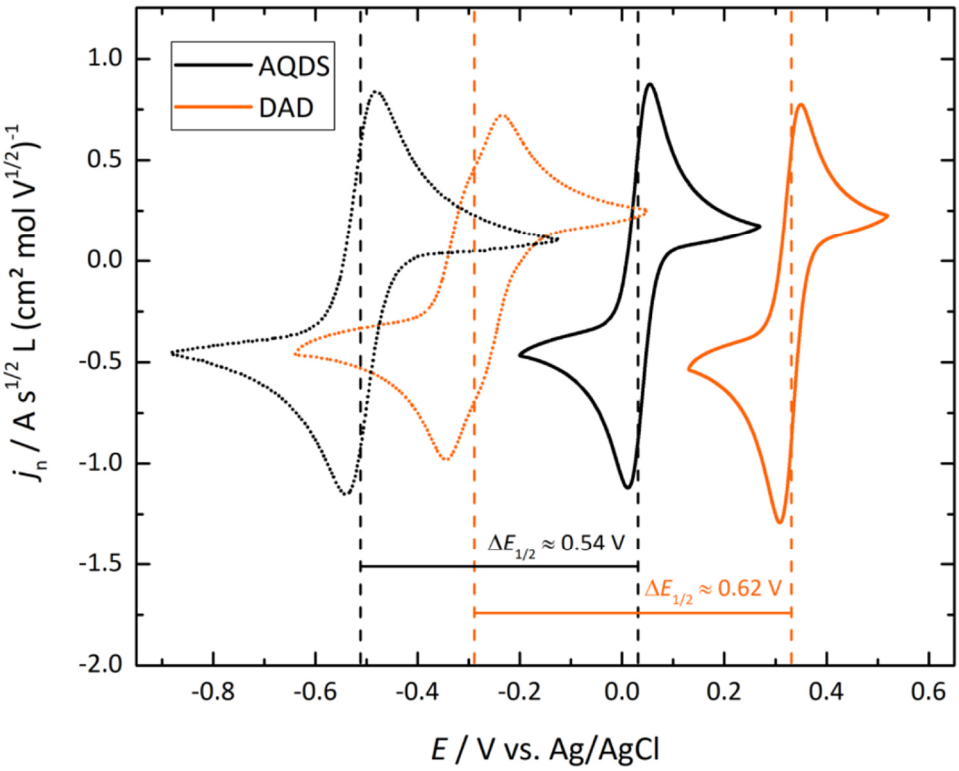

Figure S2: Normalized CVs of DAD and AQDS in 2 M H_2SO_4 (straight lines) and 1 M KOH (dotted lines). The currents were normalized by electrode surface (0.0707 cm²), active material concentration (0.5 mM) and the applied scan rate (50 mV/s) to allow for a direct comparison. The incorporation of a diaza-moiety results in a positive shift of the redox potential that amounts 220 mV (alkaline) to 300 mV (acidic), depending on the applied pH value. Regarding catholyte active materials, this effect can be very beneficial to increase the achievable cell voltage.

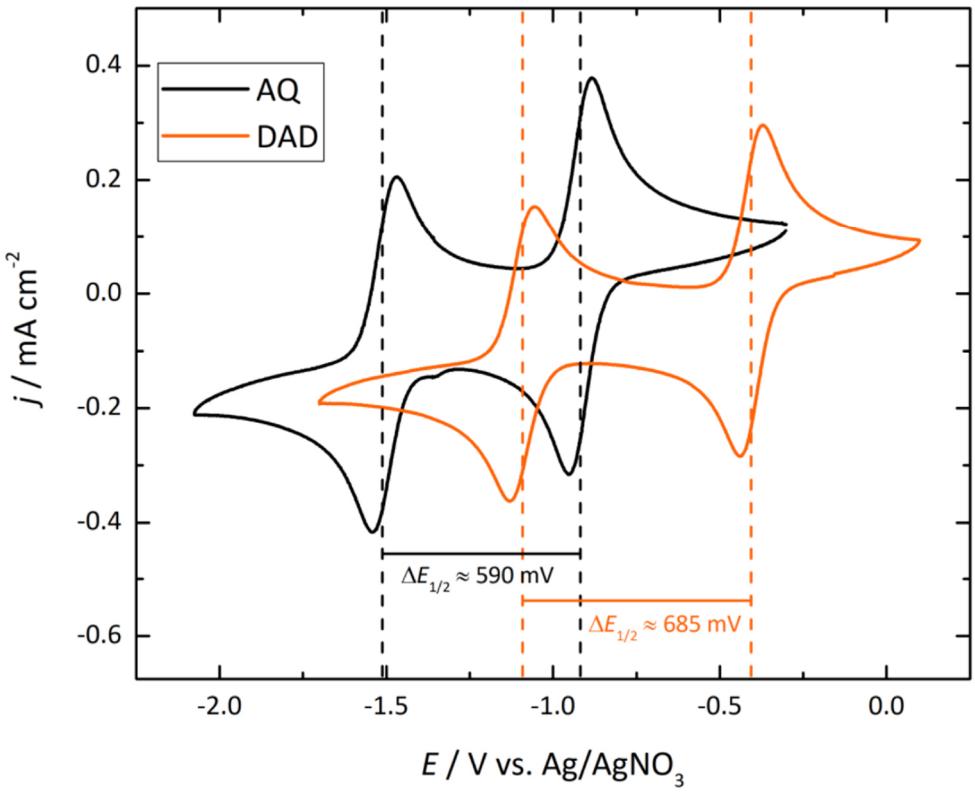

Figure S3: CV of 1 mM AQ and 1 mM DAD in 0.1 mM $TBAPF_6$/ acetonitrile at a scan rate of 25 mV/s. Although being measured under the same conditions, both curves show very different peak separation between the two correlated charge transfers. This phenomenon might indicate an enhanced stabilization of the semiquinone radical or a higher destabilization of the dianion respectively. Furthermore, the mean redox potential can be increased by the incorporation of nitrogen into the aromatic system. This is marked by the strong positive shift of the first redox process from −0.92 V vs. $Ag/AgNO_3$ (AQ) to −0.4 V vs. $Ag/AgNO_3$ (DAD).

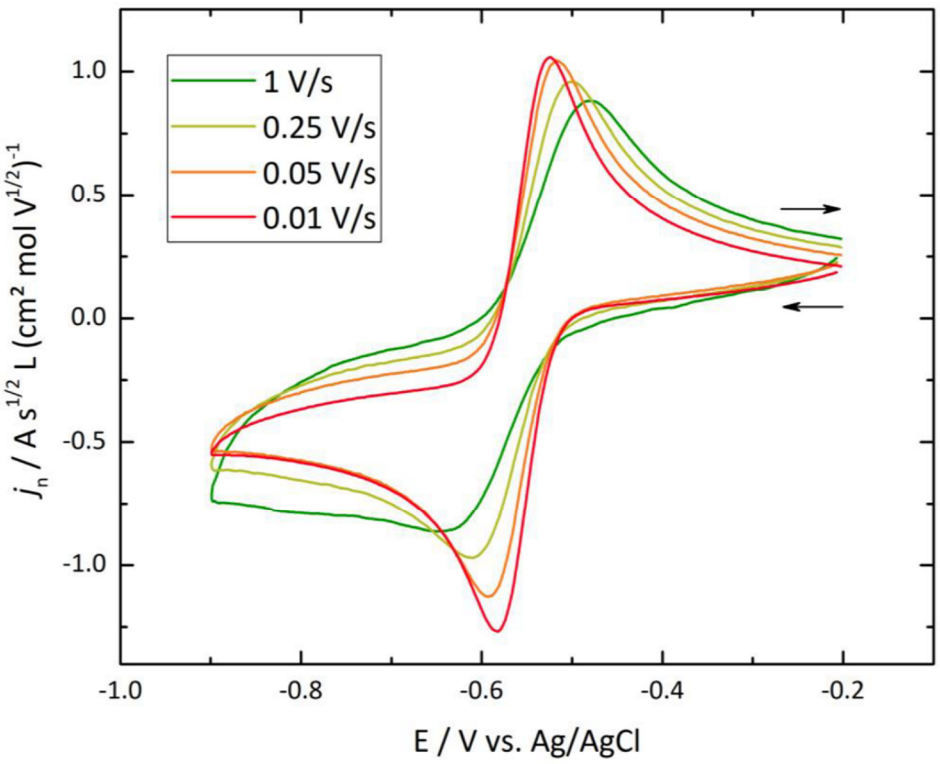

Figure S4: Normalized CVs of DADdi(OH) in 1 M KOH at different scan rates. The currents were normalized by electrode surface (0.0707 cm²), active material concentration (0.5 mM) and the applied scan rate to allow for a direct comparison. ΔE_p ranges between 56 mV at 0.01 V/s and 167 mV at 1 V/s which indicates slower charge transfer kinetics compared to DAD and DAD(MeO). Both compounds show a constantly low ΔE_p of 35 mV in the investigated range of scan rates. This is also reflected by a notably lower k^0 of DADdi(OH) (compare Fig. S6).

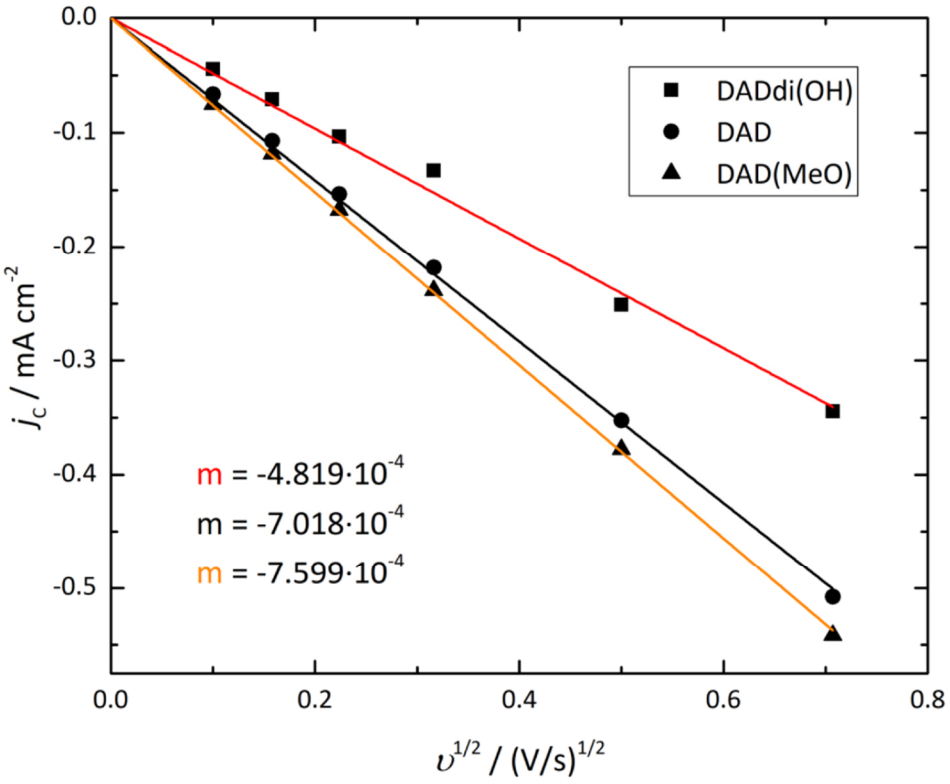

Figure S5: Randles-Sevcik plot used to determine diffusion coefficients. According to the Randles-Sevcik equation a plot of measured current densities vs. the square root of the associated scan rates yields a slope m = 0.4463 $n^{3/2}$ $F^{3/2}$ A $D^{1/2}$ $(RT)^{-1/2}$ c_0. Here n is the number of transferred electrons, F is the Faraday constant (96485 C mol^{-1}), A is the geometric area of the working electrode in cm², D is the diffusion coefficient in cm² s^{-1}, R is the universal gas constant (8.314 J K^{-1} mol^{-1}) and T is the temperature in K. The cathodic peak current densities were gathered from the CVs measured in acidic aqueous solution. Solving the equation for D gives 3.78·10^{-6} cm²/s for DAD, 4.12·10^{-6} cm²/s for DAD(MeO) and 1.61·10^{-6} cm²/s for DADdi(OH).

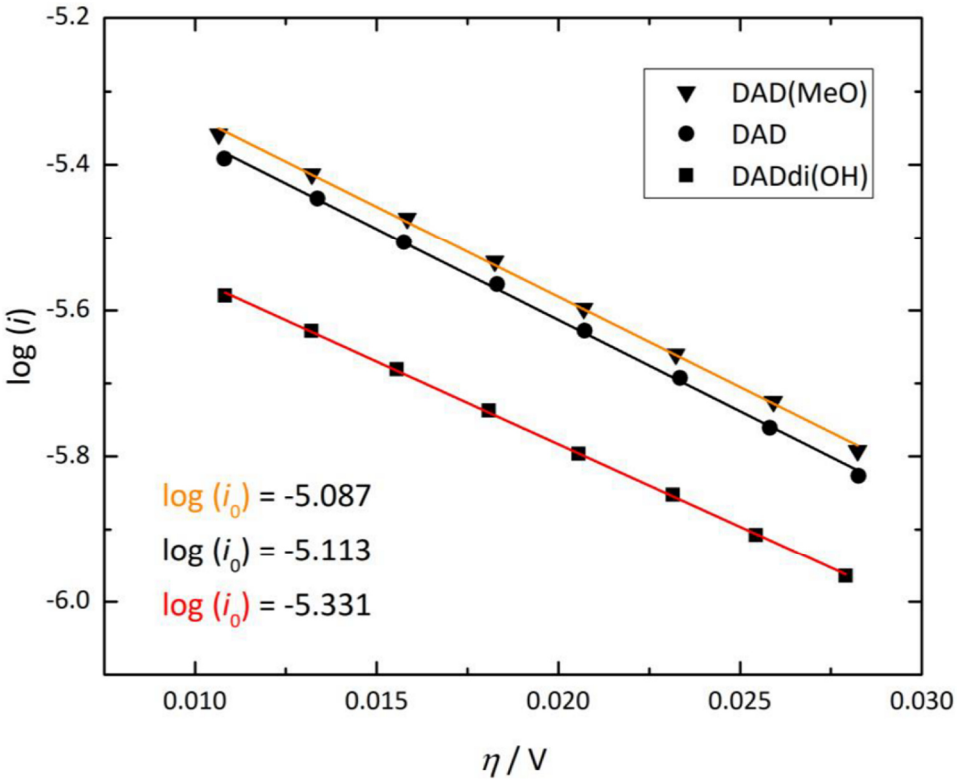

Figure S6: Tafel plot of the cathodic charge transfer of 0.5 mM DAD(MeO) in 2 M H_2SO_4. The data were gathered from the cathodic branch of the CV recorded at a scan rate of 25 mV/s. According to the Tafel equation the y-axis intercept equals the log of the exchange current i_0. Transferring this value to the equation $i_0 = k^0\ n\ F\ A\ c_0$ and solving the equation for k^0 yields a value of $1.131 \cdot 10^{-3}$ cm/s (DAD), $1.201 \cdot 10^{-3}$ cm/s (DAD(MeO)) and $6.85 \cdot 10^{-4}$ cm/s (DADdi(OH)) for the heterogeneous rate constant.

Hydrodynamic measurements

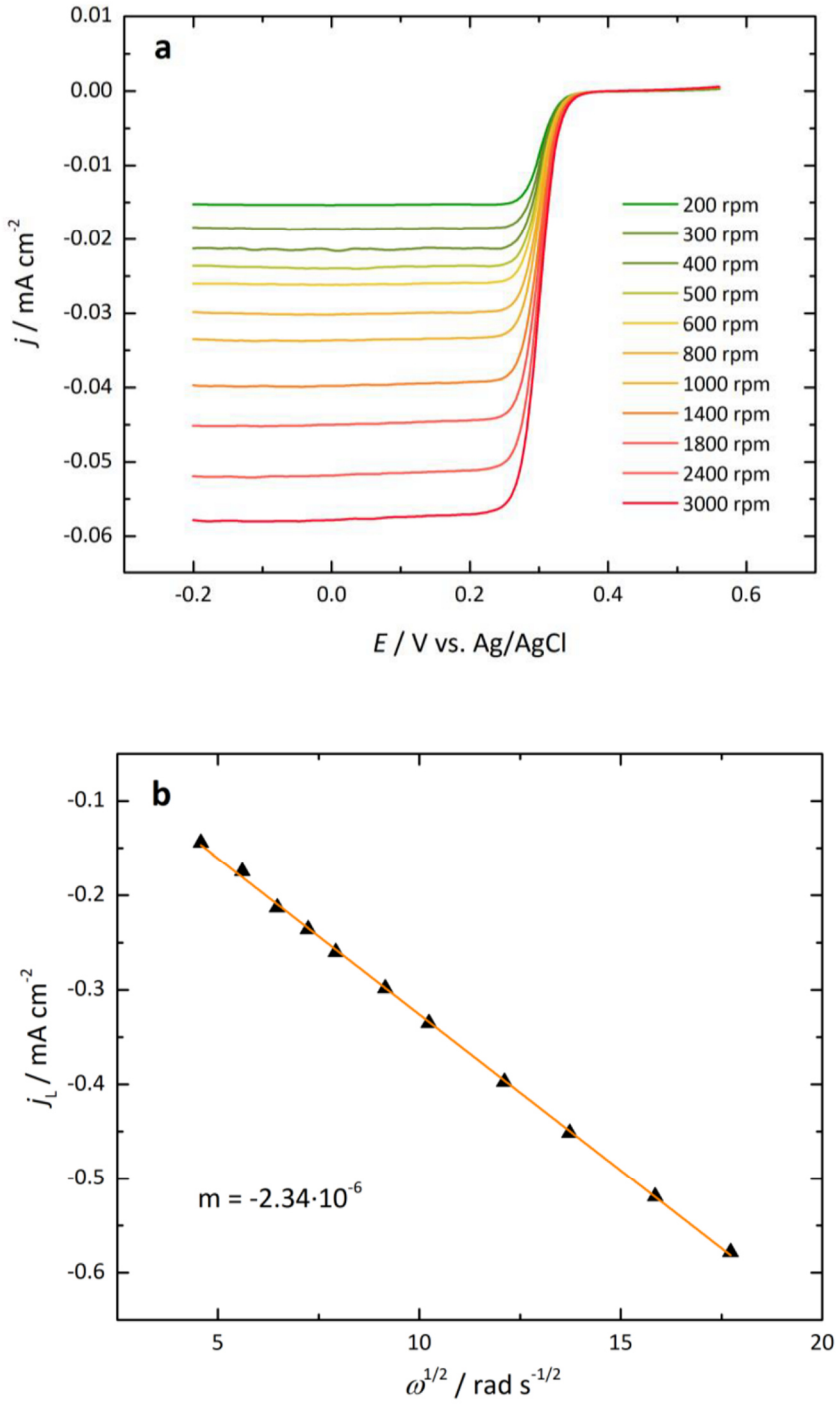

Figure S7: Hydrodynamic RDE measurements of 0.5 mM DAD(MeO) in 2 M H_2SO_4. Linear sweep voltammetry (10 mV/s) at different electrode rotation rates ω results in limiting current densities j_L (**a**) that are plotted vs. the square root of ω (**b**). According to the Levich equation a linear fit yields a slope m = 0.62 $n\ F\ A\ c_0\ D^{2/3}\ v^{-1/6}$ that was used for the determination of D. Here i_{lim} is the limiting current, v is the kinematic viscosity of the solution in cm²/s and c_0 is the concentration of the electrochemically active species in mol/cm³. For a slope of $-2.34 \cdot 10^{-6}$ we yield a diffusion coefficient of $4.23 \cdot 10^{-6}$ cm²/s, which is in well accordance to the value calculated from the Randles-Sevcik plot.

Characterization of carbon felt current collectors

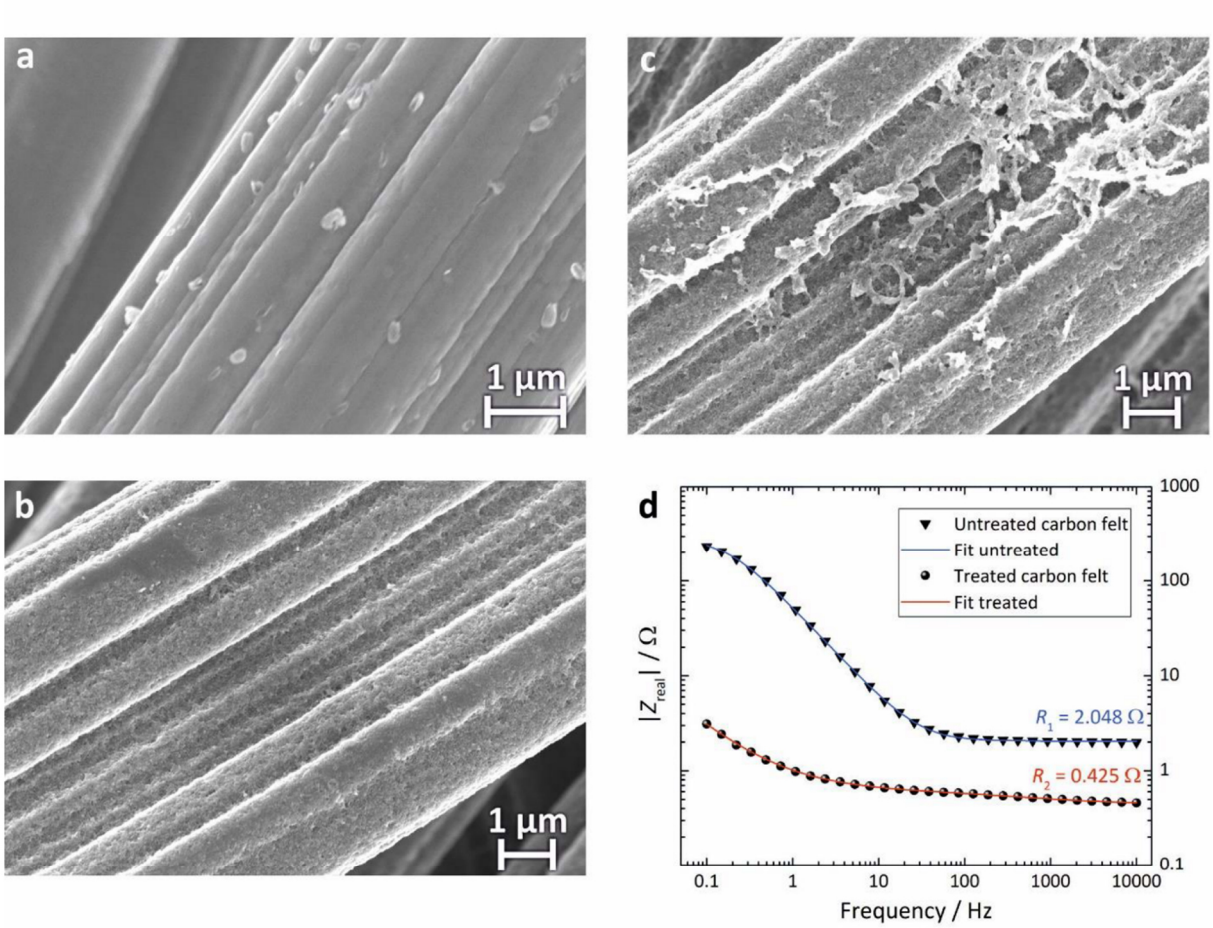

Figure S8: Scanning electron microscope (SEM) images of the carbon felt current collectors at different states of treatment. (**a**) Carbon felt as received from SGL Carbon at 15,000 x magnification. In this state the individual fibers exhibit a smooth and homogeneous surface structure. (**b**) Carbon fiber after a 24 h heat treatment at 400 °C in air at 10,000 x magnification. As a result of the high temperatures in the presence of oxygen the fibers display a roughened texture caused by the oxidation and degassing of surface material. (**c**) Heat-treated carbon felt after usage in several cycling experiments at 10,000 x magnification, cleaned with water. During cycling in a full redox flow cell the fibers underwent morphological changes leading up to not only roughened but porous regions. (**d**) Impedance data of cells built with differently conditioned carbon felts. The Bode plot illustrates the measurement results of untreated carbon felts that were used as received (blue) and heat-treated carbon felts that were annealed at 400 °C in air for 24 h (red). The data were fit with an equivalent circuit diagram comprising a series circuit of a resistor R_1/R_2 followed by an *RC*-element, yielding an inner cell resistance of 2.048 Ω for untreated and 0.425 Ω for heat-treated carbon felts.

Long-term CV measurements

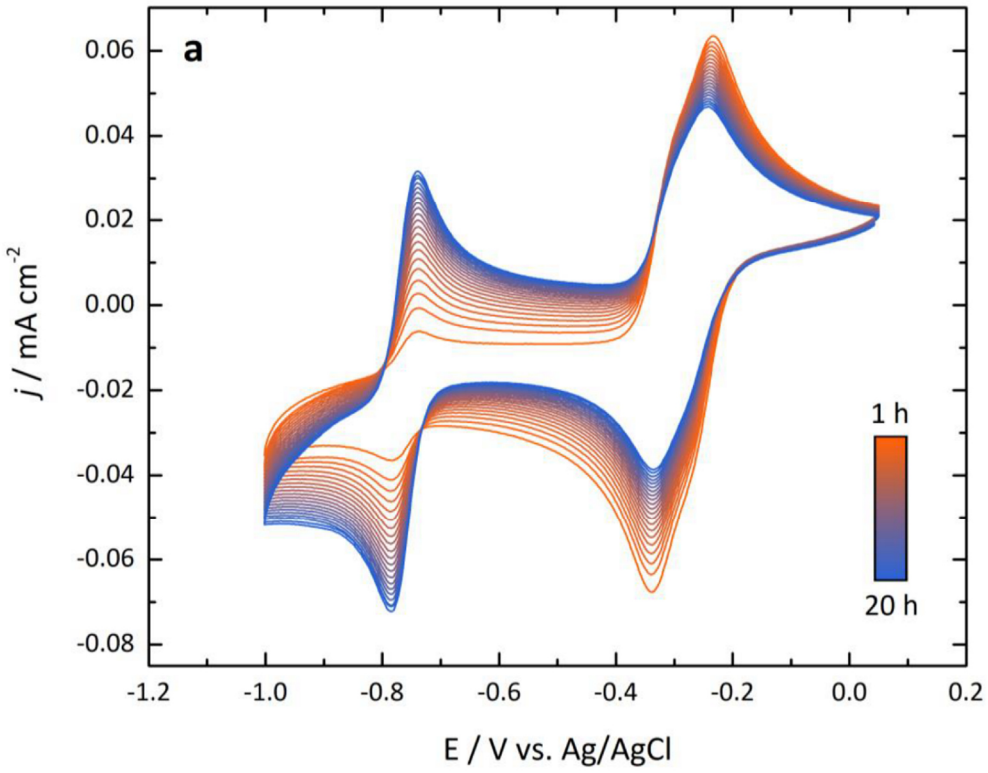

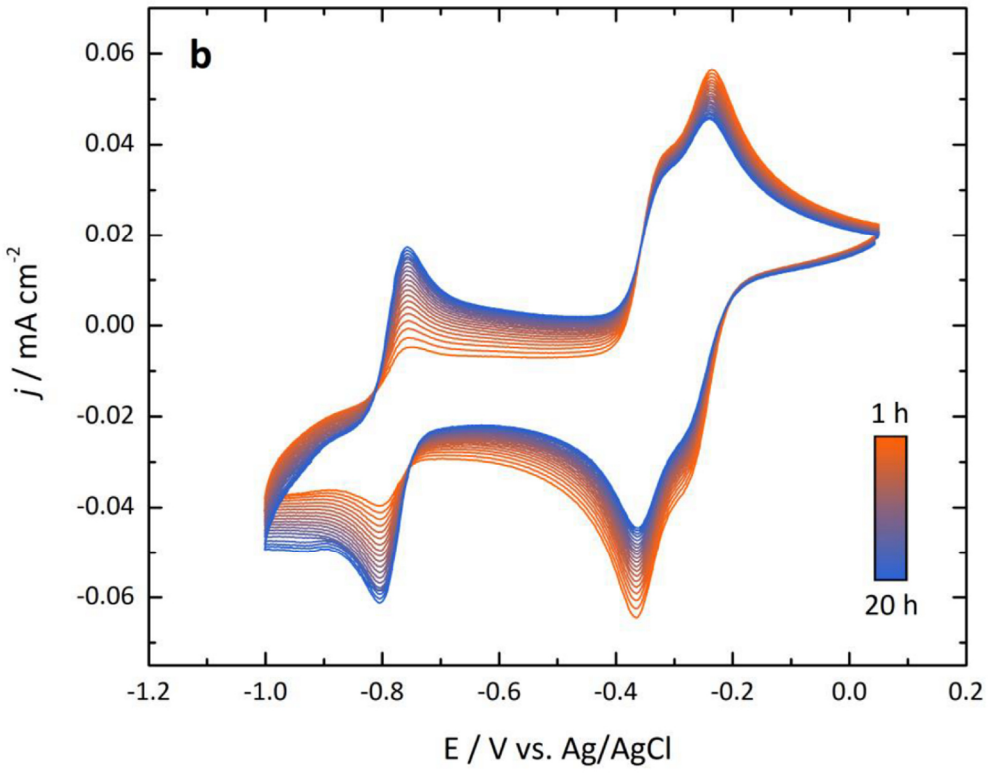

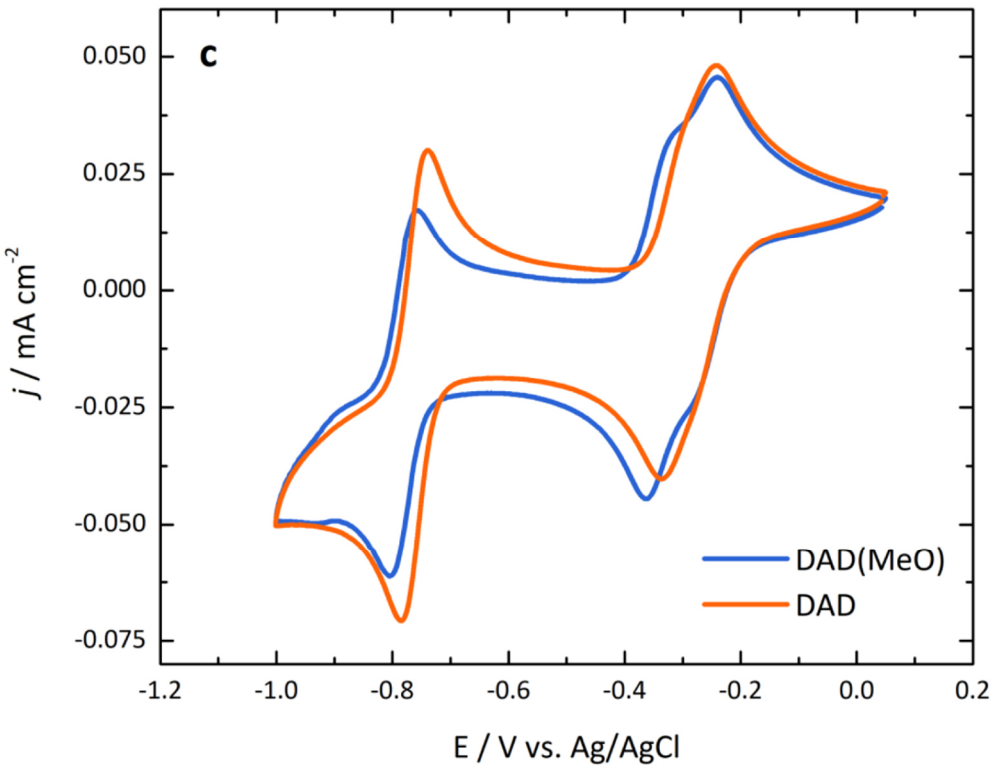

Figure S9: Time dependent CVs of 1 mM DAD in 1 M KOH (**a**) and 0.5 mM DAD(MeO) in 1 M KOH (**b**) at a scan rate of 25 mV/s. For (**a**) the characteristic features of the original compound decrease distinctly by an exposition to alkaline media over time. Within a time span of 20 h, the pristine signal between −0.4 V and −0.2 V vs. Ag/AgCl declines in favor of a new redox wave emerging at around −0.75 V vs. Ag/AgCl. The negative potential shift as well as the absent peak splitting gives rise to the assumption that the nitrogen containing part of the compound undergoes a degradation reaction. For (**b**) this reaction proceeds with a notably reduced rate, indicating a higher stability of DAD(MeO) versus alkaline media compared to DAD. This becomes even more evident by a direct comparison of the CVs of both compounds after 20 h (**c**).

DFT calculations

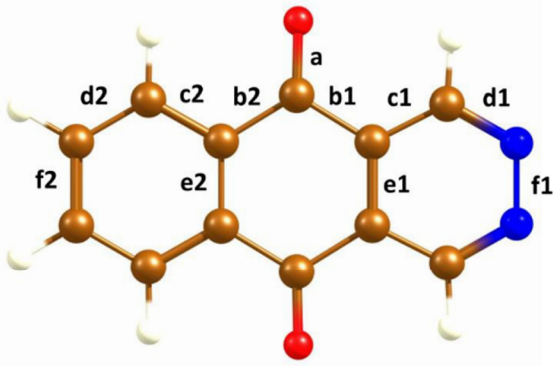

non-reduced state
reduced state
X neutral
X alkaline
X acidic

Compound	a	b1	b2	c1	c2	d1	d2	e1	e2	f1	f2
DAD	1.239	1.498	1.489	1.412	1.410	1.345	1.402	1.400	1.425	1.355	1.410
$DADH^+$	1.235	1.506	1.481	1.407	1.410	1.339	1.402	1.396	1.428	1.341	1.414
DAD^{2-}	1.303	1.440	1.466	1.423	1.427	1.334	1.392	1.459	1.454	1.407	1.426
$DADH^-$	1.393	1.441	1.426	1.438	1.434	1.326	1.389	1.446	1.453	1.392	1.423
$DADH_2$	1.370	1.409	1.425	1.433	1.432	1.326	1.385	1.438	1.456	1.392	1.426
$DADH_3^+$	1.355	1.412	1.428	1.409	1.428	1.331	1.386	1.451	1.453	1.374	1.422
DAD(MeO)	1.238	1.498	1.492	1.411	1.405	1.345	1.410	1.400	1.424	1.355	1.420
$DAD(MeO)H^+$	1.234	1.505	1.484	1.405	1.404	1.340	1.412	1.397	1.428	1.340	1.422
$DAD(MeO)^{2-}$	1.306	1.438	1.464	1.425	1.431	1.333	1.392	1.461	1.450	1.408	1.428
$DAD(MeO)H^-$	1.395	1.401	1.424	1.438	1.436	1.327	1.394	1.445	1.450	1.390	1.428
$DAD(MeO)H_2$	1.373	1.408	1.424	1.433	1.431	1.326	1.391	1.439	1.455	1.391	1.432
$DAD(MeO)H_3^+$	1.359	1.410	1.429	1.411	1.426	1.331	1.394	1.451	1.452	1.373	1.431
DADdi(OH)	1.268	1.484	1.451	1.413	1.421	1.343	1.428	1.405	1.436	1.357	1.384
$DADdi(OH)H^+$	1.267	1.485	1.445	1.407	1.424	1.338	1.432	1.408	1.434	1.344	1.382
$DADdi(OH)^{2-}$	1.330	1.427	1.449	1.424	1.442	1.332	1.398	1.456	1.448	1.405	1.423
$DADdi(OH)^{3-}$	1.348	1.412	1.457	1.431	1.441	1.330	1.398	1.455	1.473	1.410	1.410
$DADdi(OH)^{4-}$	1.309	1.441	1.481	1.419	1.479	1.340	1.428	1.458	1.500	1.426	1.404
$DADdi(OH)H_2$	1.366	1.412	1.428	1.431	1.440	1.327	1.384	1.435	1.462	1.392	1.419
$DADdi(OH)H_3^+$	1.351	1.415	1.431	1.407	1.436	1.333	1.387	1.449	1.459	1.376	1.412

Table T1: Bond lengths in Å (=0.1 nm) of the investigated DAAQs and their reduced species in aqueous solutions, calculated at UBP86-D3/aug-cc-pVDZ level of theory. Labelling of bonds is shown in the figure above. For each DAAQ the bond lengths of the unreduced molecule (for the case of protonated [indicated by positive formal charge] and unprotonated diaza group) as well as for the relevant protonation states of the reduced DAAQs for high and low pH value are shown. The values a - d may slightly vary for the non-symmetric molecules. In addition, the C-O bond length of the methoxy group in DAD(MeO) / $DAD(MeO)H^+$ is 1.356 Å / 1.350 Å, whereas in $DAD(MeO)H^-$ / $DAD(MeO)H^{2-}$ it is 1.374 Å / 1.386 Å and amounts to 1.365 Å / 1.356 Å in $DAD(MeO)H_2$ / $DAD(MeO)H_3^+$. The C-O bond length of the added hydroxyl groups in DADdi(OH) / $DADdi(OH)H^+$ comes to 1.340 Å / 1.333 Å, in $DADdi(OH)^{2-}$ it is 1.370 Å and in $DADdi(OH)H_3^+$ it amounts to 1.351 Å and

1.382 Å. The hydroxyl C-O bond length of the reduced and completely deprotonated DADdi(OH)$^{4-}$ is 1.309 Å and 1.324 Å.

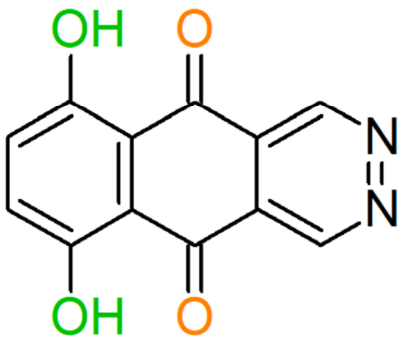

DADdi(OH) protonation state	+ 2e$^-$	+ 2e$^-$ + 1H$^+$	+ 2e$^-$ + 2H$^+$
–OH / –OH / =O / =O → **±0**	–0.270	–0.026	0.073
–OH / –O$^-$ / =O / =O → **–1**	–1.033	0.071	0.315
–O$^-$ / –O$^-$ / =O / =O → **–2**	–1.804	–0.439	0.665

Table T2: Reduction potentials (in V vs. SHE) of different protonation states of DADdi(OH) to distinctly protonated reduced species. The formal charges of the various protonation states before electrochemical reduction are given. For the sake of completeness, we also calculated the reduction potentials for the state of one protonated hydroxyl moiety (monoanion) in the case of DAD (0.094 V), DAD(MeO) (0.044 V), and AQ (–0.224 V).

Full cell performance of diaza-anthraquinones

To investigate whether the behavior of DAAQs in half cell experiments can be transferred to the full cell scale operation of RFBs, we tested several in-house RFBs with diaza compounds as redox active material at the anode. The performance was evaluated by means of cell voltage, capacity retention and cycle stability. As can be seen in Fig. S11a, DAD undergoes a severe capacity fading during cycling in alkaline solution. The discharge capacity decays very fast to about 60 % of its initial value – especially during the first 20 cycles. Prior to the long term cycling measurements several performance benchmarks (e.g. polarization curve measurements) were run. Because of this, the nominal first six cycles of the measurement were conducted under varying electrochemical conditions and are not included. The full cell measurements are solely thought of as a proof of concept within the scope of this work.
Having a closer look at the general cycling behavior up to cycle 100 reveals the following: after approximately 50 cycles, the discharge capacity of cells with DAD continues to decrease, but with a much lower rate relative to the first 20 cycles. The subtle rise of the discharge capacity, starting around the 90th cycle, may be an indication for the onset of side

reactions during the discharge process. Nevertheless, the DAD based cell showed an average Coulombic efficiency of 98.97 % during the first 100 cycles (see Fig. S11b).

In contrast, cells with DAD(MeO) do not exhibit a distinct capacity fade. Moreover, a slightly elevated discharge capacity relative to the starting value is observed in the first 10 cycles for RFBs containing DAD(MeO), which is presumed to be an activation process. This effect is likely correlated with morphological changes of the carbon felt current collectors during cycling, resulting in a higher surface area and increased porosity (see Fig. S8). With increasing cycle number, a slight capacity fade is noted, though marginal in comparison with cells containing DAD.

The reason for this slow but continuous capacity fading during cycling seems to be the general chemical sensitivity of the presented diaza-based compounds against alkaline media. A time dependent observation of their charge transfer characteristics within a relatively broad potential window reveals a decrease of the primary signal in favor of a second emerging redox wave (see Fig. S9). The later obtained curves feature a redox potential that is 470 mV more negative than the pristine wave and fast kinetics indicated by a very small peak separation of about 40 mV. Due to the fact that the redox potential shifts negatively and the aforementioned peak splitting is not observed for the new species, we assume that the nitrogen containing part of the molecule is primarily involved in the side reaction. The absence of the diaza group would most likely lead to a naphtoquinone-like structure, which offers a more negative redox potential by nature[1,2], and regularly does not feature peak splitting[3], which is in accordance to our findings.

As shown in Fig. S9, this conversion process in alkaline solution was found to be less significant in the case of DAD(MeO), which is probably the reason for its improved cycle stability compared to DAD. This also results in the highest average Coulombic efficiency of the three species, which amounts to 99.72 %.

Regarding the results of the DADdi(OH)-based cell, the applied cut-off condition for the charging process leads to the most constant discharge capacity retention. Similar to the case of DAD(MeO), the cell seems to undergo an electrochemical activation process, which results in the highest overall discharge capacity of the three investigated DAAQs. Different from the other two compounds, DADdi(OH) does not seem to suffer from discharge capacity fading within the first 100 cycles. Still, this needs to be evaluated carefully by considering the Coulombic efficiencies for DADdi(OH) (see Fig. S11b). The aforementioned initialization process is reflected by a low initial efficiency of about 88 %, ramping up to 95.15 %, which is the lowest value of the three aromatic diaza structures. Polymerization reactions, even in combination with the steady decomposition in alkaline solutions, and other degradation mechanisms have to be taken into consideration as disadvantages of DADdi(OH). Furthermore, the impact of additional redox centers created by the incorporation of hydroxyl groups in close vicinity to the carbonyl group needs to be assessed in future studies.

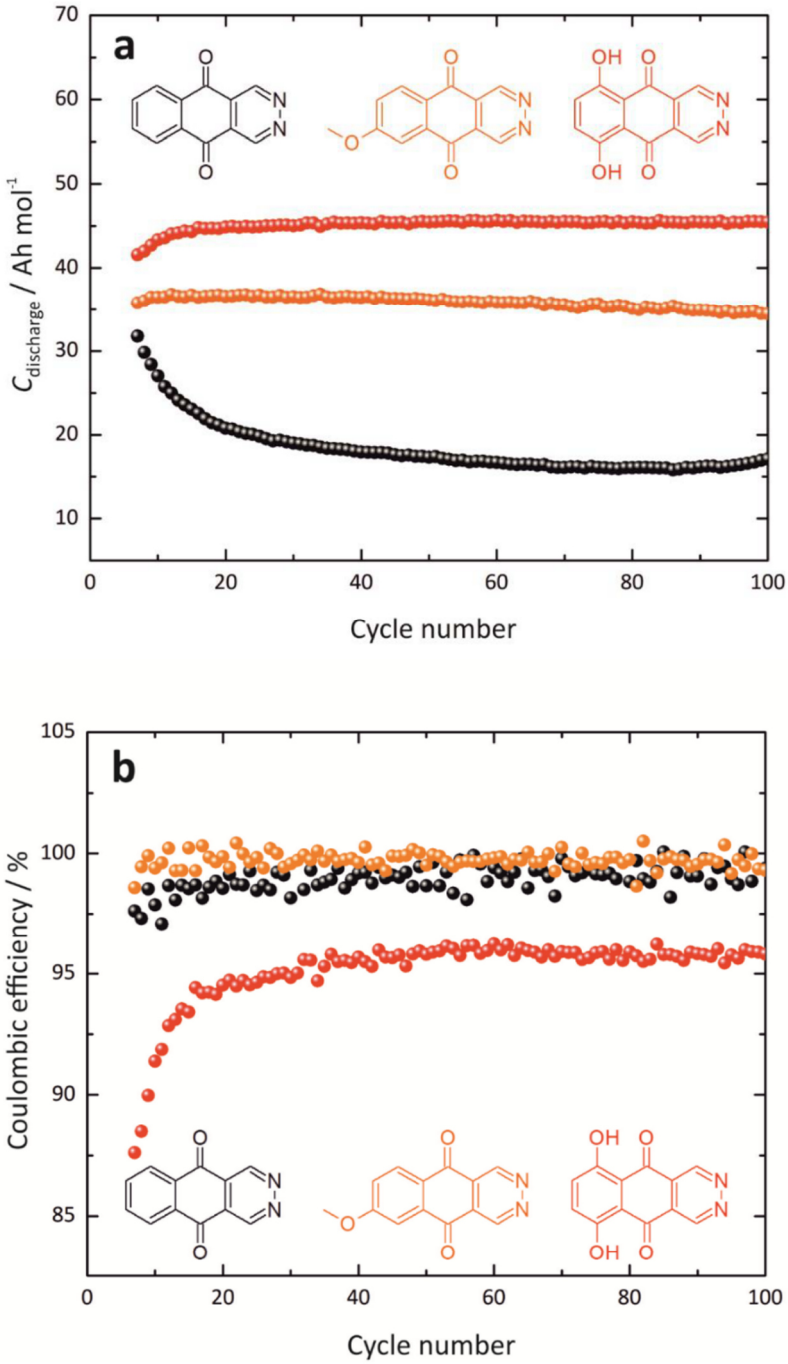

Figure S10: Full cell performance of the three investigated DAAQs in 1 M KOH. As a result of preceding polarization measurements, the nominal first six cycles are not included. (**a**) DAD undergoes a severe capacity fading during the first 100 cycles. On the contrary DAD(MeO) and DADdi(OH) exhibit a stable discharge capacity retention. For both compounds an activation process is observed, which especially for DADdi(OH) is also reflected by the Coulombic efficiency of the first depicted cycles (**b**). Starting from low values of about 87 % a constant efficiency around 95 % is attained after 40 cycles, representing the lowest overall value of the presented compounds. Compared to that, DAD and DAD(MeO) display very high mean Coulombic efficiencies of up to 99.72 %. Considering the strong capacity loss for DAD within the first twenty cycles, DAD(MeO) presumably is the most suitable of the presented compounds for RFB applications.

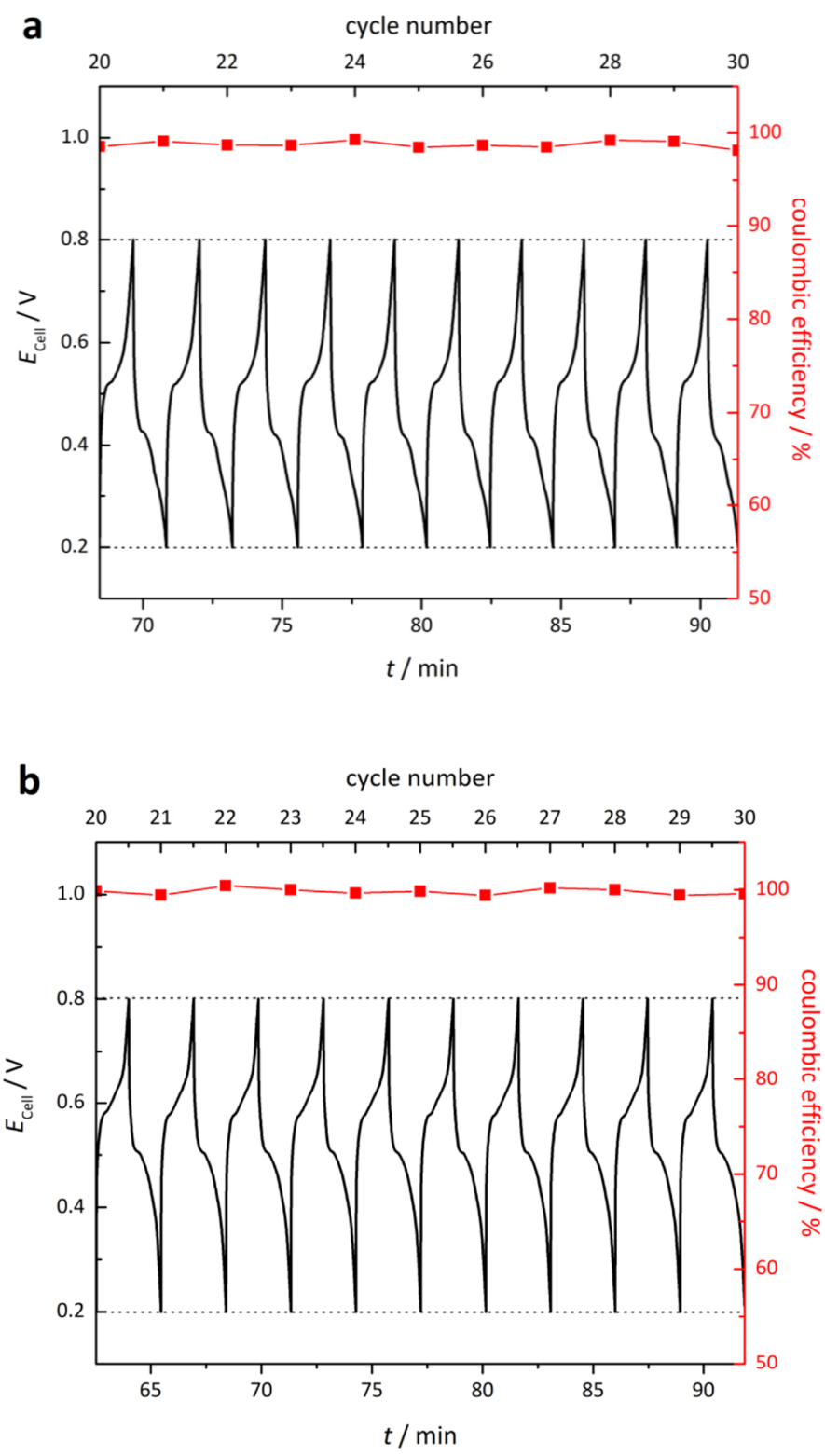
a
cycle number
20
22
24
26
28
30
1.0
0.8
0.6
0.4
0.2
E_{Cell} / V
100
90
80
70
60
50
coulombic efficiency / %
70
75
80
85
90
t / min
b
cycle number
20
21
22
23
24
25
26
27
28
29
30
1.0
0.8
0.6
0.4
0.2
E_{Cell} / V
100
90
80
70
60
50
coulombic efficiency / %
65
70
75
80
85
90
t / min

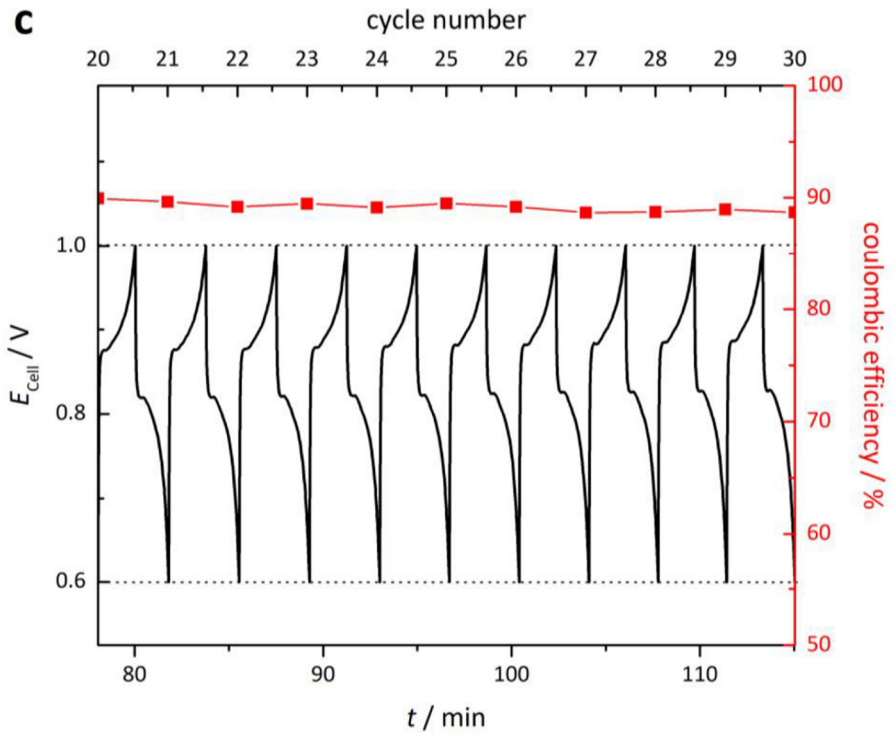

Figure S11: Temporal cell cycling behavior of the three investigated DAAQs in 1 M KOH. The figures display the progress of cell voltage during 10 subsequent cycles as well as the resulting Coulombic efficiency. The cut-off voltages are signalized by dashed lines: DAD (**a**) and DAD(MeO) (**b**) were cycled between 0.2 V and 0.8 V, whereas in the case of DADdi(OH) (**c**) the threshold values had to be set to higher potentials, which arises from its more negative redox potential relative to DAD and DAD(MeO). Hence, the cell was cycled between 0.6 V and 1 V.

DAAQ cycling stability at low pH value

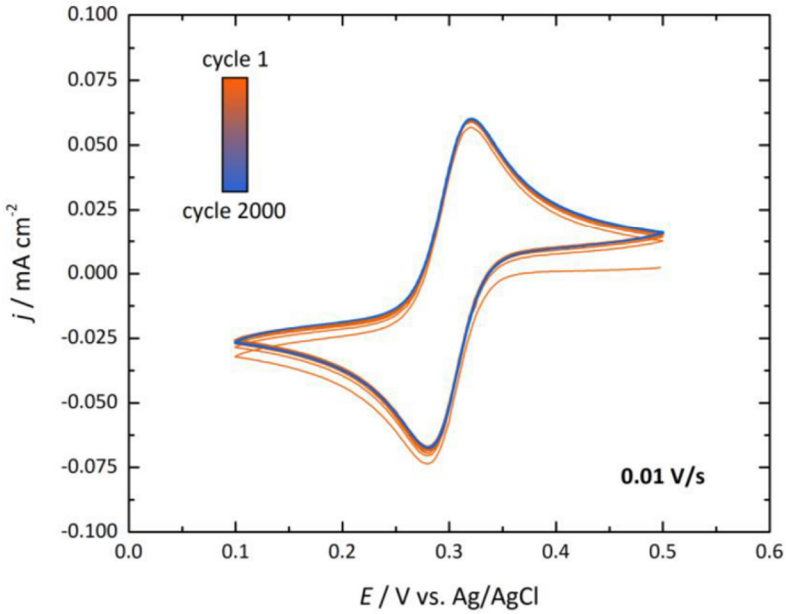

Figure S12: Cycling stability of 0.5 mM DAD in 1 M HCl. By the use of hydrochloric acid, stable cycling of DAAQs was attained. After reaching a steady state during the first cycles, a stable charge transfer characteristic was observed even for high cycle numbers up to 2000.

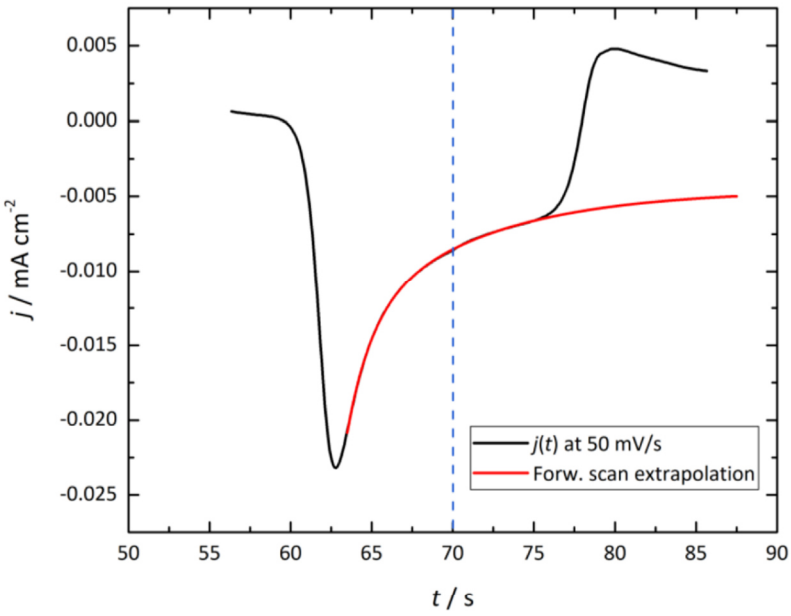

Figure S13: Extrapolation of the cathodic CV forward scan in time for DAD at 50 mV/s. As a measure of electrochemical reversibility a comparison between the anodically and cathodically transferred charge during a single cycle was made. To extract the anodic charge of the backward scan the extrapolation of the forward scan was used as a baseline for integration. Here the dashed blue line illustrates the reversal of the potential scan direction.

References

(1) Er, S.; Suh, C.; Marshak, M. P.; Aspuru-Guzik, A. Computational Design of Molecules for an All-Quinone Redox Flow Battery. *Chem. Sci.* **2015**, *6*, 885–893.

(2) Pineda Flores, S. D.; Martin-Noble, G. C.; Phillips, R. L.; Schrier, J. Bio-Inspired Electroactive Organic Molecules for Aqueous Redox Flow Batteries. 1. Thiophenoquinones. *J. Phys. Chem. C* **2015**, *119*, 21800–21809.

(3) Guin, P. S.; Das, S.; Mandal, P. C. Electrochemical Reduction of Quinones in Different Media: A Review. *Int. J. Electrochem.* **2011**, *2011*, e816202.

5.2 Supporting Information publication III

Supporting Information for

Tailoring Dihydroxyphthalazines to Enable their Stable and Efficient Use in the Catholyte of Aqueous Redox Flow Batteries

Jonas David Hofmann[a], Sebastian Schmalisch[c], Sebastian Schwan[a,d], Longcheng Hong[c], Hermann Andreas Wegner[c,d], Doreen Mollenhauer[a,d], Jürgen Janek[a,d*] and Daniel Schröder[a,d*]

[a] Institute of Physical Chemistry, Justus Liebig University Giessen, Heinrich-Buff-Ring 17, 35392 Giessen, Germany
[c] Institute of Organic Chemistry, Justus Liebig University Giessen, Heinrich-Buff-Ring 17, 35392 Giessen, Germany
[d] Center for Materials Research, Justus Liebig University Giessen, Heinrich-Buff-Ring 16, 35392 Giessen, Germany
* Corresponding Authors: Jürgen Janek, juergen.janek@phys.chemie.uni-giessen.de, Daniel Schröder, daniel.schroeder@phys.chemie.uni-giessen.de

Alternative synthesis routes of 2,3-diazanaphthoquinone (DNQ)

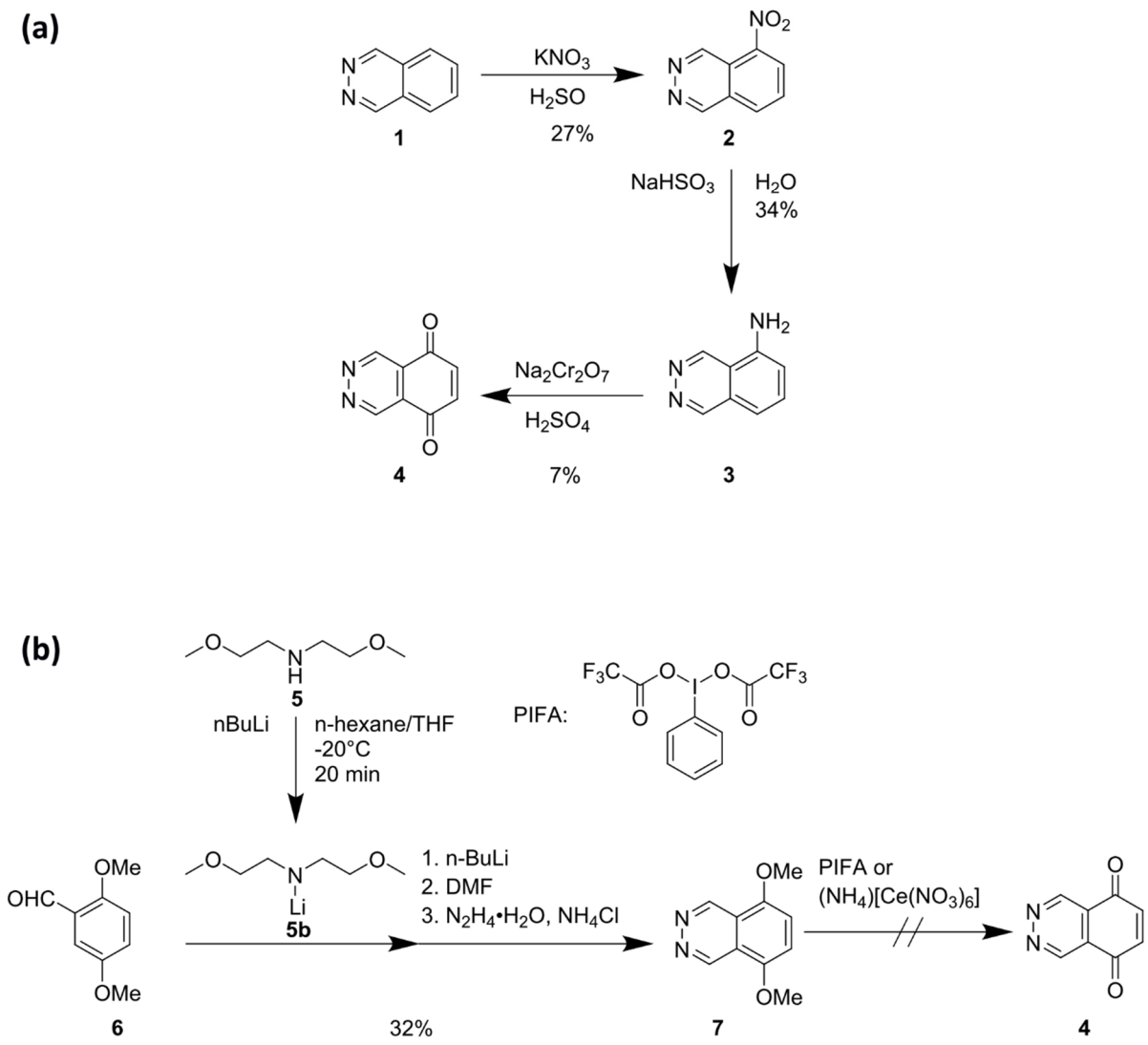

Figure S1: Alternative routes for the synthesis of 2,3-diazanaphthoquinone (DNQ). The conditions and yields are given in the scheme. Due to the low yield (7 %) of route **(a)** this approach was omitted in favor of the route reported in the manuscript. Route **(b)** was omitted completely as a result of the unsuccessful final oxidation step.

Rotating Disc Electrode (RDE) measurements

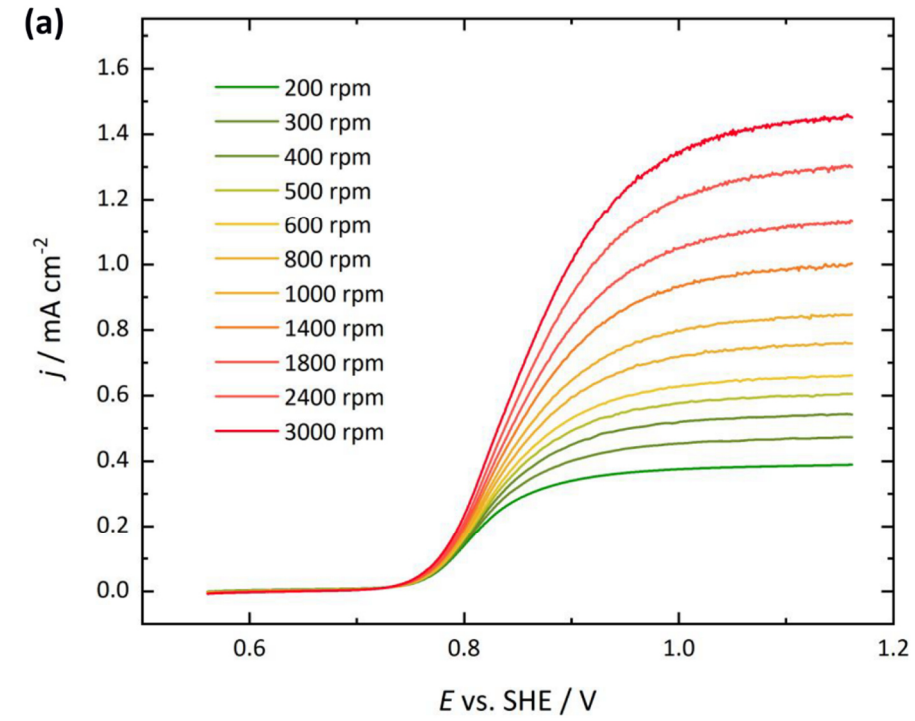

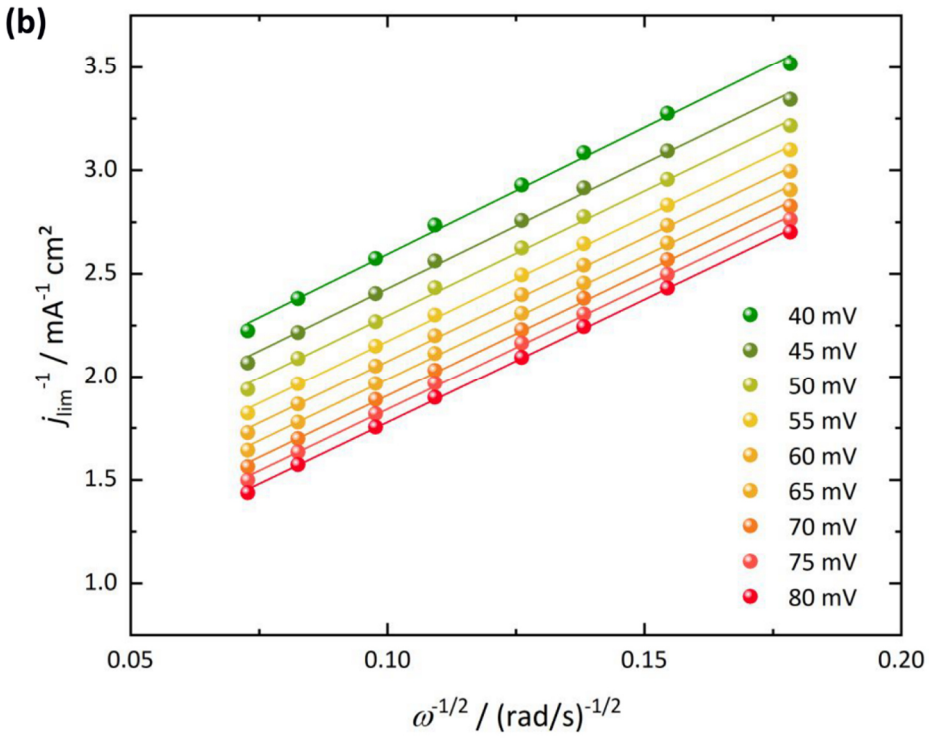

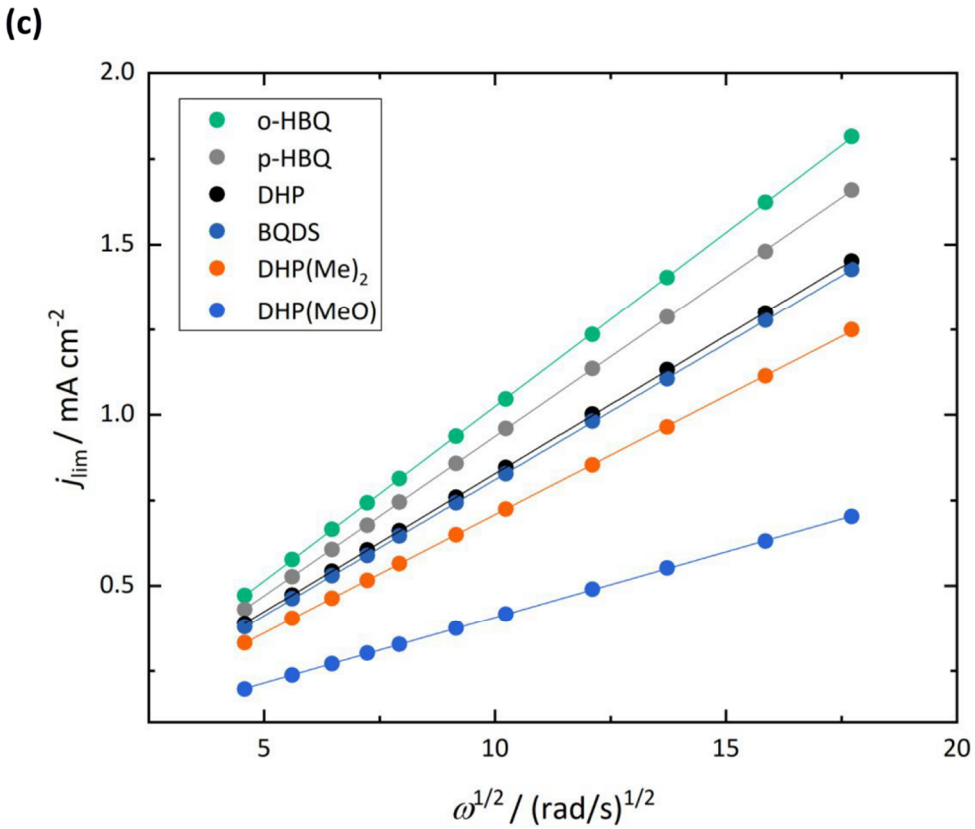

Figure S2: Determination of D and k_0 on the basis of RDE measurements of DHP: **(a)** Linear sweep voltammograms of DHP (1 mM in 1 M H_2SO_4) measured at a scan rate of 10 mV/s for electrode rotation rates ranging from 200 rpm to 3000 rpm. **(b)** Plot of the reciprocal limiting currents i_{lim} taken from (a) versus the inverse square root of the applied rotation rate ω (Koutecky-Levich plot). The varying colors hereby indicate the overpotential η (40 mV to 80 mV) the associated data points were taken from. **(c)** Levich plots of all compounds investigated in this work. The associated Levich slopes obtained by a fit of experimental data are given in Table T1.

Table T1: Summary of Levich slopes and Tafel intercepts used to calculate the values of D and k_0 given in Table 1. The underlying slopes and intercepts were obtained by fitting experimental data according to equation (1), (2), (3) and (4) (see experimental part).

Compound	Levich slope / A rad$^{-1/2}$ s$^{1/2}$	Tafel intercept
ortho-HBQ	7.2(1) x 10^{-6}	-5.22(4)
para-HBQ	6.5(9) x 10^{-6}	-5.03(6)
BQDS	5.6(3) x 10^{-6}	-5.50(1)
DHP	5.7(1) x 10^{-6}	-4.64(8)
DHP(MeO	2.7(2) x 10^{-6}	-4.80(9)
DHP(Me)$_2$	4.9(1) x 10^{-6}	-4.52(0)

Cyclic voltammograms of DHPs and other quinone species

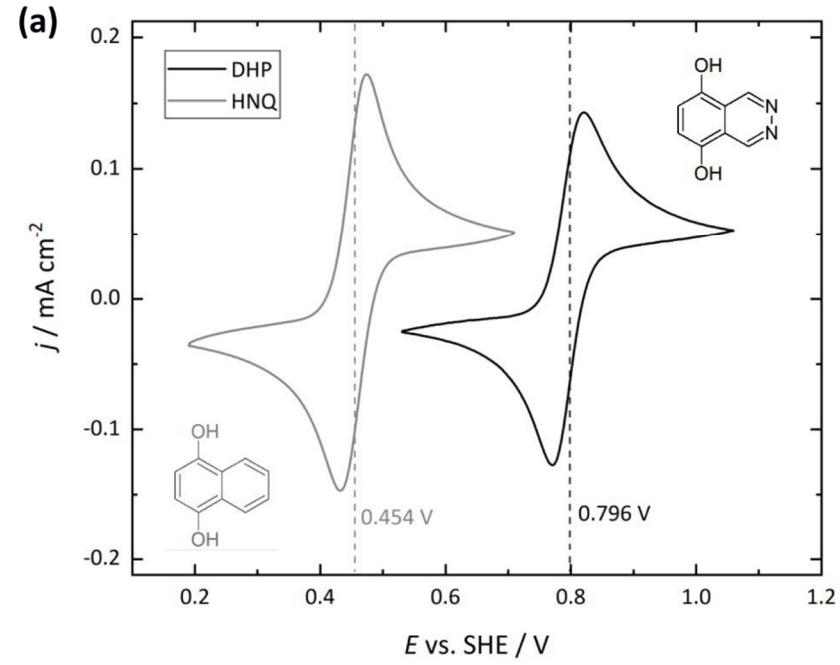

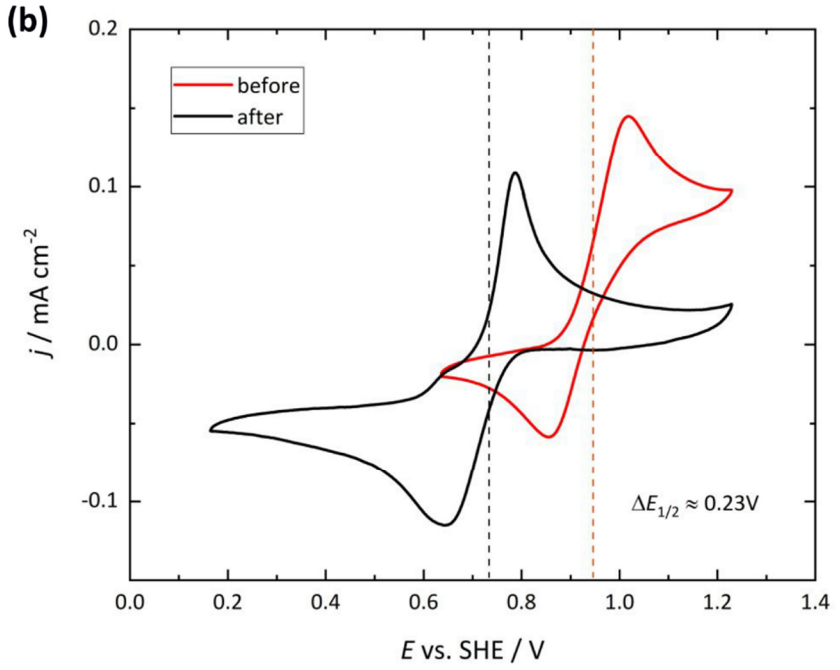

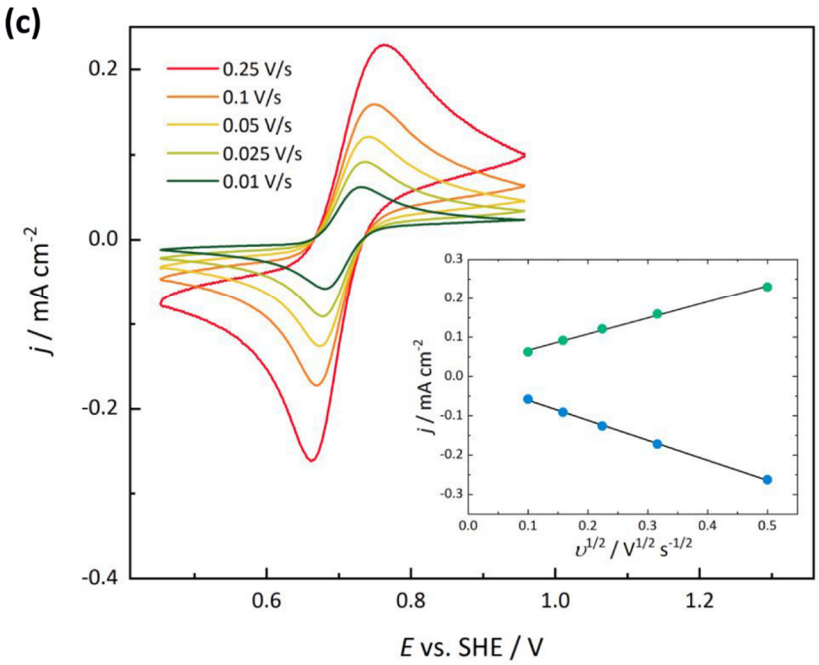

Figure S3: (a) CVs of the homocyclic 1,4-hydronaphthoquinone (HNQ) and the heterocyclic 5,8-dihydroxy-2,3-phthalazine measured at a sweep rate of 10 mV/s and an active material concentration of 1 mM in 1 M H_2SO_4. As a result of the nitrogen atoms in the aromativ system, DHP exhibits a mid-point potential of 796 mV vs. SHE, which is 342 mV higher than for HNQ. **(b)** CVs of BQDS before and after anodic exhaustive electrolysis measured at a sweep rate of 10 mV/s and an active material concentration of 1 mM in 2 M HCl. BQDS remains electrochemically active even after exhaustive electrolysis. However, the $E_{1/2}$ of the resulting compound is diminished by 230 mV which may be attributed to nucleophilic attacks of water and a deviating redox pattern (see also Scheme 1 and Figure S3). **(c)** Scan rate dependent CV studies of 1 mM $DHP(Me)_2$ in 1 M H_2SO_4, representative for the three DHP derivatives investigated in this work. The inset shows a plot of the measured anodic (mint) and cathodic (blue) peak currents I_p as a function of the square root of the applied scan rate υ. According to the Randles-Sevcik equation

$$I_p = 0.4463\, nFAc_0 \left(\frac{nF\upsilon D}{RT} \right)^{1/2}$$

where I_p is the peak current in A, n is the number of transferred electrons, F is the Faraday constant (96485.33 A s mol^{-1}), A is the electrode surface area in cm^2, υ is the scan rate in V s^{-1}, D is the diffusion coefficient in cm^2 s^{-1}, R is the universal gas constant (8.314 J mol^{-1} K^{-1}) and T is the temperature in K, there is a linear relation between the measured values of I_p and the square root of the associated υ for diffusion-controlled processes.[1] As indicated by the inset, this is given in the case of DHPs in acidic aqueous solution.

Exhaustive electrolysis

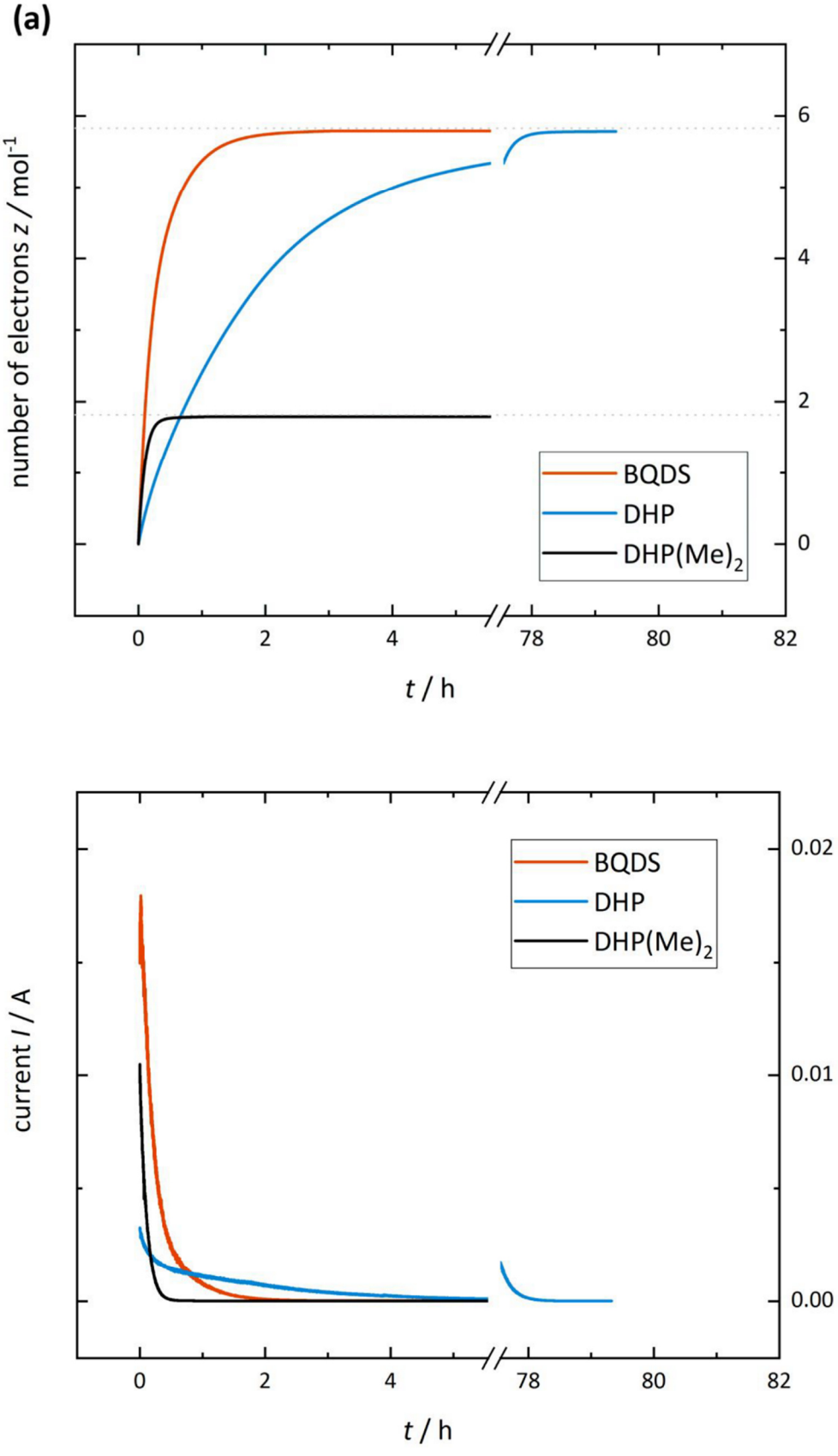

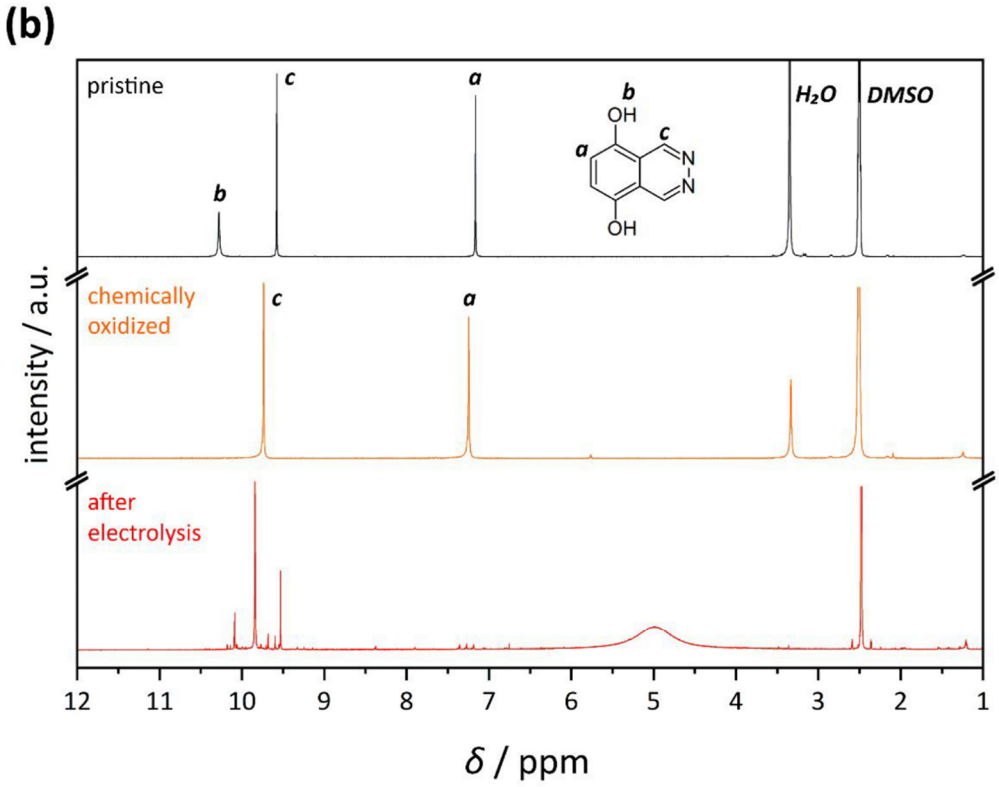
(b)
pristine
chemically oxidized
after electrolysis
a
b
c
H₂O
DMSO
OH
N
intensity / a.u.
12 11 10 9 8 7 6 5 4 3 2 1
δ / ppm

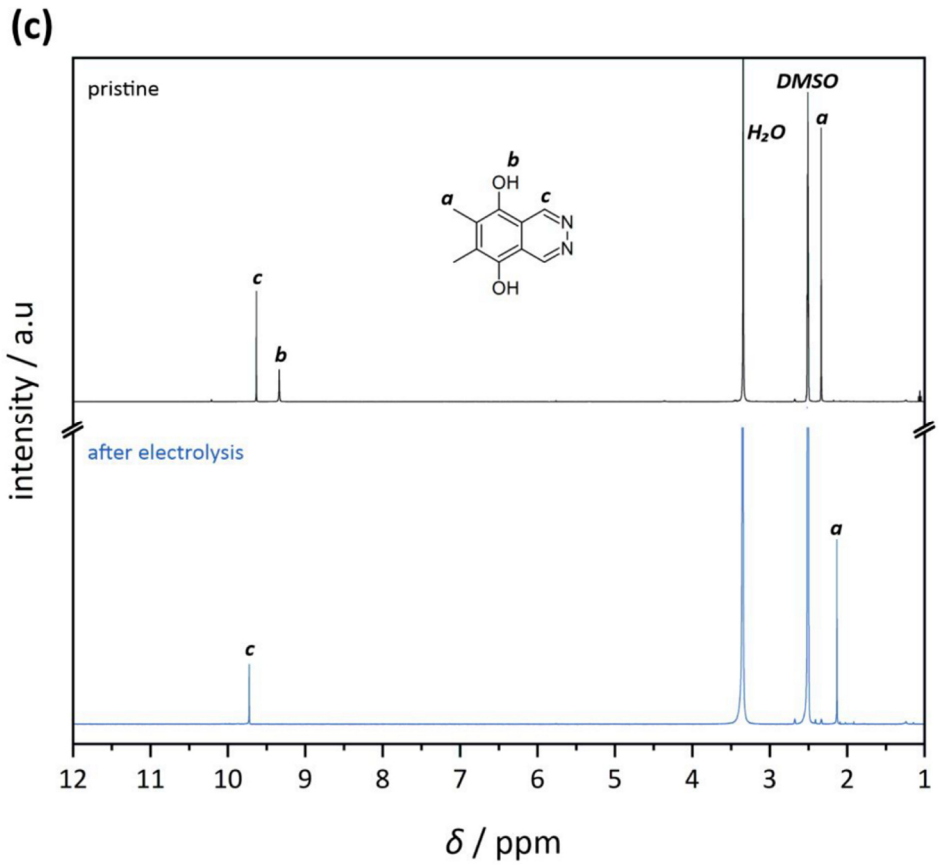
(c)
pristine
after electrolysis
a
b
c
DMSO
H₂O
OH
N
intensity / a.u
12 11 10 9 8 7 6 5 4 3 2 1
δ / ppm

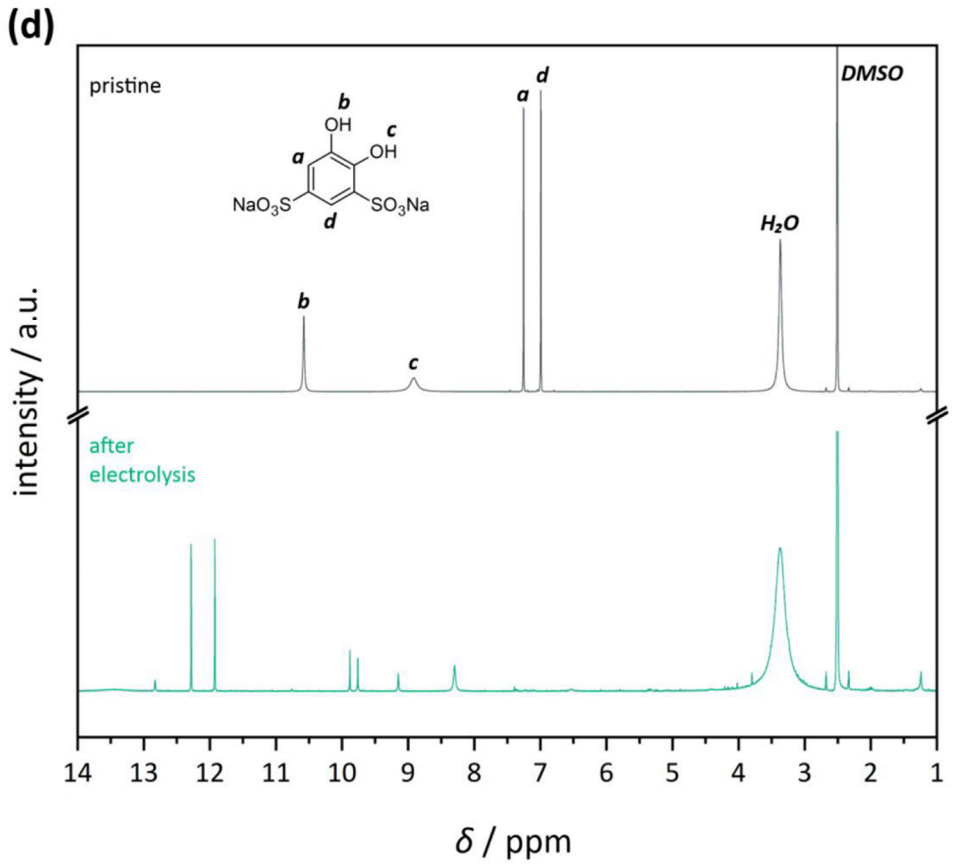

Figure S4: Electrolysis data and ^{1}H NMR spectra of DHP and HBQ species. **(a)** Results obtained for the electrolysis of BQDS, DHP and DHP(Me)$_2$. In order to achieve a complete conversion of the investigated active material, a constant voltage well beyond the redox potential of the associated species was applied (1.16 V vs. SHE for BQDS, 1.01 V for DHP and 0.96 V for DHP(Me)$_2$). During electrolysis, gas bubbles were formed at the counter electrode, probably indicating the evolution of hydrogen. For BQDS it takes about 2 h to reach a stable value which corresponds to 5.82 electrons transferred per molecule. This clearly surmounts the expected value of two electrons. The slow charge transfer and the excess amount of charge may indicate a side process, successively offering more charge to be transferred after the intended oxidation to the quinone form. A potential reaction pathway is given in Scheme 1. For DHP a similar value of 5.78 is attained. However, the shallow slope of the graph implies that the process takes place distinctly slower than in the case of BQDS. After 4.5h the measurement was stopped and the solution was stored under an argon blanket for about 74 h. When the measurement was restarted the remaining charge was extracted almost immediately further underlining the argument of a – in the case of DHP very slow– capacity generating side reaction following the intended oxidation step.

For all ^{1}H NMR measurements trace amounts of water were detected which may originate from DMSO-d_6 which was used as a reference. **(b)** For pristine DHP (black trace) three chemically equal pairs of protons are present which can be assigned to the three peaks (*a*, *b*, *c*) obtained in the spectrum. To verify the anticipated assignment we oxidized DHP with $NaIO_4$ in aqueous solution to obtain the oxidated product 2,3-diazanaphthoquinone (orange trace). As expected, peak *b*, which is correlated with the hydroxyl protons of the reduced species, is missing in the spectrum. Besides a slight shift of peak *a* and *c* is observed, which may be due to the lack of aromaticity of the oxidized compound and consequently a deviating shielding of the associated protons. However, for the electrolysis product of

DHP (red trace) a multitude of signals is obtained. An assignment of the signals hence cannot be done unambiguously. The peak at 9.86 ppm may be correlated with signal *c* of the pristine compound whereas the nature of the remaining signals remains unclear. The presence of new signals yet implies that proton-carrying moieties are involved, which is in line with the mechanism proposed in Scheme 1. The broad signal around 5 ppm may be related to the protons of water present, which is also observed in other measurements. The distinct shift and broadening of the peak may be explained by a strong hydrogen bonding interaction between the protons of water and the proton of the (after electrolysis in an acidic environment) protonated diaza-moiety. Nonetheless, the bottom line of the illustrated spectra is that no more signals were detected in the region characteristic for the pair of protons attached to the quinone ring of the compound (peak *a*) indicating nucleophilic attacks in these positions.

(c) For pristine DHP(Me)$_2$ (black trace) three proton signals are to be distinguished. As expected after oxidative electrolysis the peak assigned to the hydroxyl protons is missing in the spectrum (blue trace). Since the other signals remain unchanged the peak pattern implies the intended oxidation of DHP(Me)$_2$ to its oxidized quinone form and hence a high stability versus nucleophilic attacks as a result of the applied methyl functionalization. As in the case of DHP the shift of peak *a* may be related to the deviating chemical environment within the oxidized molecule.

(d) For pristine BQDS (black trace) a more complex 1H NMR spectrum is anticipated since in this case four protons with deviating chemical environments are present. As a result, four peaks are obtained of which *a* and *d* are to be assigned to the protons directly attached to the aromatic ring. The peaks *b* and *c* correspond to the hydroxyl protons whereas the high relative distance between both peaks is due to the strongly electron withdrawing character of the sulfonate moiety which consequently deshields the hydroxyl proton *c*. Furthermore, the broad appearance of peak *c* indicates a distribution of chemical environments of the associated proton which may be caused by hydrogen bonding interactions. Since hydroxyl group *c* features an adjacent sulfonate group this may lead to the conclusion that the interaction takes place between these moeties. For the electrolysis product of BQDS (green trace) a large number of new signals is observed. As in the case of DHP an unambiguous assignment of the peaks is not feasible. It becomes clear that the degradation process suggested in Scheme 1 does not satisfy the complexity of the spectrum. Nonetheless, as in the case of DHP it is to be noted that the signals *a* and *d* that are correlated with the protons attached to the aromatic ring completely disappeared in the course of electrochemical oxidation. This further emphasizes the initial argument that these sites are vulnerable to nucleophilic attacks. The wide distribution of the remaining signals may be explained by the interplay of different reaction mechanisms: besides the hydroxylation of unsubstituted sites described by Scheme 1 sulphonate loss as a result of β-elimination[2] or even a protodesulfonation combined with a subsequent hydroxylation[3] may occur which would lead to a multitude of different structures.

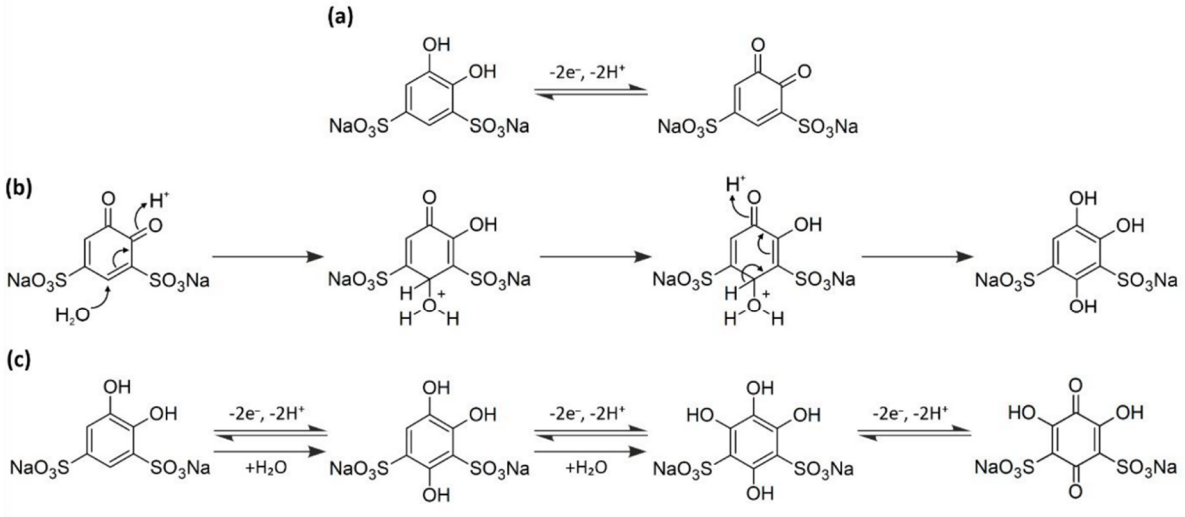

Scheme 1: Potential degradation mechanism of BQDS. The intrinsically high electron affinity of the benzoquinone base structure as well as the incorporated sulphonate groups pose a strong driving force for potential nucleophilic attacks. As long as BQDS is present in its reduced form the aromatic nature of the molecule and the concomitant delocalisation of electrons effectively prevents these kinds of side reactions. In theory, BQDS should undergo a reversible two-electron, two-proton transfer **(a)**. However, as soon as BQDS is oxidized a nucleophilic attack of water is very likely, chemically transforming the molecule back into a hydroquinone state **(b)**. As a result, the molecule structure is altered by an additional hydroxyl moiety and is available for another oxidation step. Since the oxidation of a *para*-HBQ is thermodynamically more favorable than for an *ortho*-HBQ (see also Fig. 1) the compound from this point is likely to act according to the *para*-configuration. This manifests in a lower redox potential, which is further underlined by the added hydroxyl moiety. **(c)** If the driving force for another nucleophilic attack is high enough, another addition of water and rearomatization of the molecule is feasible, leading to the fully functionalized 1,4-benzoquinone-2,6-dihydroxy-3,5-disulphonate.[4] However, as indicated by the diffuse ^{1}H NMR spectrum after electrolysis (see Fig. S3) the side reactions ocurring may not be confined to the proposed machanism. Instead an interplay of different reactions may lead to a distribution of deviating electrolysis products.

DFT calculations

Table T2: Redox potentials E_{calc} of different DHP substitution patterns, calculated at PBE-D3/aug-cc-VDZ (PCM) level of theory. The compounds are listed in the order of increasing redox potential. Abbreviations are indicated as DHP(X)-(Y) with (X) standing for the functional groups located at the homocyclic ring, and (Y) representing the functional groups located at the heterocyclic ring including the diaza moiety. The molecules discussed in the manuscript are highlighted in red (experimental data available) and blue (solely DFT-based potentials). For the phosphonic acid group redox potentials of different protonation states are given in brackets. The last column indicates the degree of structural distortion relative to the ring planarity by means of dihedral angles. A distortion larger than or equal to 5° of the oxidized/reduced molecule is indicated by an asterisk. As a measure of chemical stability, relative energies of selected DHP derivatives (ox) compared to the planar DHP are given in brackets.

Compound	E_{calc} vs. SHE / V	Ring distortion (ox/red)
DHP(Me)(SO_2iprop)	0.735	*/*
DHP($Me)_2$	0.737	
DHP-($Me)_2$	0.780	
DHP(SOiprop)	0.784	*/
DHP(MeO)	0.795	
DHP	0.858	
DHP(Br)	0.871	
DHP($CF_3)_2$-($CF_3)_2$	0.921	*/* (6.2 kcal mol^{-1})
DHP($CF_3)_2$	0.931	*/*(4.0 kcal mol^{-1})
DHP(SO_3^-)-($Me)_2$	0.934	
DHP-($COOH)_2$	0.938	/*
DHP($F)_2$-($F)_2$	0.946	
DHP(Me)(SO_2Me)	0.964	*/ (2.4 kcal mol^{-1})
DHP(Me)(SOiprop)	0.977	*/
DHP(SO_3^-)-(Me)-1	0.978	
DHP(SO_2iprop)	0.985	*/
DHP(SO_3^-)-(Me)-2	0.993	
DHP(PO_3H_2)	1.014 (1.079, 1.204)	
DHP(SO_3^-)	1.017	
DHP(SO_3^-)-($CF_3)_2$	1.027	*/*
DHP(SO_2Me)	1.029	
DHP(Me)(SO_3^-)	1.053	*/ (2.4 kcal mol^{-1})
DHP(SO_2CF_3)	1.064	
DHP(SO_3^-)-(CF_3)	1.071	
DHP(SO_3^-)-(CF_3)	1.087	
DHP(SO_3^-)(CF_3)-($CF_3)_2$	1.098	*/* (3.4 kcal mol^{-1})
DHP(SO_3^-)-($F)_2$	1.121	
DHP-($SO_3^-)_2$	1.133	*/*
DHP(SO_3^-)-($CN)_2$	1.135	
DHP(sumi)	1.137	
DHP(SO_3^-)(F)-($F)_2$	1.167	
DHP(SO_3^-)(CN)-($CN)_2$	1.197	

Bond lengths and angles

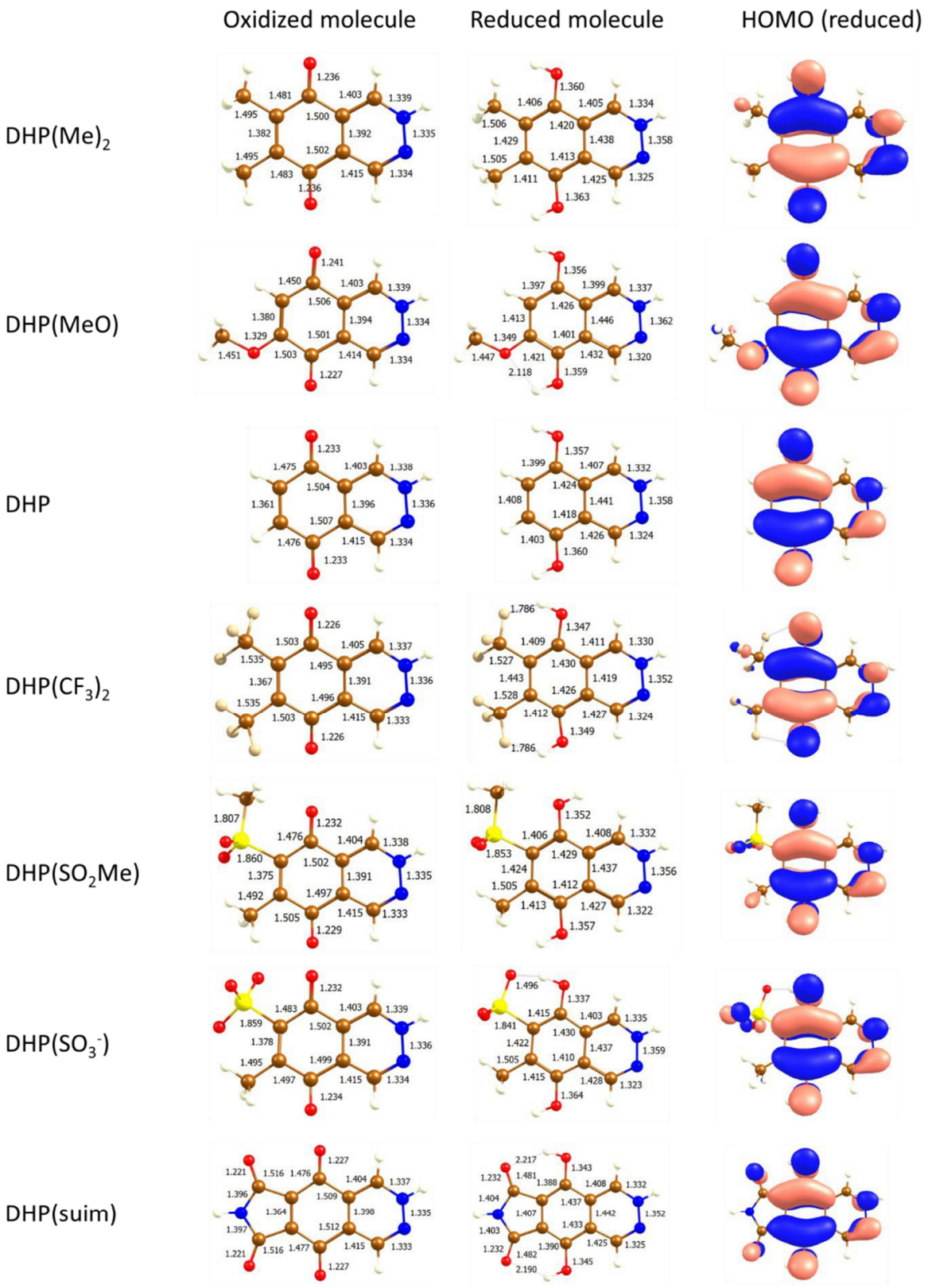

Figure S5: Bond lengths (Å) of selected DHP derivatives and the HOMO of the reduced molecule.

NMR spectra of synthesized DHP compounds

5,8-Dihydroxy-2,3-phthalazine, DHP ^{1}H-NMR

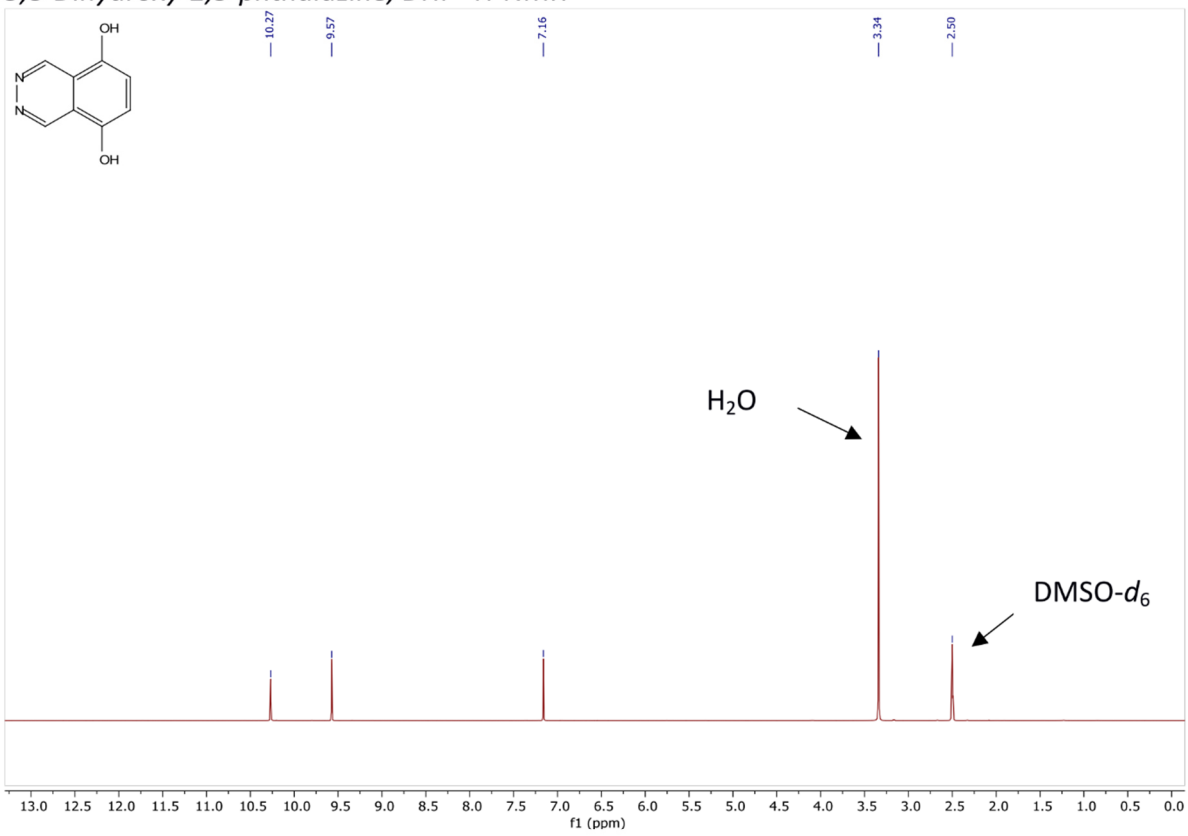

5,8-Dihydroxy-2,3-phthalazine, DHP ^{13}C-NMR

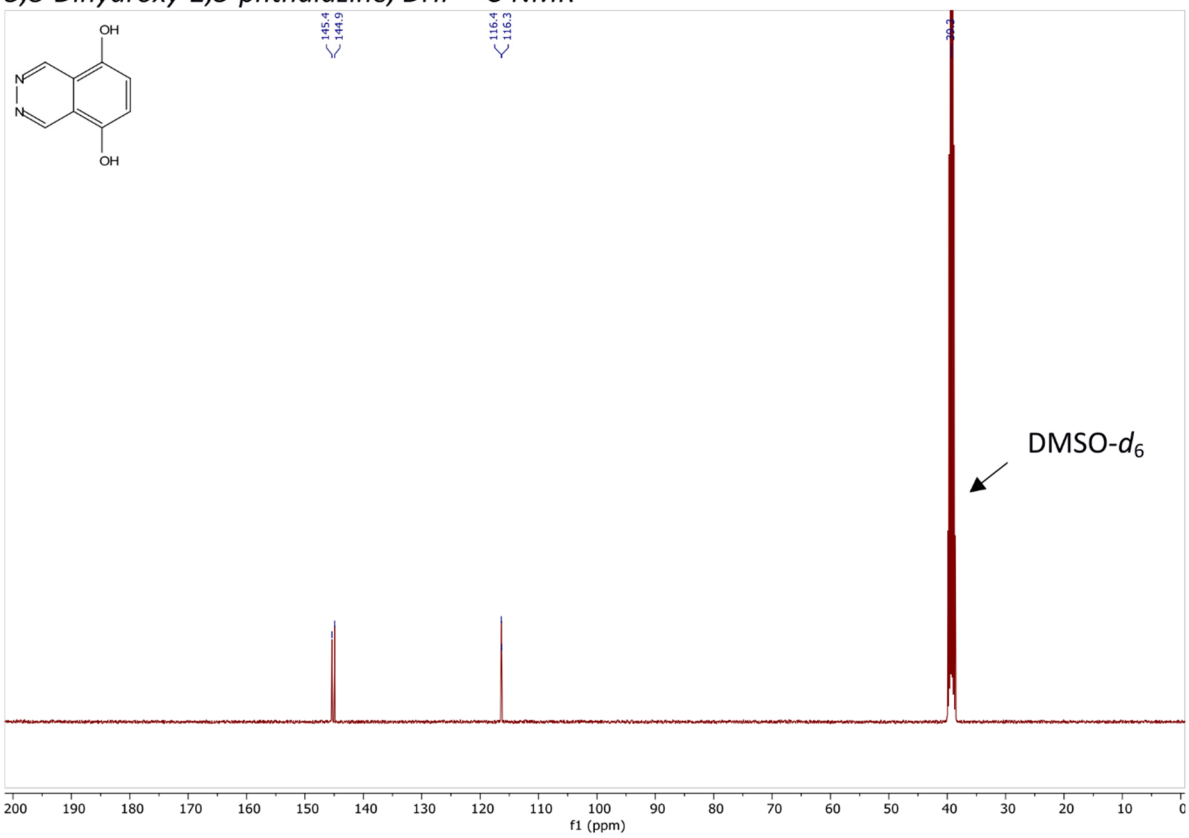

14/18

5,8-Dihydroxy-6-methoxy-2,3-phthalazine, DHP(MeO) ^{1}H-NMR

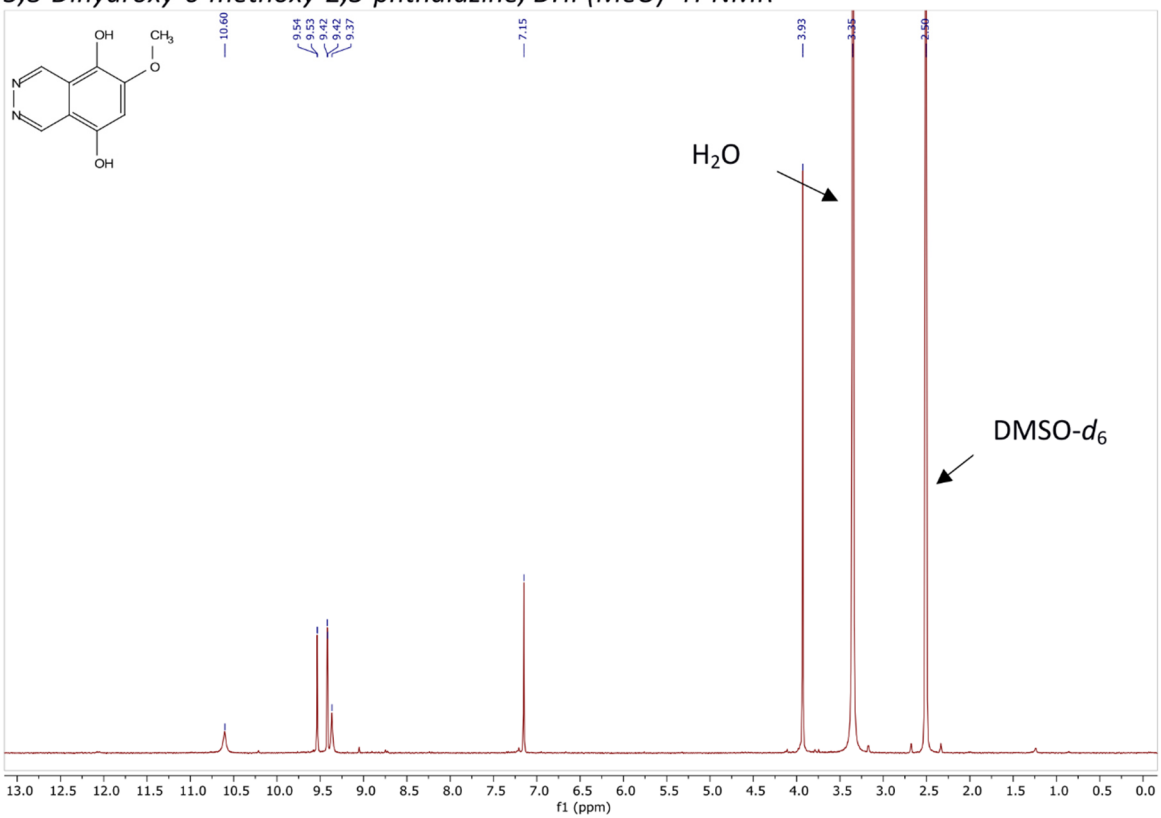

5,8-Dihydroxy-6-methoxy-2,3-phthalazine, DHP(MeO) ^{13}C-NMR

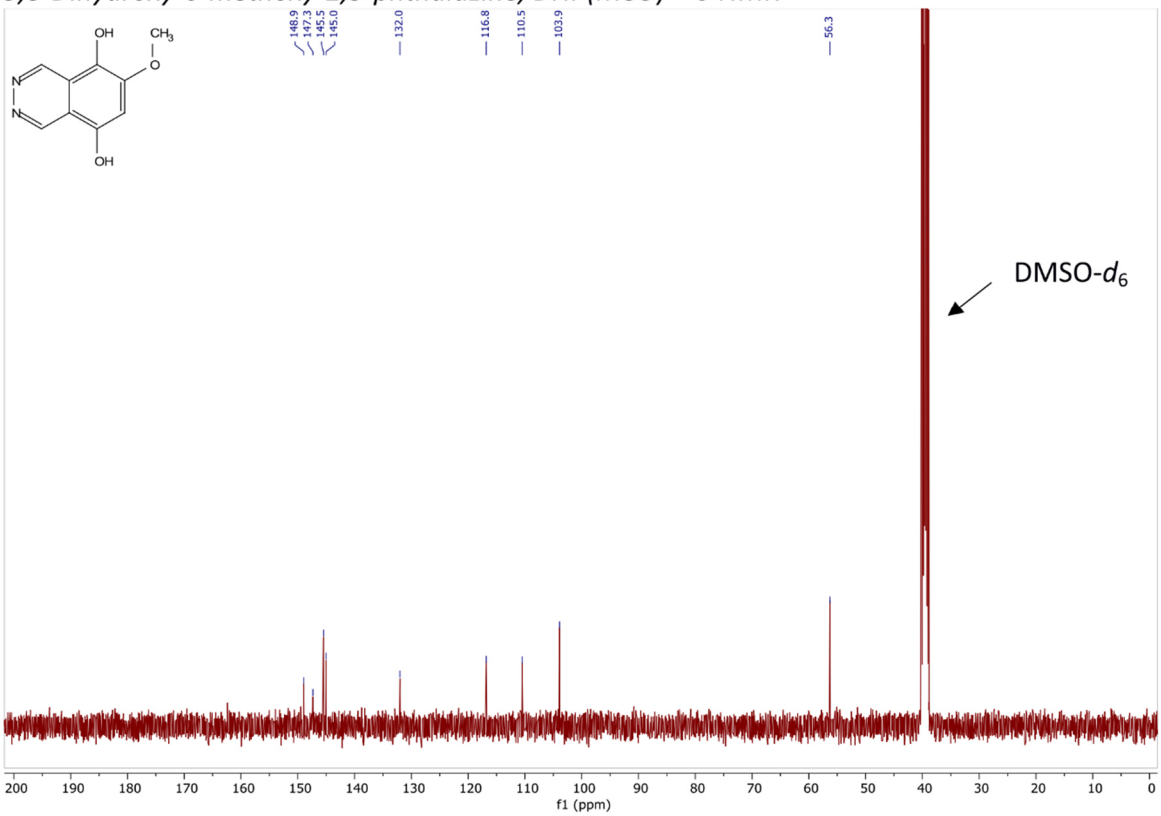

5,8-Dihydroxy-6,7-dimethyl-2,3-phthalazine, DHP(Me)$_2$ ^{1}H-NMR

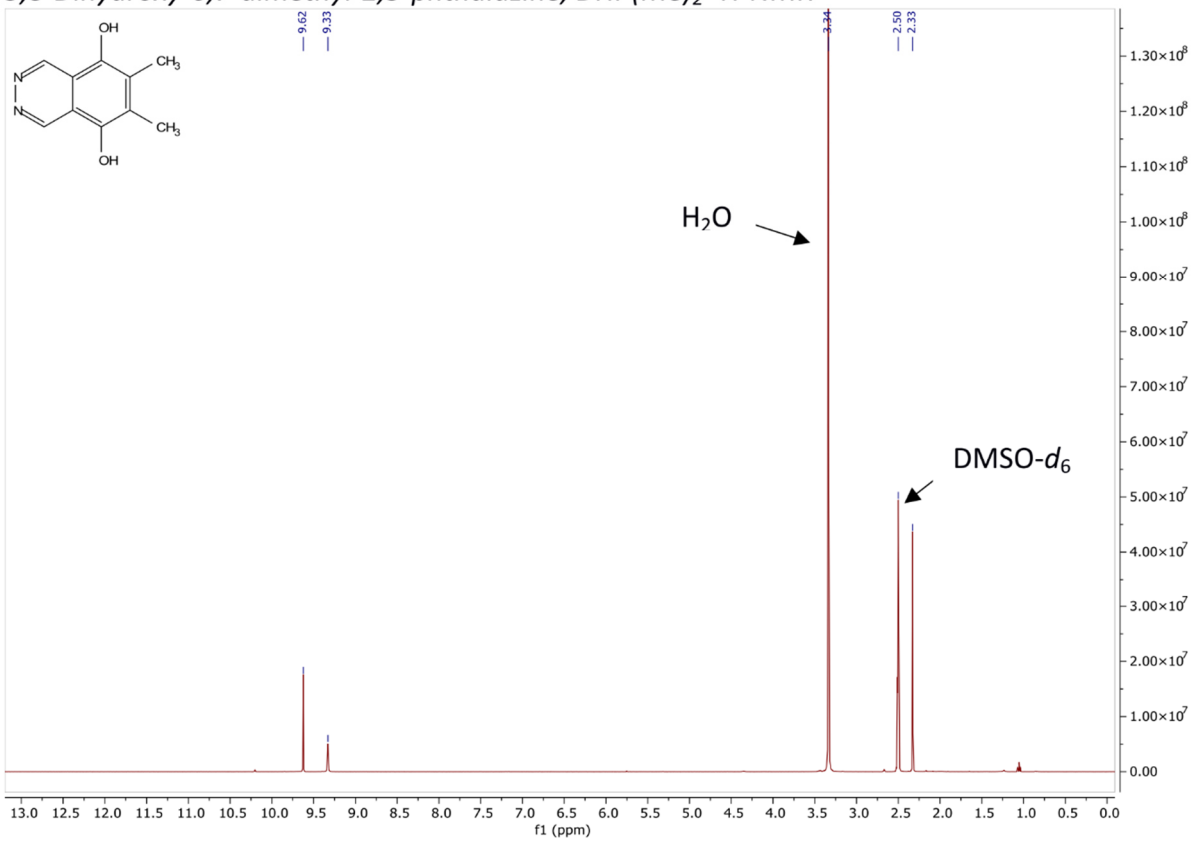

5,8-Dihydroxy-6,7-dimethyl-2,3-phthalazine, DHP(Me)$_2$ ^{13}C-NMR

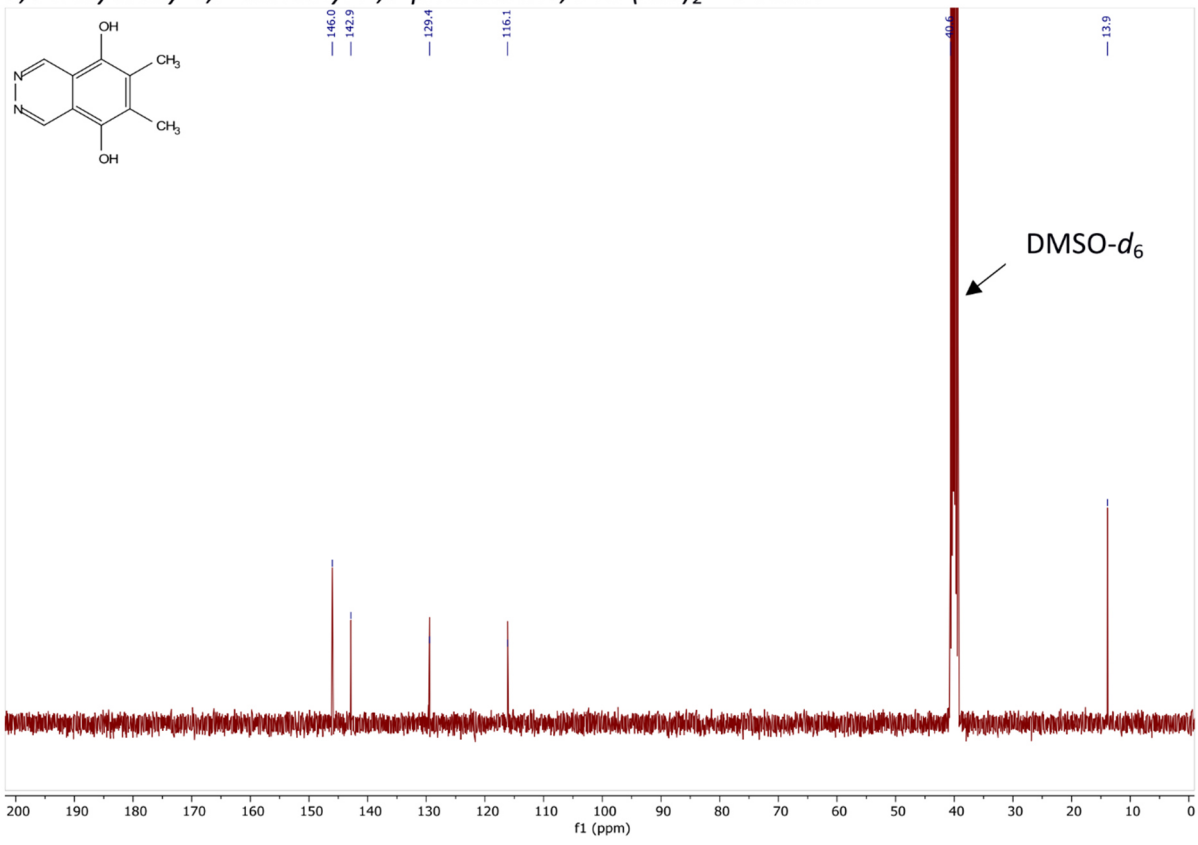

5,6-Dihydroxyphthalazine, 5,6-DHP ^{1}H-NMR

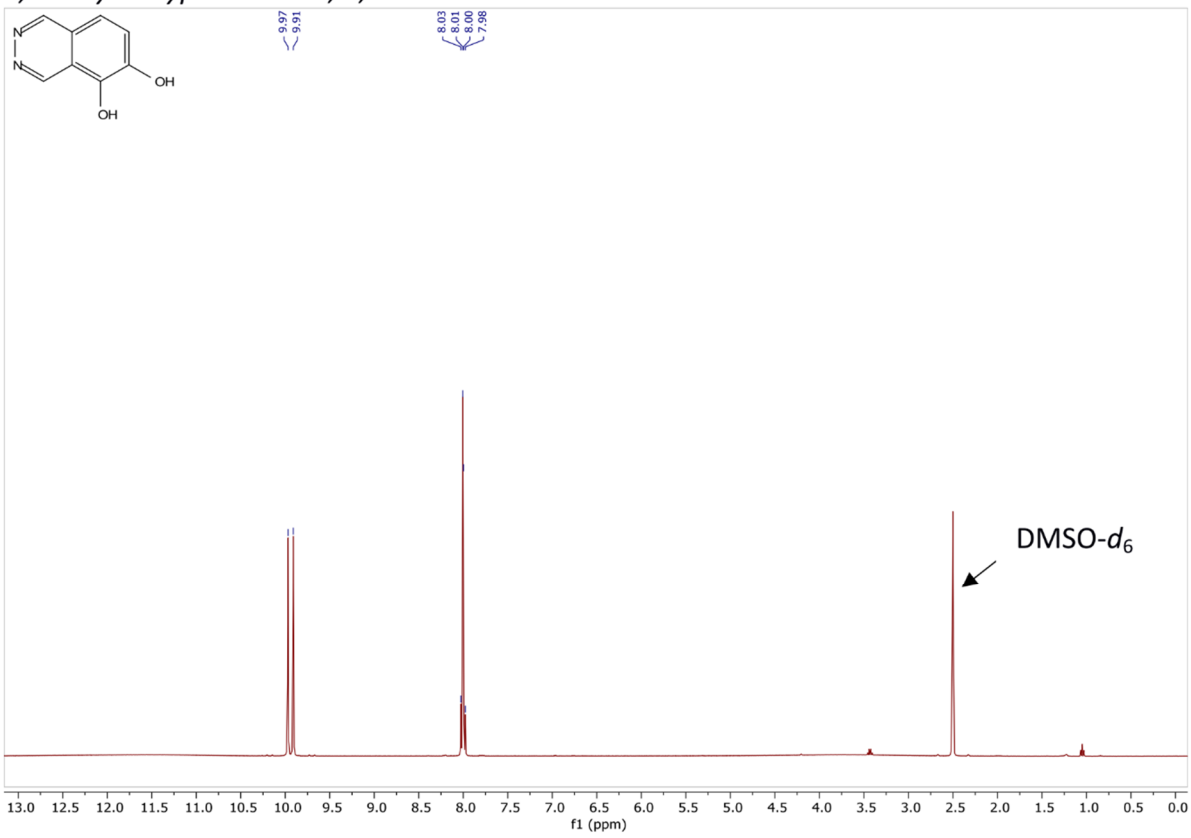

5,6-Dihydroxyphthalazine , 5,6-DHP ^{13}C-NMR

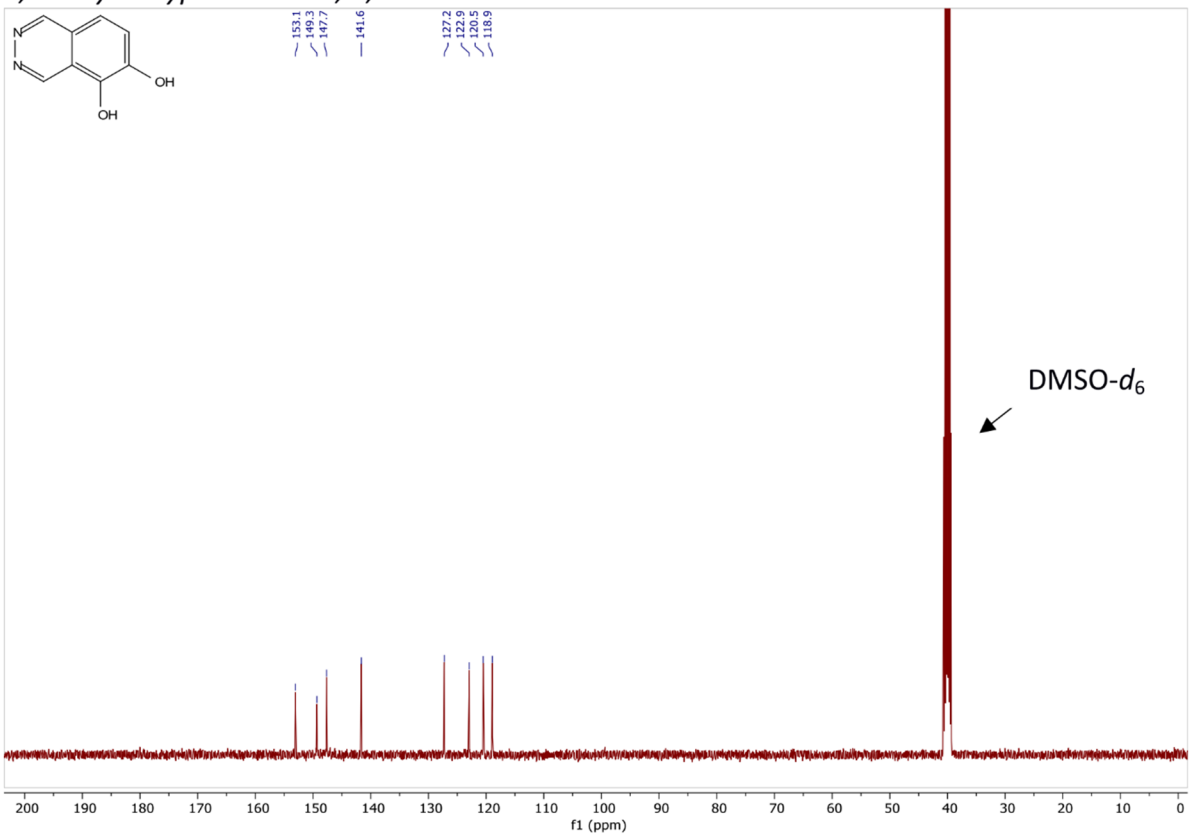

Supporting Information References

(1) Bard, A. J.; Faulkner, L. R. *Electrochemical Methods: Fundamentals and Applications*; Wiley, 2000.

(2) Mukherjee, T.; Land, E. J.; Swallow, A. J.; Guyan, P. M.; Bruce, J. M. Successive Addition of Electrons to Sodium Quinizarin-2- and -6-Sulphonate in Aqueous Solution. a Pulse and γ-Radiolysis Study. *J. Chem. Soc., Faraday Trans. 1* **1988**, *84* (8), 2855–2873. https://doi.org/10.1039/F19888402855.

(3) Murali, A.; Nirmalchandar, A.; Krishnamoorthy, S.; Hoober-Burkhardt, L.; Yang, B.; Soloveichik, G.; Prakash, G. K. S.; Narayanan, S. R. Understanding and Mitigating Capacity Fade in Aqueous Organic Redox Flow Batteries. *J. Electrochem. Soc.* **2018**, *165* (7), A1193–A1203. https://doi.org/10.1149/2.0161807jes.

(4) Permatasari, A.; Lee, W.; Kwon, Y. Performance Improvement by Novel Activation Process Effect of Aqueous Organic Redox Flow Battery Using Tiron and Anthraquinone-2,7-Disulfonic Acid Redox Couple. *Chemical Engineering Journal* **2020**, *383*, 123085. https://doi.org/10.1016/j.cej.2019.123085.

5.3 List of publications

D. Emmel, J. D. Hofmann, T. Arlt, I. Manke, G.D. Wehinger, D. Schröder, Understanding the Impact of Compression on the Active Area of Carbon Felt Electrodes for Redox Flow Batteries. *ACS Appl. Energy Mater.* **2020**, *3* (5), 4384–4393.

J. D. Hofmann, S. Schmalisch, S. Schwan, L. Hong, H. A. Wegner, D. Mollenhauer, J. Janek, D. Schröder, Tailoring Dihydroxyphthalazines to Enable Their Stable and Efficient Use in the Catholyte of Aqueous Redox Flow Batteries. *Chem. Mater.* **2020**, *32* (8), 3427–3438.

J. D. Hofmann, D. Schröder, Which Parameter Is Governing for Aqueous Redox Flow Batteries with Organic Active Material? *Chemie Ingenieur Technik* **2019**, *91* (6), 786–794.

J. D. Hofmann, F. L. Pfanschilling, N. Krawczyk, P. Geigle, L. Hong, S. Schmalisch, H. A. Wegner, D. Mollenhauer, J. Janek, D. Schröder, Quest for Organic Active Materials for Redox Flow Batteries: 2,3-Diaza-Anthraquinones and Their Electrochemical Properties. *Chem. Mater.* **2018**, *30* (3), 762–774.

Z. Lu, H. Quanz, O. Burghaus, J. Hofmann, C. Logemann, S. Beeck, P. R. Schreiner, H. A. Wegner, A Stable Organic Neutral Diradical via Reversible Coordination. *J. Am. Chem. Soc.* **2017**, *139* (51), 18488–18491.

M. T. Elm, J. D. Hofmann, C. Suchomski, J. Janek, T. Brezesinski, Ionic Conductivity of Mesostructured Yttria-Stabilized Zirconia Thin Films with Cubic Pore Symmetry—On the Influence of Water on the Surface Oxygen Ion Transport. *ACS Appl. Mater. Inter*. **2015**, *7* (22), 11792–11801.

A. Bhide, J. Hofmann, A. K. Dürr, J. Janek, P. Adelhelm, Electrochemical Stability of Non-Aqueous Electrolytes for Sodium-Ion Batteries and Their Compatibility with Na0.7CoO2. *Phys. Chem. Chem. Phys*. **2014**, *16* (5), 1987–1998.

Patents

Dihydroxyphthalazine, ihre Herstellung und Verwendung, EP 19154112.7